THESIS

This is to certify that the

dissertation entitled

**Anodic Growth and Cathodic Removal of Silicon
Dioxide Layers Utilizing an Electron
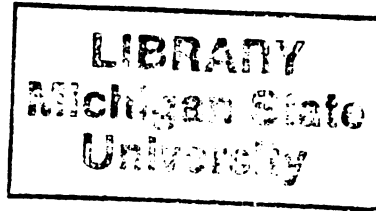Cyclotron Resonant Microwave Plasma Disk Reactor**

presented by

Geoffrey Todd Salbert

has been accepted towards fulfillment
of the requirements for

__Ph.D.__ degree in __Electrical__

__Engineering__

Major professor

Date *March 18, 1992*

O-12771

PLACE IN RETURN BOX to remove this checkout from your record.
TO AVOID FINES return on or before date due.

DATE DUE	DATE DUE	DATE DUE
————	————	————
————	————	————
————	————	————
————	————	————
————	————	————
————	————	————
————	————	————

MSU Is An Affirmative Action/Equal Opportunity Institution

c:\circ\datedue.pm3-p.1

ANODIC GROWTH AND CATHODIC REMOVAL OF SILICON

DIOXIDE LAYERS UTILIZING AN ELECTRON

CYCLOTRON RESONANT MICROWAVE PLASMA DISK REACTOR

By

Geoffrey Todd Salbert

A DISSERTATION

Submitted to

Michigan State University

in partial fulfillment of the requirements

for the degree of

DOCTOR OF PHILOSOPHY

Department of Electrical Engineering

1992

ABSTRACT

ANODIC GROWTH AND CATHODIC REMOVAL OF SILICON DIOXIDE LAYERS UTILIZING AN ELECTRON CYCLOTRON RESONANT MICROWAVE PLASMA DISK REACTOR

By

Geoffrey Todd Salbert

Two plasma processes for the modification of semiconductor substrates are investigated. In both cases a plasma is sustained in a resonant cavity applicator called a microwave plasma disk reactor (MPDR). The system operates at 2.45 GHz frequency under the condition of electron cyclotron resonance.

The first process is the low temperature (less than $265^\circ C$) anodic growth of silicon dioxide using an oxygen plasma. Three inch diameter silicon wafers are placed downstream at various distances from the oxygen plasma and biased positively. Vacuum chamber pressure is held constant at 3 mTorr. Applied dc biases range between 30 and 50 volts. Uniform growth ($\pm$ 2% standard deviation) over the wafer is achieved at 8 cm downstream with 465 Å of oxide grown in two hours of anodization. Oxide quality was investigated for several reactor configurations.

Electrical characterization of the plasma grown oxides by high-frequency capacitance-voltage measurements reveal a fixed oxide charge density of 1.137×10^{12} cm^{-2} and a minimum mid-gap interface trap density of 8×10^{11} $cm^{-2}eV^{-1}$ for oxides annealed at $450^\circ C$ for one hour

in an ambient of 95% N_2 and 5% H_2. The average oxide dielectric strength for the best annealed oxide is found to be 7.8 MV/cm.

The second process is the sputter removal of silicon dioxide layers from three inch silicon wafers using argon ions from an argon plasma which was also sustained with microwave energy in the electron-cyclotron resonant mode. The ions are accelerated to the wafer surface by use of an rf bias applied to the wafers upon which a thermal oxide has been grown. Ellipsometric measurements before and after sputtering yield an average sputtering rate of 23 Å/min over 11 experimental runs performed at -50 V induced substrate bias. Both the measured sputter rate and sputtering uniformity agree well with predictions based on Langmuir probe measurements and diffusion theory. Adding additional plasma confinement magnets improved the uniformity such that the standard deviation was $\pm$ 6% for conditions studied.

ad majorem Dei gloriam

ACKNOWLEDGEMENTS

This journey to obtain knowledge and understanding, was guided and influenced by numerous people. First and foremost, the Author wishes to express heartfelt gratitude to Dr. Donnie K. Reinhard for his guidance, encouragement and support throughout this work. Special thanks is extended to Dr. Jes Asmussen Jr. for suggestions and comments during this research. Additionally, thanks is given to Dr. Timothy A. Grotjohn and Dr. Mohammed Aslam for numerous consultations and to Dr. Thomas J. Pinnavaia for comments on this manuscript. Also, appreciation for observations, comments, and friendship is expressed to Dr. Jeffrey A. Hopwood.

In addition, the Author is deeply thankful for the love and support of my parents, Joseph and Judith Salbert without whom this work could not have taken place.

TABLE OF CONTENTS

CHAPTER ONE
Introduction

CHAPTER TWO
Background and Review

CHAPTER THREE
Microwave ECR Plasma System Description

CHAPTER FOUR
Procedures for the Plasma Anodization of Silicon

CHAPTER FIVE
Evaluation of ECR Plasma Anodization Oxides

CHAPTER SIX
ECR Argon Plasma Sputter Removal of Oxides

Chapter Seven
Summary and Conclusions

LIST OF TABLES

LIST OF FIGURES

CHAPTER ONE

Introduction

Hello

1.1 MOTIVATION FOR PLASMA PROCESSING

1.1.1 Oxygen Plasma Anodization

Integrated circuits (ICs) fulfill many roles in everyday appliances, tools, and control systems. These roles are expanding, while at the same time the space allotted to the control circuits is becoming smaller. Also there is a drive to reduce device size in an IC so that more functions can be performed on the same chip. Hence the miniaturization of IC devices is becoming more and more desirable.

IC device manufacture on single-crystalline, silicon wafers involves many steps, one of which is the growth or deposition of silicon dioxide, SiO_2. This material performs many important roles in an integrated circuit such as: device isolation, gate dielectrics for metal-oxide-semiconductor, field-effect-transistors (MOSFETs), masking for dopant implantation or diffusion, inter-layer insulation, and passivation of the surface of the IC. One of the more reliable methods of obtaining SiO_2 layers is by growing them at high temperature,

1

between 800 and 1200 $^{\circ}$C, in a furnace with an oxygen or steam atmosphere. This method has been used extensively in IC fabrication, but with decreasing device size, advanced device structures, and increasing wafer sizes, a low temperature alternative has become desirable. A low temperature method has several advantages, including: (1) fewer thermally activated stacking faults and dislocations are generated in the silicon substrate; (2) there is less redistribution of previously established doping profiles which relaxes lower limits on integrated circuit critical dimensions; (3) excessive penetration of metal alloys is avoided; and (4) less wafer warpage will occur, which is important since larger and larger wafers, up to 8 inches in diameter, are being used in IC manufacturing.

Two low temperature methods for obtaining oxide layers on silicon which have been extensively studied are chemical vapor deposition, CVD, and anodization. In CVD, silane and oxygen, for example, are reacted over silicon wafers to deposit silicon dioxide,

$$SiH_4 + O_2 \rightarrow SiO_2 + 2H_2$$
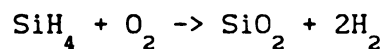
which can be carried out at temperatures below 500 $^{\circ}$C. In plasma anodization, silicon wafers are placed in a medium which contains negative oxygen ions and electrons as well as other species, and then biased positively to draw the negatively charged species to the wafer surface to grow silicon dioxide.

This second method of low temperature production of silicon dioxide is the major focus of the research presented in this dissertation, namely the use of an oxygen plasma to provide negative oxygen ions for the anodic growth of silicon dioxide on silicon.

1.1.2 Argon Plasma Soft Sputter

Another major concern as integrated circuit devices become smaller is the contact resistance between devices and conduction paths or between multi-layer conduction paths. The size of the contacts must also decrease as the devices themselves shrink in size. Therefore it becomes imperative that the resistance of these contacts not be increased by extraneous layers of oxide or other contamination. Of increasing interest and value is the development of an *in situ* method of cleaning these contacts in the same machine or vacuum system which the subsequent conduction material or epitaxial material is to be deposited or grown on the wafer being processed.

Because many of these deposition and growth processes are performed under vacuum, one possible way to clean these contacts is to physically sputter off undesirable material by bombarding the surface with ions provided by a low pressure plasma. The ions impinging on the wafer surface need sufficient energy to do only a limited amount of sputtering and it is essential that the energy of these ions be low enough so as not to damage the underlying material that is being cleaned (such as causing crystal dislocations).

One approach to doing this soft sputter clean is to use a low pressure, argon plasma and accelerate the argon ions to the surface of the silicon wafer being processed. This can be done in the same vacuum chamber which the deposition or growth takes place. This dissertation presents an investigation of such a soft sputter cleaning process.

1.2 RESEARCH GOALS

1.2.1 Anodization of Silicon with an Oxygen Plasma

The primary objective of this research is to investigate conditions for growing uniform oxides on silicon wafers at low temperatures with a downstream electron-cyclotron resonant Microwave Plasma Disk Reactor (ECR MPDR) system (the MPDR is described in detail in Chapter 3). Several experimental conditions which can be varied that effect the growth and uniformity of the silicon dioxide layers are:

1.   distance from the plasma discharge

2.   wafer bias

3.   microwave input power

4.   vacuum chamber pressure

Of these four experimental parameters, the first two were investigated. The microwave power and chamber pressure were kept at constant values of 265 Watts of 2.45 GHz power and 3 mTorr belljar pressure.

At this time, microwave plasma anodization has been reported with up to 2 inch diameter wafers and inductively coupled rf systems with up to 4 inch diameter wafers. A goal of this research is to achieve microwave plasma anodization over 3 inch wafers with an apparatus design that is readily scalable to 6 to 10 inch wafers. An additional goal is to investigate oxide quality and to correlate this quality with reactor configurations and process conditions.

1.2.2 Removal of SiO$_2$ Layers with an Argon Plasma

The second goal of this research is to investigate conditions for the uniform removal of silicon dioxide layers from 3 inch diameter silicon wafers by sputtering the surface with argon ions from an argon plasma sustained in the MPDR operating in the ECR mode. The argon ions are accelerated to the surface of the silicon wafers by a negative potential induced by the use of an rf bias. The same experimental conditions as mentioned above are again valid here. Also as above, the apparatus is scalable to 6 to 10 inch diameter wafers. In addition, correlation between the sputtering results, plasma characteristics and theoretical models of the plasma are studied.

1.3 DISSERTATION OUTLINE

This dissertation has two distinct topics involving silicon dioxide and plasma processing. The first is the anodic growth of silicon dioxide on silicon wafers biased positively with a dc potential using an oxygen plasma sustained with microwave power in the MPDR. The second is the sputter removal of silicon dioxide layers from silicon wafers biased with an rf (13.56 MHz) signal which induces a negative dc potential on the wafer using an argon plasma also sustained with the MPDR.

The first two sections of Chapter Two provide a more detailed description of the role of silicon dioxide in semiconductor technology and methods of the growth and deposition of silicon dioxide. This is

followed by a literature review of plasma anodization and argon plasma sputtering for cleaning the surface of wafers. Chapter Two ends with a review of ECR Plasma processing.

Chapter Three describes the MPDR, the vacuum system, the various biasing and associated measuring circuits, and the data collection systems that were used during plasma processing. In addition to this hardware description, the theory and typical operation of a plasma diagnostic tool, the double Langmuir probe, which was used to characterize both the oxygen and argon plasmas, is presented.

The experimental configurations and procedures used in the oxygen plasma anodization of silicon is detailed in Chapter Four. Also included in this chapter is an account of the sample preparation, the temperature measurement of the substrate during anodization and characterization of the oxygen plasma with the double Langmuir probe.

Chapter Five details the substantial work done in characterizing the plasma grown oxides in regards to the thickness, uniformity of the thickness, chemical constituency, and electrical properties.

The sputtering work using an argon plasma is described in Chapter Six. The experimental configurations, method, argon plasma characterization, sample preparation, experimental results and a discussion of these results is detailed. The experimental rate of sputtering and uniformity of sputtering are compared to predicted values based on diffusion theory and plasma characterization.

Chapter Seven is a summary of the major results achieved in this research as described in Chapters 3 through 6 and the conclusions that were reached. Recommendations for future research in each of these areas of oxygen plasma anodization and argon plasma sputtering is also included.

Chapter Two

Background and Review

To go forward, we must know where we've been

2.1 INTRODUCTION

In this chapter, a review and description of the role of silicon dioxide in semiconductor technology is presented. A description of its uses as a dielectric, insulator, mask and passivator is given in section 2.2. In section 2.3, a review of the several techniques that are currently used to grow, deposit and remove silicon dioxide is discussed with emphasis on methods currently used or proposed for use in integrated circuit fabrication. The anodization of silicon utilizing an oxygen plasma as an alternative method of silicon dioxide growth is reviewed in section 2.4. Oxides of silicon must also be removed and in section 2.5, a review of previous research on the soft sputter removal of silicon dioxide using an argon plasma is presented.

2.2 THE ROLE OF SILICON DIOXIDE IN SEMICONDUCTOR TECHNOLOGY

Current integrated circuit fabrication requires an economical, reliable, and repeatable method of growing or depositing high quality

dielectrics on silicon wafers. The most often used dielectric is the oxide of silicon, silicon dioxide, SiO_2. This important material performs many different and vital roles in the semiconductor industry as described in the following paragraphs. Indeed the attractive properties of SiO_2 and the SiO_2/Si interface are a major reason that silicon remains the principal semiconductor for integrated circuits as compared, for example, to GaAs which does not have a high quality native oxide.

When fabricating integrated circuits, impurities are often desired in only selected areas of a silicon substrate, commonly referred to as a silicon wafer. One role that silicon dioxide plays is as a mask for dopant implantation or diffusion. A layer of silicon dioxide is first grown or deposited over the entire wafer, then predetermined silicon regions where the dopants are desired are exposed by etching through this oxide layer, and dopants are introduced over the entire wafer. The silicon dioxide acts as an effective barrier to the dopants in the areas where it covers the silicon substrate.

SiO_2 is also used as a means of achieving electrical isolation between circuit elements. In today's very large scale integrated (VLSI) and ultra large scale integrated (ULSI) circuits, devices and multiple layer metallizations must be separated by a highly resistive and stable insulator. Because of its high resistivity, typically 10^{14} - 10^{16} Ω-cm, and long term stability, silicon dioxide fulfills this requirement for isolating devices and metal layers very well.

Another use of silicon dioxide is as a surface covering for protection from the environment. After fabrication of an integrated circuit is completed, silicon dioxide is often times deposited over the

entire circuit. This covering protects and passivates the surface, preventing contaminants, such as water vapor and mobile metallic ions, from being incorporated in the circuit in subsequent handling or processing steps.

Finally, of special importance is the role silicon dioxide plays as a gate dielectric in field effect transistors. State of the art field effect transistors, FETs, require a thin, 100 to 500 Angstrom, (Å), high quality oxide layer for proper performance. For example, representative gate oxide thicknesses for random access memory chips are 170 Å for a 1 megabit chip [1] and 100 Å for a 16 megabit chip [2]. Gate oxides must have a sufficiently low density of states at the semiconductor- dielectric interface and high breakdown strength. In addition to its high resistivity and long term stability, silicon dioxide also has a high dielectric strength and makes a good interface with a crystalline silicon substrate. Thus, silicon dioxide fulfills the requirements of a gate dielectric very well.

2.3 CONVENTIONAL METHODS OF OXIDE GROWTH, DEPOSITION, AND REMOVAL

For over three decades, the most common method of obtaining high quality silicon dioxide layers has been by growing them at high temperature, between 800 and 1200 $^{\circ}\text{C}$, in a furnace with an oxygen or steam atmosphere. Silicon wafers are placed in a "boat" usually made of quartz (fused silica), then this vessel is pushed into a quartz tube that passes concentrically through the furnace. Steam ("wet" oxidation) or oxygen ("dry" oxidation) is then flowed through this tube. This method has been studied and refined extensively [3-6]. The

reactions are straightforward as:

$$Si + O_2 \longrightarrow SiO_2$$
$$Si + 2H_2O \longrightarrow SiO_2 + 2H_2 \, .$$
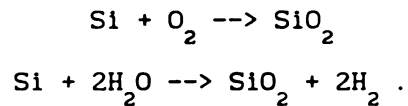
The newest oxide is formed at the interface of the silicon substrate and the oxide layer. The high temperature of the furnace provides the energy for the reaction and for the diffusion of oxidants through the growing oxide layer to the interface.

This high temperature processing can affect the silicon wafer in adverse ways. Integrated circuits are fabricated on single crystalline silicon, but if exposed to high temperatures, the crystalline lattice can be disrupted by stacking faults and dislocations which are heat activated. Larger wafers can be warped by high temperatures and with industrial fabrication moving toward eight inch and larger diameter wafers, this possibility of damage is increased. Also, exposure of the wafer to high temperature processing causes impurities to diffuse through the silicon crystal. Impurity profiles of VLSI and ULSI circuits are shallower than their predecessors and must be tightly controlled. Thus the length of time that a wafer can undergo processing at elevated temperatures must be limited. Hence the need for a low temperature method of obtaining high quality oxides on silicon has become very attractive, and desirable, if not critical.

A low temperature method currently used for depositing oxide layers on silicon is chemical vapor deposition, CVD, which has several variations: Plasma Enhanced CVD, (PECVD); Low Pressure CVD, (LPCVD); Remote Plasma Enhanced CVD, (RPECVD); and photo-enhanced low-pressure

CVD, [7-11]. In these processes, silane and oxygen, for example, are reacted over silicon wafers to deposit silicon dioxide,

$$SiH_4 + O_2 \longrightarrow SiO_2 + 2H_2$$
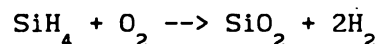
which can be carried out at temperatures below 500 $^\circ$C. These processes have received much study and application since silicon dioxide must be deposited, rather than grown, on the surface of a partially completed circuit that must be passivated or requires insulation between multiple interconnection layers. Also, CVD SiO_2 is being studied as a dielectric for III-V compounds which do not readily grow a native oxide possessing the same desirable characteristics [11,12]. Generally, however, the SiO_2/Si interfacial quality is better with thermally grown oxides than with deposited oxide layers, hence deposited oxides are not usually used as gate dielectrics in standard silicon integrated circuit processing.

Once silicon dioxide layers are in place, techniques must also exist for removing them in a controllable, uniform and selective manner. This is easily achieved in a "wet etch". Most commonly, buffered oxide etches, consisting of a variable ratio of NH_4F and HF is used. The chemical reaction is

$$SiO_2 + 4HF \longrightarrow SiF_4 + 2H_2O \ .$$
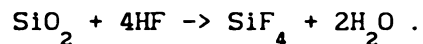
The salt, ammonium fluoride, is added as a buffer so that the pH of the solution remains fairly constant as the HF is consumed. Also any mixture of $HF:H_2O$ will remove SiO_2, but not as controllably or selectively.

Removal of SiO_2 can also be achieved in a "dry etch". This is done under vacuum with a plasma generally containing fluorine radicals

obtained for example from CF_4. This gas, when excited or dissociated, will again provide the necessary F ions or radicals to remove the silicon dioxide by forming SiF_4 and O_2. Dry etching is becoming more and more desirable due to the fact that it can be very anisotropic (proceeds in one direction preferentially over another), whereas wet etching is isotropic (proceeds at a rate in all directions equally). Thus when etching, there will be little undercutting of the mask containing the pattern to be etched into the oxide layer. This attribute of anisotropic etches allows for the increased packing density required in todays VLSI and ULSI circuits. Also, dry processes offer generally higher purity than wet processes.

The ability to remove very thin layers of oxide and impurities is also gaining importance in integrated circuit fabrication. Interfaces between the silicon substrate and a conductor or epitaxial silicon layer, must be very clean. If any residual oxide exists between these two materials, the contact resistance may be high or the interface disrupted, adversely affecting circuit performance. To this end, a method called a soft sputter clean is sometimes implemented just prior to the deposition of the desired material. This is performed in the same vacuum system that the deposition takes place, ensuring cleanliness. The sputter clean uses heavy ions, commonly Ar^+, to bombard the surface of the silicon wafer. The kinetic energy of these particles must be high enough to physically remove the undesired layers, sputtering SiO_2 particles or contaminants from the surface, but not so high as to cause appreciable substrate damage. Ion energies are typically less than 100 eV.

2.4 PLASMA ANODIZATION GROWTH OF SILICON DIOXIDE

In the previous section it was noted that thermally grown oxides, in which the oxidant reacts directly with the silicon substrate, provided a higher quality SiO_2/Si interface than do CVD oxides in which the oxide forms as a gas-phase precipitate which settles on the wafer. However it is desirable to avoid high temperature processing conditions. Consequently there is interest in investigating low temperature means for growing oxides on semiconductors, with the intended goal of achieving a high quality interface at low temperatures.

Toward this purpose, a low temperature process which has received much attention and study and is the main topic of this dissertation is the anodization of silicon. In anodization, silicon wafers are placed in a medium which contains negative oxygen ions and then biased positively to draw these ions to the wafer surface to grow silicon dioxide.

For silicon anodization, several mediums which contain negative oxygen ions have been studied. The gaseous plasma is one medium which has been investigated extensively. As early as 1964, Ligenza [13] reported the use of a microwave generated plasma to grow silicon dioxide over small areas, 1.27 cm in diameter. A wave guide was used to apply microwave power to a quartz vacuum vessel containing oxygen pressures from 0.1 to 2 Torr. Oxide thicknesses as high as 6000 Å were achieved in one hour using 300 Watts of 2.45 GHz input power. The oxides grown had an index of refraction of 1.47 as measured with an

ellipsometer and a dielectric breakdown strength of 10 MV/cm. These results compare well with thermally grown oxides which have an index of refraction of 1.46 and maximum breakdown strengths of 10 to 13 MV/cm. However, the apparatus was not practical for production, since it involved glass to silicon seals for the sample and was limited to small oxidation areas. Since Ligenza's pioneering work, research has been aimed at achieving uniform growth rates over large areas with high wafer throughput, while maintaining oxide quality.

Results similar to Ligenza's were presented in 1967 by Kraitchman [14]. As with Ligenza's work, a growth rate of 6000 Å in one hour was achieved using a microwave generated oxygen plasma, but again with a small area of about 36 square mm. Attempts at larger area anodization by Kraitchman resulted in non-uniform films. Again, the small area oxides showed useful properties. Temperature-bias stressing of the oxide films using an MOS capacitor structure revealed no mobile ion contamination, indicating a clean process. Etch rates of the plasma grown oxides in a P-etch (15 parts of 49% HF, 10 parts of 70% HNO_3, and 300 parts of H_2O) were 2 Å/sec, the same as for thermally grown oxides.

Ligenza also reported anodic growth of oxides on silicon in an oxygen plasma sustained by a dc arc. These films however had a relatively high density of interface states [15]. A comprehensive review of plasma anodization of metals and semiconductors prior to 1970 is presented in a paper by O'Hanlon [16].

Pulfrey, et al. [17,18] in 1973 and 1974, reported growth in an rf discharge maintained by 1 MHz, 3 kW RF power. The oxygen plasma was created in a 5 cm diameter, 1 m long quartz tube by inductively coupling the rf power by use of a two-turn coil. Bias was supplied to

keep a constant anodizing current of between 0.5-4.0 mA over a 1.5 cm diameter silicon substrate. The temperature of the substrate was estimated to be 240 $^\circ$C during anodization. For these samples, however, MOS measurements indicated a large fixed charge in the oxide based on the large shifts observed in the flatband voltage, V_{FB}.

In 1980, Ho and Sugano [19,20] showed that with anodic oxidation of silicon the problem with the growth of the "bird's beak" structure when selectively growing oxide layers is suppressed. In this work, approximately 1 kW of 420 kHz RF power was used to generate the oxygen discharge. The rf power was inductively coupled to the plasma and 1 inch diameter wafers were oxidized. The temperature of the wafer could be varied by changing the distance of the wafer from the coil, from 1000 $^\circ$C at the center of the coil to less than 100 $^\circ$C with the wafer 20 cm from the coil. A constant 40 VDC bias was used to grow the oxides which exhibited breakdown strengths reaching 7 MV/cm and etch rates in a P-etch of 2 $\mathring{A}$/sec.

Ho and Sugano [19] also reported the effects of a low temperature annealing process by which the density of interface states could be reduced. Using a forming gas consisting of 5% hydrogen and 95% nitrogen, the plasma grown oxides were annealed for 60 minutes at 450 $^\circ$C. The density of interface states, D_{it}, was reduced from 10^{12} states/cm^2/eV to about 10^{10} states/cm^2/eV. However, subsequent high temperature processing steps increased D_{it}. This was thought to be due to the out diffusion of the hydrogen. Consequently, an annealing step at 1000 $^\circ$C for 20 minutes in which argon was bubbled through CCl_4 was investigated [20]. The hypothesis was that the halogen would not out diffuse as the hydrogen did. *C-V* measurements on capacitors fabricated

with anodic oxides annealed in such a fashion showed ideal characteristics. MOSFET's formed on the same oxide showed better characteristics than MOSFET's fabricated with thermally grown oxides without an anneal.

Haneji, et al. [21], in 1985 reported an extension of the work of Ho and Sugano, [19,20]. In Haneji's investigation, a few percent of chlorine was added to the oxygen plasma while anodically growing silicon dioxide. This was an attempt to improve the interface trap density and the growth rate. The setup was the same as that of Ho et al. [19]. Chlorine percentages of 0.0, 0.75, 1.5, and 3.0 were studied. With a 3 percent chlorine, 97 percent oxygen plasma, the growth rate of the oxide was almost doubled. With a 1.5 percent chlorine, 98.5 percent oxygen plasma, the density of interface traps was reduced at midgap to 8×10^8 /cm^2/eV.

In 1982, Moruzzi et al. [22] at the University of Liverpool, confirmed by mass spectrometry that the primary negative ion in a Ligenza-type microwave generated oxygen plasma was the O^- ion. A system very similar to that of Ligenza with a 100 micron hole in the anode was used to allow a sample of the charged particles incident on the anode to pass through it into a second vacuum chamber containing the mass spectrometer. Results showed that the negative ions passing through the anode hole were O_1^-. This test method was applied to plasmas maintained by a glow discharge and it was found, in contrast to the microwave generated plasma, that almost equal amounts of O_1^-, O_2^-, and O_3^- were extracted from the glow discharge. The investigation also reported a pressure dependence of the O^- species concentration and hence the oxide growth rate. The greatest concentration and growth

rate occurred around 0.1 Torr.

The study of anodic growth of silicon dioxide at the University of Liverpool was continued and expanded by Kiermasz et al. [23]. In 1983, the use of a resonant microwave cavity to sustain an oxygen plasma at 0.1 Torr was reported. Oxides were grown on silicon using a 50 VDC bias and heating the substrate to 550 °C. Oxides of 800 Å thickness were achieved in 8 minutes while thickness of 4000 Å (the maximum thickness attempted) were grown in 330 minutes.

Subsequent reports from the University of Liverpool [24-29], have traced further developments in their anodization work. Both rf and microwave generated oxygen discharges have been studied for use in the anodic growth of oxides on silicon. In an rf inductive discharge, uniform oxides were achieved over 4 inch wafers, while in the microwave discharge 1 inch diameter wafers were uniformly covered. In the microwave system, 200 W of 2.45 GHz power was applied to a resonant cavity while in the rf system, 1 KW of 27 MHz power was inductively coupled to the discharge via coils surrounding the chamber. Substrate temperatures were varied, using a heater, up to 580 °C. At this temperature film thicknesses of 3000 Å were achieved in one hour. By a combination of Cl_2 partial pressure in the oxygen discharge, post oxidation anneal, and post metal anneal, high quality films were achieved. The films were reported to have a density of interface states as low as 5×10^{10} states/cm^2/eV, an average breakdown field of 10 MV/cm, a mobile charge density in the oxide of 2×10^{10}/cm^2, and a fixed charge density of 6×10^{10}/cm^2.

In 1986, Roppel [30-32] reported the use of a cylindrical resonant cavity named the Microwave Plasma Disk Reactor (MPDR)

operating with 2.45 GHz microwave power, to anodically grown silicon dioxide films on small substrates, 3.2 cm^2. Substrates were placed in direct contact with the plasma which was contained in a quartz cylinder 10 cm in diameter and 1.5 cm in height at the bottom of the cavity. Using the anneal suggested by Ho et al. [18], the post anneal density of interface states were found to be $D_{it} \cong 2 \times 10^{10}$ states/cm^2/eV and the fixed oxide charge, Q_f, was found to be 1×10^{11} /cm^2. Electrical breakdown fields were reported to average 6.3 MV/cm.

Nelson and Buhrman [33,34] in 1987 reported the growth of silicon dioxide in a plasma produced by 13.56 MHz rf power. The rf power was applied between two water-cooled electrodes covered with quartz to prevent sputtering contamination. Typical rf power densities used were 2.5 W/cm^2 and wafer temperatures 475 - 500 $^{\circ}$C. Three different plasmas were investigated: pure argon plasma, pure oxygen plasma and a mixture of argon and oxygen plasma. The pure argon plasma was used for sputter deposition of silicon dioxide, the pure oxygen plasma was used for anodic growth of silicon dioxide, and the combination plasma was used for a mixed sputter deposition/anodic growth process. The best oxides obtained by this method were half deposited/half grown. As grown oxides were characterized by C-V measurements and had a midgap density of interface states of $D_{it} \leq 2 \times 10^{11}$ states/cm^2/eV and an oxide fixed charge of $Q_{ox} \leq 1 \times 10^{11}$. Electric field breakdowns were also measured and reported as $E_B \geq 13$ MV/cm. Rapid thermal anneals, 15 to 30 secs at 800 - 850 $^{\circ}$C, reduced D_{it} to 7×10^{10} and Q_{ox} to less than 5×10^{10}. E_B was only slightly improved.

Most anodic plasma systems grow oxides on only one silicon wafer at a time. In 1984, Wong and Oldham [35] reported an investigation of

the possibility of a high throughput, and clean multiwafer system for anodic growth of silicon oxide and silicon nitride layers using an rf driven plasma. Wafers alternatingly contacted one of two graphite rods to which rf power of 13.56 MHz was applied. Oxide thicknesses of 250 Å were grown in 2 hours by anodization in a 2 torr O_2 plasma. Oxides exhibited an index of refraction of 1.45 as measured by ellipsometry.

Experiments aimed at elucidating the plasma oxidation mechanisms have produced mixed results. Perriere et al. investigated the plasma anodization oxidation mechanisms in an rf inductive system by using ^{18}O tracing techniques [36,37]. Thin ^{18}O enriched ZrO_2 overlay films were used as a source of oxygen tracer during subsequent silicon anodization in an ^{16}O plasma. Subsequently, nuclear micro analysis was performed on the films with a 2MeV Van de Graff accelerator. Their results indicated that oxygen order was preserved in the film and consequently that anodic plasma oxidation involves only short range oxygen or silicon ion transport through the oxide layer.

However, tracer experiments with ^{18}O by Ho and Sugano [19], also with an rf inductively coupled plasma, produced different results. In this case, ^{18}O was found throughout the film which indicates the possibility of long range ionic migration.

More recently, Vinckier and De Jaeger [38] have reported calculations correlating yields of oxidation due to atomic oxygen or negative oxygen ions with growth rates presented in the literature. Their calculations show that the yield of silicon dioxide due to negative oxygen ions, ϕ_{o^-,SiO_2}, is at least a thousand times more than the yield of silicon dioxide due to atomic oxygen, ϕ_{o,SiO_2}. This is

consistent with the experimental work of Moruzzi, et al. [22] which indicated that the responsible particle for oxidation by anodization is the O^- ion.

In any case, anodic plasma oxidation is believed to be a result of the migration of oxygen and possibly silicon ions (and/or their vacancies) which results from the electric field across the oxide. Thermally induced ion transport is negligible.

Kiermasz, et al. [23], Roppel [30,31] and Taylor, et al. [28] have found that microwave plasma anodic oxide growth rates are consistent with separately developed high field discrete hopping models. In these models, a high field in the growing oxide layer promotes the drift of negative oxygen ions to the silicon-silicon dioxide interface. All three models were used to accurately fit data from experimentally grown oxide layers, further supporting the negative oxygen ion migration hypothesis.

Three investigations, Ray and Reisman [39,40,41], Kimura, et al. [42-46], and Bardos, et al. [47,48,49], while not anodic methods since no d.c. bias was applied to the silicon wafers are briefly noted due to the use of an oxygen plasma as a low temperature alternative for growing oxide layers. The former used rf discharges while the later used a microwave discharge. Both Ray and Reisman and Kimura, et al. obtained thin, high quality films on 57 mm and 40 mm diameter wafers respectively, however the oxidation times were rather long. Up to four hours were required to produce 400 Å of oxide.

Bardos, et al. reported much higher rates (over 1000 Å per hour) on electrically floating silicon wafers with microwave powers of 1.5 to 2 kW. Their apparatus also had a longitudinal magnetic field applied

to the plasma.   Uniformity of ±10% was obtained on 40 mm diameter
wafers, but fast electrons in the discharge were found to degrade the
films.

Additional background is found in a review article by Gourrier and
Bacal [50] and in an extensive review of plasma oxidation of III-V
compounds as well as silicon in a 1985 book by Sugano [51].

2.5   SPUTTER-CLEAN REMOVAL OF THIN OXIDE LAYERS

Because silicon forms a thin oxide, 4-10 Å thick within minutes on
exposure to air, an *in situ* method to remove this small layer and other
contaminants just before the addition or growth of other layers, such
as metallizations, epitaxial silicon, silicon dioxide and other
interconnection materials, is desirable and has been studied for the
last two decades.   One way of performing this cleaning procedure is to
do a "soft sputter etch" of the surface.   Using an argon plasma and
accelerating the Ar^+ ions to the surface with only a small kinetic
energy sputter cleans the surface without damage to the silicon
substrate.   This procedure can be done just prior to deposition or
growth of desired layers in the same vacuum chamber.   The need for
transferring the silicon wafer from one processing station to another
is thus eliminated and prevents exposure of the silicon substrate to
atmosphere.

An early use of a sputter clean is reported by McCaughan and
Heilig [52].   Just prior to anodic growth of silicon dioxide in an
oxygen plasma sustained by a dc arc, the silicon surface was rf
sputter-cleaned.   Dielectric strengths of the resulting films were

greatly improved, from 4-5 MV/cm without sputter cleaning, to 7-8 MV/cm with sputter cleaning.   No details were given on the method of sputtering.

Broadbent [53], reports the use of an argon beam sputter clean just prior to the evaporation of a metal onto silicon wafers for metal-metal contact resistance improvement.   An ion source provided Ar^+ ions which were accelerated via two graphite grids to 500-1500 eV. Contact resistances between two metals were decreased significantly with the sputter clean as compared with a chemical dip-rinse-dry procedure.

Donahue, et al. [54] at MIT investigated the use of an *in situ* argon ion sputter clean of silicon substrates just prior to the deposition of epitaxial layers of silicon for the fabrication of transistors.   In subsequent work by Burger and Reif [55,56], Comfort et al. [57], and others at MIT [58-62], the process was optimized to produce a very clean surface evidenced by the fact that the transistors fabricated had "characteristics *at least* as good as those fabricated in bulk silicon" [55].   The final optimized process consisted of an argon plasma sustained by 2.5 W of RF 13.56 MHz power, a separate DC supply for the application of -100 V DC bias, constant argon pressure of 4.2 mTorr, 2 to 27 minute sputter time and a substrate temperature of 750 - 800 $^\circ$C.

Faith, et al. [63] reported an investigation comparing the contact resistance of junctions that were cleaned by a dilute HF dip, CF_4 plasma etch and an argon plasma sputtering.   The CF_4 plasma etch and the argon plasma sputter cleaning both had pre-alloy contact resistances lower than the contacts cleaned with the dilute HF dip.   In

this case, the sputter cleaning with the argon plasma was not really "soft", having used 1000W of RF power applied between the substrate holder and the grounded vacuum chamber. After a thermal anneal step to alloy the contact, resistances were found to increase, sometimes by a factor of 3, for the argon sputter cleaning, most likely due to damage of the silicon substrate from the high energy bombardment.

Ohmi, et al. [64,65] investigated an even lower temperature and lower kinetic energy particle process. They argued that the process of Burger, et al. [55,56], would introduce significant substrate damage, thus the 750 - 800 °C wafer temperature was needed in fact to anneal the silicon crystal. Subsequently, they studied a process which utilized 100 MHz RF excitation and separate DC biasing supplies for the substrate and target. An optimized soft sputter cleaning process was found to consist of 5 W RF power, a silicon target bias of -25 V DC and a substrate bias of +7 V DC. The energy of the ions bombarding the surface was estimated to be 32 eV, taking into account the added self bias from the rf plasma. This particle energy is below the threshold of silicon sputtering by argon of 40 eV, but above the energy required to sputter silicon dioxide. The substrate temperature was measured to be 320-350 °C.

One of the first investigations to utilize an argon plasma excited by 2.45 GHz power, microwave power, was reported by Salimian, et al. [66]. In this system, the microwave power is enhanced by a magnetic field provided by two electromagnets. Thus the plasma operates in an electron cyclotron resonant mode. This they believed would enable them to separately control plasma density and ion energy as opposed to a conventional rf plasma system in which it is difficult to achieve high

densities without high particle energies. The substrate was biased with 13.56 MHz rf power which self-induces a negative substrate bias. Etch rate vs DC bias was investigated in the range of -25 to -350 VDC. Etch rates varied linearly from about 20 to 270 Å per minute. The substrate holder was water cooled with an estimated wafer temperature less than 200 °C in all experiments. The advantage of this system was reported to be the very low and controllable ion energies at high densities.

In a review paper, Holwill [67] points out the need for advanced techniques for cleaning contact vias before deposition of metallization layers. Holwill's report cites several sources [53,68,69] in which sputter cleaning of silicon-metal and metal-metal junctions resulted in the reduction of contact resistances. At time of publication, Holwill was also investigating AlSi-Si and inter-metal contact resistance reduction using an argon sputtering technique.

2.6 ELECTRON-CYCLOTRON RESONANT MICROWAVE PLASMA PROCESSING

As mentioned in the preceding sections, the use of a plasma for processing silicon in the fabrication of integrated circuits has distinct advantages over alternative wet-chemical or high temperature methods of processing. Also noted was that microwave sustained plasmas have merits not shared by other means of plasma powering. Some advantages of the microwave sustained plasma and in particular the microwave plasma operating in an electron-cyclotron resonance (ECR) manner will be discussed in this section.

One of the first advantages unique to microwave plasmas is their

ability to sustain a plasma with higher electron and ion densities than lower frequency discharges. If one considers "the *(electron) plasma frequency*" [70] given by :

$$\omega_{pe} = 2\pi f_{pe} = [\ n_e e^2 / (m_e \varepsilon_O) \ ]^{1/2}$$

where n_e is the electron density, m_e is the mass of an electron, ε_O is the permitivity of free space, and e is the charge of an electron, then the conventional maximum critical density for wave propagation in the plasma [71] is governed by:

$$n_e = 1.2 \ X \ 10^{-2} \ f_{pe}^2 \quad (m^{-3}).$$

Using the FCC designated microwave heating frequency of 2.45 GHz, the calculated density is 7.2 X 10^{10} particles/cm^3. However, densities measured in an ECR cavity applicator [72] and in a waveguide applicator [73] have indicated that densities even higher than this critical density can be achieved with a microwave sustained plasma. These higher than critical densities are "due to evanescent wave penetration in the plasma" [71], that is, the electromagnetic wave does not propagate through the plasma, but the skin depth is large enough to allow sufficient microwave penetration to provide good coupling of microwave energy to the plasma.

In addition to this high density of charged particles, an ECR plasma is capable of operating at milli Torr (mTorr) and sub-mTorr pressures where there is currently significant interest in performing IC plasma processes. As the pressure is lowered, other things being equal, fewer collisions occur between the electron gas and the ion or neutral gas. Therefore Joule heating of the plasma does not occur as efficiently as at higher pressures. But if the electron-cyclotron resonance condition exists, efficient energy coupling can occur even at

lower pressures. The ECR condition is achieved when a static magnetic field of proper magnitude is impressed on the plasma perpendicular to the time varying electric field provided by the microwave power. When the magnetic field lines are perpendicular to the electric field lines, the electrons can cycle in an orbit parallel to the electric field and perpendicular to the magnetic field. This provides a more efficient coupling of the microwave power to the electron gas because the electrons can now spiral, enhancing the probability of an eventual collision. When the electron's orbital frequency equals the frequency of the exciting electric field, resonance occurs. The condition for electron-cyclotron resonance to exist is:

$$\omega_{ce} = qB/m_e$$

where ω_{ce} is the cyclotron resonant frequency of the electron, q is the charge on the electron, B is the magnetic field strength, and m_e is the mass of the electron. Operating with 2.45 GHz excitation, the magnetic field strength required for electron cyclotron resonance is 875 Gauss.

Coupling the two preceding advantages, higher plasma densities and the ability to sustain a plasma at lower pressures, indicates that plasma processing with a microwave sustained discharge operating in the electron cyclotron resonance mode can achieve higher rates of processing at lower pressures. This advantage holds attractive economic potential for a higher through-put which would reduce the cost of manufacture of an integrated circuit.

Another important advantage is that in contrast to parallel plate, RF sustained plasmas, a discharge maintained by microwave radiation has a lower and more controllable plasma potential. In rf parallel plate plasma processing, the substrate to be processed is most often placed

directly on one of the plates used as an electrode. The plasma is maintained by high electric fields between the plates and therefore the substrate is subject to bombardment by high energy ions often on the order of 200 eV. With ECR microwave plasmas, the electron gas is heated in the ECR zones and impart their energy to the ion and neutral gases. Ions produced have energies usually less than 50 eV. Substrates can be placed near the discharge and biased with a dc or rf bias separate from the fields maintaining the plasma. Therefore the possibility of damaging the substrate due to bombardment by high energy particles is reduced. This becomes more and more important in the processing of integrated circuits whose dimensions are on the order of one micron or less.

Due to its ability to exist at low pressures in a stable manner, an ECR microwave plasma holds another advantage over other plasmas. At these low pressures the diffusion lengths of charged particles is longer thus giving the possibility of having a more uniform plasma at greater distances from the discharge region.

CHAPTER THREE

Microwave ECR Plasma System Description

Such wonderful toys, where did we get such wonderful toys?

3.1 THE MICROWAVE PLASMA DISK REACTOR

The main focus of this dissertation is the use of a microwave plasma for the processing of silicon in certain steps of the manufacture of integrated circuits. The unique applicator used in this study to sustain the plasma is named the Microwave Plasma Disk Reactor (MPDR). The MPDR was developed by Asmussen, et al. at Michigan State University and has several features described as follows.

The MPDR [30-32,71,72,74-81], shown in Figure 3.1, consists of a circular cylindrical cavity (10) which can be adjusted to a single resonant mode by means of two degrees of tuning. A variable length input probe (antenna) (12) and an adjustable sliding short (11), which serves as one termination of the cavity, allow the MPDR to be matched to the input line impedance under a variety of cavity loads. Thus no external tuning is required and essentially all forward power from a microwave power generator can be coupled into the cavity.

The lower termination of the MPDR, referred to as a baseplate (14), is made up of several important individual parts. A circular
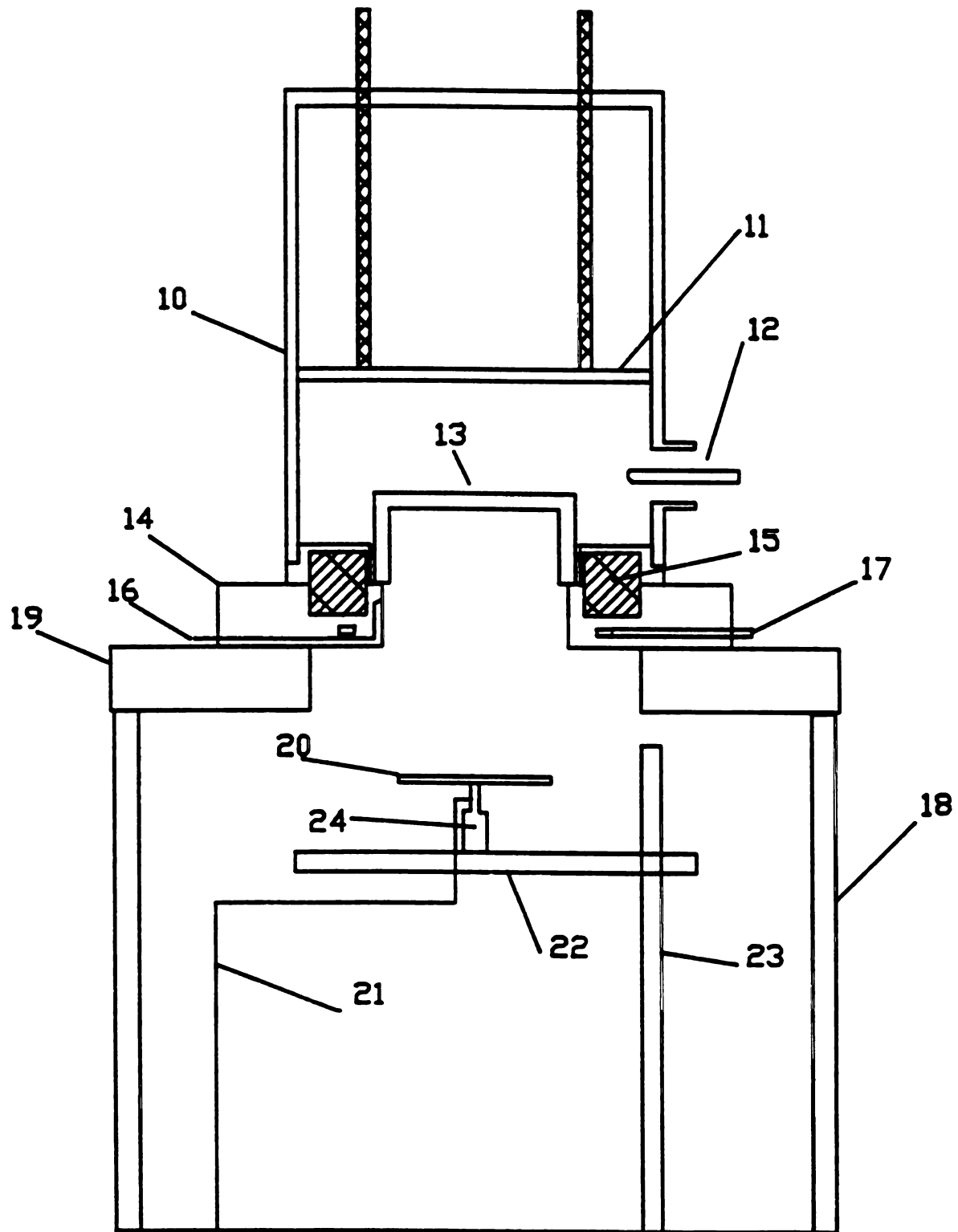
Figure 3.1 Cross Section of the Microwave Plasma Disk Reactor

quartz dish (13), which serves as the containment for the plasma, is surrounded by eight rare earth magnets (15). These magnets are imbedded in the baseplate with alternating poles facing the discharge. Process gas flows into an inlet passage (16) and out of eight holes just under the quartz dish. In a channel (17) under the magnets flows cooling water.

Figure 3.2 shows a detailed cross section of the baseplate. In this can be seen the magnets (15) the working gas inlet (16) and the water cooling input/output and channel (17). Also shown are the details of the gas channel and openings into the discharge zone.

The MPDR generates and sustains a plasma under vacuum. The quartz dish is vacuum sealed by a vacuum gasket to the baseplate which in turn is sealed to the vacuum chamber by a rubber o-ring. The vacuum chamber itself consists of a circular stainless steel plate (19) and a cylindrical pyrex chamber (18). The entire apparatus is placed on a vacuum station described in section 3.2.2.

Inside the vacuum chamber and connected to the vacuum station is the supporting structure for holding a silicon wafer that is to be processed. This consists of a stainless steel rod (23) to which is attached a support arm (22). A circular stainless steel disk (20) that is welded to a threaded bolt serves as the wafer holder. The wafer holder is insulated from the support arm by a ceramic dowel (24) which has threaded holes at both ends into which the wafer holder is bolted and a bolt can be inserted to fastened the structure to the support arm. A bias wire (21) is attached to the wafer holder and passes through a glass tube to a vacuum feedthrough.

For this work, an applicator designed to operate at 2.45 GHz was
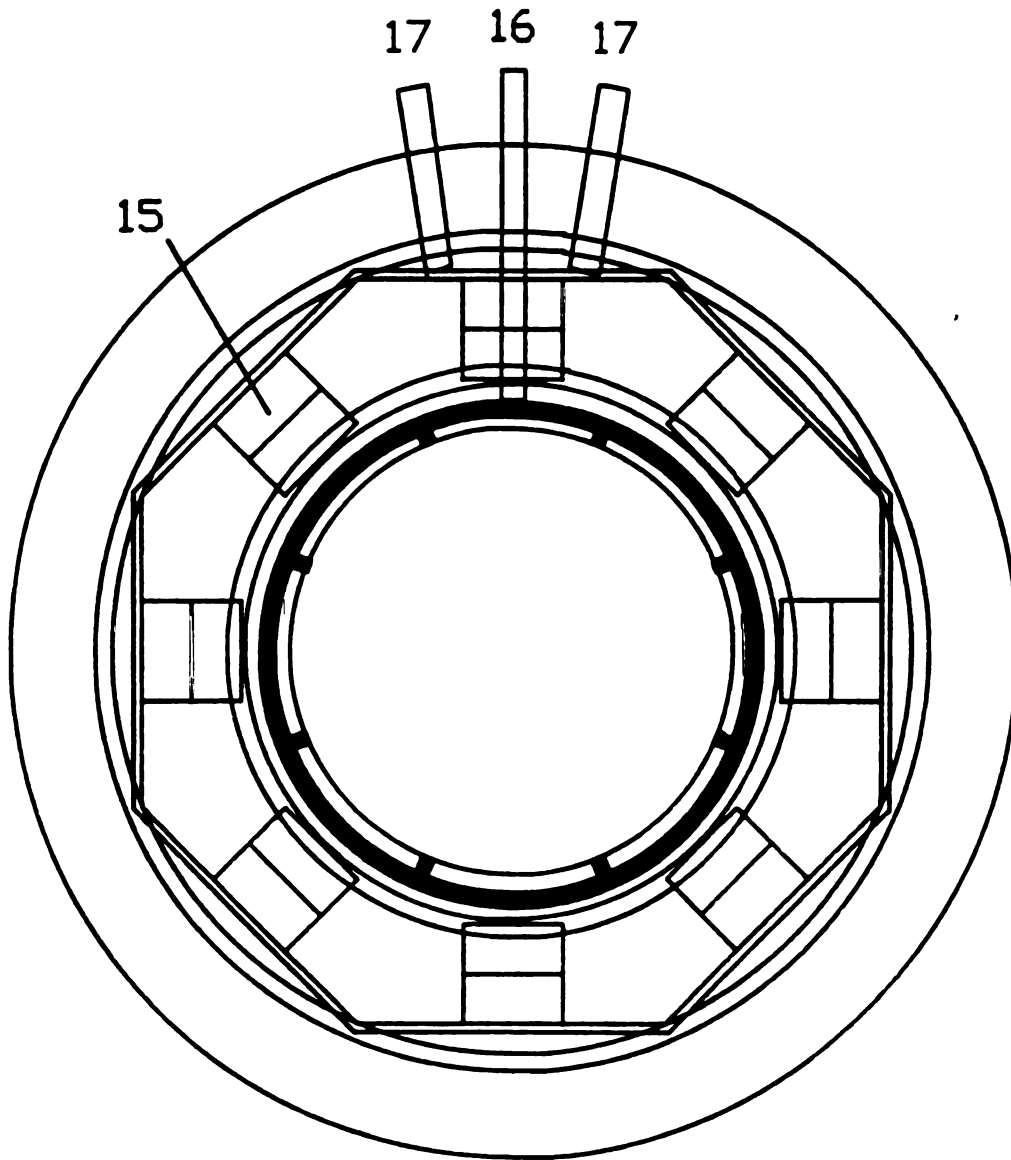
Figure 3.2   Detailed Cross Section of the MPDR Baseplate

used. The inside diameter of the brass cylinder of the MPDR is 17.8 cm. The quartz containment dish has an 8.7 cm inside diameter while the discharge zone of the baseplate has a 9 cm diameter. The MPDR is scalable with frequency which allows for the possibility of a larger diameter discharge zone. Recently, an 18 inch cavity with an 8 inch discharge excited with 915 MHz and 2.45 GHz microwave power has been studied and shows promise for processing 6 to 8 inch wafers [80].

The theory and practice of operation of the MPDR has been extensively reviewed by several authors [30-32, 73-80] and only a brief description will be given here. The rare earth magnets in the baseplate {(15) in Figure 3.2} provide the static magnetic field necessary for ECR operation. The alternating poles form eight magnetic cusps inside the discharge zone. The necessary magnetic field strength of 875 for ECR resonance gauss exists inside the discharge zone approximately 1 cm from the discharge zone wall.

All work in this study was done using the TE_{211} mode. Typically, the cavity height is 7.2 to 7.4 cm high and the input probe depth is 1.6 to 2.1 cm. The cavity is tuned to the TE_{211} mode to take advantage of the magnetic field arrangement. In this resonant mode, the time varying electric field forms four lobes of intense electric field strength in the cavity. The magnets and input probe are positioned such that these four regions are aligned with and perpendicular to four of the eight magnetic cusps provided by the rare earth magnets. Hence, in this configuration, the plasma has four large bright lobes were the strong electric field lobe is perpendicular to a magnetic cusp and four smaller lobes where a weaker part of the electric field is perpendicular to a magnetic cusp.

3.2 SYSTEM DESCRIPTION

3.2.1 Microwave Circuit

Figure 3.3 is a block diagram of the equipment used to supply and measure the amount of microwave energy incident on the MPDR (38). A MicroNow 420B1 precision microwave power generator (31) supplies the required continuous wave 2.45GHz energy. To protect the power supply from reflected power, a 300 watt coaxial 3-port circulator (32) is first attached. Any microwave power reflected from the MPDR is channeled through this circulator away from the power supply to a 500 watt, 50 ohm dummy load (33).

To measure the power incident on and reflected from the MPDR a very small portion of each of these must be sampled. Therefore, a 500 watt, 20 dB dual directional coupler (34) is connected between the circulator and the MPDR. The reflected and incident power are further reduced by 20 dB attenuators (35) before being measured by two Hewlett-Packard Model HP435a microwave power meters (36).

The microwave power system described is a coaxial one. All the connections are made via n-type coaxial connectors. A 500 watt capacity coaxial cable (37) connects the MPDR to the dual directional coupler. As with any finite impedance conductor, some of the energy carried by the cable and connectors is lost as resistive heat rather than delivered to the plasma/cavity combination. This loss was determined to be 18% of the power measured by the power meters.
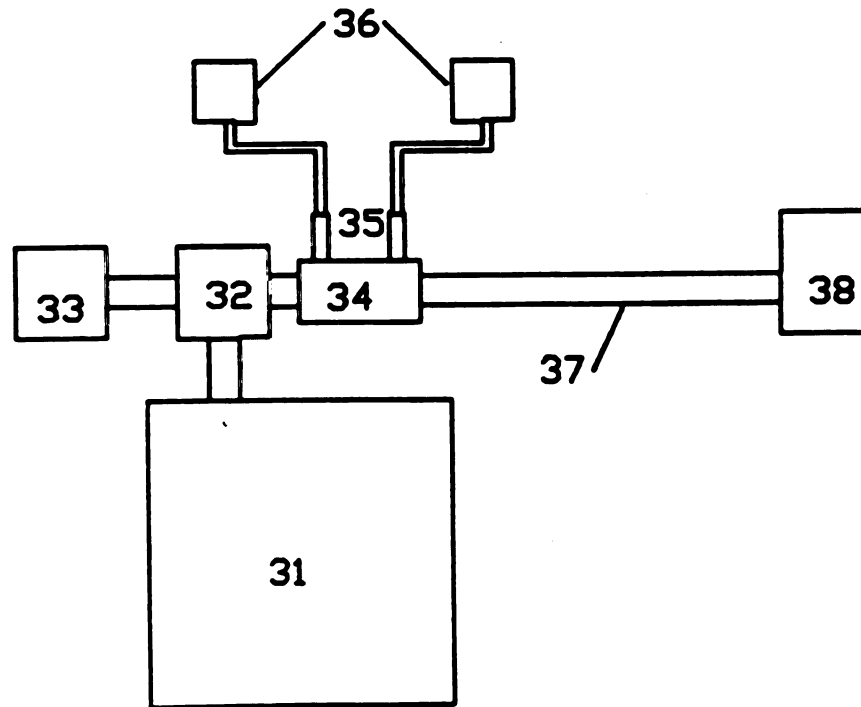
Figure 3.3   The Microwave Power Supply and Measuring Circuit

3.2.2 Gas Flow and Vacuum System

Figure 3.4 shows the working gas measurement and control system and the vacuum system used for this work. Working gases are metered into the baseplate gas inlet by use of an MKS Flow Ratio Controller Type 254 flow and pressure system. This system consists of 3 channels for gas flow; Channel A, consisting of an MKS Type 251-100 Flow Control Valve (45a) and Thermal Mass Flow Transducer (44a), has a 100 standard cubic centimeter per minute (sccm) flow capacity, and Channels B and C, each consisting of MKS Type 251-10 Flow Control Valves (45b) and Thermal Mass Flow Transducers (44b) have 10 sccm capacity. The flow controller has a control precision of 0.1 sccm on channel A and 0.01 sccm on Channels B and C.

The working gases are contained at high pressures in commonly used compressed gas cylinders. The high pressure of the oxygen (42) and argon (41) are reduced to working levels by the use of high purity, stainless steel Matheson Model 3803 pressure regulators (43). Connected directly to these regulators is a shut off valve to which 1/4 inch stainless steel tubing is then connected to carry the gas to the flow controllers.

In the gas feed line between the flow controllers and the gas inlet of the baseplate of the MPDR (46) is a shut-off valve and a length of glass tubing. This glass tubing is used to electrically isolate the MPDR from the flow controllers to prevent any large voltage anomaly from damaging the flow controller and also to dc isolate the MPDR in certain experiments.

Gas flow continues from the MPDR gas inlet to the discharge zone
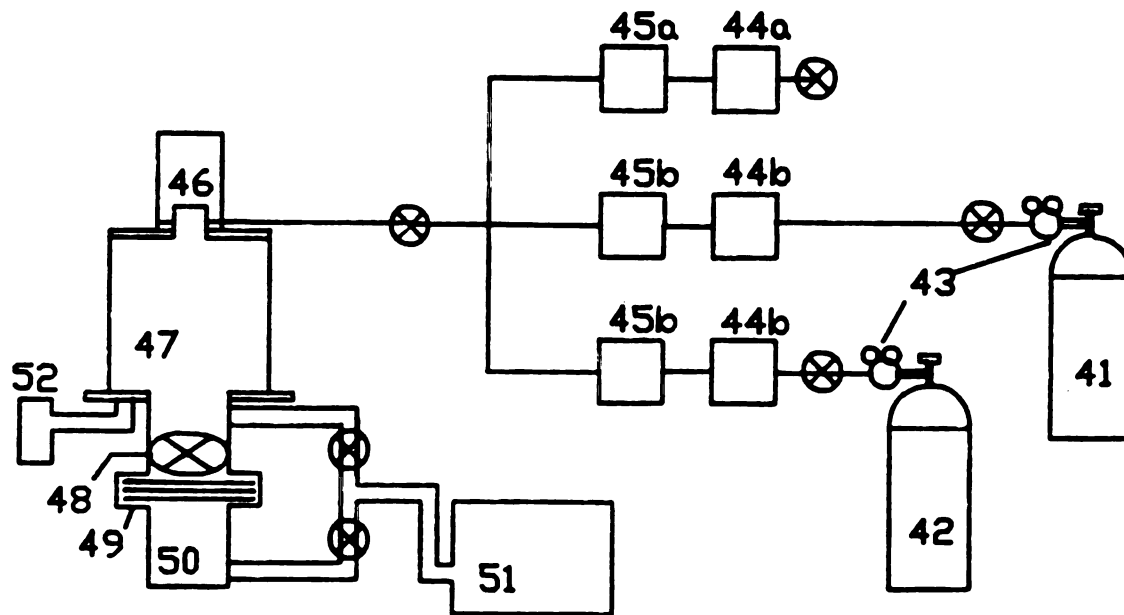
Figure 3.4 Gas Flow System and Vacuum System for the MPDR

of the baseplate below the quartz dish then into the vacuum chamber (47). The vacuum chamber (described in section 3.1) is mounted on a stainless steel plate which is the top surface of a Consolidated Vacuum Corporation LC1-14B Vacuum Pumping Station.

The vacuum station consists of a 400 liter/min mechanical pump (51) and a 4-inch diffusion pump (50). The mechanical pump can be switched via two valves to pump directly on the vacuum chamber or to back the diffusion pump. Between the diffusion pump and the vacuum chamber are a cold trap (49) and a high vacuum gate valve (48). The cold trap is cooled by a compressed freon refrigeration unit and is used to absorb the heat from boiling oil from the diffusion pump thereby condensing the oil and preventing it from reaching the processing chamber (the vacuum chamber).

Pressure in the vacuum chamber is measured using a capacitance manometer (52). This consists of an MKS-390HA absolute capacitance manometer and a MKS-270B signal conditioner. This measurement system can accurately determine the pressure from 1×10^{-5} Torr to 1 Torr.

3.2.3 RF Biasing

In the argon-ion sputtering of silicon dioxide work, which will be described in Chapter Six, it was necessary to apply an rf bias to the wafer holder {(20) in Figure 3.1}. This rf bias is connected to the wafer holder through a coupling capacitor so that a negative potential, a negative self-bias, can be induced on the wafer. This self bias then accelerates the positively charged argon ions to the surface of the wafer with enough energy to "knock off" atoms and clumps of atoms from

the silicon dioxide.

To explain why one electrode can be made more negative than the other, first consider the random thermal particle flux of an arbitrary type of particle, α, which can be expressed as [82]:

$$\Gamma_\alpha = n_\alpha \, [kT_\alpha/2\pi m_\alpha]^{1/2}$$

where n_α is the average density of the arbitrary species, T_α is the temperature of the particle and m_α is the mass of the particle. From this expression then, it is quite evident the electrons of a plasma will have a much higher flux than even a hydrogen ion not to mention an argon ion. Thus with a time varying potential applied to an electrode, a much higher electron current will flow in the positive half cycle than will an ion current in the negative half cycle. If a blocking capacitor is attached in series with the electrode that is to be "driven", i.e. made more negative, then because of this much higher mobility of the electrons and with the capacitor to block any dc current in the outer circuit to compensate for the higher charge density, a negative bias will be induced on that electrode.

Figure 3.5 is a block diagram of the rf biasing system. A Plasma-Therm, Inc. Model HFS-500E 0-500 Watt 13.56 MHz Radio Frequency Generator (61) was used to supply the necessary rf power. Connected first to this supply is a matching network (62), to match the impedance of the wafer/plasma load. Figure 3.6 shows the details of this network which consists of a variable capacitor, C_1, in parallel with the generator followed by a center tapped variable inductor. A blocking capacitor, C_2, was placed in series with the wafer/plasma load to block dc currents and allow a negative potential to be maintained on the substrate holder. The matching network is housed in a metal box which

to
wafer

to
filter

63

62

61
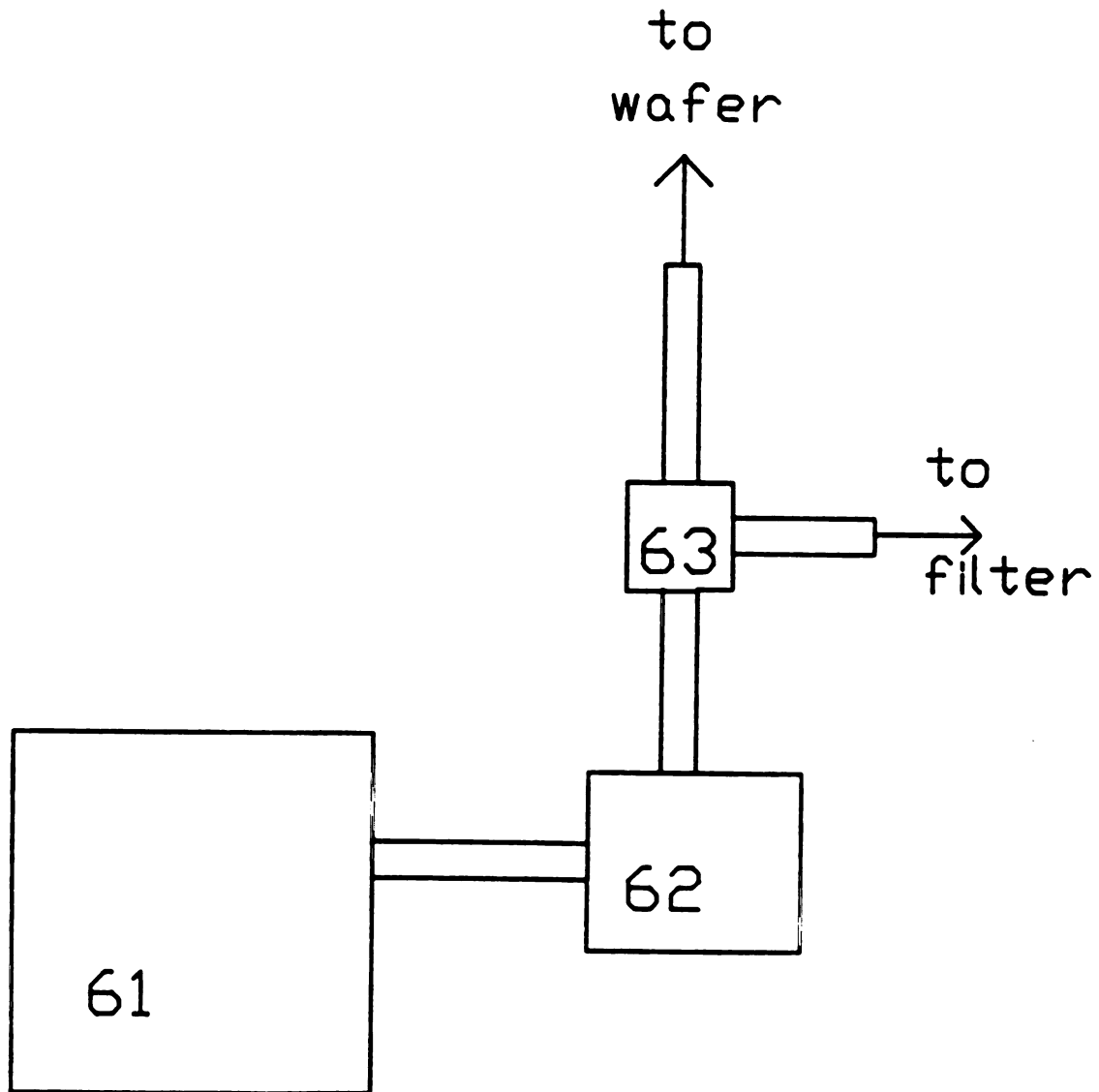
Figure 3.5   The RF Biasing Circuit for Sputtering
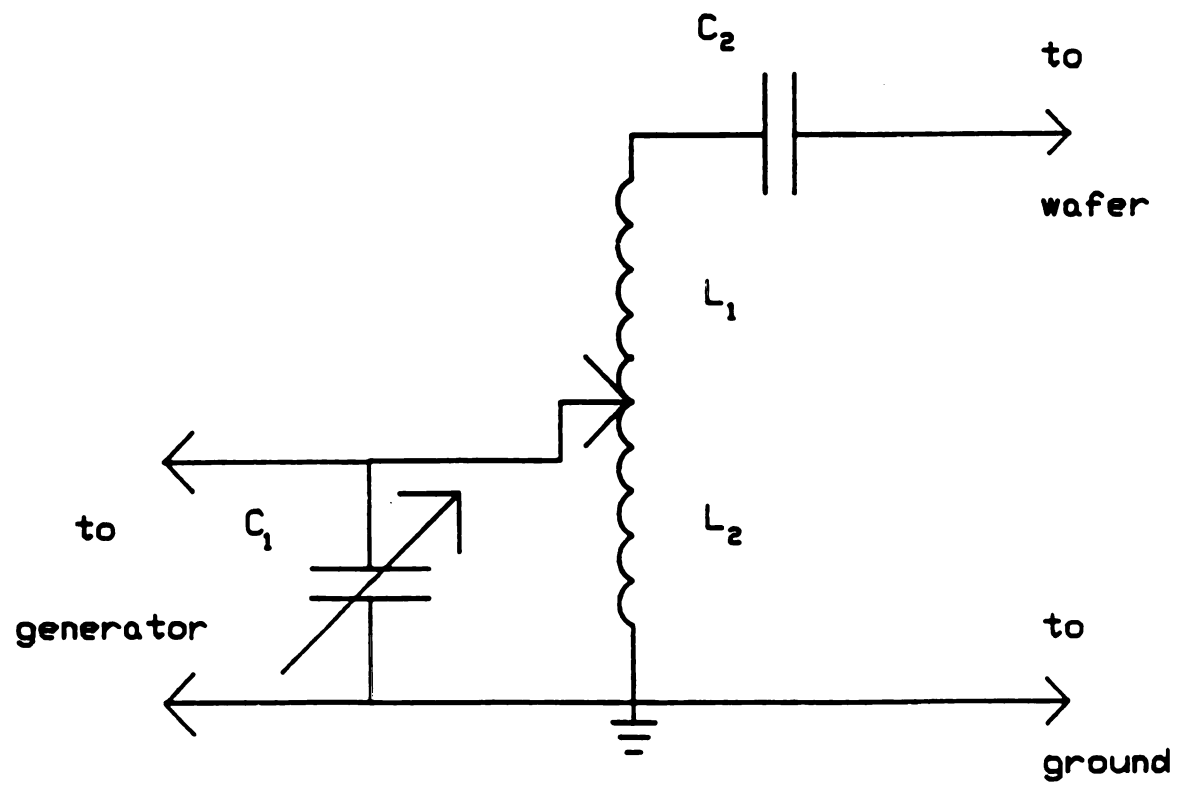
Figure 3.6   The Matching Network for the RF Circuit

is grounded to contain the rf signal.

Two n-type connectors are mounted on this metal box and connected to the matching network such that 50 ohm coaxial cables could be easily attached to carry the rf power. In Figure 3.5, a coaxial cable connects the RF power supply (61) to matching network (62). A cable is then connected to the matching network but is bared at the other end to attach to a vacuum feedthrough (63). This vacuum feedthrough is a single 1/2 inch diameter copper post. The center conductor of the coaxial cable is connected to this post and the outer conducting braid is attached to the vacuum system itself which is grounded. A brass mesh is grounded and placed around this post to contain the RF power. Inside the vacuum system is another coaxial cable again with the center conductor connected to the copper post and the outer braid grounded. The coaxial cable inside the vacuum carries the rf power to the wafer holder with the center conductor being attached to the wafer holder and the outer conductor grounded to the support arm.

To control the sputtering, it was necessary to monitor the dc bias induced on the wafer. A two stage low pass filter, to filter out the high frequency power of the rf generator, consisting of a series inductor, a parallel rf capacitor, another series inductor, and a second rf capacitor, was connected to the copper post on the atmosphere side of the vacuum chamber. The bias is then measured via a Hewlett-Packard 10X probe and a Hewlett-Packard Model 1727A Storage Oscilloscope.

3.2.4 Data Collection and DC Biasing

For the anodization work, a positive dc bias for the wafer was required. To apply this bias, two Trygon Model HR40-750 Power Supplies were connected in series to supply the dc power required. The bias was connected to the wafer holder {(20) Figure 3.1} by wires running from the power supplies to a low power vacuum feedthrough. On the vacuum side of the feedthrough, the biasing arrangement described in section 3.1 was used to supply power to the wafer holder. To complete the circuit, the MPDR was grounded. Thus the current flow was through the plasma to the baseplate of the MPDR.

Anodization current and bias were measured and recorded by an automated means developed and described by Roppel [30], therefore only a brief overview will be presented here.

The anodization current was measured by means of a Hewlett-Packard Model 428B Clip-On DC Milliammeter. This instrument provides an output proportional to the measured current, but to increase the resolution of this measurement, this output was connected to a Keithly Model 610 Electrometer. A second identical electrometer was used to directly monitor bias potential. The two electrometers provide a high resolution output signal proportional to the input signal. These output signals were recorded by a laboratory computer, an IBM PC with a Data Translation 8-channel, 12-bit A/D converter.

The incident and reflected microwave power levels were also recorded with the laboratory computer. The HP 435a power meters provide an output signal proportional to the input signal. Coaxial cables, for transmitting the analog signals to the A/D board of the

computer, were connected to the power meters and the electrometers used for the recording of the substrate bias and microwave power.

3.2.5 Double Langmuir Probe Procedure

It was desirable to measure the plasma density at various radial and downstream distances in the plasma in order to compare plasma properties with the processing results in the anodization and sputtering work.   To do this, a double Langmuir probe with an automated current-voltage measuring and analysis system was utilized.   This automated system has been developed and refined by many workers [83]. The procedure and theory of the double Langmuir probe have been well documented and explained [77,78,84], so only a brief explanation will be given here.

To perform a double Langmuir probe measurement, two probes of equal diameter and length are constructed and insulated from each other. A simple method employed here is two tungsten wires encased in a pyrex tube with insulated wires exiting from the other end.   The probes are small enough so as not to significantly disturb the plasma, but large enough to be larger than the plasma sheath.   Another consideration is the separation of the probes.   The distance between the probes should be greater than several Debye lengths such that the plasma sheath of one probe does not interact with the other, but close enough together such that the plasma potential near each probe is the same.   The dimensions of the probes used in this work are: 0.89 mm diameter tungsten wires, 7 mm length of wire extending above the pyrex enclosure and 5 mm separation between the probes.

When the probes are immersed in the plasma, each collects ions and electrons. Since the probes are made of equal area, if the probes are allowed to float with the plasma potential, i.e. no potential is applied between the two probes, each collects the same number of charged particles and no current flows between the probes or in the circuit. When a potential is applied between the probes, the more positive collects more electrons and repels some ions. If the potential is increased between the two probes to a high enough level, the more positive electrode will attract only an electron current since all positively charged ions are being repelled. The other probe meanwhile will only collect an ion current since the electrons will be repelled. The magnitude of this current is called the ion saturation current, I_s.

At this potential difference where the current becomes saturated, the I-V characteristics "bend" forming a knee in the curve. In reality the current in the circuit does not saturate, but increases at a much slower but still steady manner. In the development of the theory, the ions were assumed to be so massive as to be immobile. In fact, the ions are much more massive than the electrons but are still mobile but to a much smaller degree than the electrons. The increase in potential accelerates the ions and hence the I-V characteristics still increase but at the slower rate.

The potential difference between the two probes is usually swept from a negative to a positive voltage with the range being large enough to form two knees. With equal area probes, the I-V curve is symmetric about the voltage axis. Figure 3.7 shows a typical I-V curve of a double Langmuir probe measurement. From this curve, the electron
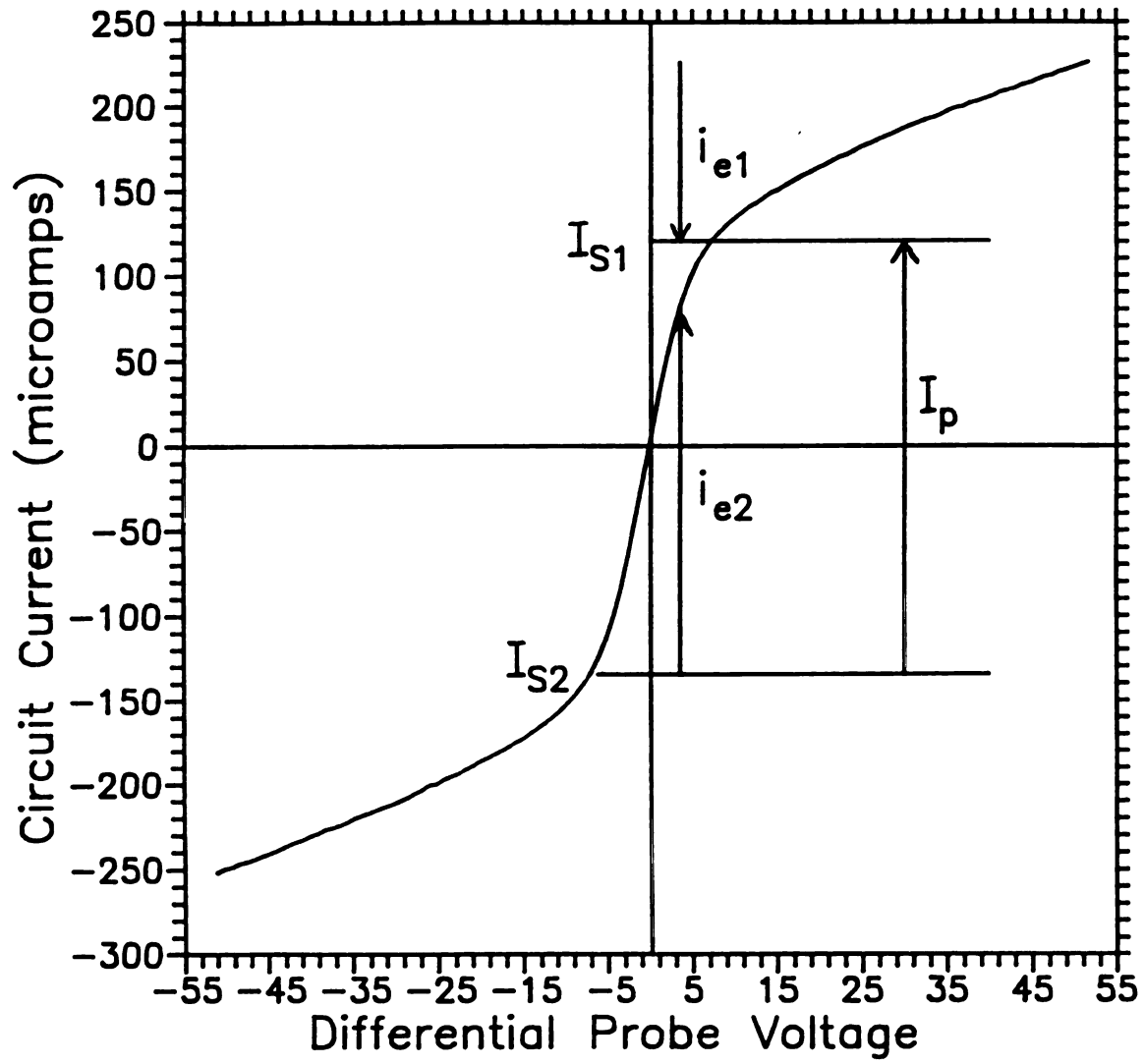
Figure 3.7 Typical I-V Characteristics of a Double Langmuir Probe

temperature of the plasma can be calculated. To do so, consider the current between the two electrodes. The current arriving at one electrode must equal the current leaving the other electrode:

$$i_1 = -i_2 .$$

These two currents can be broken down into the ion and electron components as:

$$i_{11} - i_{e1} = i_{e2} - i_{12}$$

where i_{11} and i_{12} are the ion currents to probe 1 and probe 2 respectively and i_{e1} and i_{e2} are the electron currents to probe 1 and probe 2 respectively. Now one may define I_p, the total ion or electron current collected by the two probes as:

$$I_p \equiv i_{11} + i_{12} \equiv i_{e1} + i_{e2} .$$

If the electron energy distribution is assumed to be Maxwellian, this can be rewritten as:

$$I_p = i_{e1} + i_{e2} = I_{01}\exp(-eV_1/kT_e) + I_{02}\exp(-eV_2/kT_e)$$

where I_{01} and I_{02} are the electron currents collected on the respective probes when the potential applied between the probes is zero. V_1 and V_2 are the voltages of probes 1 and 2 respectively. Now $V_1 - V_2$ is just the differential probe voltage, i.e. the potential applied between the two probes, V. Rearranging the above equation and taking the natural logarithm of both sides, this equation can be rewritten as:

$$ln\left(\frac{I_p}{i_{e2}} - 1\right) = -\frac{eV}{kT_e} + ln\left(\frac{I_{01}}{I_{02}}\right) .$$

If one uses two probes with the same area, then I_{01} is equal to I_{02}, and the natural log of 1 is zero. From the slope of ln (I_p/i_{e2}) versus V, the electron temperature can be determined. Then using this

electron temperature, the ion density can be determined from:

$$I_s \approx 0.6\ n_i\ e\ A_p \left(\frac{kT_e}{m_i}\right)^{1/2}$$

where I_s is the ion saturation current, n_i is the ion density, e is the electronic charge, A_p is the area of the probe and m_i is the ion mass.

This development assumes an equal number of positively charged ions and electrons so that the ion density, n_i is equal to the electron density, n_e. This procedure gives ion densities of reasonable accuracy provided a plasma of a simple gas, such as argon, is being measured. With argon, the species present are electrons, positively charged argon ions, neutral argon atoms and some excited states of the positive ions and the neutrals. With a plasma formed of a complex gas, such as oxygen, the species present are electrons, positively charged oxygen ions, negatively charged oxygen ions, positively charged oxygen molecules, negatively charged oxygen molecules, neutral oxygen atoms and molecules, and excited states of all of these. Hence with a complex plasma, m_i may be the mass of a single ion or a molecule, which gives rise to some uncertainty in the true ion density.

CHAPTER FOUR

Procedures for the Plasma Anodization of Silicon

Amazing growth!   Simply amazing!

4.1   EXPERIMENTAL CONFIGURATION

This section describes in detail the various configurations of the equipment used to study the anodic growth of silicon dioxide using an electron-cyclotron-resonance microwave oxygen plasma sustained with the Microwave Plasma Disk Reactor.   Several configurations were investigated in the process of achieving oxides with improved quality as discussed in subsequent sections of this chapter and in chapter 5.

4.1.1   With and Without Tube

As described in section 3.1 and shown in further detail in Figure 4.1, an MPDR was used to sustain an oxygen plasma operating in the electron-cyclotron-resonance mode.   This plasma was used to grow silicon dioxide on silicon in an anodic fashion.   The baseplate (14) was used as the cathode while the wafer was attached to a 2.8 inch (71 mm) diameter stainless steel wafer holder (20) by a conductive paint. The wafer holder was isolated from the supporting arm (22) and the

48
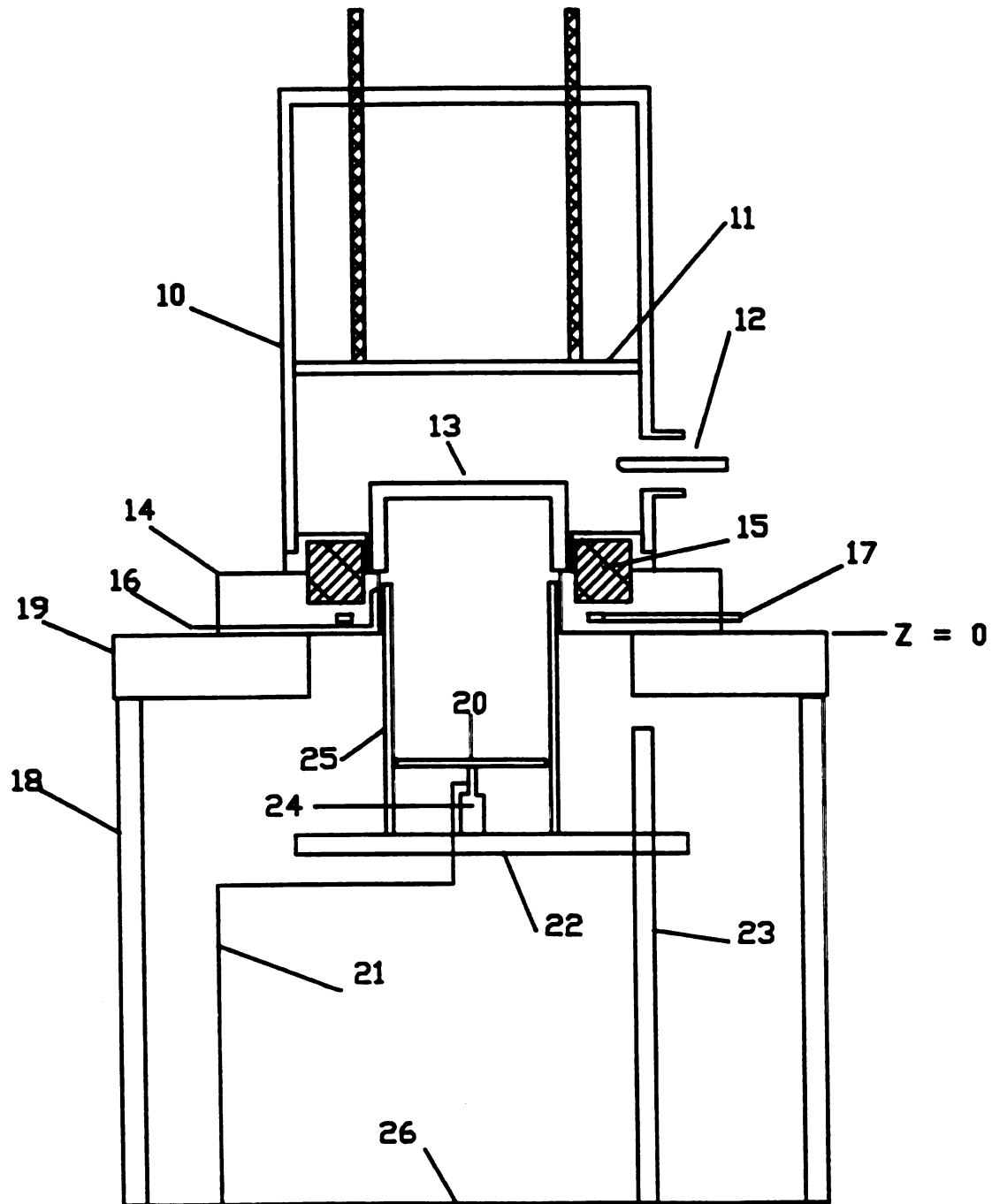
Figure 4.1 The Plasma Anodization Configuration

support rod (23) by means of a threaded ceramic dowel (24). This ceramic dowel was attached firmly to the support arm by a bolt and the wafer holder was screwed into the dowel. A bias wire (21) was attached to the wafer holder and enclosed in a glass tube through which it passed to a low power vacuum feedthrough. Most of the oxidation experiments were performed using this arrangement of silicon wafer as anode and baseplate as cathode with the plasma being the conduction path between the two.

As will be discussed in section 5.2, some sputtering contamination from the baseplate was found in the silicon dioxide layers. A dc current results from the applied dc wafer bias, and as a result positive ions are collected at the stainless steel cavity baseplate. These ions strike the baseplate with sufficient energy to cause sputtering. Since there is a direct line-of-sight between the cavity baseplate and the wafer, contamination results. In order to reduce this contamination, a quartz tube {(25) in Figure 4.1} was added to the setup. The quartz tube has an outer diameter of 8.4 cm and an inner diameter of 8.0 cm. As shown in Figure 4.1 the tube was positioned such that only 0.5 to 0.8 cm of the stainless steel was exposed to the plasma above the quartz tube. This greatly reduced, but did not totally eliminate the contamination. Consequently further modifications were made, which are described as follows.

4.1.2 Floating Baseplate

As a second attempt to eliminate the contamination from the baseplate, the baseplate was allowed to electrically "float" with the

plasma potential. To do this, all paths to ground from the MPDR were eliminated.   An insulating Teflon choke was inserted between the Andrews connector and the input power probe.   Thus the outer conductor, which is the ground of the microwave power cable, was isolated from the oxidation apparatus. A glass tube was also inserted in the gas feed line, eliminating that path to ground as well.

With the floating baseplate arrangement, the very large lower stainless steel plate {(26) in Figure 4.1} of the vacuum pumping station was used as the cathode. This plate is 35 cm downstream from the ECR plasma discharge. The rationale for this approach was that any stainless steel sputtering would occur well downstream from the wafer. Two experiments were attempted using this configuration. In the first, the quartz tube was left in place as shown in Figure 4.1. With this arrangement, no current flow was measurable. With no current flow there is negligible oxide growth. In a second trial, the quartz tube was removed and the cavity baseplate was again isolated to allow it to float with the plasma potential. With this second arrangement a small current was measurable, but again not enough to account for significant oxide growth. Consequently, it was concluded that there were too few ions at a distance of 35 cm downstream from the discharge to support a sufficiently large current.

4.1.3 Silicon Cathode

The third and final approach to eliminate metallic contamination in the oxide films was the use of silicon as a cathode. Figure 4.2 is a cross section of this configuration. Three pieces of silicon were
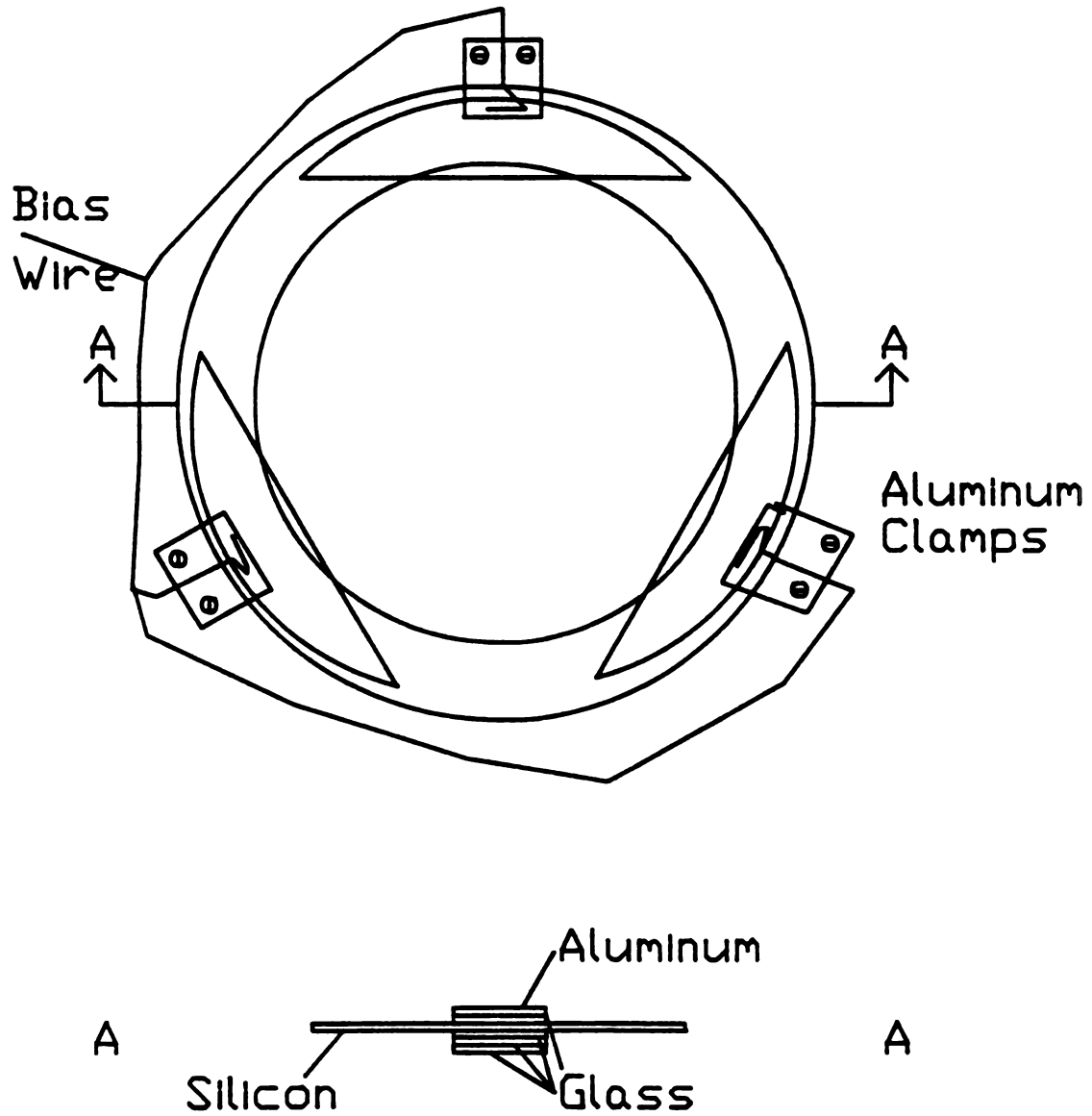
Figure 4.2 The Silicon Cathode Arrangement

attached to the baseplate and isolated from the baseplate by pieces of glass. A ground wire was clamped between a piece of glass and the wafer by use of custom fitted aluminum pieces. Existing threaded holes in this baseplate, from grid experiments [76], provided the necessary means of clamping the aluminum pieces to the baseplate with screws. The cavity baseplate (14) was again floating so that only the silicon pieces serve as the cathode. Consequently any sputtering of the cathode material would result in silicon atoms rather than metallic species from the stainless steel. With this arrangement, as will be discussed in section 5.4, XPS analysis did not detect any sputtering contamination from the baseplate in the oxide.

4.2 SAMPLE PREPARATION

4.2.1 Cleaning

Three inch (76 mm) silicon wafers, both n- and p-type, were used throughout this study. The first step in all experiments was to clean the wafers in order to ensure as clean a start, with as little contamination, as possible. The procedure used was the RCA method [85]. Briefly, this procedure consists of a three minute bath in boiling trichloroethylene (TCE) followed by rinses in acetone, methanol and a two minute rinse in de-ionized water (DI). This bath was followed by a 70°C, 10 minute bath in a solution called a degrease etch. The degrease etch consists of 5:1:1 mixture of $H_2O:H_2O_2:NH_4OH$. This was followed by a 2 minute rinse in DI. Next was a 70° C, 10 minute bath in a solution called demetal etch which consists of 8:2:1

mixture of $H_2O:H_2O_2:HCl$. This was followed by another 2 minute rinse in DI. Finally, a 10 second rinse in a 50:1 $H_2O:HF$ solution followed by a 3 minute rinse in DI completed the cleaning of the wafers.

4.2.2 Mounting

The wafers were mounted in the vacuum chamber on the wafer holder {(20) in Figure 4.1} by use of a conductive paint to insure a good electrical contact between the silicon wafer and the wafer holder. The major flat of the wafer was positioned 180° from the microwave power input probe to provide a repeatable reference point in the experimental setup.

The arm {(22) in Figure 4.1} of the wafer support arrangement can be secured to the vertical rod (23) at various positions. This allows the wafer to be positioned at any distance below the discharge. Referring to Figure 4.1 where z = 0 is the bottom of the cavity baseplate, distances of z = 2, 4, 6, 8, and 10 cm below the discharge were used to study the growth and uniformity of the silicon dioxide layers grown.

4.3 OXIDATION PROCEDURE

After a wafer is mounted on the wafer holder, the vacuum system is assembled and pumped down. Using the mechanical pump, the pressure is reduced from atmosphere to 15 mTorr within approximately 15 minutes. The valves are then adjusted such that the vacuum chamber is isolated and the mechanical pump is used as a foreline pump. The diffusion pump

is now turned on and allowed to warm up for a minimum of 15 minutes at which time the high vacuum valve (gate valve) is opened. The vacuum chamber is now evacuated using the diffusion pump for a minimum of 30 minutes to approximately 10^{-6} Torr.

At the end of this evacuation time, the oxygen flow is initiated and the gate valve partially closed to allow the pressure to rise to approximately 60 mTorr. Microwave power to the MPDR is then increased until the plasma ignites. When the plasma is ignited, some power is reflected from the MPDR and some slight adjustment of the tuning is required. The gate valve is then gradually opened to reduce the pressure from 60 mTorr to 3 mTorr over a time period of approximately 5 minutes.

All experiments were conducted with a Baratron pressure reading of 3 mTorr. A low pressure is desired because diffusion lengths of plasma species increase as the pressure is lowered resulting in a more uniform plasma density distribution. Three mTorr is near the lower end of the pressure range at which an oxygen plasma could be reliably maintained with the particular cavity, cavity mode, and magnet configuration used in this work.

When the pressure of 3 mTorr was achieved and the MPDR tuned for maximum power transfer to the plasma (minimum reflected power), the anodization potential was applied to the wafer and oxide growth commenced. The time of anodization for all experiments, (except DS-38 and DS-18) was 120 minutes.

Table 4.1 is a summary of the conditions used in the anodization work. This list contains all the physical parameters and conditions used in the study.

Table 4.1   Parameters and Conditions for Silicon Anodization

Vacuum chamber pressure	3 milli Torr
Microwave power input	260 - 265 Watts
Microwave power reflected	$\leq$ 5 Watts
Oxygen Flow	7.5 - 10 sccm
Input Probe Depth	1.6 - 1.8 cm
Cavity Height	7.3 - 7.5 cm
Time of Anodization	120 minutes

Table 4.2 is a list of all experiments run with the MPDR operating in the electron-cyclotron-resonant mode and the wafer placed downstream of the reactor. Trials DS-1 through DS-6 were conducted with a grid attached to the bottom of the baseplate to terminate the reactor and the wafers were placed below this grid. Initially, a grid was thought necessary to contain the microwave power, so that biological hazards were not created. This grid was a stainless steel mesh with circular holes in it. The oxides grown with the grid in place had the pattern of the grid transferred to them in terms of the oxide thickness. Sharply defined, small round areas of the oxide, which correspond to the hole pattern in the grid, were thicker than the rest of the oxide (for example 1350 Å compared to 1240 Å for sample DS-1). This is possibly an indication of light stimulated growth since the thicker oxide regions correspond to those portions of the substrate which were exposed to radiation from the plasma.

Beginning with experiment DS-6a, the grid was removed to take

Table 4.2 Partial List of Oxidation Experiments

DS	Z	VB	TYPE	DIAM	COMM
1	1.0	30	N	2	
2	2.0	25	N	2	
3	2.5	30	N	2	
4	3.0	30	N	3	Low current-bias circuit
4a	3.0	30	N	3	Additional anodization of DS-4
5	3.0	30	P	3	
6	3.0	30	N	3	
6a	3.0	30	N	3	Additional anodization of DS-6, no grid
7	3.0	30	P	3	Magnets oriented with alternating poles
8	3.0	40	N	3	Plate (19) changed to stainless steel
9	3.0	40	P	3	
10	6.0	30	N	3	
11	4.0	40	N	3	no paint, very non-uniform
12	4.0	40	N	3	
13	4.0	40	N	3	New Baratron installed
14	4.0	40	N	3	
15	4.0	40	N	3	
16	4.0	40	N	3	
17	2.0	40	N	3	
18	5.0	40	N	3	3 hour run
19	2.0	40	N	3	
20	6.0	40	N	3	
21	6.0	40	N	3	C paint rather than Ag paint from here
22	8.0	40	N	3	
23	8.0	40	N	3	
24	10.0	40	N	3	
25	10.0	40	N	3	
26	2.0	40	N	3	New bias wire in glass tube
27	6.0	40	N	3	
28	8.0	40	N	3	
29	10.0	40	N	3	
30	8.0	40	N	3	
31	6.0	40	P	3	quartz tube (QT)
32	6.0	40	N	3	QT
33	6.5	40	P	3	QT
34	6.5	40	P	3	QT
35	3.3	40	P	3	QT
36	6.5	50	P	3	QT
37	6.0	30	P	3	QT
38	6.0	40	P	3	dc isolation, no current, QT
38a	6.0	40	P	3	dc isolation, no quartz tube, small i
SC	8.0	40	P	3	silicon cathode, dc isolation

advantage of conditions noted in section 5.6.2 of [78]. After the plasma is ignited, the highly conductive plasma acts as the termination of the cavity thereby containing the microwave power. Oxides grown with this arrangement did not have any specific pattern evident upon them except for some slight non-uniformities caused by the plasma density distribution when the wafer was placed very near the plasma discharge.

Also, for samples DS-1 through DS-6a, the rare earth magnets which provide the static magnetic field to create the ECR zones in the plasma were not positioned with alternating poles. This caused a slight non-uniformity in the distribution of plasma species which was transferred to the oxide thicknesses grown. Beginning with DS-7, the magnets were positioned correctly such that the plasma was sustained under the ECR conditions outlined in Section 2.6.

Experiment DS-11 was performed without conductive paint between the wafer and the wafer holder. This was to see if the conductive paint could be eliminated from the procedure as it may cause contamination in consequent processing steps. However, the oxide grown without the conductive paint showed a higher degree of non-uniformity than other oxides. This was most likely due to the wafer and wafer holder not being in good electrical contact. In all other trials, a conductive paint was used, either silver paint or carbon paint. Beginning with DS-21, carbon paint, a very pure mixture of graphite and isopropanol, was used to provide the electrical contact between the wafer and holder.

Before experiment DS-13, the Baratron used was not a high accuracy unit and even though the pressure reading was 3 mTorr, the actual

pressure in the vacuum chamber is estimated to be from 3 to 6 mTorr of pressure during these initial experiments.

4.4 PLASMA CHARACTERIZATION

As mentioned in section 3.2.5, it was desirable to ascertain the density of plasma species at various points in the vacuum chamber to compare this distribution with the uniformity results. The results of a double Langmuir probe measurement in oxygen is summarized in Figure 4.3. As noted in section 3.2.5, multiple positive species exist in an oxygen plasma, i.e. O_1^+ and O_2^+. The results shown in Figure 4.3 were computed assuming that the dominant positive ions in the plasma were O_1^+. In reality, both species do exist in the plasma, but the relative populations were not determined in this study. Consequently, the data shown is the lower limit of the possible density. Multiplying these numbers by the square root of 2 will give the upper limit on the density, i.e. making the assumption that all the positive species are O_2^+. Conditions used to to perform the double Langmuir probe study were the same as those used to grow the oxides, i.e. 3 mTorr bell jar pressure, 7.5 sccm oxygen flow, 260-265 watts of incident microwave power, and 1-3 watts of reflected microwave power.

Each double Langmuir probe data point on Figure 4.3 represents a separate probe positioning, vacuum system assembly, pumpdown and plasma initiation experimental run. Once the operating conditions were reached, the plasma was allowed to "warm up" for 15 minutes before the probe data was acquired.

The data in Figure 4.3 show that the plasma density becomes more
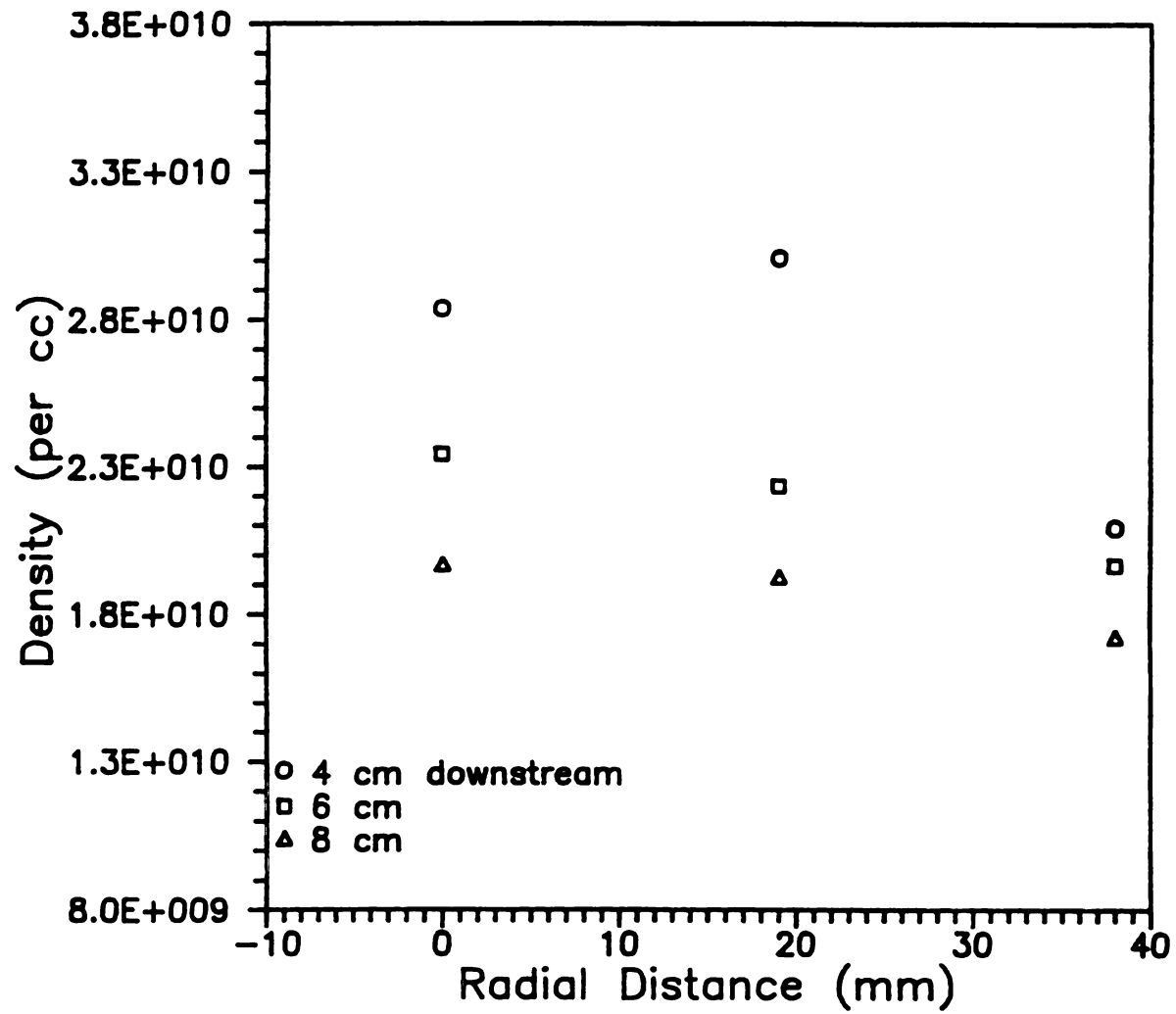
Figure 4.3 The Measured Density of Oxygen Ions.

uniform, radially, as the downstream distance is increased. Using the measured ion density numbers, at 4 cm downstream, the plasma density at a radial distance of 38 mm is 26% lower than the center value and 30% lower than the value at a radial distance of 19 mm. This lateral data point may appear to be anomalous in Figure 4.3, but a similar behavior was observed in measurements performed with an argon plasma as will be discussed in Section 6.3. This may represent the effect of an ECR zone, as this data was taken along a radius moving directly toward an ECR zone, i.e. a position between two magnets. At 8 cm downstream, the plasma density at a radial position of 38 mm is only 12% lower than the center value.

The improved uniformity with increasing downstream distance is due to diffusion. This can also be seen by analyzing the plasma assuming it follows the theory of ambipolar diffusion. Following the development of Hopwood [78], an analytic expression for the distribution of charged plasma species can be obtained from the ambipolar diffusion equation [86]:

$$D_a \nabla^2 n(r, \phi, z) + \nu_i n(r, \phi, z) = 0$$

where ν_i is the ionization frequency, n is the density of the charged species as a function, in three dimensions, of radius, angle and distance (cylindrical coordinates) from the discharge, and D_a is the ambipolar diffusion constant given by:

$$D_a = \frac{\mu_i D_e + \mu_e D_i}{\mu_e + \mu_i} .$$

Here μ_i and μ_e are the mobilities of the ions and electrons respectively and D_i and D_e are the diffusion constants of the ions and

electrons. Solving the ambipolar equation in the manner of Hopwood, the analytic expression is:

$$n_{e,i}(r,z) = N_o\left(\frac{2b}{a}\right)\sum_{n=1}^{\infty}\frac{1}{x_{On}}\left[\frac{J_1\left(\frac{x_{On}b}{a}\right)}{J_1^2(x_{On})}\right]J_o\left(\frac{x_{On}r}{a}\right)\exp\left(-k_z z\right),$$

where N_o is the constant density of the plasma in the discharge region, a is the radius of the opening of the top plate of the vacuum chamber {(19) in Figure 4.1}, b is the radius of the discharge zone, and x_{On} is the nth root of the zero order Bessel Function of the first kind. The expression in square brackets in the equation are the coefficients of each term found in solving the differential equation. In solving the equation, angular symmetry is assumed, hence there is no dependence on ϕ, the angle measured about the z axis. As observed in the theoretical expression, the density distribution has a Bessel function dependence on the radial variable, r, and a decaying exponential dependence on the vertical variable, z. The eigenvalue, k_z, which is a measure of the z dependence of the density distribution, is expressed as:

$$k_z = \sqrt{\left(\frac{x_{On}}{a}\right)^2 - \frac{\nu_i}{D_a}}\quad,$$

where ν_i is the ionization frequency of the gas in the plasma. To calculate this expression, a knowledge of the ionization frequency, ν_i, and the ambipolar diffusion constant, D_a, is required. For an argon plasma, ν_i is on the order of 15,000 - 20,000 s^{-1} and D_a is on the order of 2 - 5 X 10^6 cm^2/sec. Consequently, ν_i/D_a is in the range of approximately 0.003 to 0.01 cm^{-2}. The quantity $(x_{01}/a)^2$ for this particular geometry is 0.0597 with higher order terms being larger. As

a first-order approximation, a simplification is made on the basis of ν_i/D_a being much smaller than x_{On}/a and k_z is simplified to:

$$k_z \approx x_{On}/a \ .$$

Using the theoretical expression for the ion density, a comparison can be made between the measured density and what could be expected from plasma theory. Figure 4.4 is a comparison of the measured density distribution and the theoretical density distribution as calculated using the above expression for $n_e(r,z)$ and neglecting the ν_i/D_a term. N_o is chosen such that the curve corresponding to the calculated 6 cm downstream density distribution matches the measured 6 cm downstream density distribution at a radial distance of 19 mm. As can be seen, the calculated distribution becomes more uniform radially as the distance from the discharge is increased. However, the calculated theoretical density does not match the measured density exactly. Observing the calculated numbers, the theoretical density of ions falls off more rapidly than the measured density. This may be due to the assumption in the theoretical calculation that k_z, the z variable eigenvalue, can be simplified to just x_{On}/a since ν_i/D_a was very much smaller. This assumption works well for argon, (see Section 6.3 and Hopwood [78]) but for oxygen, it may not be a good assumption. Oxygen is a much more complex gas with more and different energy exchange mechanisms. Also, the work done in oxygen was at a higher pressure, 3 mTorr, as opposed to 0.76 mTorr for argon. Therefore, it is very probable that ν_i is larger and D_a smaller for oxygen under these operating conditions. So using 50% of $(x_{O1}/a)^2$ (= 0.02985) for ν_i/D_a, Figure 4.5 is another comparison of the theoretical calculation of the
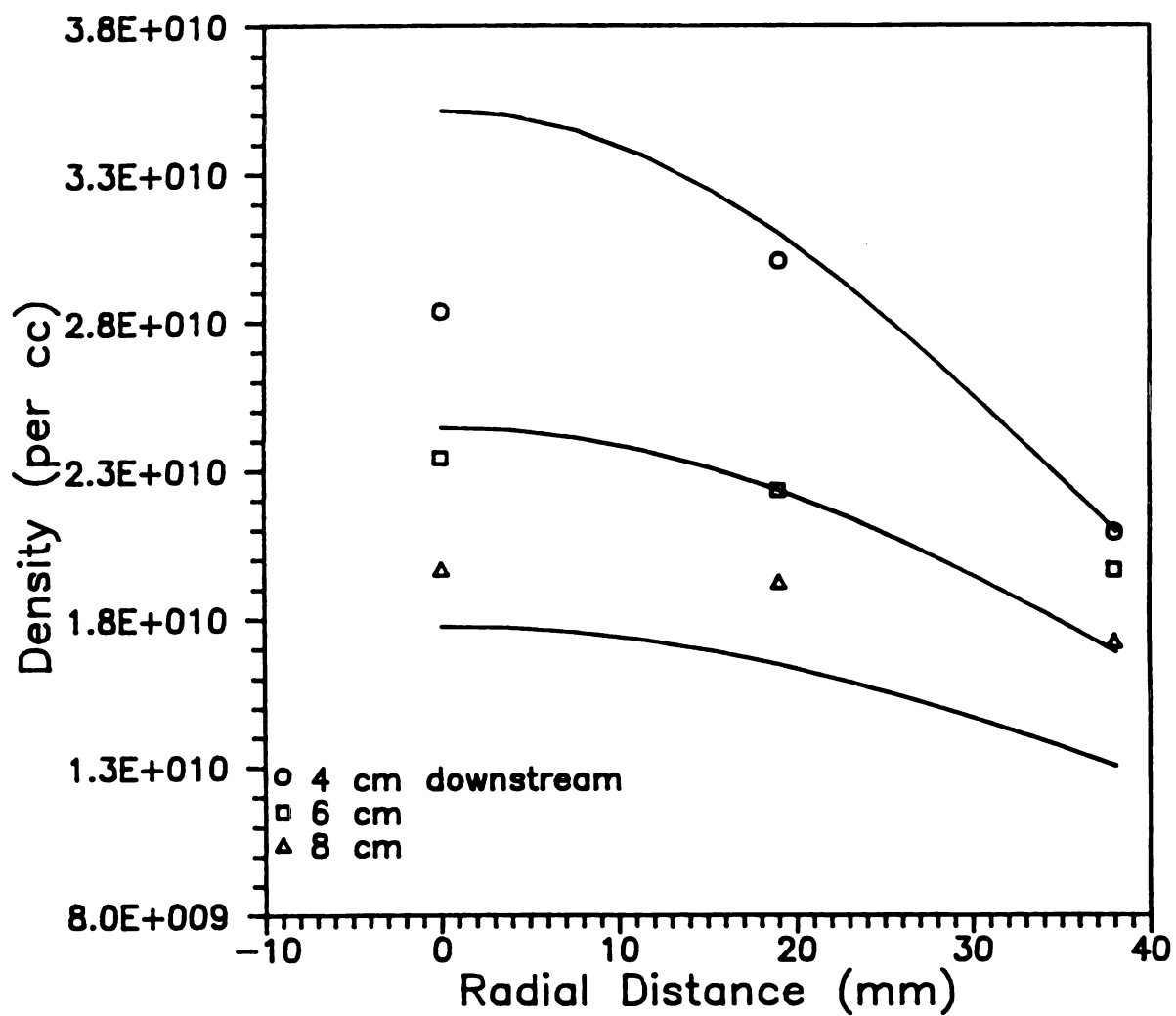
Figure 4.4 Comparison of the Measured Density with the
Calculated Density of Oxygen Ions Assuming $v_i/D_a \ll (x_{01}/a)^2$
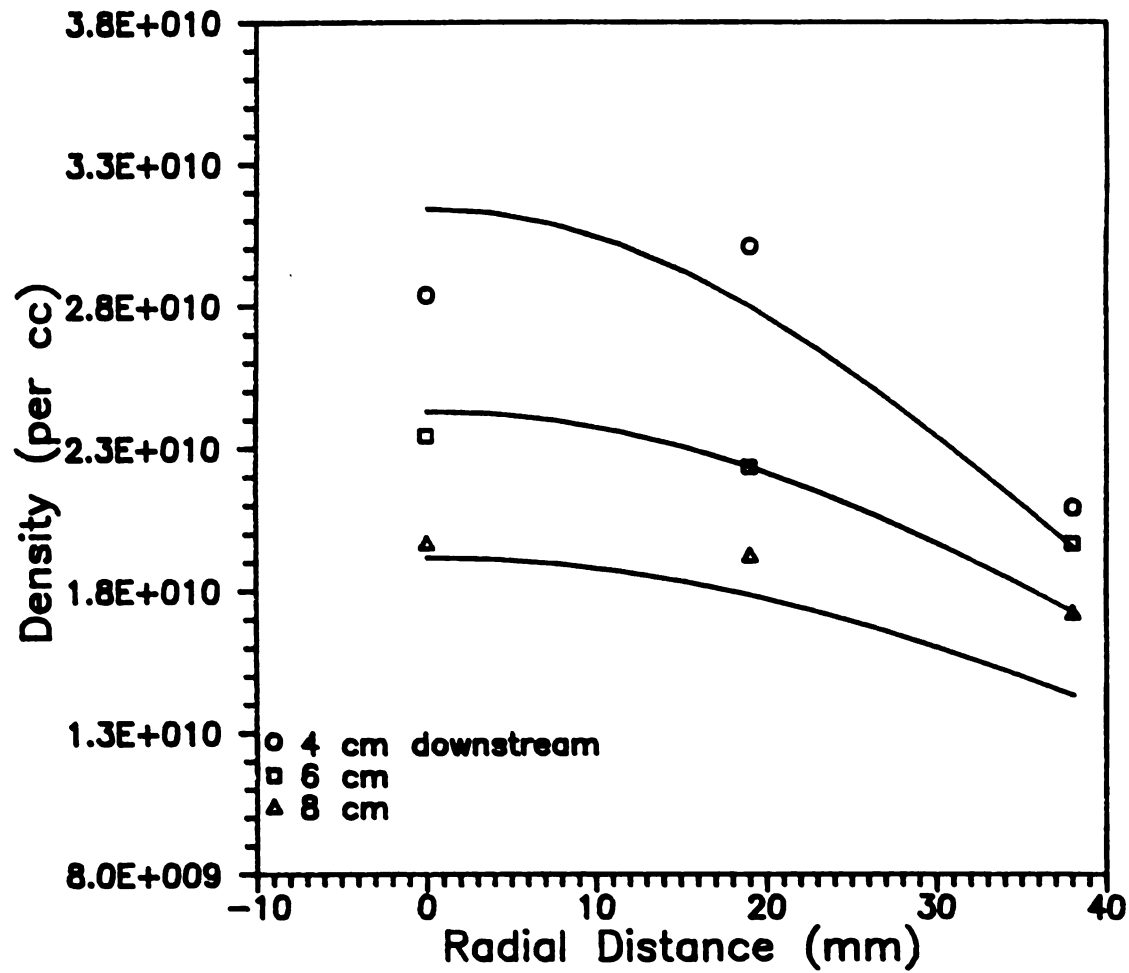
Figure 4.5 Comparison of the Measured Density with the
Calculated Density of Oxygen Ions Assuming $v_1/D_a = 0.50(x_{01}/a)^2$

ion density with the actual measured values. As is shown, these values are in much closer agreement.

4.5 TEMPERATURE MEASUREMENT

The main purpose of using an oxygen plasma to anodically grow oxide layers on silicon is because it is a low temperature process. In the process described above, it was confirmed that the temperature of the wafer was indeed less than 300° Celsius by indirectly measuring the temperature of the wafer using a thermocouple.

To get the thermocouple wires into the vacuum chamber, two small holes were drilled in one of the blank brass feed-throughs. The wires were then passed through two small pieces of glass tubing and the whole arrangement epoxied using a vacuum epoxy called Torr Seal.

The thermocouple wires were attached to the threaded bolt that supports the wafer holder above the ceramic dowel. The temperature of two different oxide growth arrangements were then measured. Both trials were conducted under the same conditions as those used in the growth of oxides as mentioned in section 4.3, Table 4.1 except that the time of anodization was shortened to 30 minutes.

In both experiments, the plasma was ignited, operating conditions of microwave power and pressure were adjusted, a bias was applied and an oxide was allowed to grow for 30 minutes. The bias was then disconnected, the plasma extinguished (the microwave power turned off), and the thermocouple wires attached to the electronic signal readout. The bias and plasma were turned off so as not to disrupt the electric signals the thermocouple wires send to the electronic interpretation

circuits.　The results of the two experiments are as follows:

Trial 1:

2 cm downstream, 40 V bias, no quartz tube:

Temperature = 255° Celsius

Trail 2:

6 cm downstream, 50 V bias, quartz tube:

Temperature = 195° Celsius

As can be seen from these results, the temperature of the wafer is indeed well below that of temperatures used to grow oxides in furnaces, which is generally above 900 $^{\circ}$C.

CHAPTER FIVE

Evaluation of ECR Plasma Anodization Oxides

What an absolutely marvelous substance!

5.1 INTRODUCTION

If a new process is to replace a reliable, tried and true process, it must hold some advantages over the old process while producing the same or improved results.   Plasma anodization of silicon using an oxygen plasma sustained with the MPDR operating in the ECR mode provides a low temperature means of growing oxide layers on silicon which holds the advantages outlined in Section 2.3.   But the oxides grown must be of the same or better quality as those obtained by thermal means if plasma anodization is to be a competing process.

Therefore, the oxides grown anodically must be rigorously tested to see if they do indeed have the necessary quality to be used in integrated circuit manufacture.   This chapter describes the many tests and instruments brought to bear in measuring the various properties of the plasma grown oxides.   Results of these test and comparison with oxides grown thermally are also presented.

5.2 UNIFORMITY AND THICKNESS EVALUATION

5.2.1 Dek Tak Procedure

One of the first physical characteristics of the oxides that must be quantified is the thickness and uniformity of the oxide layer. The first method employed in this endeavor was the use of a stylus instrument, a Dek Tak IIa. This instrument has a stylus with a 20 micron tip which is gently lowered onto the sample. After the stylus has made contact with the surface, the stage which holds the sample moves with respect to the stylus. The stylus and arm which holds it will move vertically with respect to the sample surface if valleys or peaks that may exist on the sample surface are encountered while the sample is moving. Thus the surface is mapped out with respect to the contact point in a manner which shows any points on the surface that are higher or lower than the contact point. Manufacturer's specifications claim a 10 Angstrom resolution. However, at time of use this instrument was mounted on an ordinary table in the basement of the Physics-Astronomy Building. Whenever a motor vehicle rumbled past outside, the readings would vary greatly.

To use this instrument, a checkerboard pattern was etched into the oxide layer using photolithographic methods and the mask shown in Figure 5.1. First, the wafers were cleaned using the cleaning procedure outlined in section 4.2.1 without the $H_2O:HF$ final rinse. Then the wafers were coated with HR-200 negative photoresist, exposed to ultraviolet light through the mask with a mask aligner, the photoresist developed and hard baked, and then the oxide etched. The
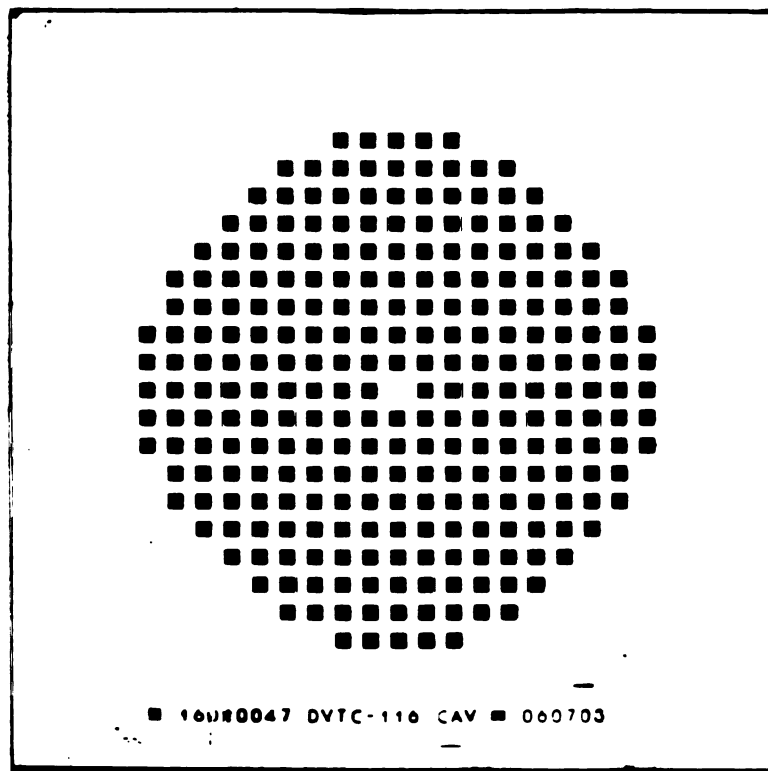
Figure 5.1 Mask with Checkerboard Pattern Used in Dek Tak Measurements

solution used for the oxide etch was a buffered oxide etch consisting of 7 parts 40% NH_4F and 1 part 50% HF. After the oxide was etched, the photoresist was removed with Olin Hunt Microstrip etch.

At this point, the checkerboard pattern was clearly visible on the wafer and ready for the Dek Tak measurement. The size of the squares etched through the oxide down to the silicon surface is 1.96 mm X 1.96 mm. From one edge of a square to the next, the distance is 1.84 mm. The Dek Tak was used to measure the vertical distance between the oxide surface and the bottom of a square (the silicon surface) that was etched through the oxide layer.

As an example measurement, first the level of the silicon surface was determined relative to zero, then the level of the oxide was measured again relative to zero. But each of these measurements had relatively large uncertainties, 10 - 20 Å. Thus the oxide thickness and the uncertainties were computed as follows:

$$(x_1 \pm e_1) - (x_2 \pm e_2) = x_1 - x_2 \pm (e_1^2 + e_2^2)^{1/2}$$

A sample calculation from DS-16 is presented here as an example:

oxide surface:	1000 ± 20 Å
silicon surface:	170 ± 15 Å
oxide thickness	830 ± 25 Å.

5.2.2 Ellipsometer Procedure

The preferred method of oxide thickness and uniformity character- ization employed in this work was the use of an ellipsometer. The specific instrument used is a Gaertner L115 B Scanning Ellipsometer. As the name suggests, the ellipsometer will automatically scan a

surface in several different ways that can be chosen by the operator. For example, an X-Y grid can be chosen with the coordinate points separated by any desired distance and the oxide thickness measured at the coordinates. This automatic system is controlled by an IBM PS/2 Model 30 computer.

The ellipsometer utilizes an monochromatic light provided by a Helium-Neon laser which emits a red light with a wavelength of 6328 Angstroms. The laser light is polarized and focused on the oxide layer. The oxide layer is transparent to and non-absorbing of this particular wavelength of light. However, SiO_2 has an index of refraction different from that of air. Thus the laser beam is diffracted and partially depolarized. Following Snell's Law of Reflection, the beam is reflected from the silicon surface below the oxide layer at an angle equal to the incident angle. A rotating analyzer placed in the path of the reflected beam determines the amount of diffraction and depolarization and from this determines the thickness of the oxide film.

The theory of the use of ellipsometers for silicon dioxide film characterization is well documented as a highly accurate and reliable method for determining thicknesses of pure, thermally grown oxide layers. The specifications of this instrument claim an oxide can be measured to within $\pm$ 3 Angstroms. A very obvious advantage of this method of oxide thickness and uniformity characterization is the ease and much shorter time needed for the analysis as compared with the Dek Tak IIa instrument described in section 5.2.1, as well as the fact that photolithography and oxide etching were not required.

5.2.3 Results of Dek Tak and Ellipsometer Measurements

One of the first experiments performed was an investigation into the amount and uniformity of oxide that could be grown as a function of distance from the plasma discharge region. To do this, 3 wafers were anodized at 40 V dc under the conditions described in Section 4.3 at distances of 2, 4, 6, 8, and 10 cm below the discharge. Three wafers were done at each distance to investigate repeatability. All fifteen of these wafers were anodized using the baseplate as the cathode and without the quartz tube in place to shield the wafer from sputtering contamination. Figure 5.2 shows the oxide thickness measured at the center of each wafer. Center thicknesses are reported due to the very apparent non-uniform oxide thickness, when viewed by eye, of the wafers anodized at 2 cm downstream from the plasma discharge. In this case, the center of the wafer had a thicker film grown than the edges. The wafers anodized at 4, 6, 8 and 10 cm downstream, however, appeared to the eye to be very uniform.

The oxide thicknesses in Figure 5.2 were measured using the Dek Tak instrument. Four measurements around the center square of the checkerboard pattern on each of the three wafers grown at a given downstream distance were performed. Thus each data point represents the average of twelve measurements and the error bar represents the standard deviation. Studying this data, it is seen that the oxide thickness grown falls off in an exponential manner as the distance between the wafer and the baseplate is increased. This is also evidenced by a best fit line. This follows, qualitatively, diffusion theory of plasma species as discussed in Section 4.4 and also the
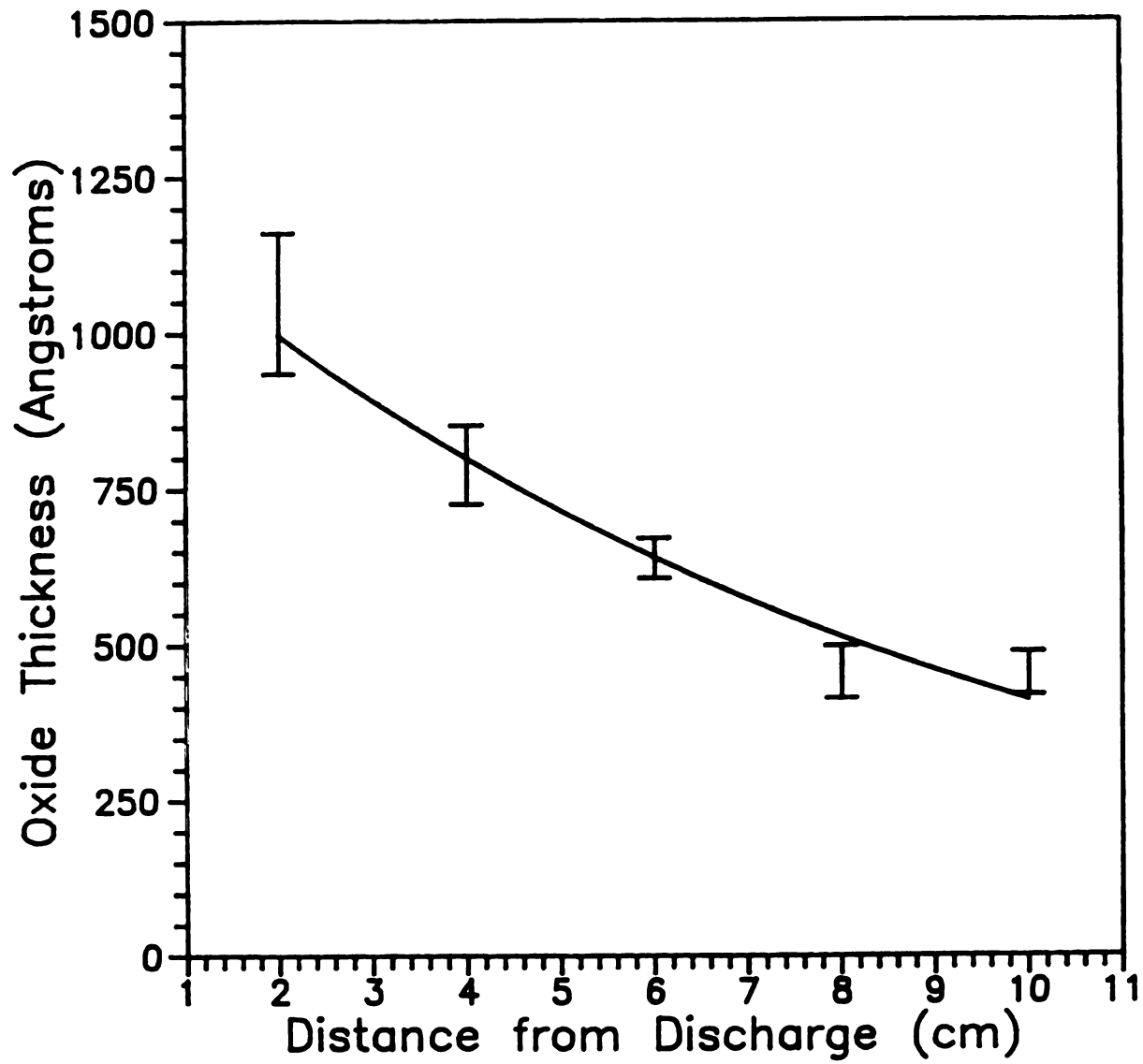
Figure 5.2 The Oxide Thickness Grown vs. Down Stream Distance
The solid line is a data fit using $d_{ox} = 1245\ e^{-0.111z}$

measured density of ions.

Measurements to investigate the uniformity of the oxide on the wafers were done relative to two diagonals of the wafer that were parallel to and perpendicular to the orientation of the input power probe axis during anodization. As mentioned in Section 4.2.2, the major flat of the silicon wafer was oriented 180° from the input power probe. Figure 5.3 is a cut-away, top view of the experimental configuration which depicts this orientation along with Cartesian coordinates that were used in the measurement of oxide uniformity. In the oxide thickness results reported below, values at positive distances on the parallel axis were on the part of the wafer closest to the input power probe. For example, in Figure 5.4a, the oxide thicknesses measured parallel to the power input probe axis from +38 mm to -38 mm are measurements performed along the wafer diagonal from a point on the wafer nearest the power input probe to a point furthest from the power input probe, i.e. from (0,40) to (0,-40). The values measured along the perpendicular axis were measured from (40,0) to (-40,0).

Measurements to investigate the uniformity of the oxide on the wafers anodized at each distance downstream were begun using the Dek Tak instrument. Figures 5.4a, 5.4b, and 5.4c show the thickness of oxides measured with this instrument, Figures 5.4a and 5.4b on a wafer anodized 4 cm below the discharge and Figure 5.4c on a wafer 8 cm downstream. In Figures 5.4a and 5.4c the values are the oxide thicknesses measured across the wafer parallel to the input probe axis. In Figure 5.4b, the oxide thickness was measured along a diagonal perpendicular to the power input probe axis. As can be seen, these
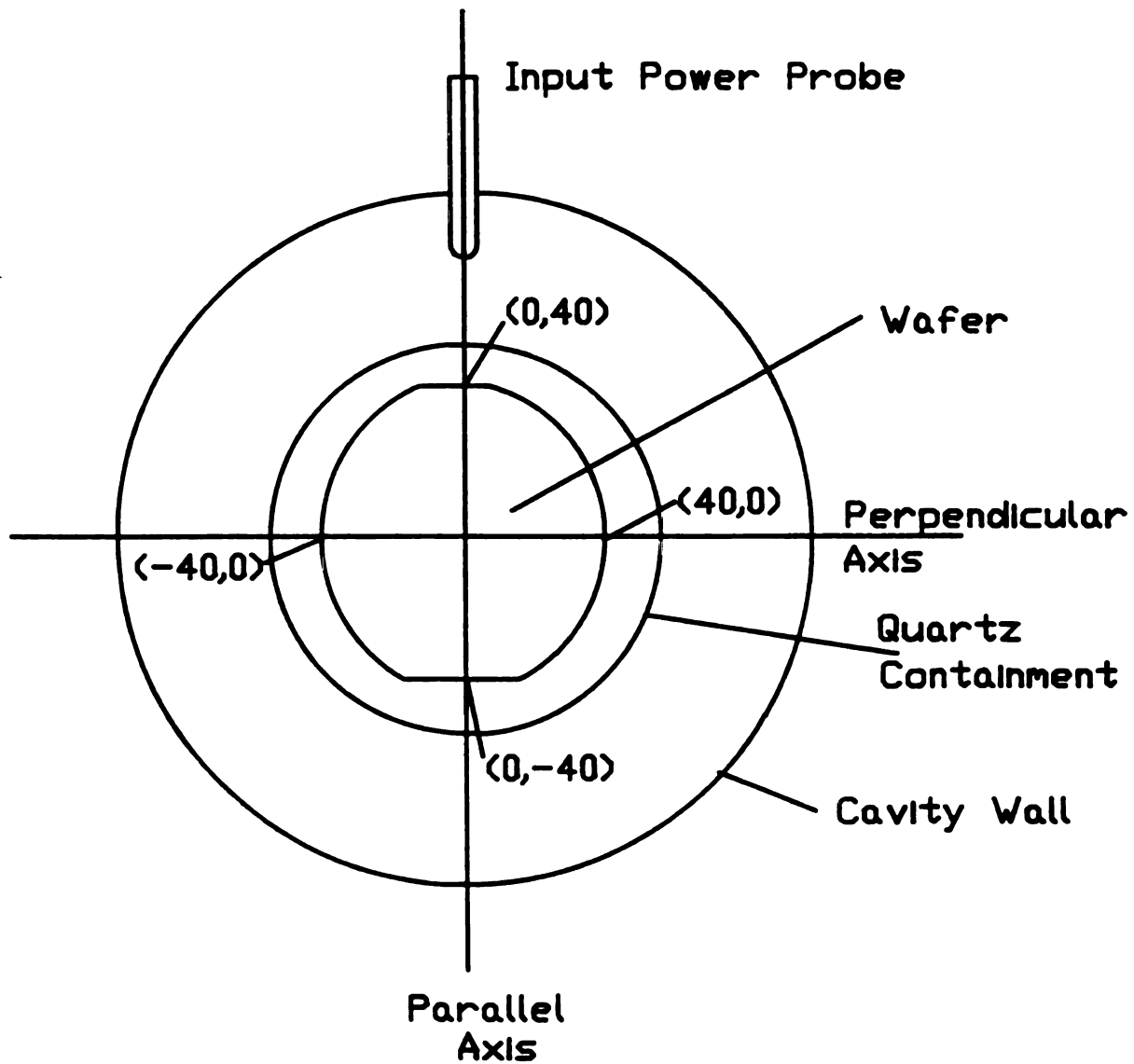
Figure 5.3 Cut-Away, Top View of the Experimental
Configuration Depicting the Orientation of the Silicon
Wafer Relative to the Input Power Probe Axis
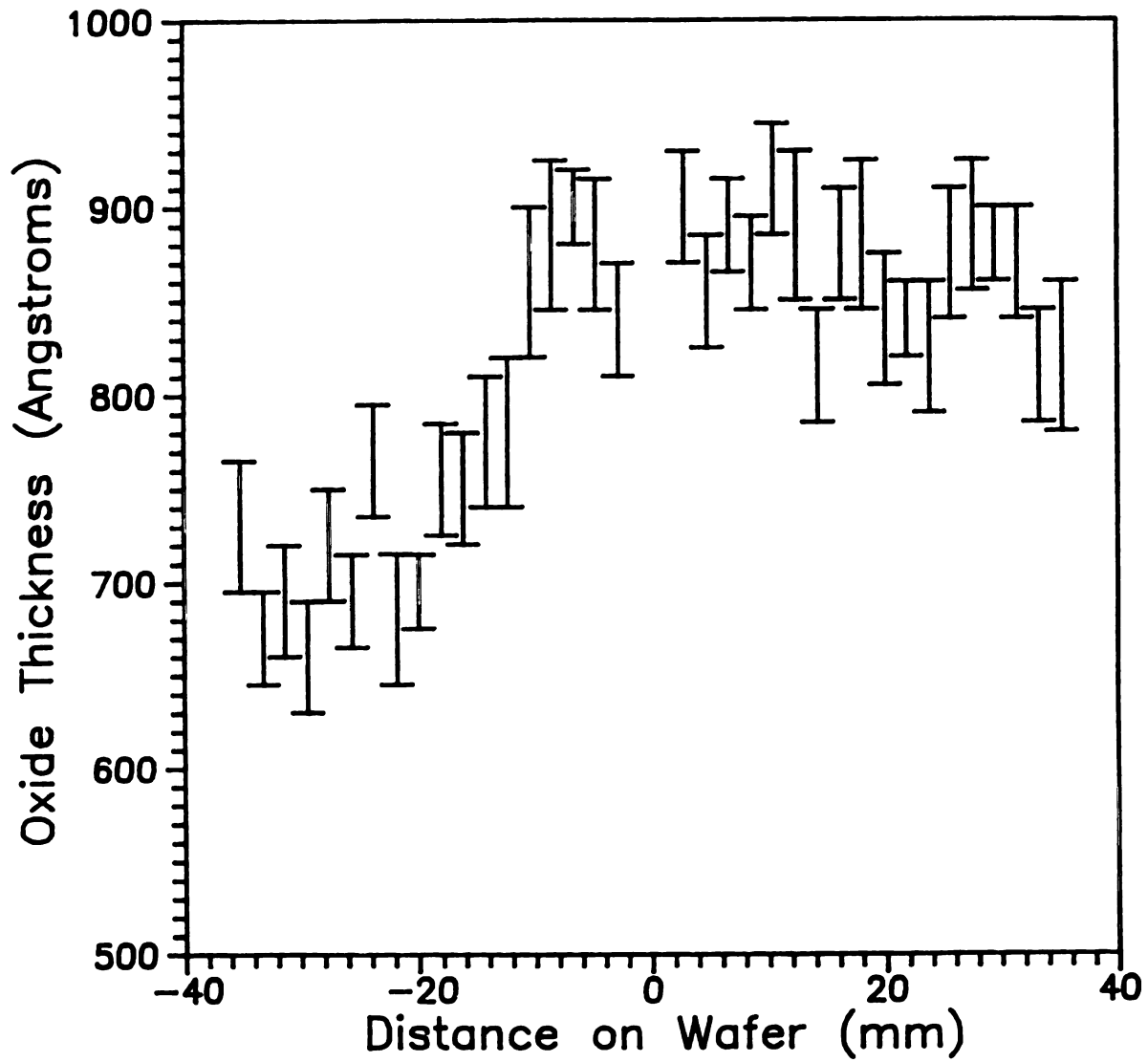
Figure 5.4a   Oxide Thickness Uniformity Grown 4 cm Downstream from
the Plasma Discharge, Parallel to the Probe Axis (Dek Tak Values)
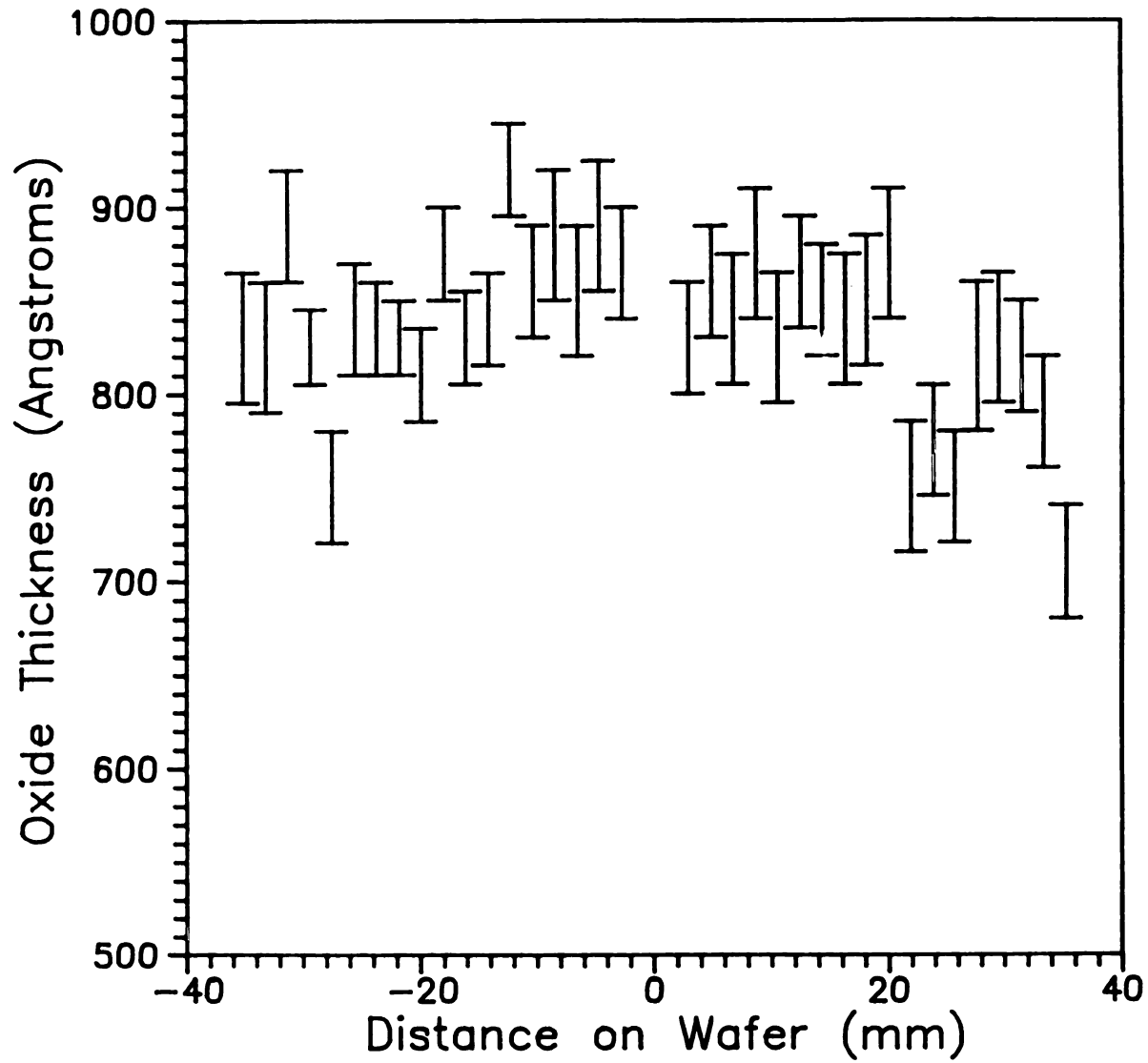
Figure 5.4b Oxide Thickness Uniformity Grown 4 cm Downstream from
the Plasma Discharge, Perpendicular to the Probe Axis (Dek Tak Values)
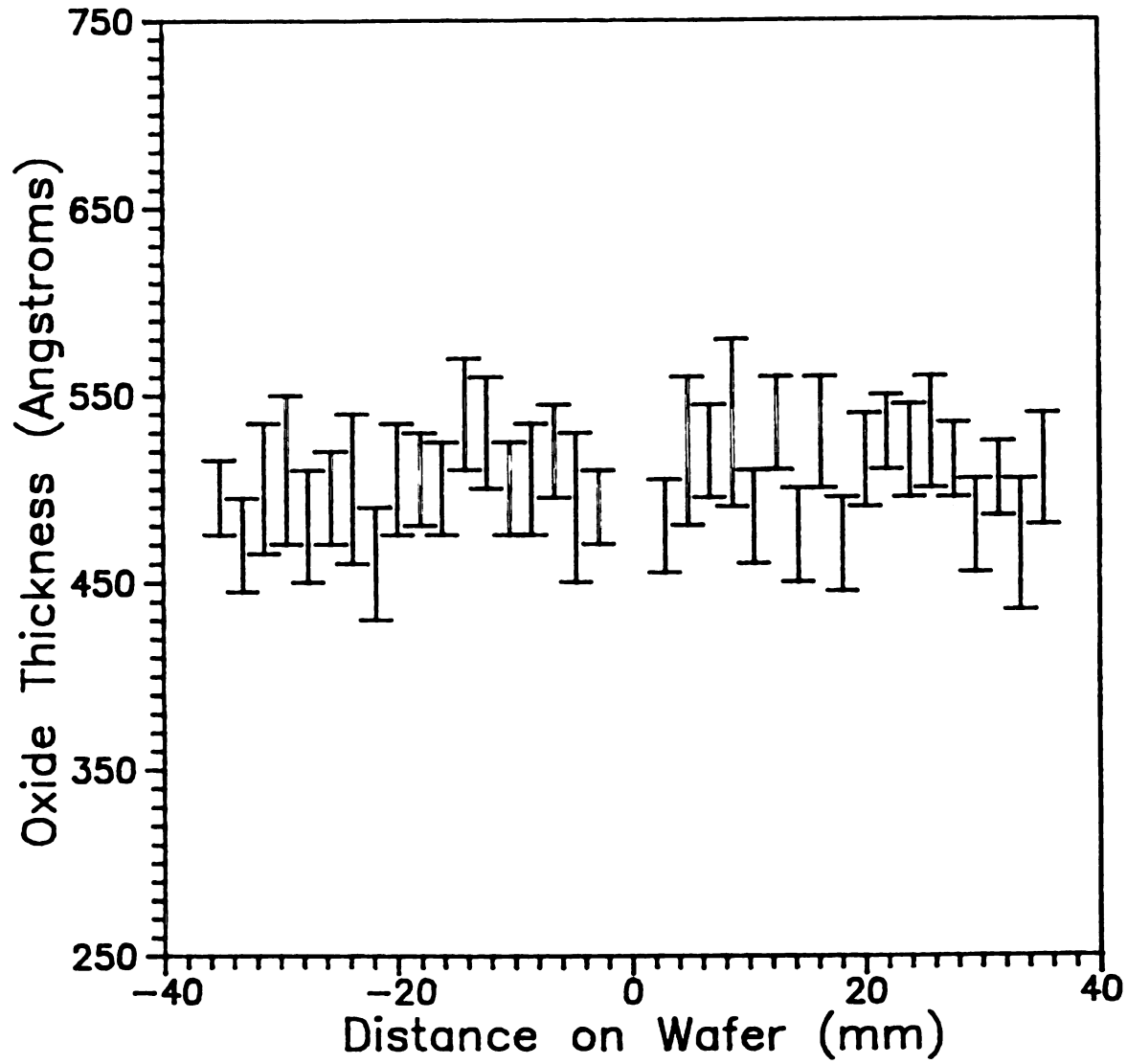
Figure 5.4c Oxide Thickness Uniformity Grown 8 cm Downstream from the Plasma Discharge, Parallel to the Probe Axis (Dek Tak Values)

measurements had a high degree of uncertainty. This is due to the limitations of the Dek Tak instrument mentioned in section 5.2.1. Thus measurements using this instrument were discontinued with the arrival of the ellipsometer.

The oxide thicknesses measured at the center of the wafers did not vary significantly within each group of three wafers grown at the same distance from the oxygen plasma. Hence, measurements using the ellipsometer to determine the uniformity of the oxides were performed on one wafer anodized at each distance downstream. These measurements were done in three different manners. The first two types of measurements were similar to the Dek Tak measurements, i.e. a line of oxide thicknesses were measured parallel to and perpendicular to the input power probe axis, with the points spaced every three millimeters. The third measurement was a grid measurement with oxide thickness values determined at X,Y coordinates spaced every seven mm's.

The results of the measurements taken parallel and perpendicular to the input power probe for each wafer are summarized in Figures 5.5a and 5.5b through 5.9a and 5.9b. The oxide thickness axis (y-axis) are all plotted with a range of 500 Å to show the differences in uniformity of the oxide thickness grown at each distance downstream.

The results of the measurements taken on an X,Y grid are summarized in Figures 5.10 through 5.14. These measurements are shown with a vertical range of 300 Å to again show the differences in uniformity.

Table 5.1 is a summary of the oxide thickness measurements. For each downstream distance, all oxide thickness values were used, i.e. all 89 points from the X,Y grid and all 27 points from each line of
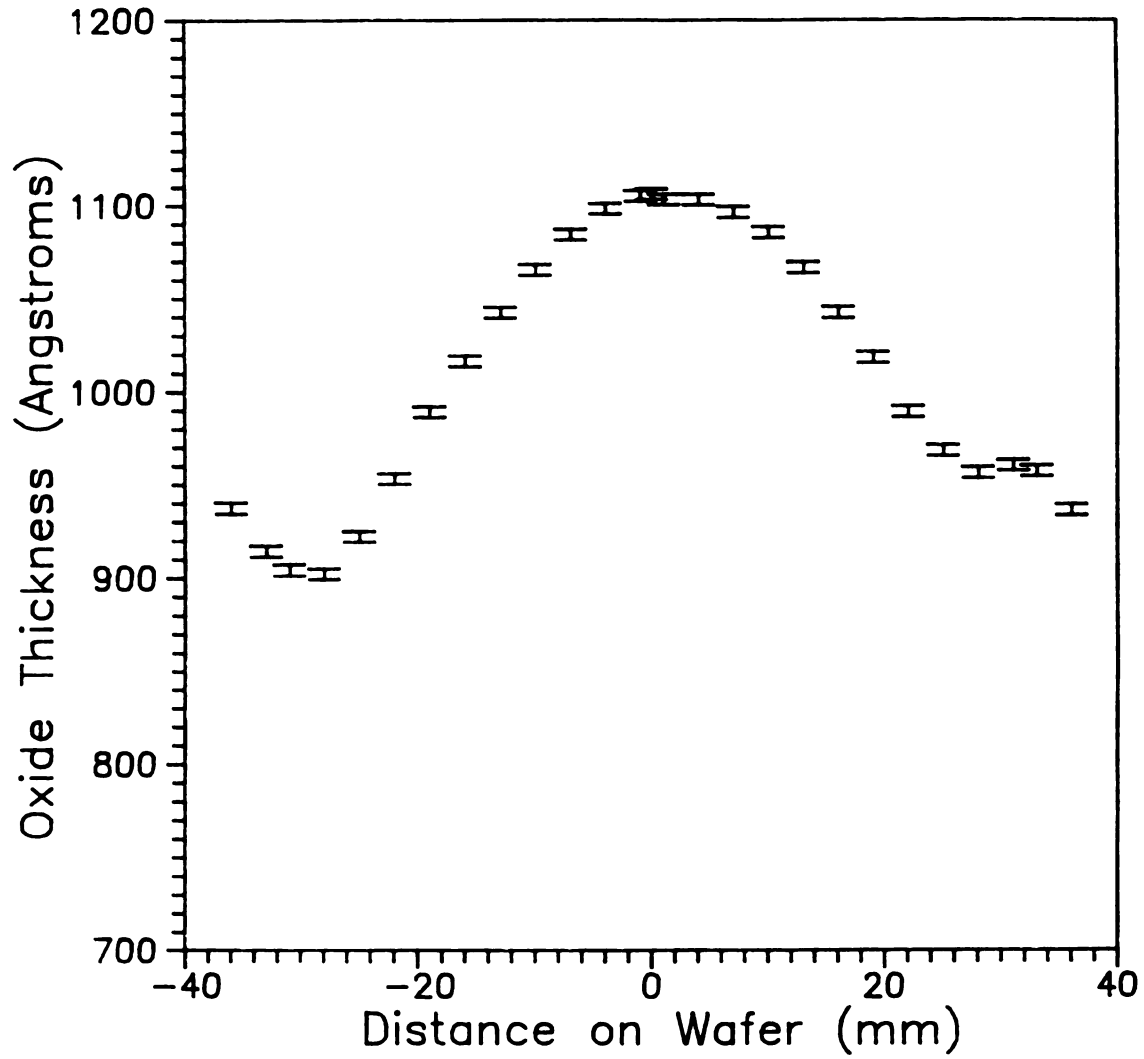
Figure 5.5a Oxide Thickness Uniformity Grown 2 cm Downstream
from the Plasma Discharge, Parallel to the Probe Axis
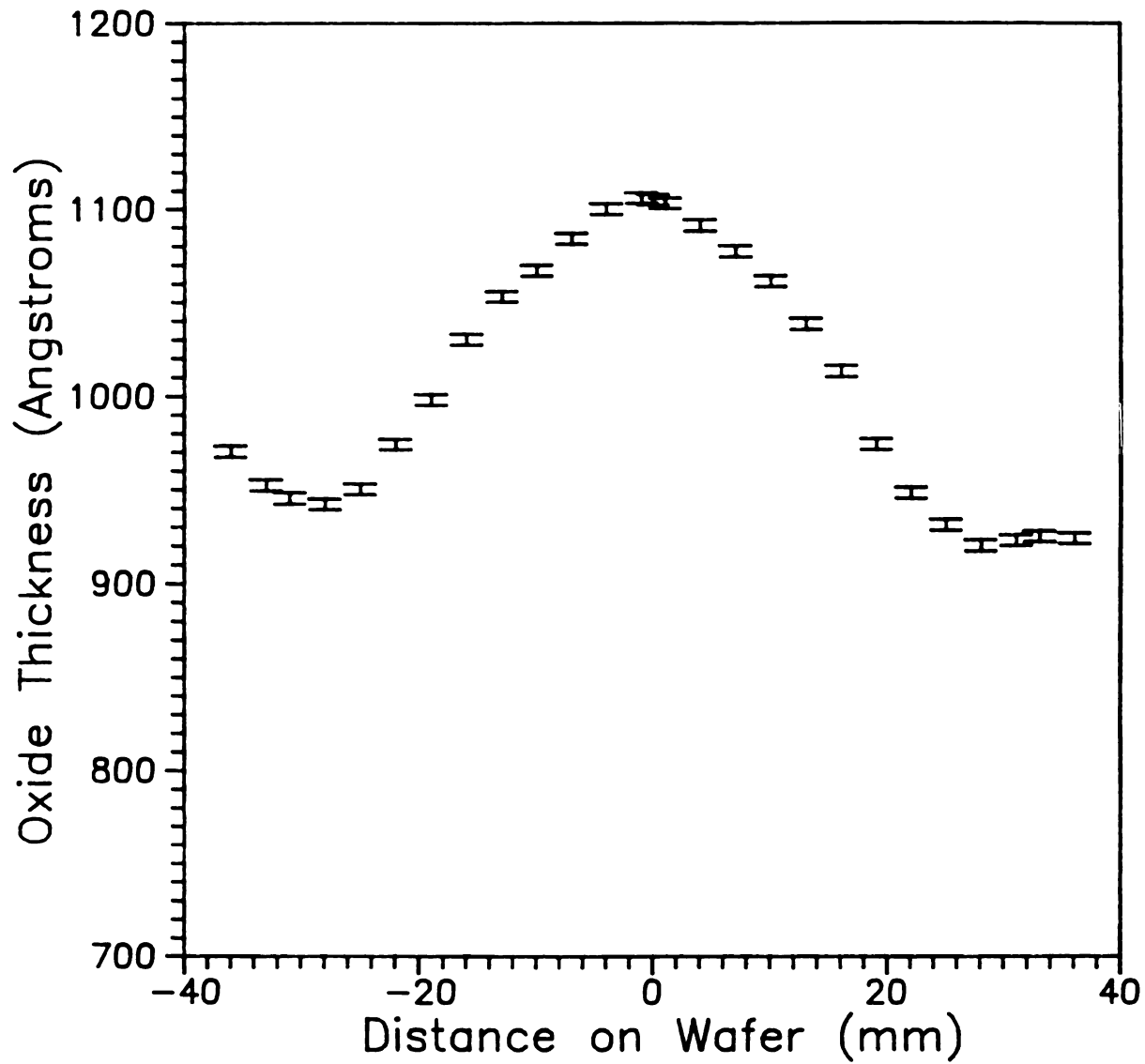
Figure 5.5b Oxide Thickness Uniformity Grown 2 cm Downstream
from the Plasma Discharge, Perpendicular to the Probe Axis
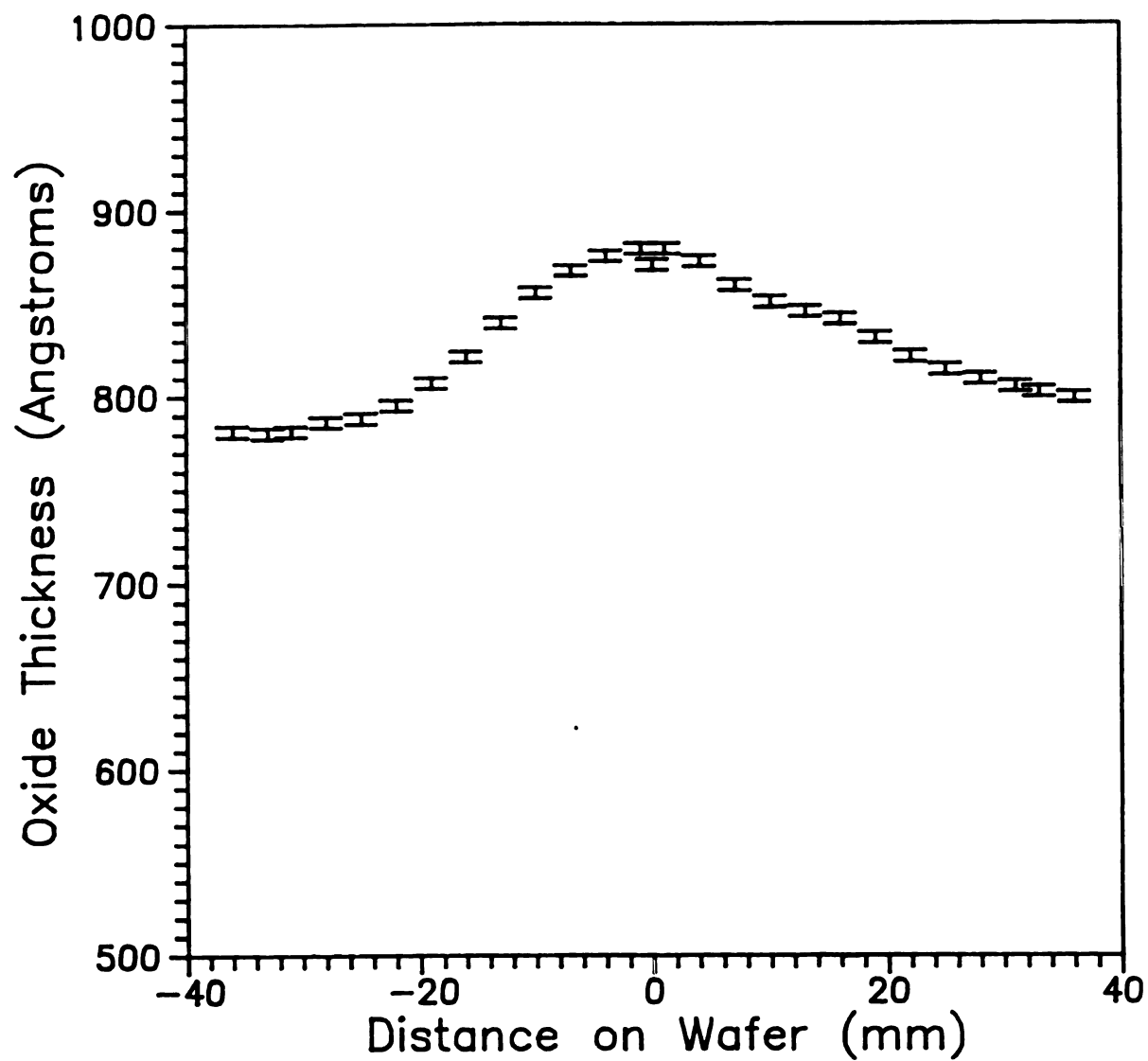
Figure 5.6a Oxide Thickness Uniformity Grown 4 cm Downstream
from the Plasma Discharge, Parallel to the Probe Axis
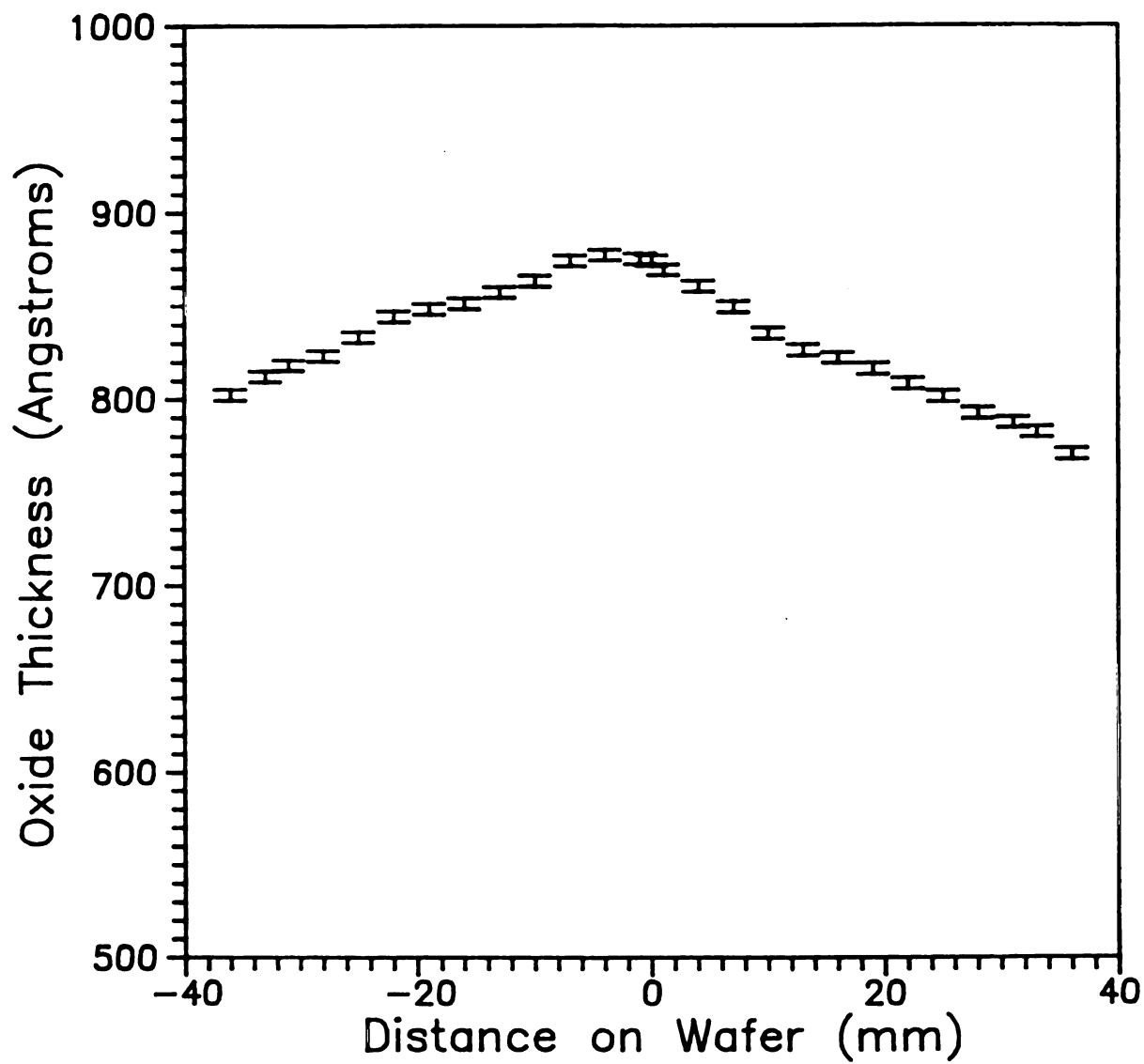
Figure 5.6b Oxide Thickness Uniformity Grown 4 cm Downstream
from the Plasma Discharge, Perpendicular to the Probe Axis
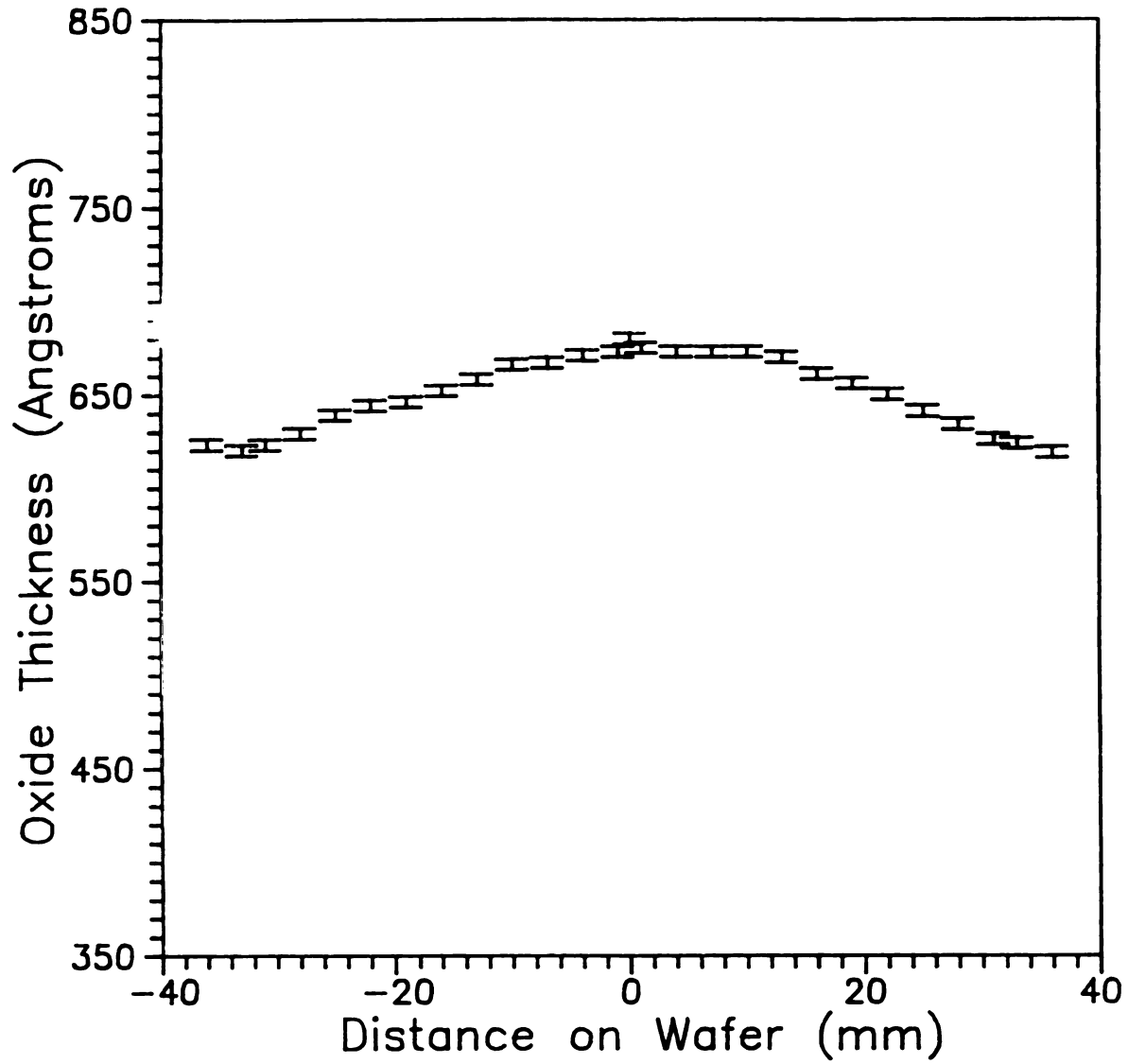
Figure 5.7a Oxide Thickness Uniformity Grown 6 cm Downstream
from the Plasma Discharge, Parallel to the Probe Axis
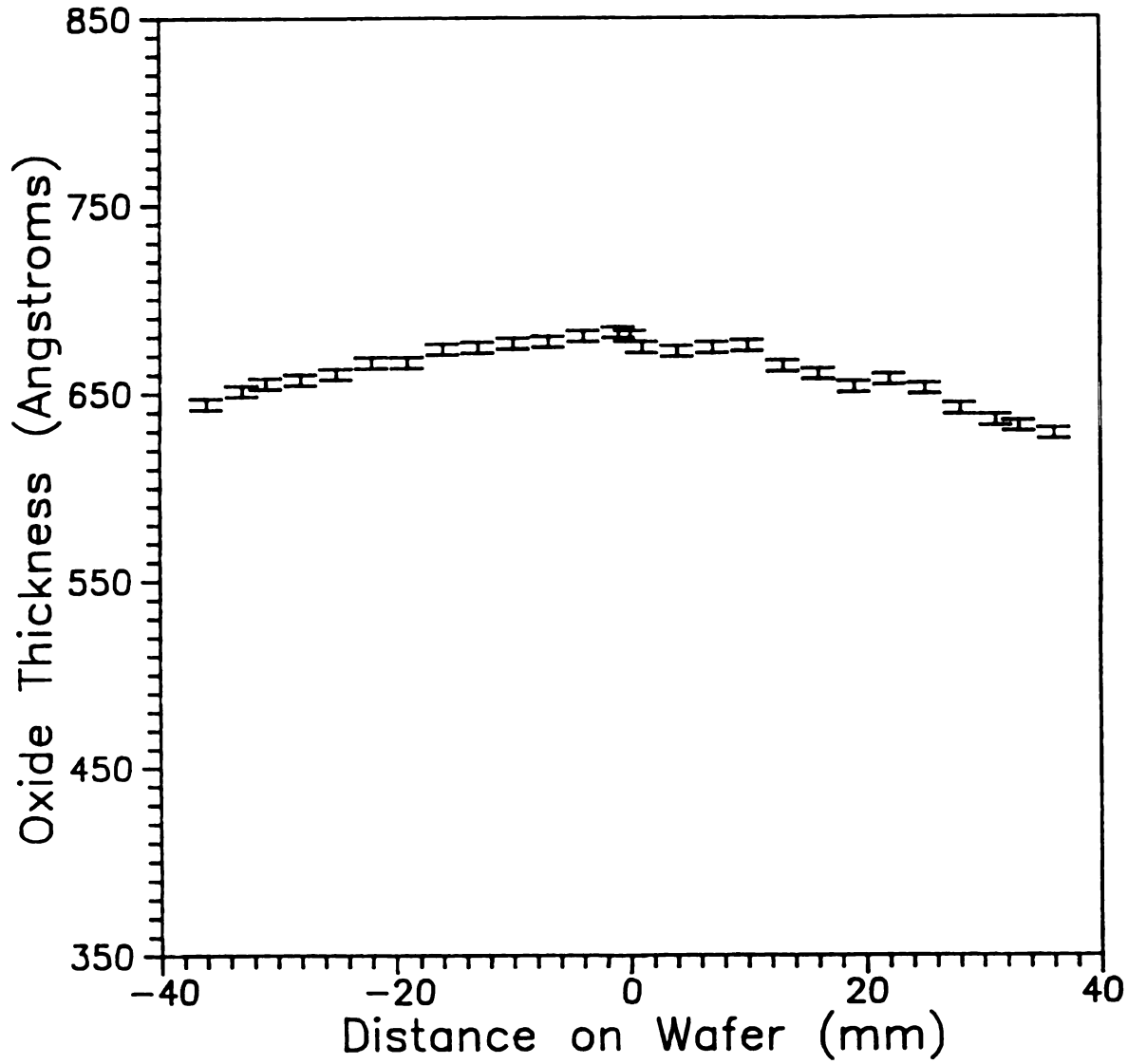
Figure 5.7b Oxide Thickness Uniformity Grown 6 cm Downstream
from the Plasma Discharge, Perpendicular to the Probe Axis
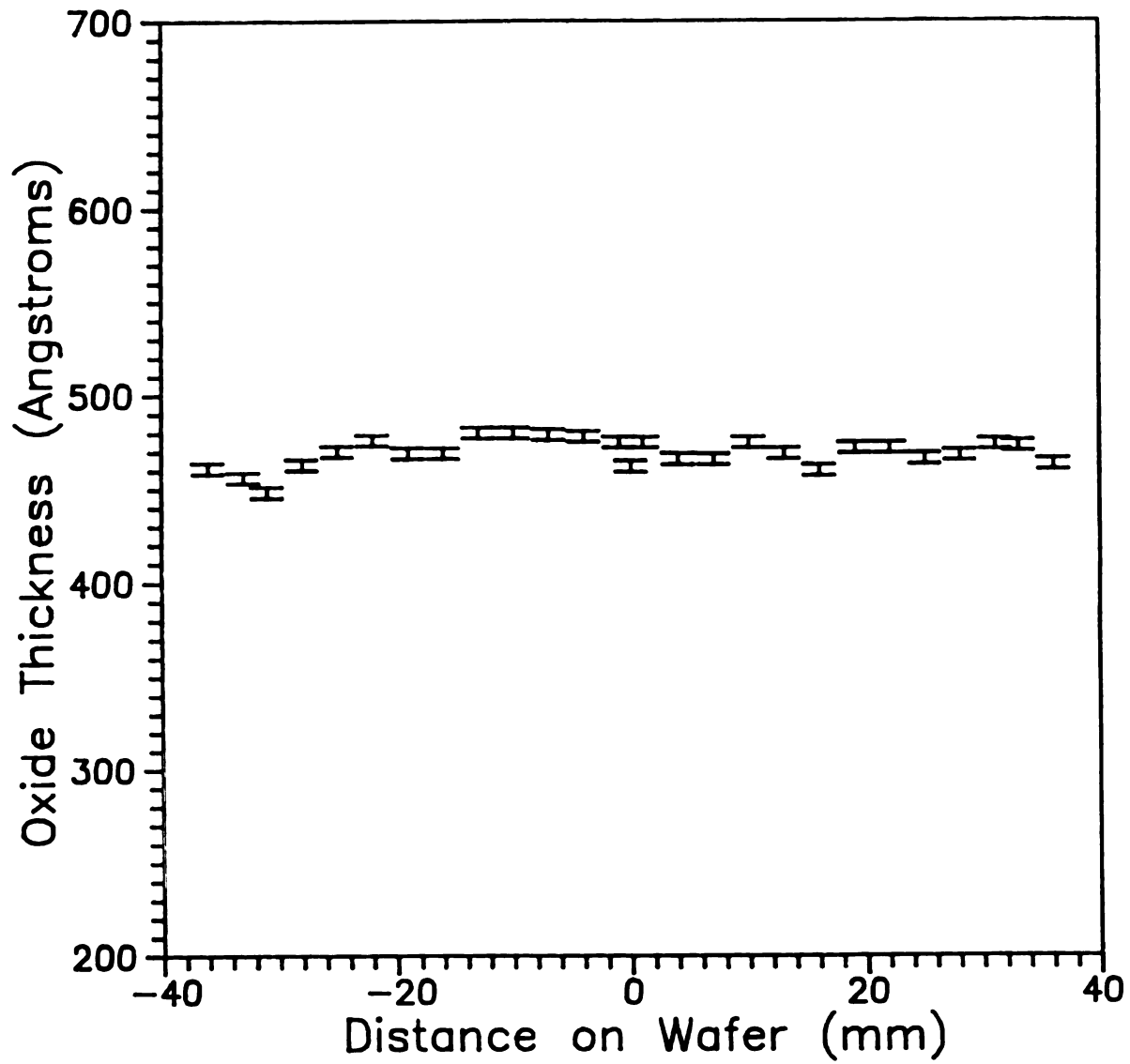
Figure 5.8a Oxide Thickness Uniformity Grown 8 cm Downstream
from the Plasma Discharge, Parallel to the Probe Axis
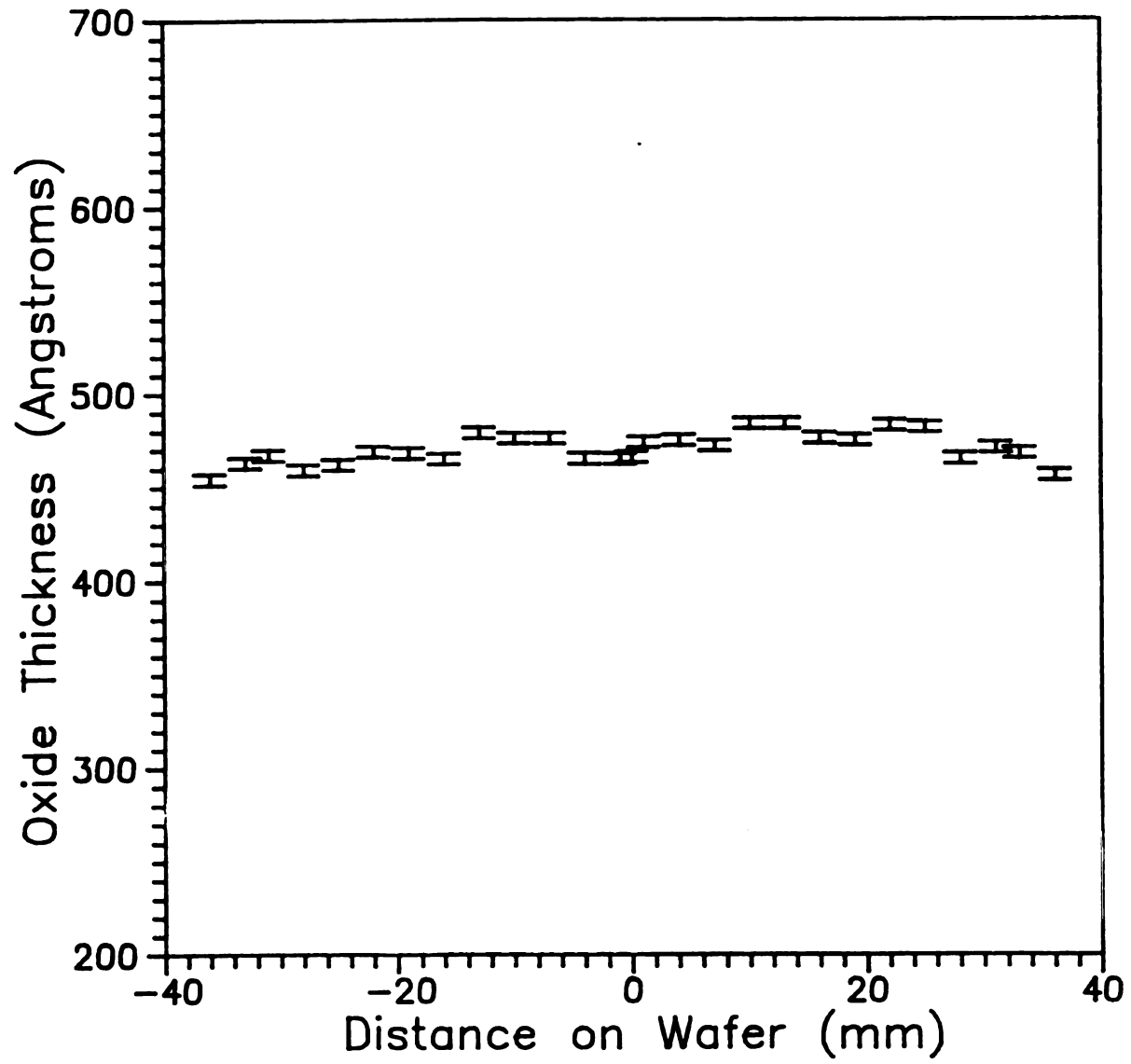
Figure 5.8b Oxide Thickness Uniformity Grown 8 cm Downstream
from the Plasma Discharge, Perpendicular to the Probe Axis
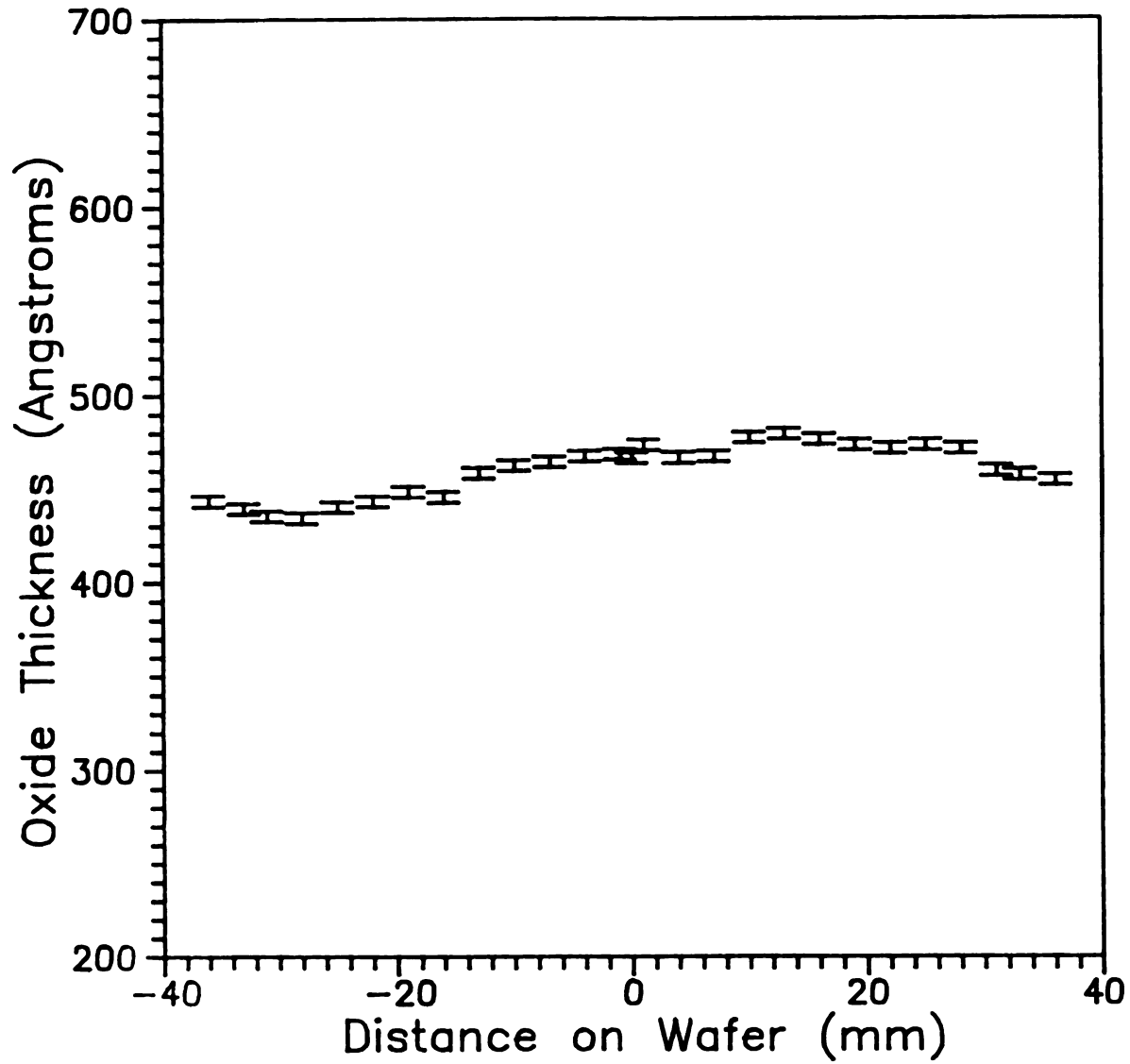
Figure 5.9a Oxide Thickness Uniformity Grown 10 cm Downstream
from the Plasma Discharge, Parallel to the Probe Axis
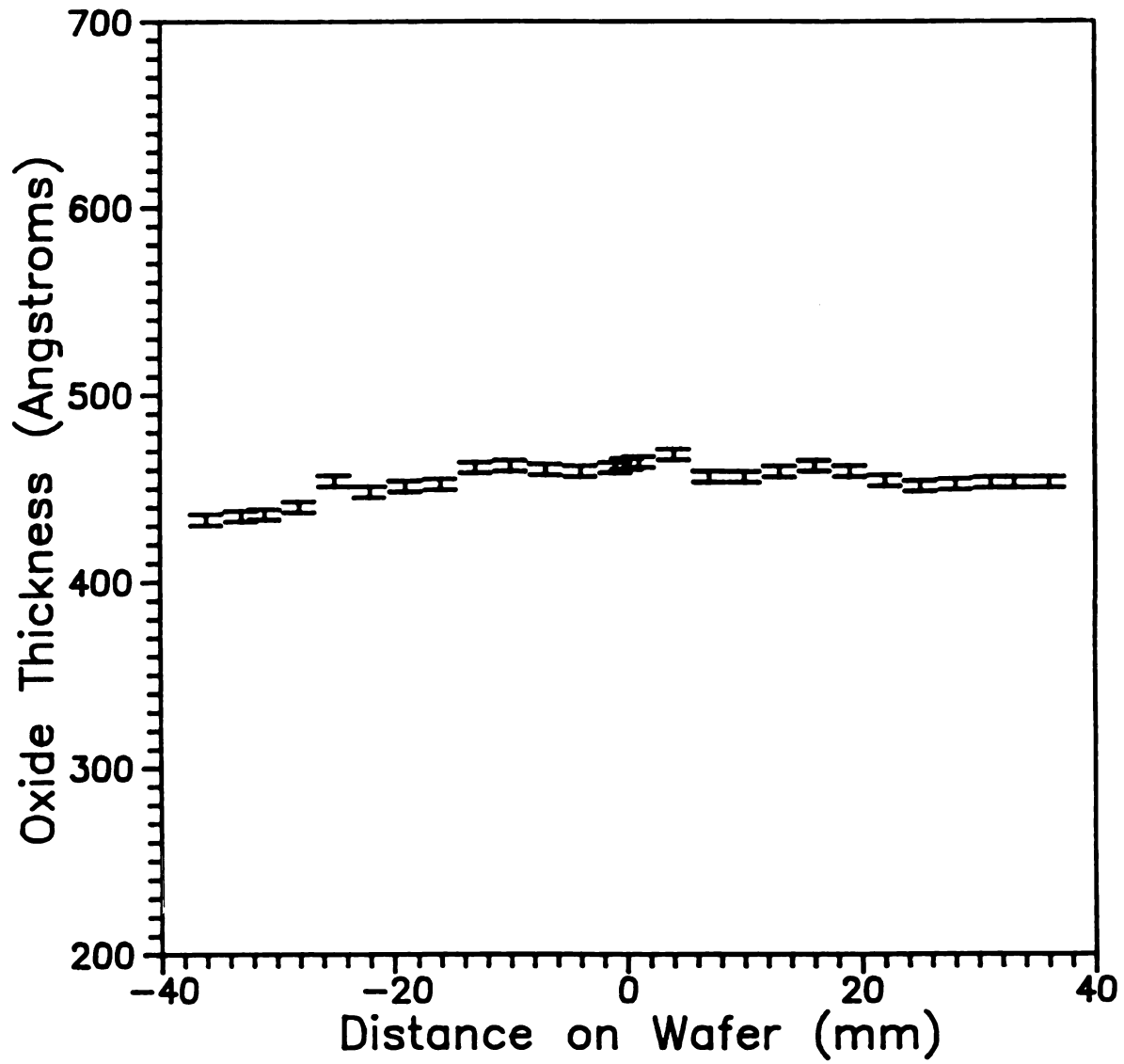
Figure 5.9b Oxide Thickness Uniformity Grown 10 cm Downstream
from the Plasma Discharge, Perpendicular to the Probe Axis

PROBE
SIDE

800

700

600
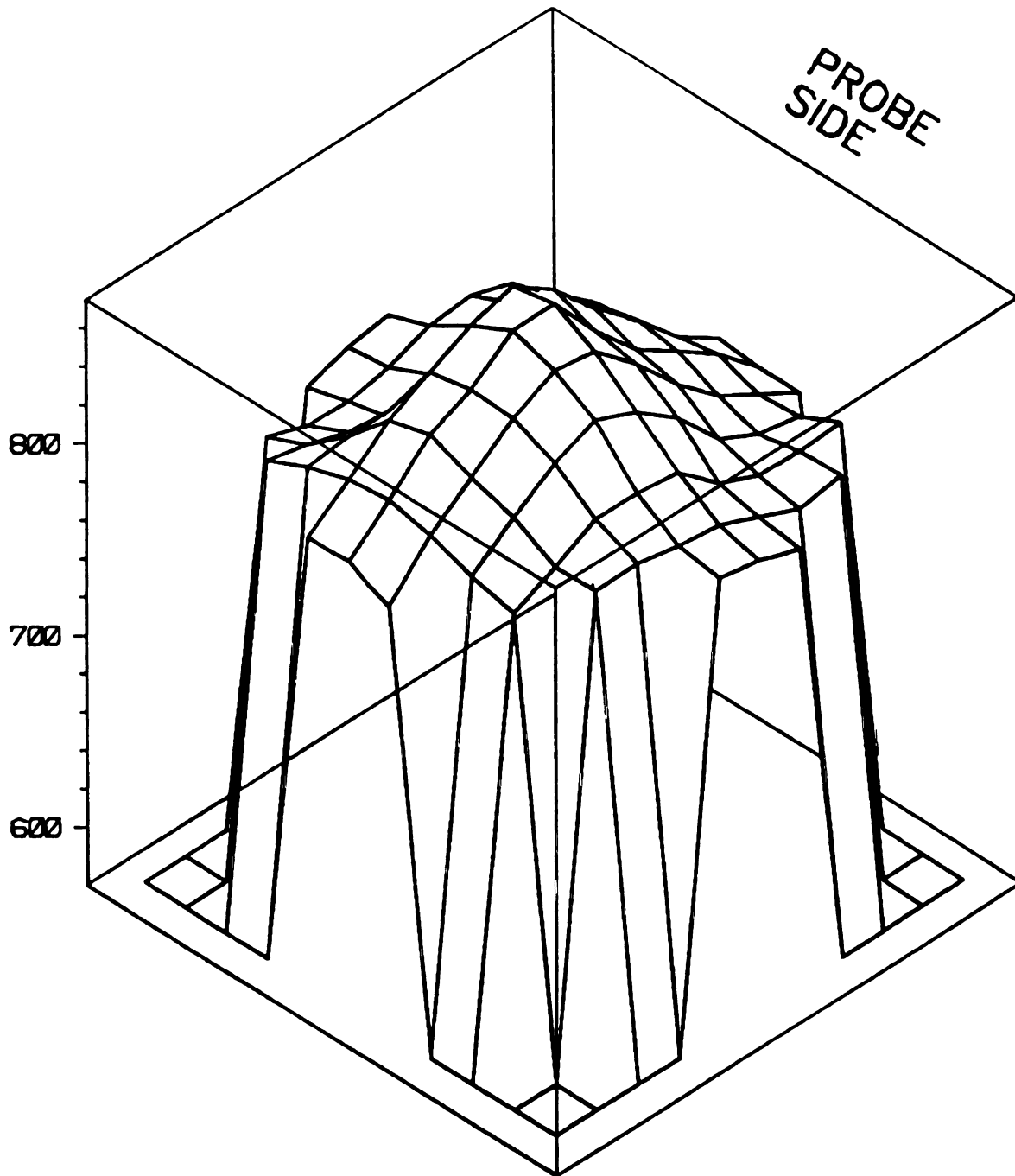
Figure 5.11 Oxide Thickness Uniformity Over Wafer
Surface Grown 4 cm from the Plasma Discharge
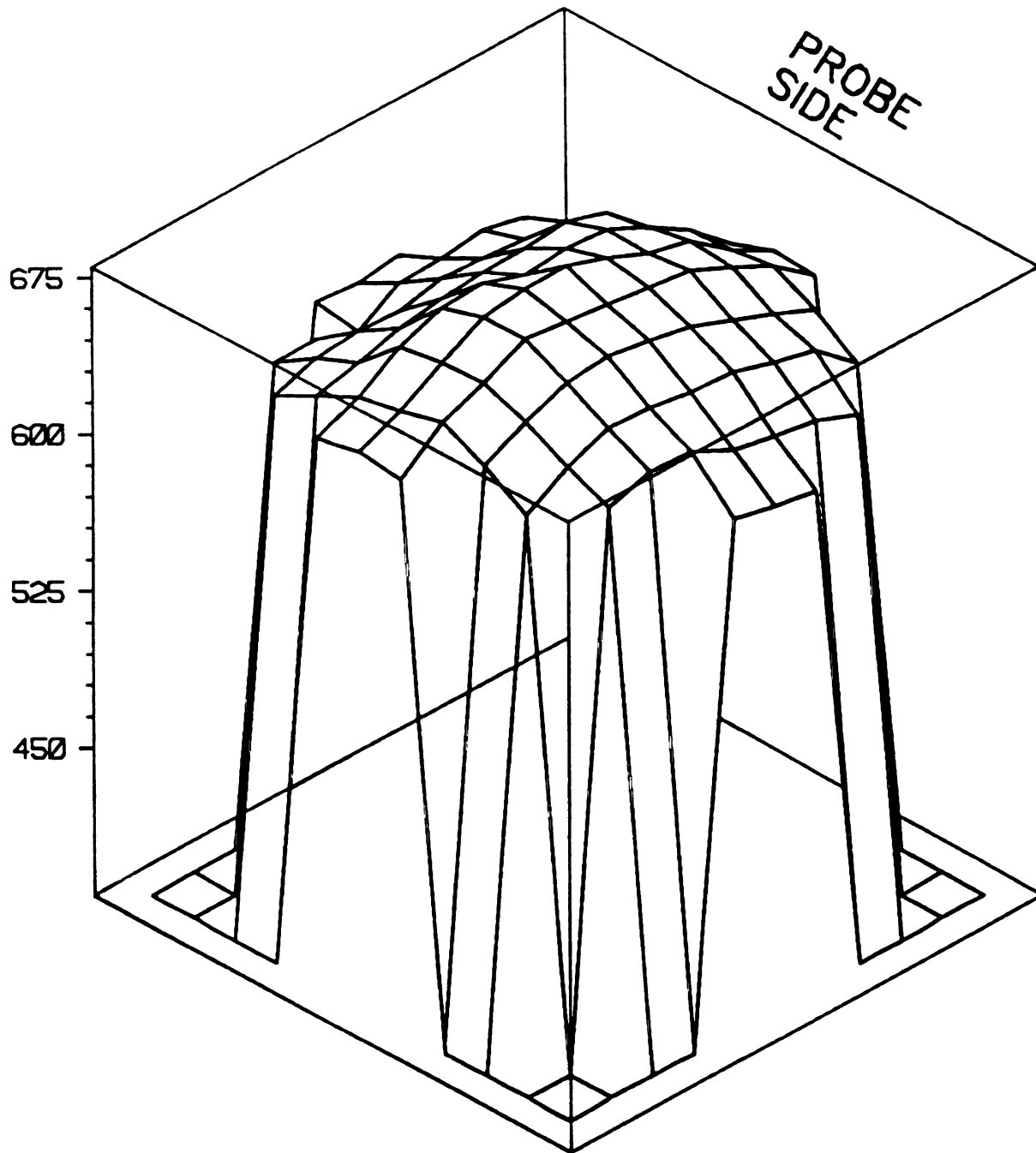
Figure 5.12 Oxide Thickness Uniformity Over Wafer
Surface Grown 6 cm from the Plasma Discharge
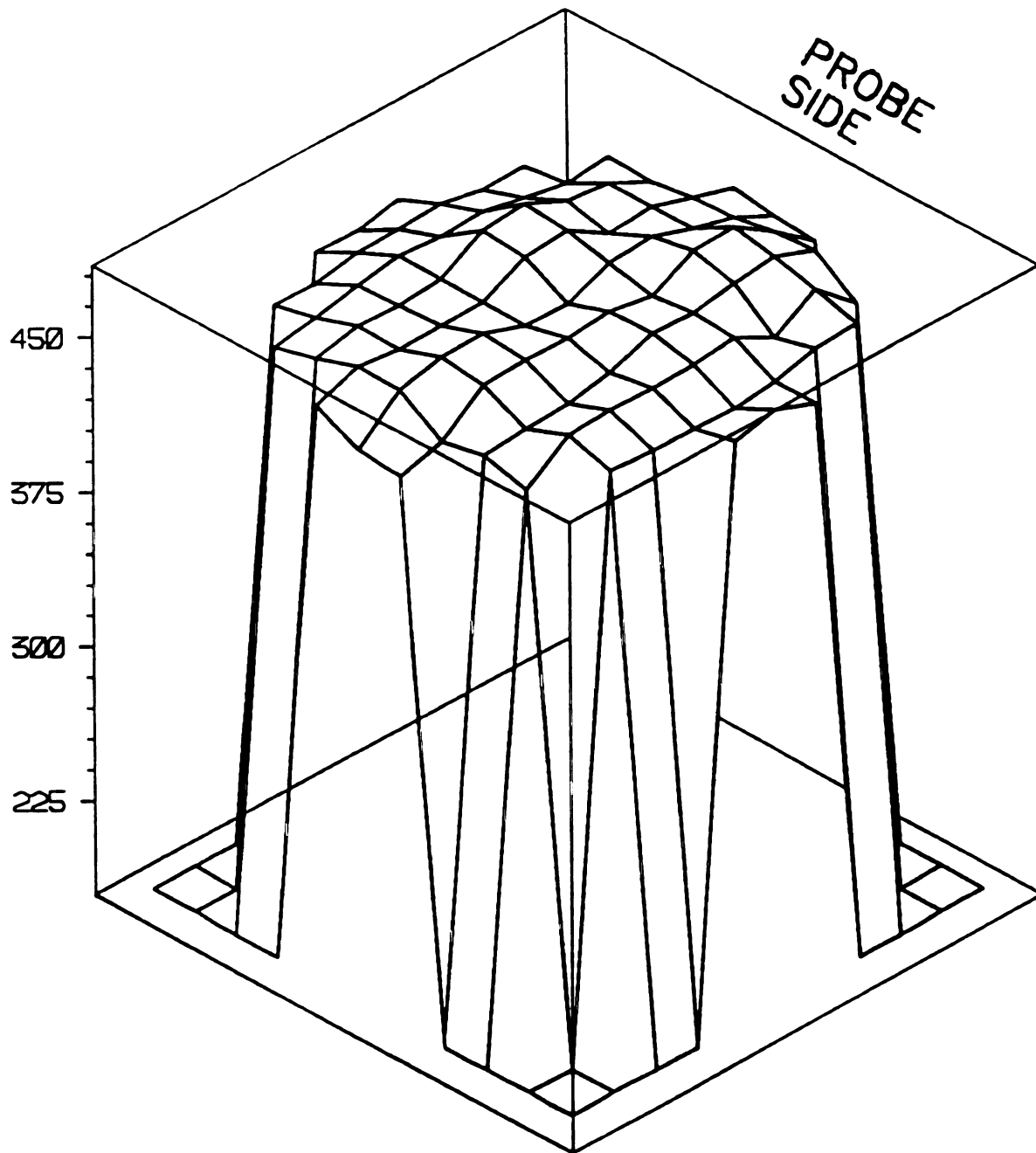
Figure 5.13 Oxide Thickness Uniformity Over Wafer
Surface Grown 8 cm from the Plasma Discharge
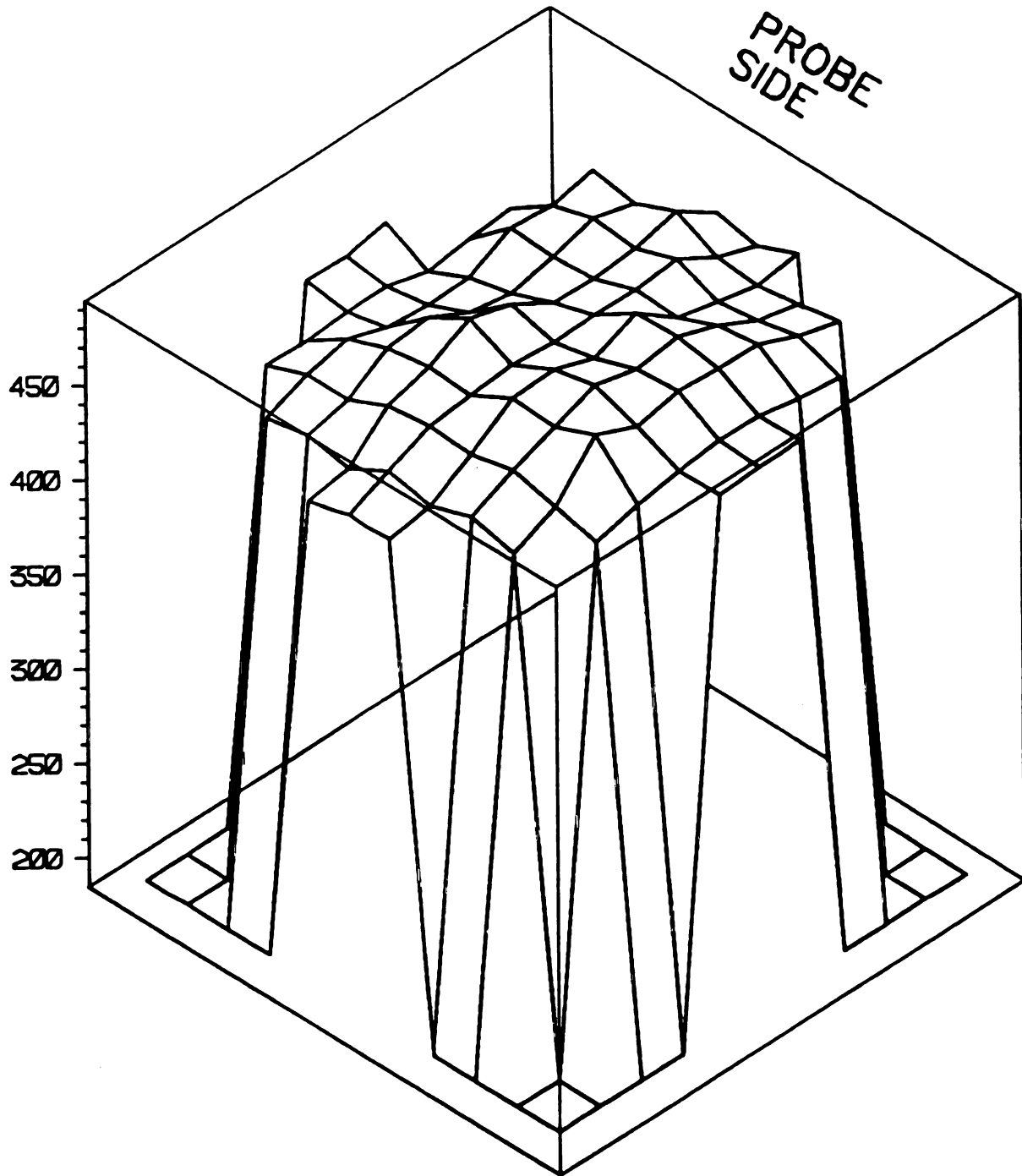
Figure 5.14 Oxide Thickness Uniformity Over Wafer
Surface Grown 10 cm from the Plasma Discharge

Table 5.1 Summary of Oxide Thickness and Uniformity Results

Distance Downstream	Largest Thickness	Smallest Thickness	Average Thickness	σ	$\%_1$	$\%_2$
2	1106	902	990	61	6.2	18.4
4	879	770	819	29	3.5	12.4
6	682	616	651	18	2.8	9.7
8	484	448	467	8	1.7	7.4
10	489	433	462	13	2.8	11.5

oxide thickness values. The last two columns are percent variations determined by two methods, $\%_1$ was determined by dividing the standard deviation, σ, by the average oxide thickness and $\%_2$ was determined by subtracting the smallest thickness from the largest thickness and dividing by the largest thickness.

Upon examination of this data, it is observed that the oxide thicknesses become more uniform as the distance is increased between the wafer and the plasma discharge up to the oxide grown at 8 cm below the discharge. This is due to the ion density distribution becoming more uniform or less bell shaped as a function of radial distance from the center of the cylindrical vacuum chamber. This is qualitatively consistent with diffusion theory as discussed in Section 4.4. However, there is actually a slight increase in non-uniformity from the oxide grown at 8 cm below the discharge to the oxide grown at 10 cm downstream. The reason for this is not obvious. One possibility is that as the downstream distance is increased, more of the substrate support rod is exposed to the processing plasma. There may eventually be a

trade off between increasing uniformity due to diffusion and increasing introduction of a perturbation to the plasma.

Another observation that can be made after consideration of the graphs of oxide thickness measured parallel to the input probe during oxidation, is that the oxide thickness nearer the probe are somewhat larger than those on the opposite side of the wafer. This is very noticeable in Figures 5.5a and 5.6a (oxides grown 2 and 4 cm downstream respectively), with the oxides becoming more equal on either side of the wafer in Figures 5.7a, 5.8a, and 5.9a. The larger oxide thickness grown on the wafer edge that was nearest the input probe during anodization is the result of a near-field effect, i.e. the field nearest the input power probe is stronger, hence there is a slightly higher density of ions in this region of the discharge.

In Section 4.4, results from double Langmuir probe measurements were presented. These measurements showed a much higher degree of variation than did the resulting oxide films. For instance, if the smallest measured ion density is subtracted from the largest density and then divided by the largest density to obtain a percent variation, then at 4 cm downstream the variation is 30.5%, at 6 cm, 16.2% and at 8 cm, 12.5%. When compared with the percent variations presented in Table 5.1, the variations in ion density are much higher than the variations measured in oxide thickness. One possible explanation is that oxide growth is self limiting, i.e. as the oxide grows thicker, the growth rate slows because of the larger distance the ions must travel through the oxide film to reach the interface between the oxide and silicon substrate where it is believed that the formation of new oxide takes place. A second possible explanation is that the ion

density distribution may become more uniform if an obstacle (or boundary) that is also an equipotential surface such as a three inch diameter silicon wafer, is placed perpendicular to the z axis in the path of the diffusing plasma species.

Using the analytic expression developed in Section 4.4, a comparison between the theoretical uniformity of the ion distribution and the oxide thickness uniformity is presented in Figures 5.15, 5.16 and 5.17 for the oxide thicknesses grown at 4, 6, and 8 cm downstream respectively. The ion density was calculated and then scaled such that the center values of oxide thickness and ion density matched. Again, the oxide thicknesses are more uniform than the theoretical ion distribution would suggest they should be.

One note that should be made here, however, is that the analytic expression was developed assuming that the z dimension of the cylindrical coordinate system was infinite and free of obstacles such as a three inch silicon wafer. Also, the double Langmuir probe measurements were made without any type of obstacle in the path of the diffusing plasma species. It is highly likely, as mentioned above, that a three inch diameter wafer place in the vacuum chamber will tend to "smooth out" the ion density distribution [87].

The oxides grown with the quartz tube in place showed an exaggerated non-uniformity very much like that of the oxide films grown at 2 and 4 cm downstream, i.e. a thicker oxide, approximately 380 Å, near the edge where the input power probe was during oxidation, and a thinner oxide, approximately 300 Å, near the furthest edge. Also, these oxides were grown at a distance of 6 cm downstream from the plasma and comparing them to the oxides grown without the quartz tube
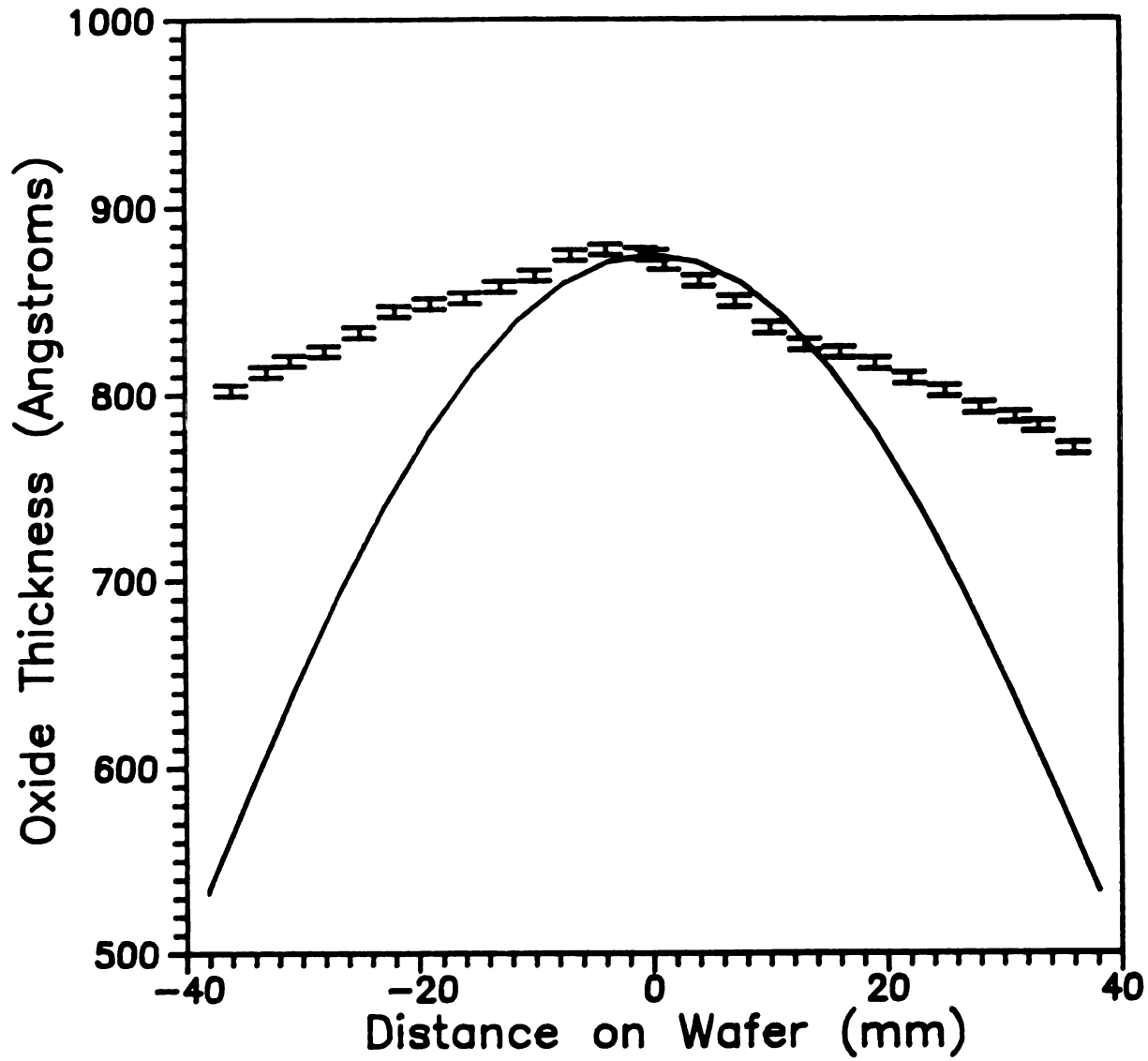
Figure 5.15 Comparison of the Oxide Thickness Grown 4 cm from
the Discharge and the Theoretical Ion Density Distribution
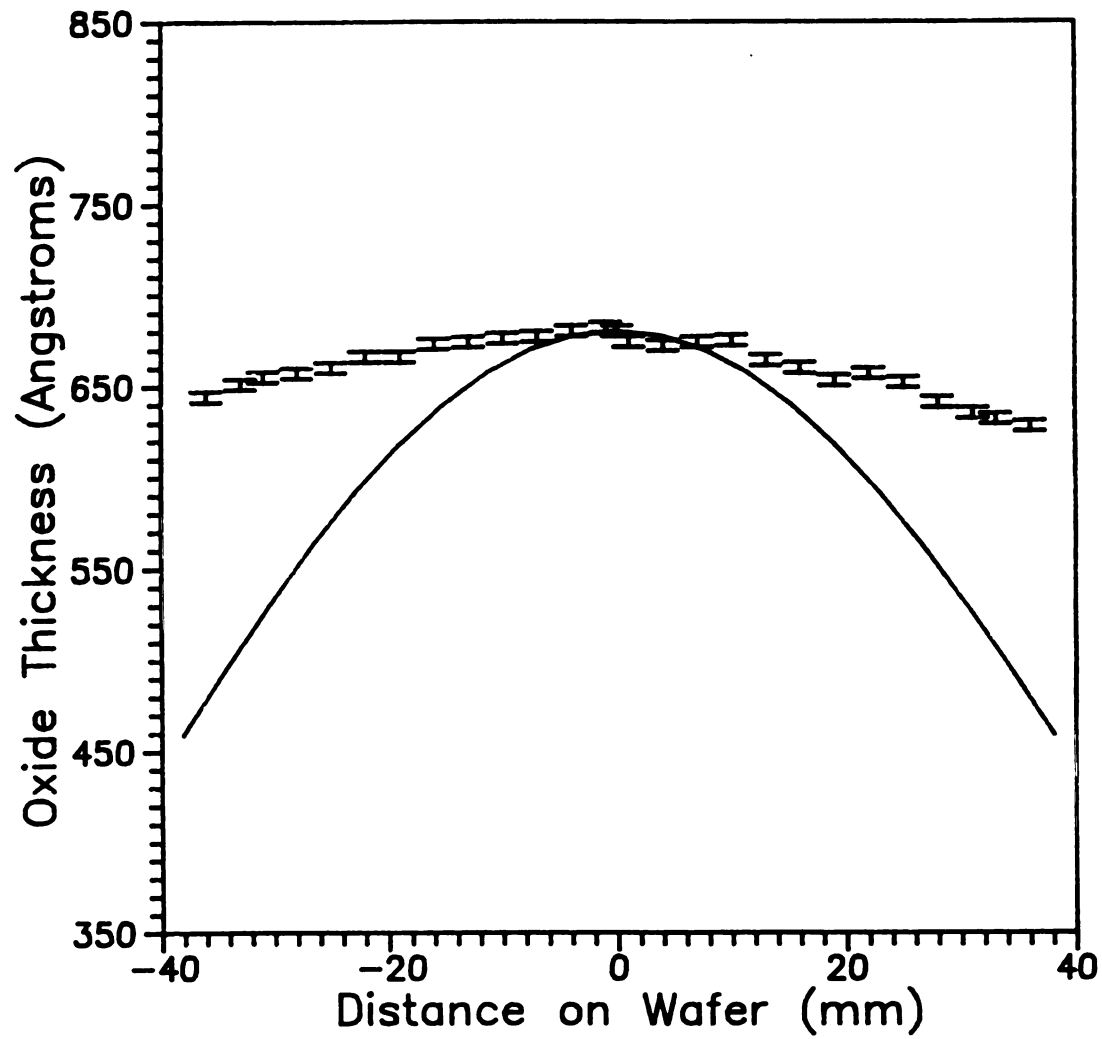
Figure 5.16 Comparison of the Oxide Thickness Grown 6 cm from
the Discharge and the Theoretical Ion Density Distribution
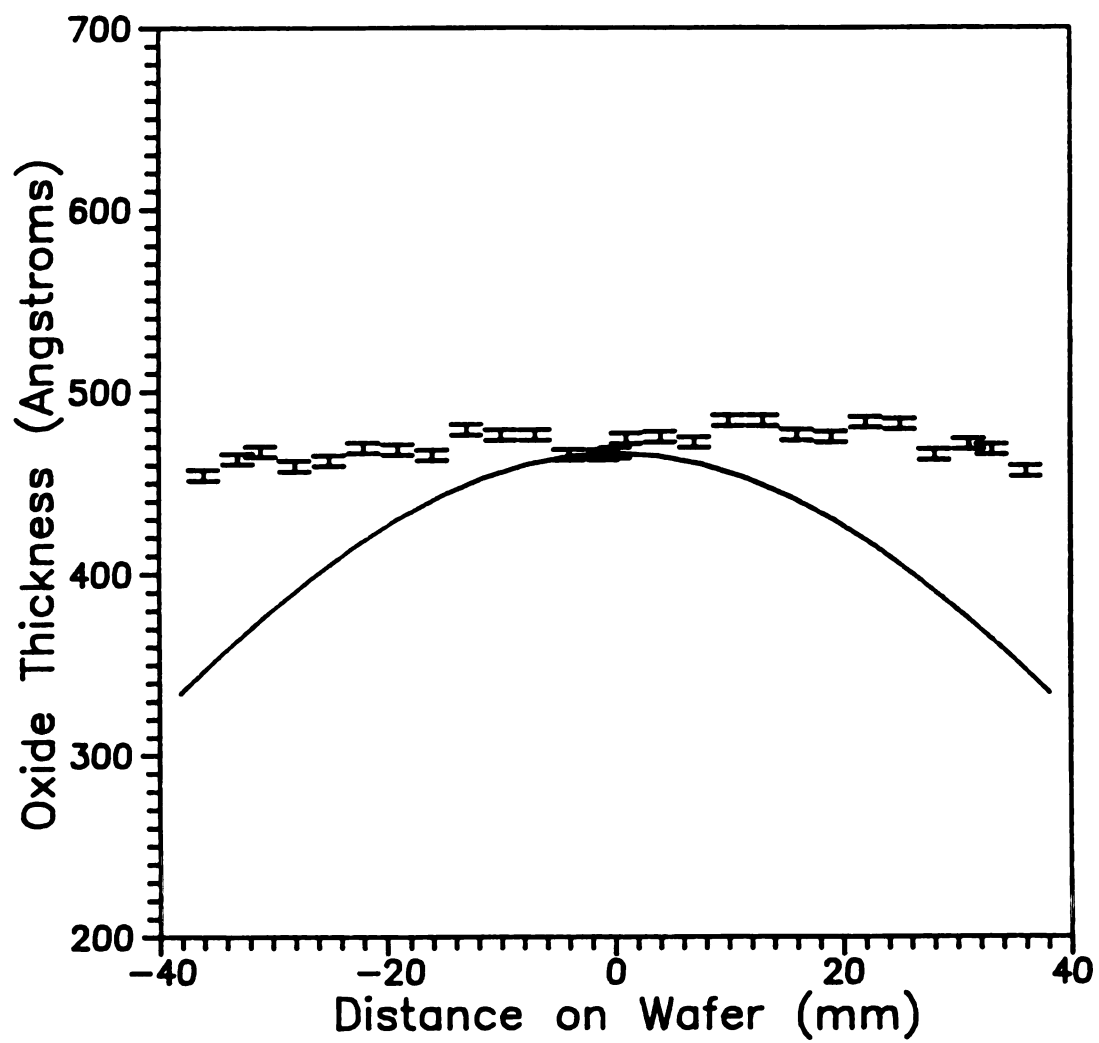
Figure 5.17 Comparison of the Oxide Thickness Grown 8 cm from
the Discharge and the Theoretical Ion Density Distribution

Both these phenomena are due in part to the much smaller radius of the quartz tube in comparison with the vacuum chamber which gives a much smaller cross sectional area for diffusion of charged particles and hence a much higher loss of particles due to recombination on the walls of the quartz tube. Figures 5.18a and 5.18b are the oxide thicknesses measured, again parallel and perpendicular to the input power probe, of an oxide grown under these conditions, i.e. 6 cm downstream with the quartz tube in place.

In an effort to increase the oxide thickness and reduce the near-field effect of the probe while growing oxides in the quartz tube, the entire support arm was lowered to increase the area of the baseplate exposed to the plasma in the discharge region from a ring of 0.5 cm to a ring of 1.0 cm, and hence increase the current during anodization. This also increased the distance between the wafer and the discharge from 6 cm to 6.5 cm. Figures 5.19a and 5.19b show the oxide thicknesses achieved with this arrangement, Figure 5.19a measured parallel and Figure 5.19b measured perpendicular to the power input probe. As can be seen, there was only a small increase in the overall oxide thickness with just a slight reduction in the near-field effect from the input power probe.

Mention should be made here of experiment DS-35. In this trial, the quartz tube was again used but two ceramic dowels were put together to place the wafer only 3.3 cm from the discharge. This was an attempt to grow a thicker, higher quality oxide. A very apparent "lobe" pattern was evident in the oxide grown on this wafer. This was most likely due to the wafer-quartz tube-baseplate confining the plasma in such a small volume that the plasma species in the ECR zones in the
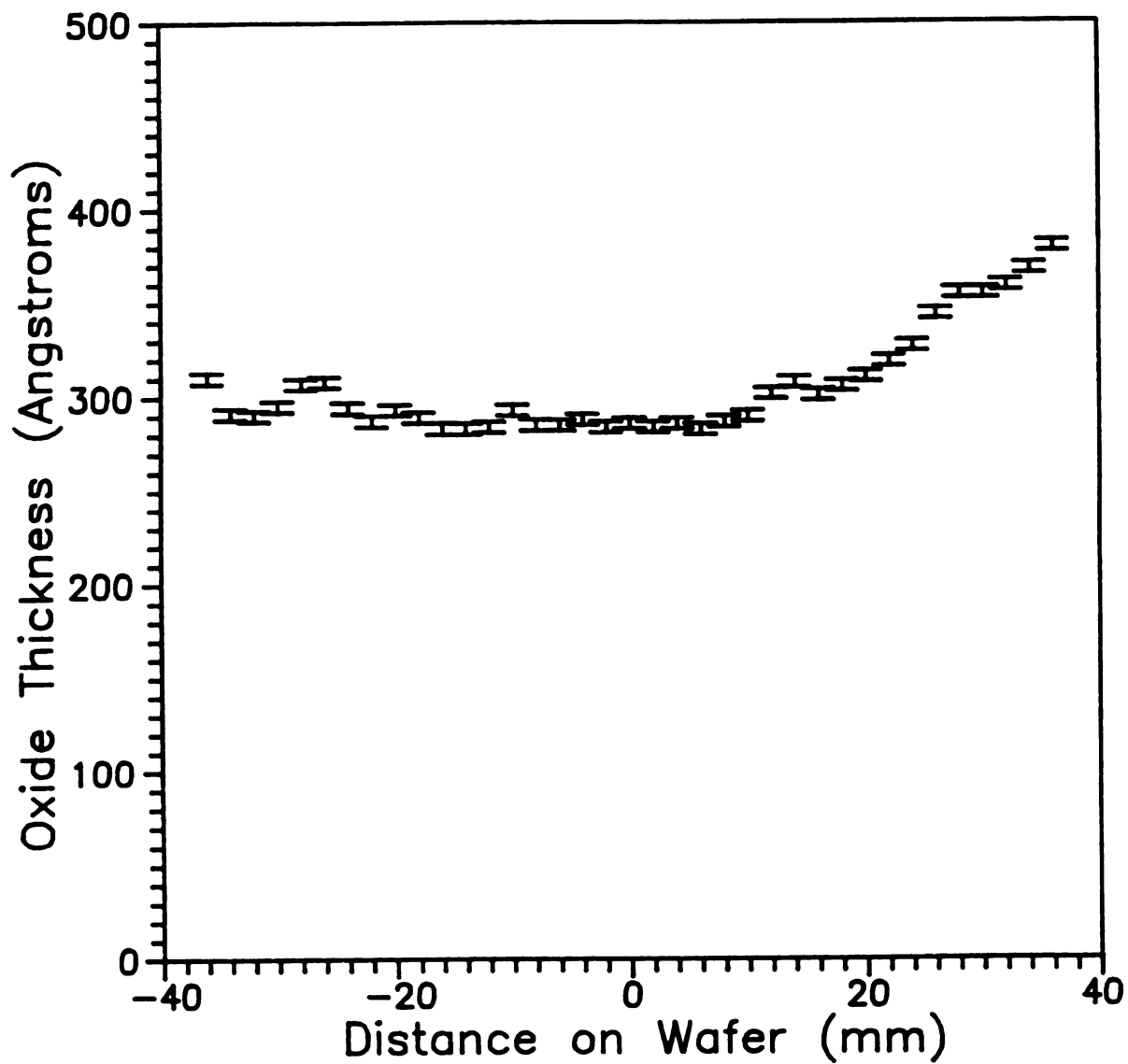
Figure 5.18a Oxide Thickness Uniformity Grown 6 cm
Downstream from the Plasma Discharge with the Quartz Tube
in Place, Measured Parallel to the Probe Axis
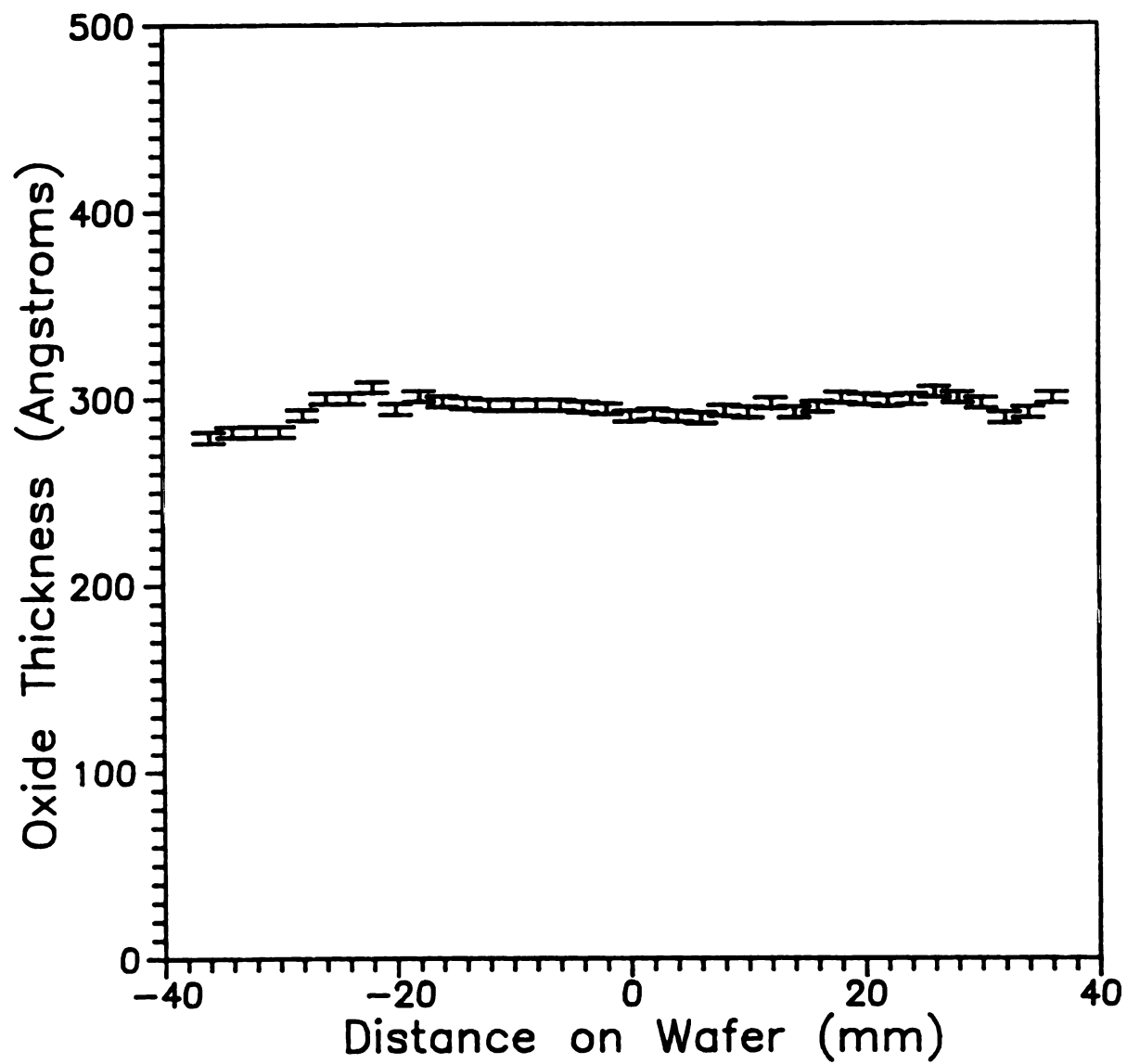
Figure 5.18b Oxide Thickness Uniformity Grown 6 cm
Downstream from the Plasma Discharge with the Quartz Tube
in Place, Measured Perpendicular to the Probe Axis
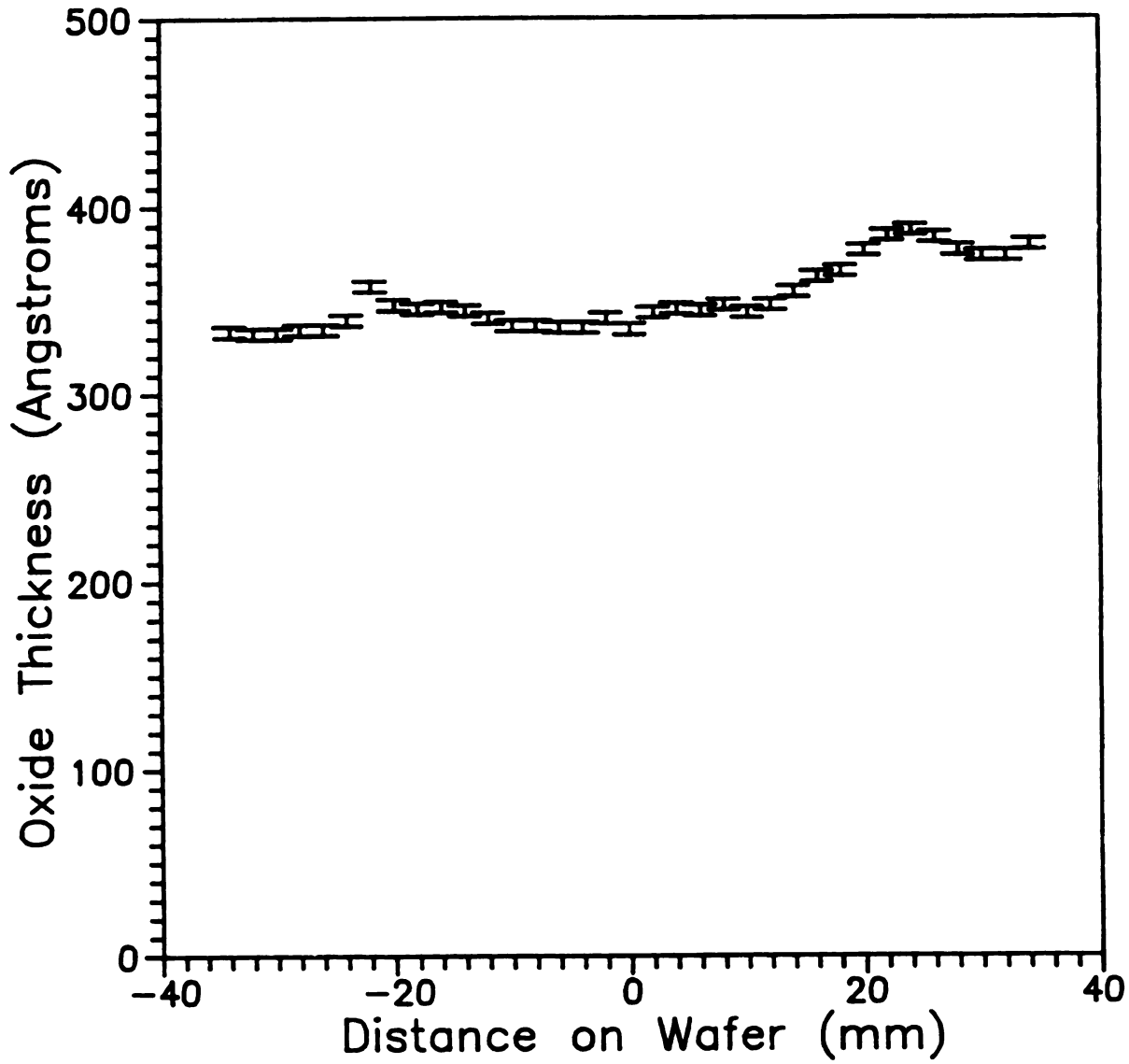
Figure 5.19a   Oxide Thickness Uniformity Grown 6.5 cm
Downstream from the Plasma Discharge with the Quartz Tube
in Place, Measured Parallel to the Probe Axis
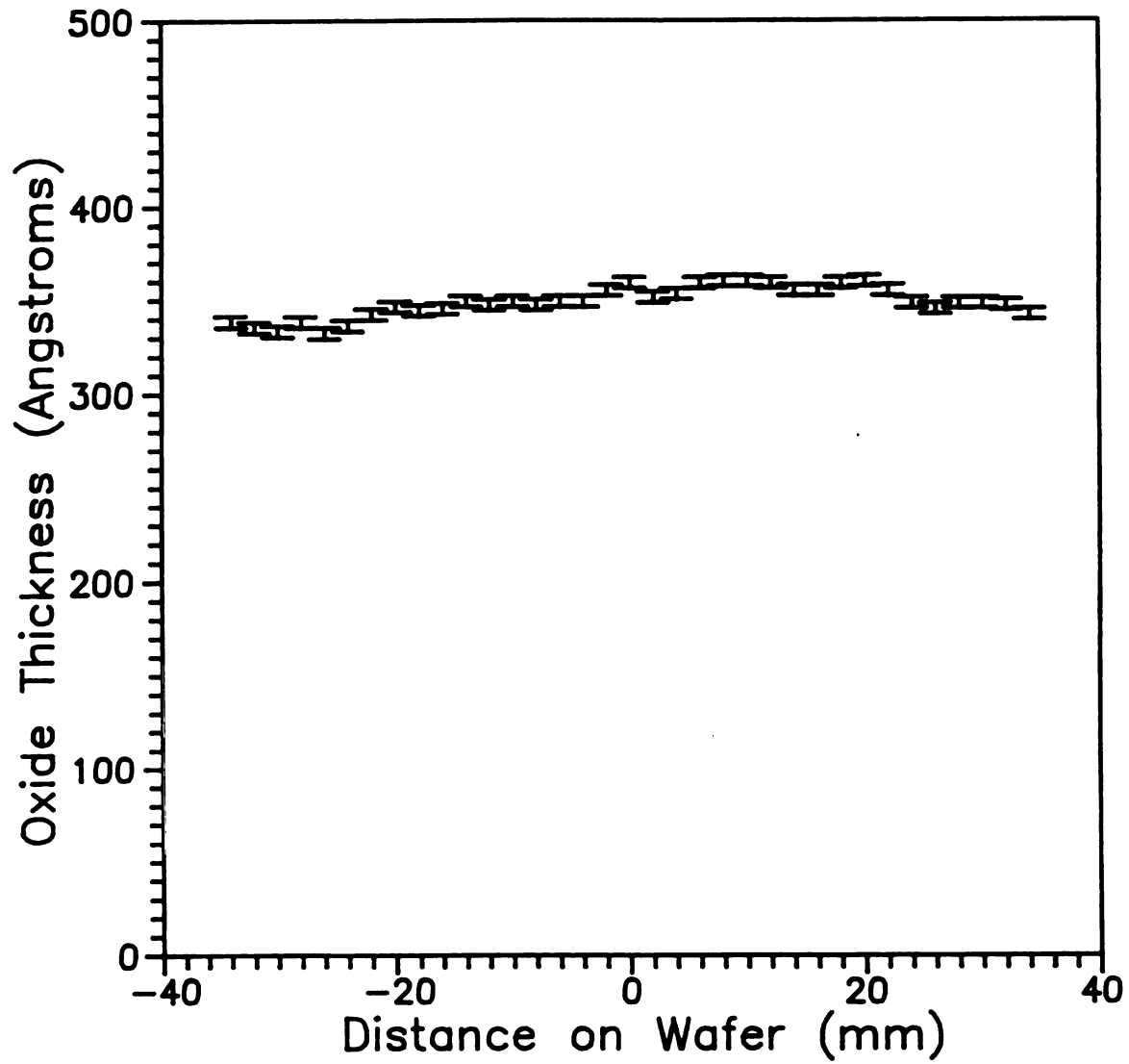
Figure 5.19b   Oxide Thickness Uniformity Grown 6.5 cm
Downstream from the Plasma Discharge with the Quartz Tube
in Place, Measured Perpendicular to the Probe Axis

plasma did not have enough space to diffuse out into a more uniform distribution.

The oxide grown with the silicon cathode arrangement was measured with the X-Y grid method and the results are shown in Figure 5.20. The vertical distance is relative to 200 Å as the maximum oxide thickness grown was 190 Å. This oxide was grown 8 cm downstream from the oxygen plasma. Comparing this to the other oxides grown at 8 cm downstream using the cavity baseplate as the cathode, this oxide is slightly more than one-third the thickness. This could be due to three things: 1. the cathode area was much smaller, 2. the cathode was some distance from the discharge, and 3. the cathode itself grew an oxide layer thereby limiting the current that could be drawn from the plasma.

The three pieces of silicon used as the cathode were briefly measured and found to have an oxide grown on them of slightly more than 300 Å. This may be due in part to the cathode being very near a high density of oxygen ions, and also partly due to heating by the discharge and by the current flowing through the silicon pieces.

Another physical characteristic of silicon dioxide that can be measured with an ellipsometer is the index of refraction. For thermally grown oxides, the index of refraction is between 1.457 and 1.461. Table 5.2 is a summary of the index of refraction for the plasma grown oxides. From this data it is seen, except for DS-14, that all the indices of refraction are below that which would be expected for a thermally grown oxide. This is a possible indication of either an oxygen rich oxide or an oxide with a lower density, i.e. a more porous oxide.
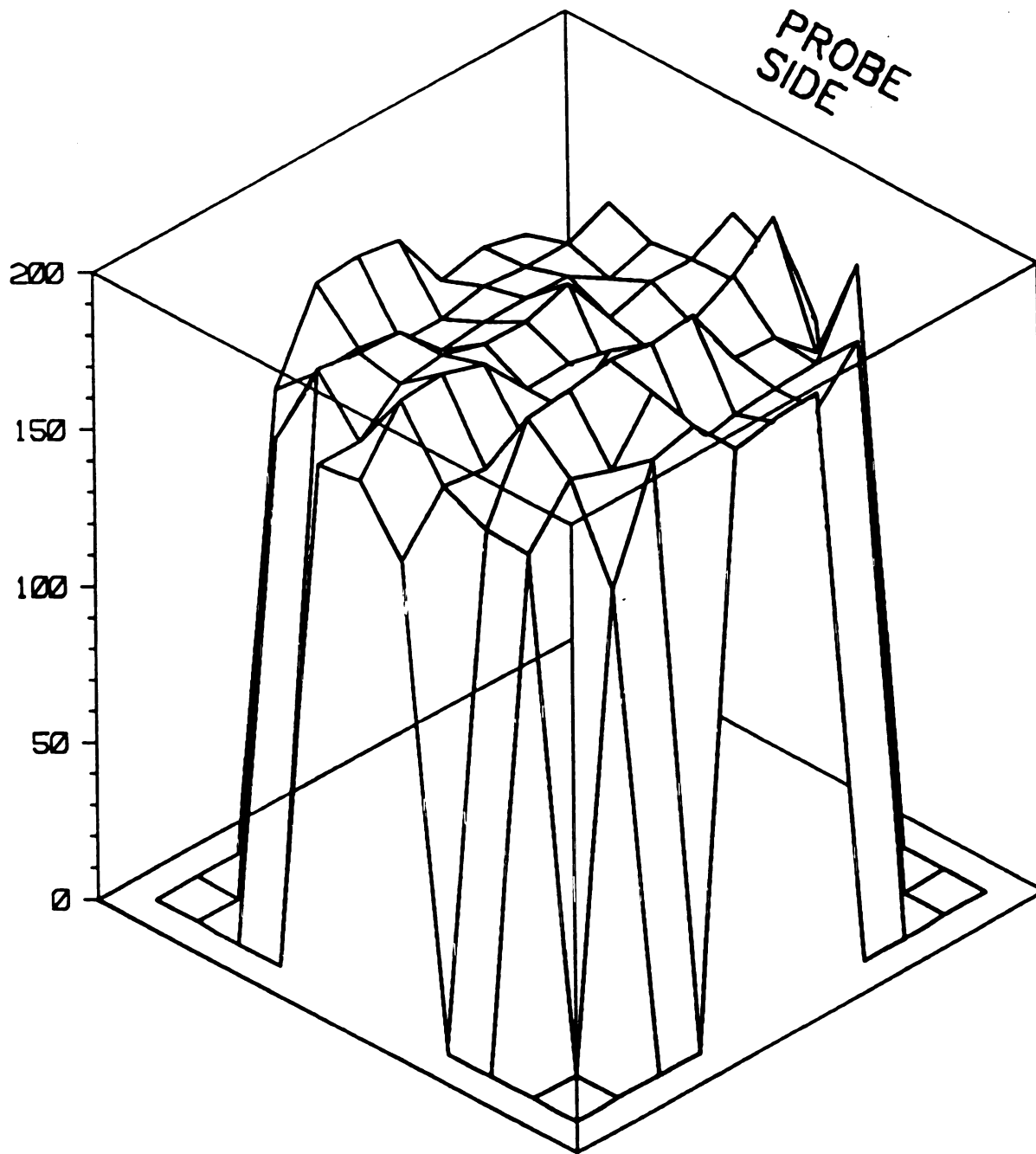
**Figure 5.20 Oxide Thickness Uniformity Over Wafer Surface
Grown 8 cm from the Plasma Discharge with the Silicon Cathode**

Table 5.2 Index of Refraction for the Plasma Grown Oxides

Sample	Distance from Plasma	Index of Refraction
DS-26	2 cm	1.455
DS-14	4 cm	1.464
DS-20	6 cm	1.429
DS-28	8 cm	1.371
DS-24	10 cm	1.385
DS-31	6 cm (QT)	1.358
DS-33	6.5 cm (QT)	1.419
SC-1	8 cm	1.424

5.3 CHEMICAL ANALYSIS

5.3.1 Methods – AES, XPS, and FTIR

One of the most basic questions that needs to be answered, in addition to the uniformity and oxide thickness questions, is "Is this substance grown on these wafers really SiO_2?" To answer this question, three instruments housed in the Michigan State University Composite Materials and Structures Center (CMSC) were used to measure the chemical, elemental, and stoichiometric properties of the films grown.

The first machines used in this evaluation was an AES (Auger electron spectroscopy) Perkin-Elmer PHI 660 Auger multiprobe system.

This machine bombards a sample's surface with energetic electrons which imparts enough energy to electrons of atoms in the sample such that they are emitted from the sample. The electrons that are emitted from these atoms are then analyzed to determine their energy. From this analysis the element from which it came can be determined. AES has excellent capabilities for determining the elemental composition of a sample to within approximately 1×10^{-3} parts of a monolayer. The sampling depth of AES is on the order of 5 to 50 Angstroms. The particular machine in the CMSC also had a calibrated and highly spatially defined argon sputtering system built into it. With this capability a depth profile of the film was also measured, i.e. was the film of uniform elemental composition through out?

The second machine used in the evaluation of the composition of the plasma grown oxides was an ESCA (electron spectroscopy for chemical analysis) or XPS (x-ray photoelectron spectroscopy) Perkin-Elmer Physical Electronics PHI 5400 system. This machine uses Al $K\alpha$ monochromatic x-rays to bombard the surface of a sample to again impart energy to electrons in the atoms of the sample. The energy of these emitted electrons is again analyzed to determine what elements are present in the sample. But unlike AES, ESCA can determine what kind of bonds exist in the sample. For instance elemental silicon and silicon bonded to oxygen have different energy peaks in the spectrum given by the emitted electrons. With this instrument the ratio of silicon to oxygen in the oxide layer was determined, i.e. the stoichiometry of the film. AES and ESCA results are given in Section 5.3.2.

Another instrument that was used to determine the stoichiometry of the oxide films was a Perkin-Elmer Physical Electronics 1800 Fourier

Transform Infrared Spectrophotometer. This particular Fourier Transform of Infra-Red Spectroscopy (FTIR) instrument uses infrared radiation in the range 700 to 3,500 cm^{-1} (1.43 to 2.86 microns or 2,100 to 1,050 GHz). The transmission mode was used to analyze the oxides. Oxides of silicon have very definite energy absorption features in this spectrum as described below.

A concise and thorough review of the use of FTIR in determining the stoichiometry of SiO_x ($0.0 < x < 2.0$) is given in [88] so only a summary will be given here. The interpretation of the IR spectra involves the knowledge of the vibrational states of Si-O-Si bonds. Table 5.3 lists these vibrational properties of SiO_2 in the range of frequencies of interest to this study.

Table 5.3 Vibrational Properties of SiO_2 [88]

Frequency (cm^{-1})	Activity[1]	Vibrational assignment
800	Raman (P)	
	IR	Oxygen bending + Si
1075	Raman (D)	
	IR	Oxygen stretching + Si
1150	IR	Oxygen stretching
1200	Raman (D)	

[1]P indicates a polarized Raman mode, and D indicates a depolarized Raman mode.

Using the vibrational state of oxygen stretching plus silicon, and

plotting this vibrational frequency versus X in the SiO_x, Figure 5.21 can be drawn where X = 0.0 for oxygen doped amorphous silicon occurs at 940 cm^{-1}, X = 1.0 for SiO occurs at 1,000 cm^{-1} and X = 2.0 occurs at 1,075 cm^{-1}. With this information, a quantitative measure of the stoichiometry of the plasma grown oxides can be made. Results are given in the next section.

5.3.2 Chemical Analysis Results

This section presents the results of the AES, ESCA, and FTIR tests performed on oxides grown under various conditions of anodization using an oxygen plasma sustained with the MPDR. These same tests were also done on thermally grown oxides for comparison with the plasma grown oxides.

As will be discussed in Section 5.5, the electrical tests suggested possible contamination of the oxides. The first tests performed on the plasma grown oxides were to determine if there was indeed some contamination of the films from the process.

Tests were first performed on DS-30 and DS-15, oxides grown without the quartz tube in place to shield the wafer from sputtering contaminants as discussed in Section 4.1.1. Significant contamination levels of iron and tin were found in the film, corresponding to heavy metal contamination sputtered from the baseplate. Using AES and ESCA, the iron content of the film was found to range from 8 to 14 percent and the tin content was found to be approximately 0.3 to 2 percent.

Tests were next performed on DS-33 and DS-37, oxides grown with the quartz tube in place. AES tests were unable to detect iron or tin,
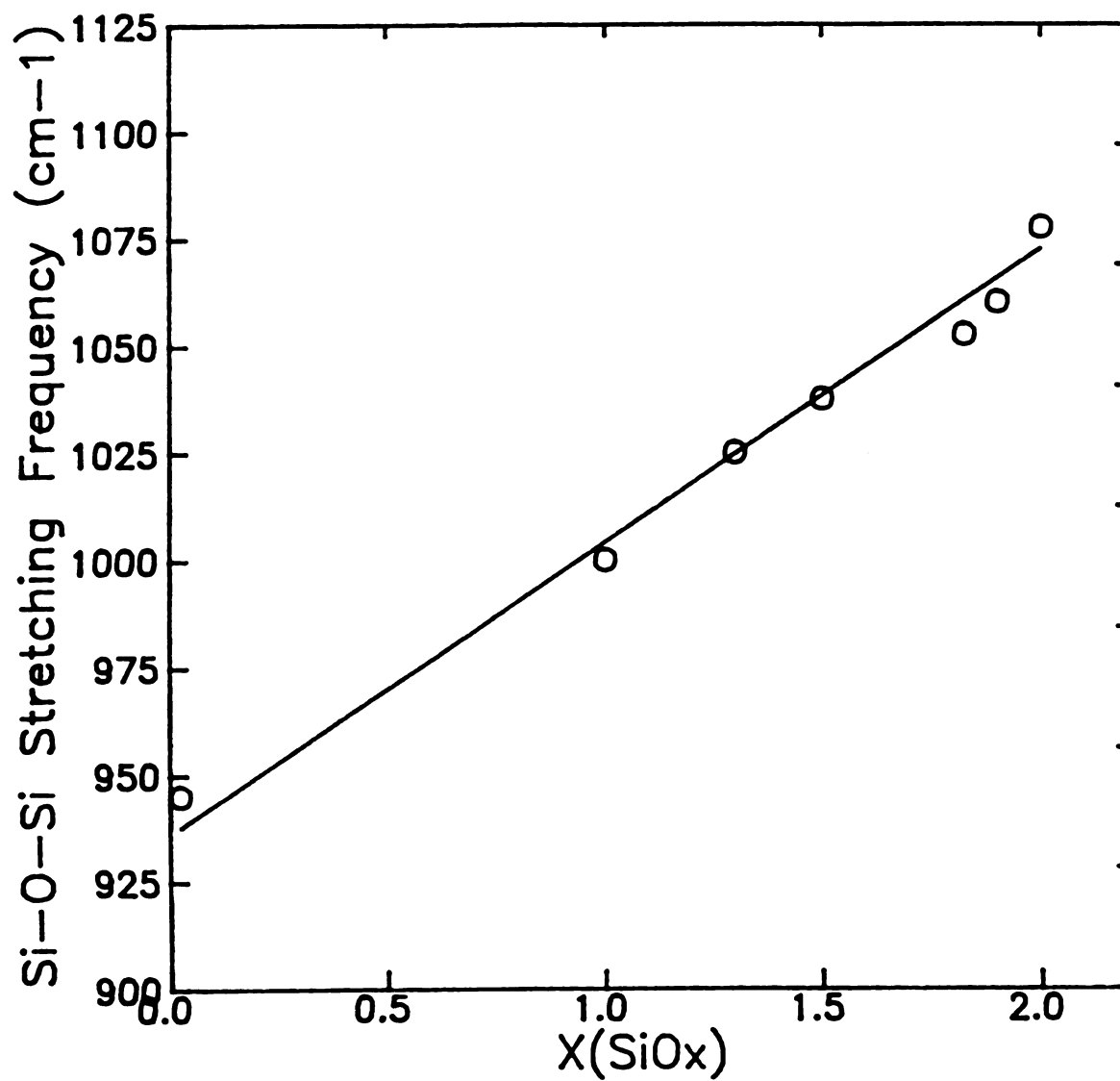
Figure 5.21 Si-O-Si Stretching Frequency as a Function of Oxygen
Composition, x in SiO$_x$ (from [88])

but ESCA tests detected approximately 0.5% iron.

Combining these facts and examining the baseplate, the tin exists only on the bottom of the baseplate as solder to hold a metal ring in place to cover the gas channel. The trials run with the quartz tube in place shielded the wafer from the bottom of the baseplate, and only a small fraction of the baseplate was exposed to the plasma above the quartz tube to act as the cathode. Hence the elimination of the tin contamination and the reduction of the iron contamination to a barely detectable level.

The experiment in which a silicon wafer was anodized with the silicon cathode arrangement described in Section 4.1.3 resulted in a film in which an ESCA analysis was unable to detect any metallic contamination.

Beside contamination detection in the films, it was desirable to use these instruments to determine the stoichiometry of the oxide layer, i.e. "What is the x in SiO_x for these oxide grown films?" and "Is the oxide of uniform stoichiometry throughout entire film?" Table 5.4 is a list of stoichiometry analysis results as determined with AES, ESCA and FTIR. In addition to plasma grown oxides, interspersed with the stoichiometry results of plasma grown oxides are results from tests performed at the same time with the same instrument on thermally grown oxides. These are oxides with x = 2.0 which provide a "standard" for comparison and are labeled "ST" directly below the corresponding plasma grown oxide(s). The entries which belong to the same group of samples that were tested together with a thermal oxide standard are double spaced to distinguish between the different groups. Also included is a column with information that indicates if a sample was sputter cleaned

or not. The samples were exposed to atmosphere for usually more than a week and this is time enough for contamination such as carbon to settle on the wafer. Hence, the top 10 to 20 Angstroms of the sample were sputtered off to expose the true oxide material.

The main conclusion that can be reached from the results presented in Table 5.4, is that all plasma grown oxide films were slightly oxygen rich as compared to a thermally grown oxide. This was observed in all oxides tested, with the lowest ratio of silicon to oxygen for an

Table 5.4 Stoichiometry Results of Plasma Anodized Silicon Oxide Films

DS	Annealed?	Sputter?	Technique	X(raw)	X(adj'd)
33	yes	yes	ESCA	2.045	2.045
33	no	yes	AES	2.53	2.05
36	no	yes	AES	2.53	2.05
37	no	yes	AES	2.63	2.13
ST	no	yes	AES	2.47	2.00
37	no	yes	ESCA	2.34	2.26
ST	no	yes	ESCA	2.07	2.00
SC	no	no	ESCA	2.30	2.11
SC	no	yes	ESCA	2.30	2.11
ST	no	yes	ESCA	2.18	2.00
33	no	no	FTIR	2.43	2.28
ST	no	no	FTIR	2.13	2.00

as-grown oxide being 2.05. An annealed film, (the anneal is described in section 5.5.1) was only slightly closer to the stoichiometrically correct ratio, i.e, x = 2.0 in SiO_x, with a portion of DS-33 that was annealed having an x = 2.045.

The FTIR results were analyzed by placing the Si-O-Si stretching frequency shift data point of the plasma grown oxide on Figure 5.21 and also noting that this test shifted the frequency of a thermal oxide from 1075 cm^{-1} (the literature reported frequency of SiO_2) to 1086 cm^{-1}. Thus the thermal oxides were shifted by 6.5% and likewise the plasma grown oxides were assumed to be shifted by this amount. Figure 5.22 shows that the FTIR measurement also indicates an oxygen rich film. FigureS 5.23 and 5.24 show the IR spectra of a thermally grown SiO_2 film and a plasma anodized film respectively.

To answer the second question of uniform stoichiometry, advantage was taken of the AES instrument's sputtering capability. Using this capability, the oxide of DS-33 was alternately sputtered and analyzed to detect the oxygen and silicon bonded to oxygen elements. This was continued until the interface was clearly passed. Figure 5.25 shows the sputter time versus elemental signal. On the vertical scale are plotted three signals, silicon bonded to oxygen, oxygen and elemental silicon. This scale is a relative measure of each signal and does not show quantitative silicon to oxygen ratios. As can be seen, the oxide grown with the plasma anodization system was of uniform stoichiometry throughout. The interface seems to be rather broad, approximately 50 Å, but this can be explained by a phenomena referred to as ion knock-on mixing [90,91] due to the highly energetic, 4 KeV, argon ions used in the sputtering process.
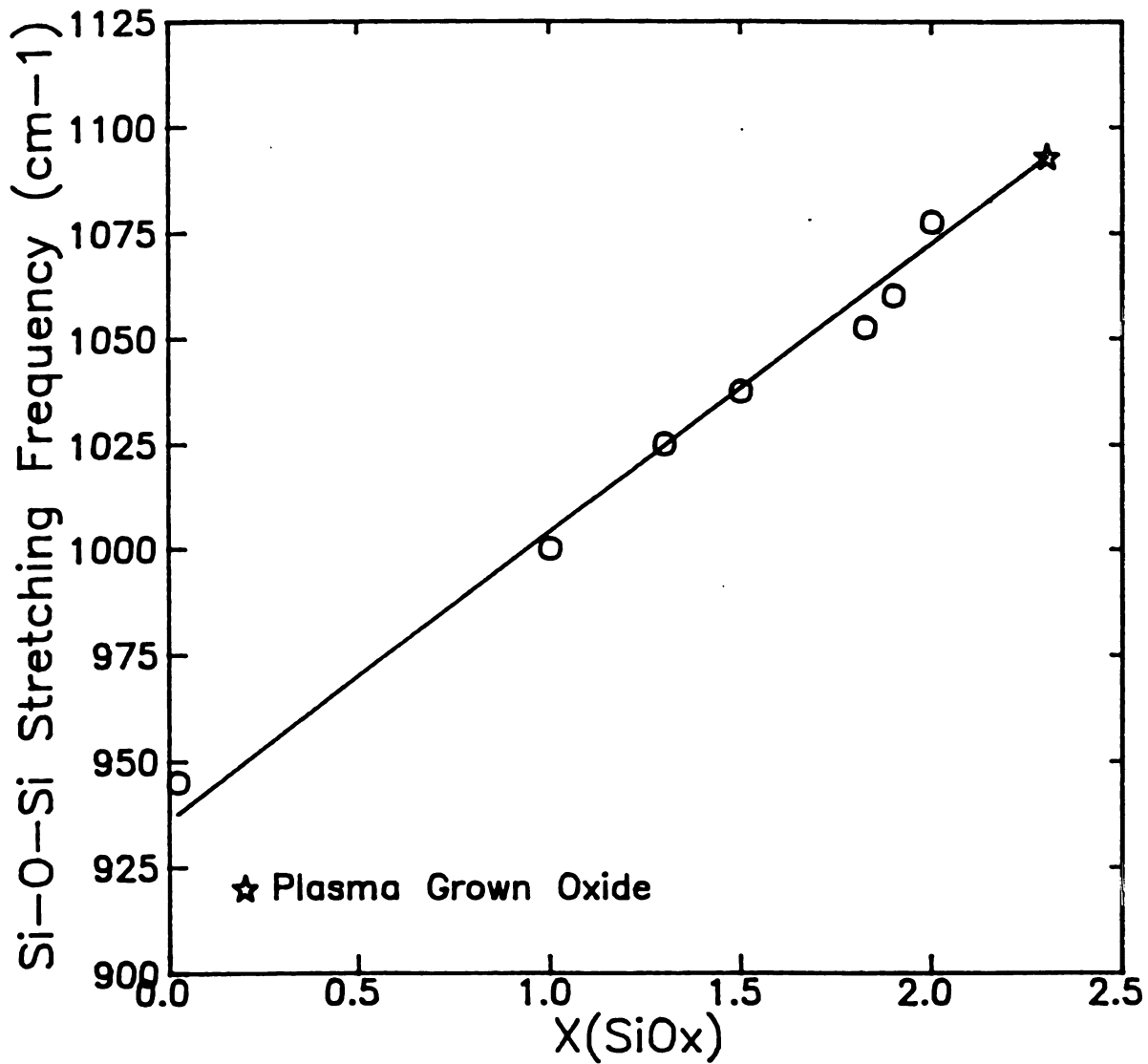
Figure 5.22 Si-O-Si Stretching Frequency of a Plasma
Grown Silicon Oxide (DS-33, no anneal, no sputter) Plotted
with the Data of Figure 5.21
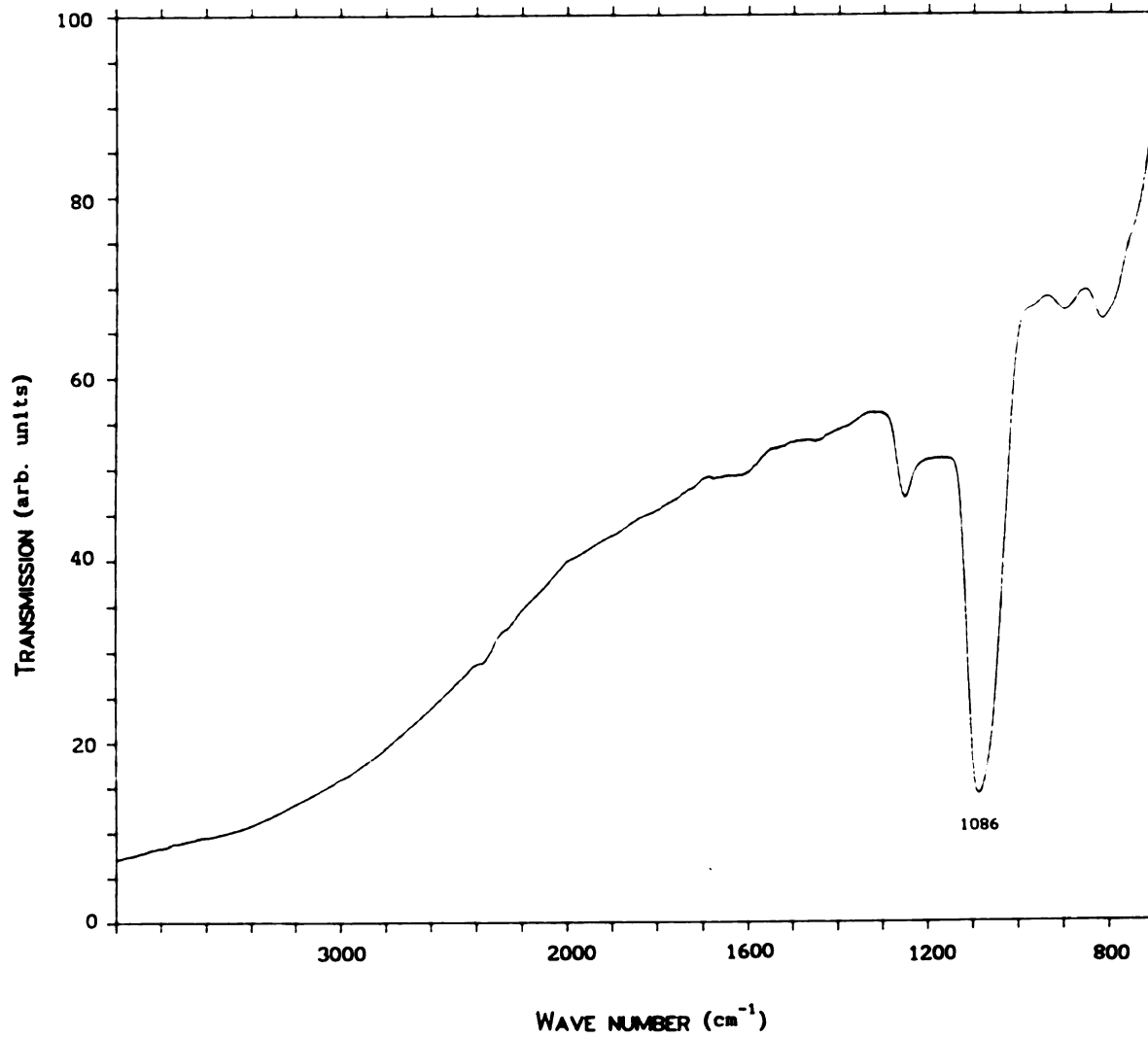
Figure 5.23 IR Spectra of a Thermally Grown Silicon Dioxide Film
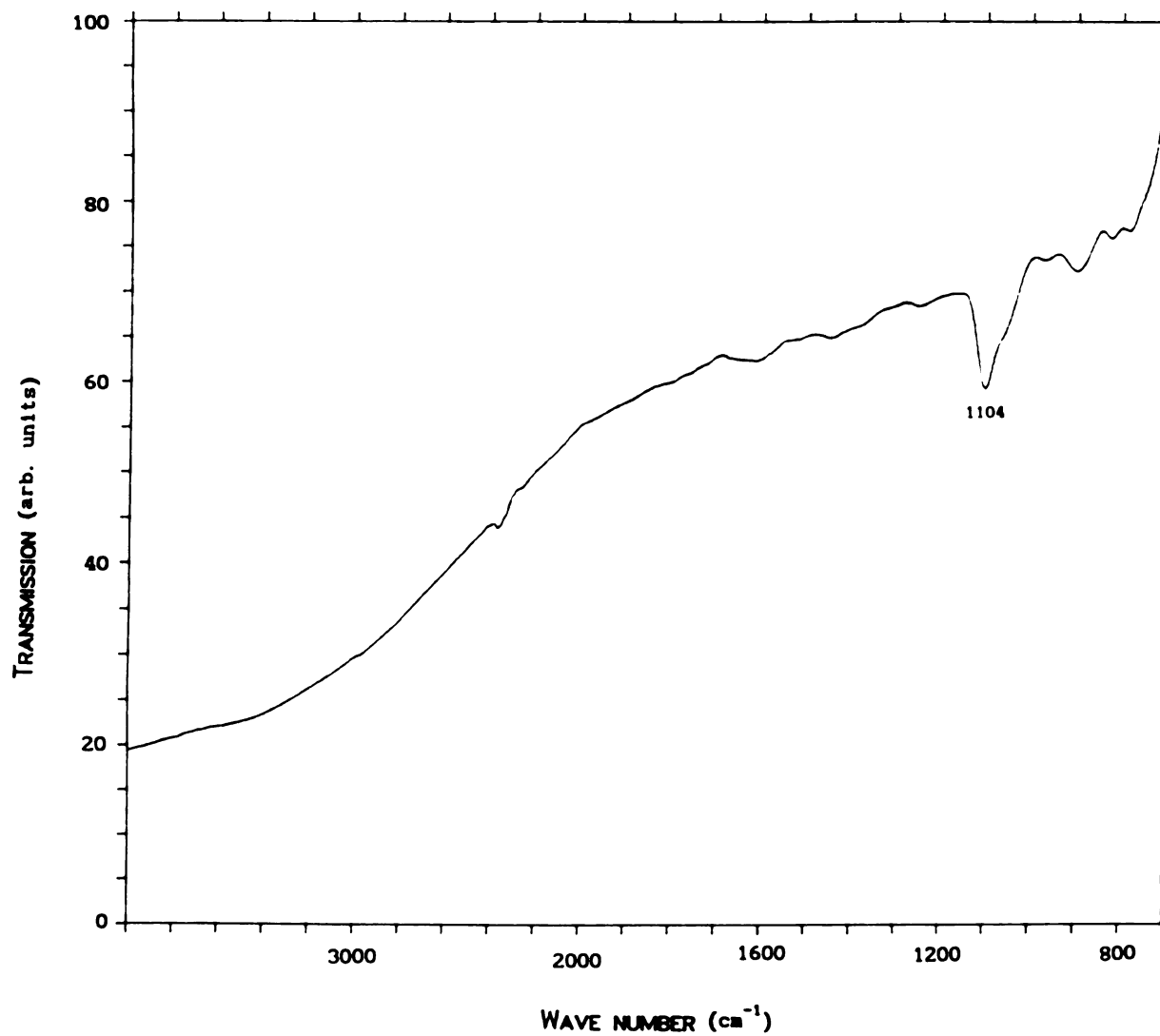
Figure 5.24   IR Spectra of a Plasma Anodized Silicon Dioxide Film
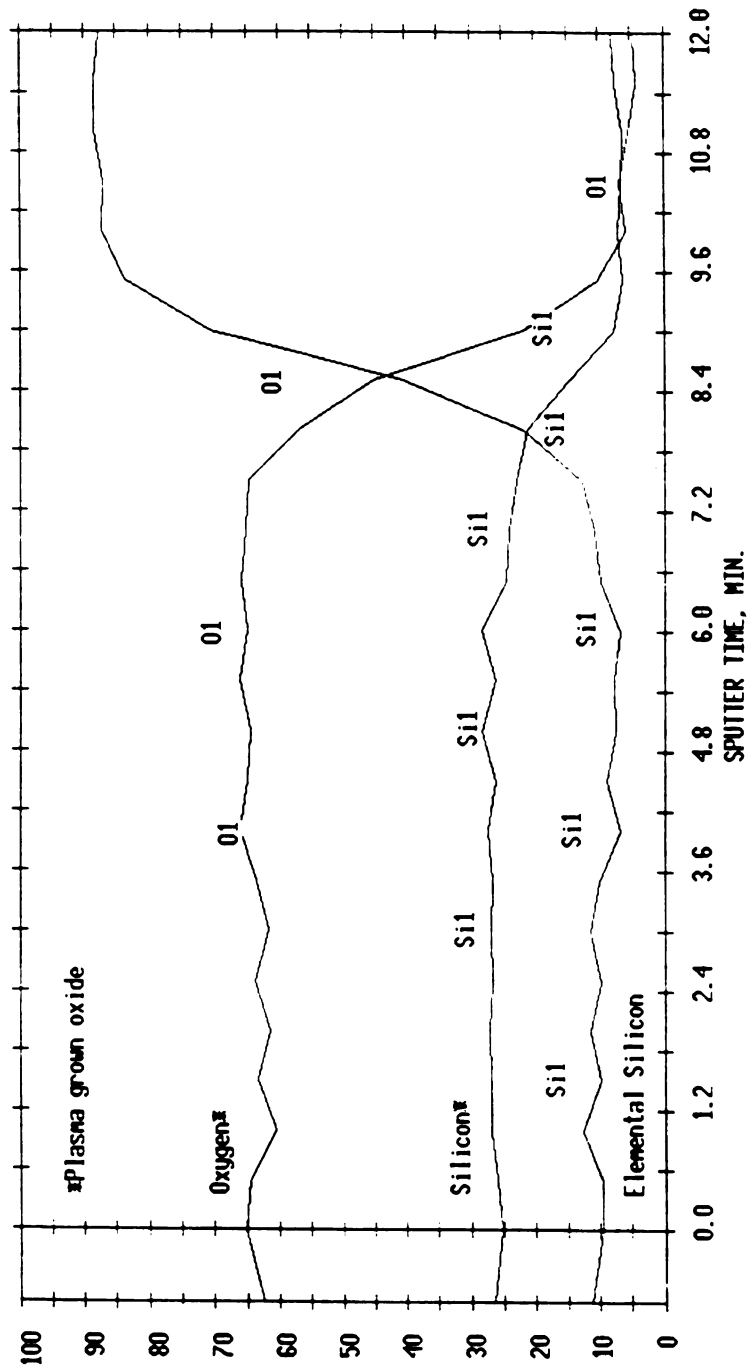
Figure 5.25 Auger Scan of the Oxide Film vs. Sputtering Time (Depth)

5.4 WET ETCHING RESULTS

In Section 2.4, one of the tests cited for use in oxide comparison [14] was the rate of etching of the silicon oxide films in a P-etch consisting of 15 parts of 49% HF, 10 parts of 70% HNO_3, and 300 parts of H_2O. This test was carried out on some of the non-annealed plasma oxides grown in this study and a thermal oxide standard. The results are summarized in Table 5.5. The thermal oxide etch rate of 2 Å per

Table 5.5 Etch Rates of Silicon Oxide Layers in a P-Etch.

Sample	Etch Rate (Å/sec)
Thermal	2
DS-14	10.1
DS-22	4.5
DS-34	2.6
DS-SC	4.5

second measured in this study is the same as the literature reported value for thermally grown SiO_2. However, it is seen that the etch rate for the plasma oxides is higher. These results, combined with the results of the stoichiometry tests and the index of refraction measurements, may indicate a higher oxygen content film, or an oxide of higher porosity and lower density. DS-14's etch rate is seen to be much higher than that of any other oxide layer. This may be due to the higher metallic impurity concentration in this particular film.

5.5 MOS CAPACITOR CHARACTERIZATION

The most important characteristics of the oxide layers that must be considered are the electrical properties. Several electrical tests were performed on the plasma grown oxides. The tests performed were to characterize several properties of the oxide: the interface between the silicon and oxide, the oxide dielectric strength, the fixed charge density in the oxide, and mobile ion contamination in the oxide. These tests and the results are described in detail in this section. Many of the results presented in this section were determined from capacitance-voltage (C-V) measurements of a metal-oxide-semiconductor system. Therefore, a brief description of the fabrication of the capacitors is presented, followed by a review of the theory of Metal-Oxide-Semiconductor capacitors. Then the instruments and tests used to characterize the oxide properties are explained and described. Finally, the results of the electrical tests performed on the oxides will be presented.

5.5.1 MOS Sample Preparation

The tests conducted on the oxides to determine the electrical properties utilized Metal-Oxide-Semiconductor capacitors (MOS-Caps) with the anodically grown films used as the oxide. To create MOS-Caps, a metal electrode on the top of the oxide is needed. This electrode is often referred to as the gate, because the structure formed is much like that of a gate in a MOS Field Effect Transistor (MOSFET). The fabrication of these gates to form capacitors is as follows.

The first step was a cleaning as described in Section 4.2.1 omitting the 10 second 50:1 H_2O:HF rinse. Then aluminum was evaporated over the entire wafer using a resistively heated, low-sodium, tungsten coil inside a dedicated vacuum evaporation system. The aluminum was then patterned to form the gate or electrode of the capacitor. Circles of 200 micron diameter were created using standard photolithographic techniques, i.e. coat the wafer with negative photoresist, soft bake at 65° Celsius for 15 minutes, expose the photoresist to ultraviolet radiation through a mask using a mask aligner, develop the photoresist using standard developing chemicals, hard bake the photoresist, etch the aluminum and strip the photoresist. The aluminum etch consists of a 16:1:1:2 mixture of H_3PO_4:HNO_3:acetic acid:H_2O. The capacitors were then annealed in a 95% N_2/ 5% H_2 gas mixture at 450° Celsius for one hour [19]. The capacitors were then ready for testing.

5.5.2 C-V Theory

One of the first tests the oxides were subjected to was a high frequency, C-V measurement, using the oxide as the dielectric in an MOS capacitor which was fabricated as described above. In this test, a bias is applied to the capacitor which consists of a small, high frequency ac signal combined with a dc potential. The dc bias is then swept to trace out a characteristic capacitance vs. dc voltage curve.

The characteristics of the curve depend on the thickness of the oxide, the number of doping impurities in the silicon, and whether the semiconductor is p- or n- type material. Silicon is a column four element of the periodic table, i.e. it has four electrons in its outer

she

bo

th

Th

th

P

b

i

a

T

C

c

c

C

shell.   If a silicon crystal has a small percentage of the element
boron, a   column three element in the periodic table, added to it, then
these boron atoms will accept an extra electron from the valence-band.
This leads to a lack of electrons, or conversely a surplus of holes in
the valence-band. This surplus of holes determines that the silicon is
p-type since the majority carriers are positive.   For these reasons,
boron is called an acceptor impurity or p-type dopant.   If silicon is
doped with a column five element such as phosphorus, arsenic, or
antimony, these impurities donate an electron to the conduction-band.
This leads to surplus of electrons or conversely a lack of holes in the
conduction-band. Now the semiconductor is n-type because the majority
carriers are negative.   Thus, these column five impurities are called
donor impurities or n-type dopants.

The   capacitance of an MOS structure is really the result of two
capacitances, that of the oxide and that of the silicon depletion
layer. The capacitance of the oxide, per unit area, is:

$$C_{ox} = \frac{\varepsilon_{ox}}{d_{ox}}$$

where ε_{ox} is the permittivity of the oxide, which is equal to the
permittivity of vacuum multiplied by the dielectric constant of silicon
dioxide (3.9 X 8.854 X 10^{-14} Farads per cm), and d_{ox} is the thickness
of the oxide. The capacitance associated with the silicon, per unit
area, is:

$$C_{s} = \frac{\varepsilon_{s}}{x_{D}}$$

where ε_{s} is the permittivity of the silicon, which is equal to the
permittivity of vacuum multiplied by the dielectric constant of silicon
(11.9 X 8.854 X 10^{-14} Farads per cm), and x_{D} is the width of the

depletion region in the silicon. The depletion width of the silicon is dependent on the bending of the energy bands in the silicon substrate which is controlled by the dc bias applied to the metal of the capacitor. The depletion width is expressed as:

$$x_D = \left[\frac{2\varepsilon_s |\psi_s|}{qN} \right]^{1/2}$$

where N is the doping concentration of the silicon substrate, $|\psi_s|$ is the magnitude of the bending of the energy bands in the silicon, and q is the electronic charge.

The capacitance of an MOS structure is the series combination of the oxide capacitance and the silicon capacitance. The expression for this series combination is:

$$C = \frac{A}{d_{ox}/\varepsilon_{ox} + x_D/\varepsilon_s}$$

where A is the area of the capacitor. Since x_D is dependent upon the band bending which in turn is dependent on the bias applied to the gate of the capacitor, it is seen that the total capacitance of the MOS structure is bias dependent.

A sample calculated, high frequency C-V curve for an MOS capacitor is shown in Figures 5.26 and 5.27 for p- and an n-type material respectively. For each curve, the silicon substrate was doped with 1 X 10^{15} impurities per cubic cm, the oxide thickness is 290 Å, and the area of the metal electrode on top of the oxide is 3.14 X 10^{-4} square cms. These curves were calculated assuming zero oxide charges and are referred to as ideal C-V curves.

CAPACITANCE (pF)
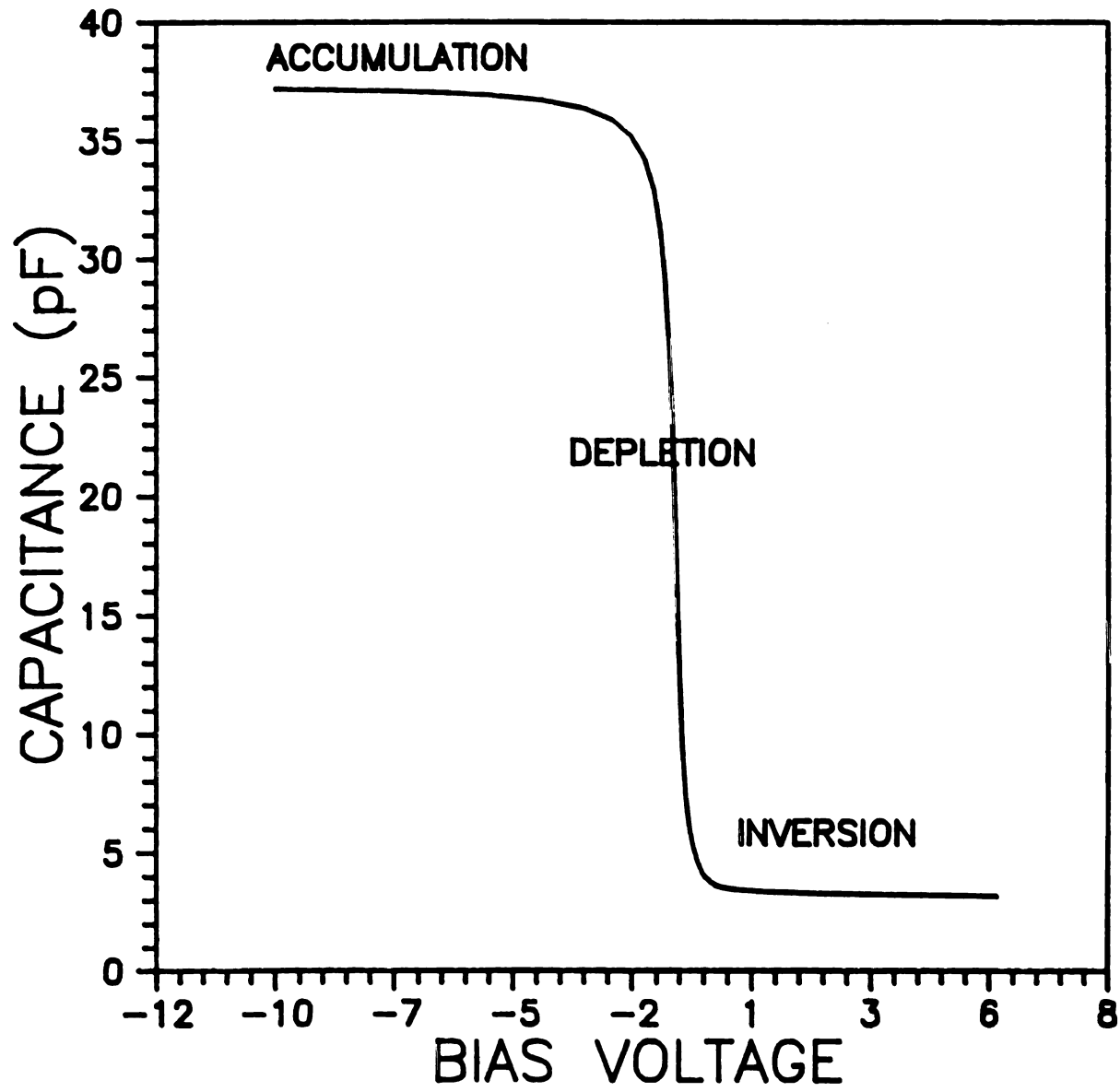
Figure 5.26 Ideal High Frequency C-V Curve (p-type silicon)
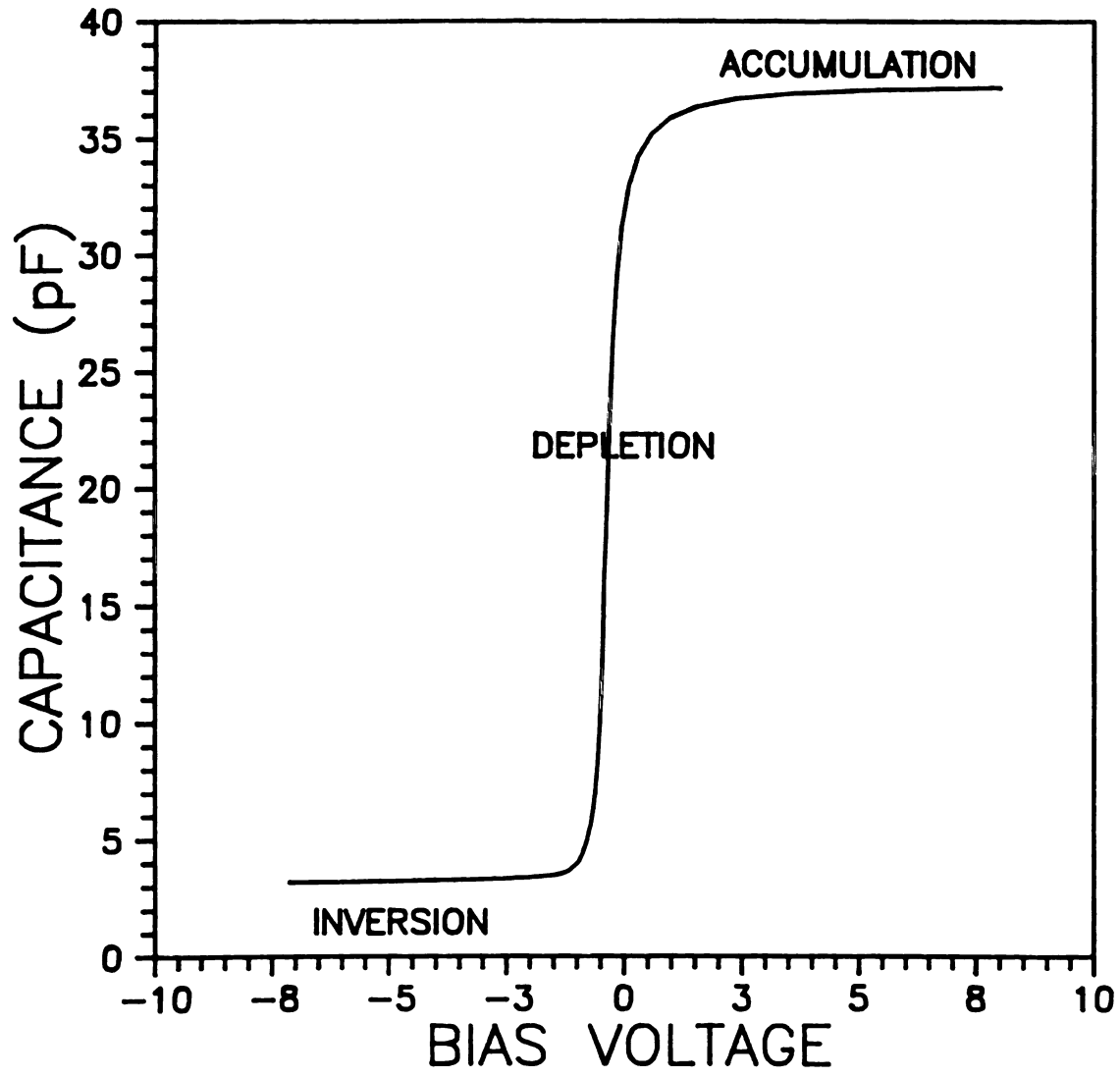
Figure 5.27   Ideal High Frequency C-V Curve (n-type silicon)

capac

with

inte

firs

appl

(ele

sill

the

depl

majo

the

inve

maxi

subs

Here

onse

ener

ener

of

semi

bulk

bulk

adde

As mentioned, the two C-V curves presented are examples of MOS capacitors measured with a high frequency ac voltage signal combined with a dc potential biasing the structure. There are three regions of interest to such characteristics which are labeled on the curves. The first region of interest is the accumulation region. This is where the applied dc potential is such that it attracts the majority carriers (electrons for n-type silicon and holes for p-type silicon) in the silicon substrate to the silicon-oxide interface. Thus, x_D is zero and the capacitance of the structure is just that of the oxide. In the depletion region, the dc potential is such that it is repelling the majority carriers and x_D is increasing so that the capacitance is then the series combination of the oxide and silicon capacitances. In the inversion region, all majority carriers have been repelled to the maximum extent that the dc potential can influence the silicon substrate. This maximum depletion width, x_{Dmax}, is given by:

$$x_{Dmax} = \left[\frac{4\varepsilon_s |\psi_F|}{qN} \right]^{1/2}$$

Here, $2\psi_F$ replaces ψ_s because this is the point that is defined as the onset of strong inversion. This onset of strong inversion is where the energy band bending at the surface of the silicon, ψ_s, is twice the energy difference of the intrinsic energy level, E_i, (E_i is a measure of the electron energy level in an intrinsic, i.e. undoped, semiconductor) and the Fermi energy level, E_F, ($q\psi_F = E_i - E_F$) in the bulk of the silicon substrate. This difference in energy levels in the bulk of the silicon substrate is dependent on the number of impurities added to the crystal. The expression for this energy is:

$$\psi_F = \begin{cases} -(kT/q)[\ln(N_D/n_i)] & \text{(n-type silicon)} \\ \\ (kT/q)[\ln(N_A/n_i)] & \text{(p-type silicon)} \end{cases}$$

where n_i is the intrinsic carrier concentration equal to 1.45×10^{10} carriers per cubic centimeter.

With a high frequency signal, minority carriers are not able to be generated or to react so as to be attracted into the depletion region. (Minority carriers are the carriers of opposite sign than the carriers that are introduced from the doping.) When x_{Dmax} is reached, the result is the flat, almost constant, capacitance of the structure in inversion. However, if a low frequency ac signal is combined with a dc potential instead of a high frequency ac signal to measure the C-V curve, the minority carriers can react to this bias. Then after inversion is reached, minority carriers will be attracted to the region of the silicon near the oxide which decreases x_D, and the capacitance will again rise to the value of that in accumulation. Figures 5.28 and 5.29 are examples of calculated, low frequency C-V curves for p- and n-type MOS capacitors respectively.

Another piece of information that can be obtained from a C-V measurement is the flat band voltage, V_{FB} which is the bias voltage required to produce zero energy band bending in the semiconductor. In isolation, each material, metal, oxide, and semiconductor, has its own Fermi energy. When the three materials are put together to form a capacitor, at equilibrium the structure must be characterized by a single Fermi energy level. Hence the energy bands in the silicon and oxide bend so to align the Fermi level of the semiconductor with that of the metal.

The V_{FB} of the capacitor can be found from the measured C-V curve
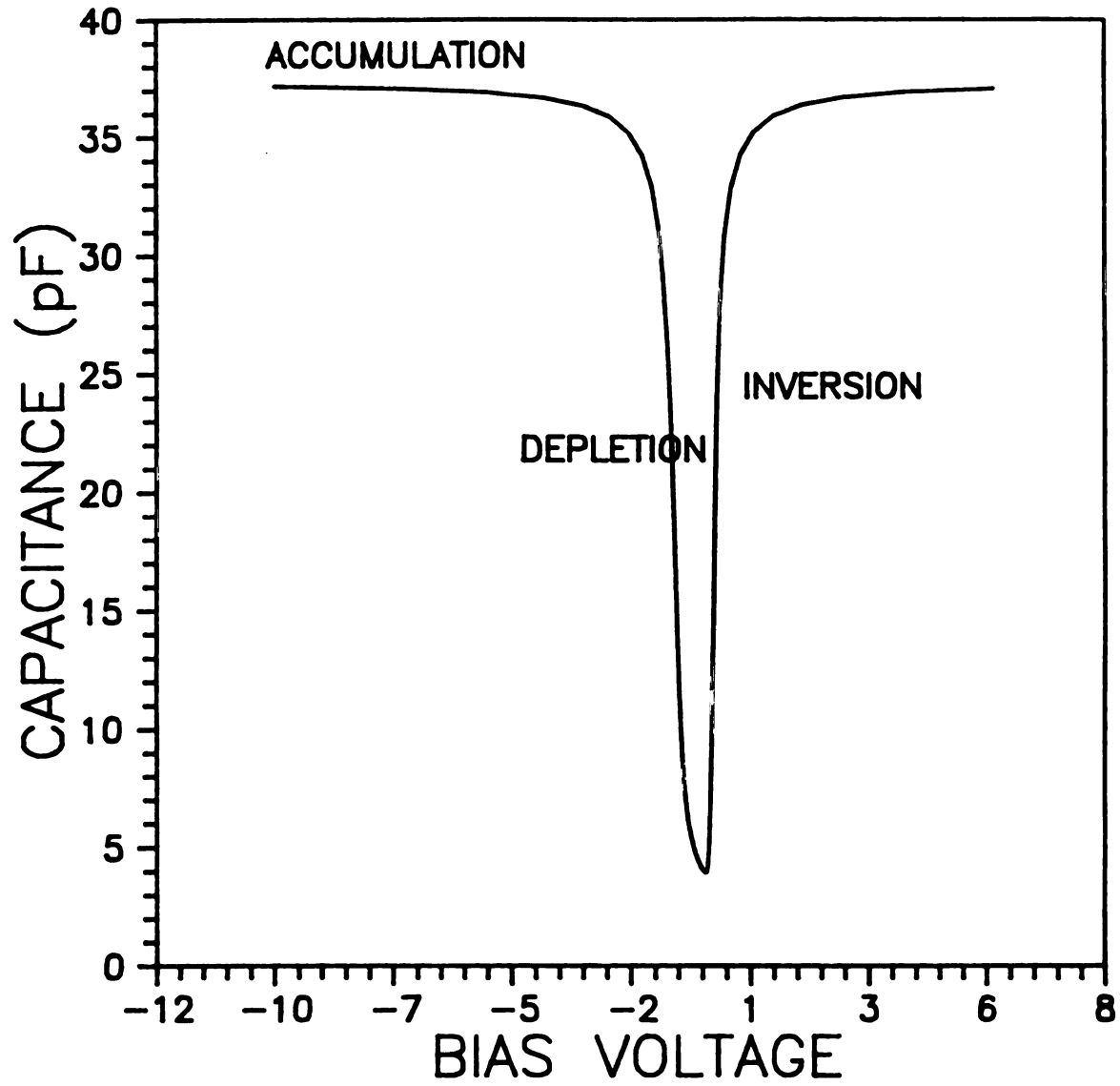
Figure 5.28   Ideal Low Frequency C-V Curve (p-type silicon)
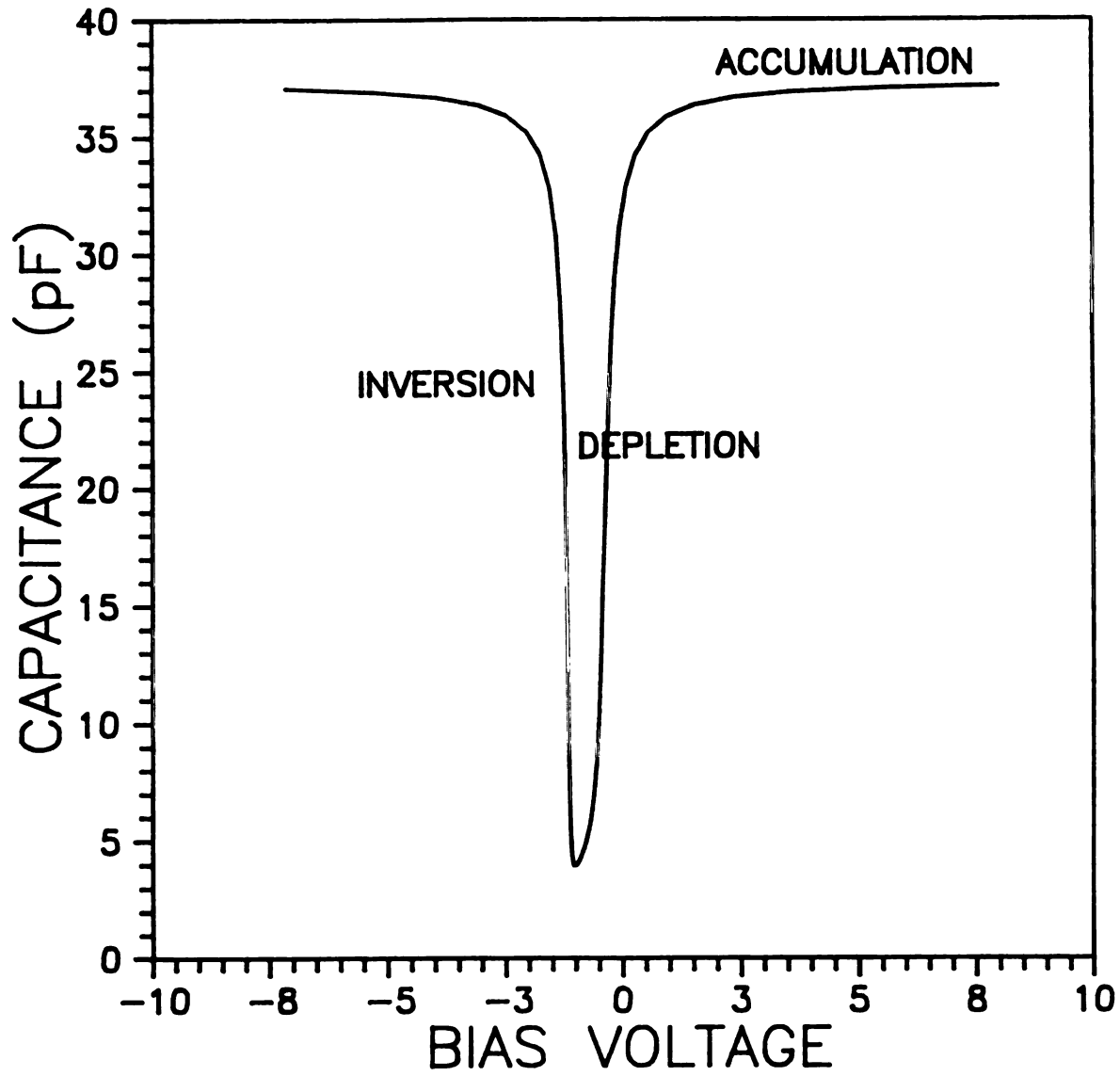
Figure 5.29   Ideal Low Frequency C-V Curve (n-type silicon)

since it occurs at the flat band capacitance given by

$$C_{FB} = A/[d_{OX}/\varepsilon_{OX} + L_{D}/\varepsilon_{S}]$$

where L_{D}, $= [\varepsilon_{S} (kT/q) (N/q)]^{1/2}$, is the extrinsic Debye length which is a measure of the maximum separation at which a given carrier will be influenced by the electric field of an ionized impurity atom.

The theoretical value of the flat band voltage, V_{FB}, can be calculated, in the absence of oxide charges, as:

$$V_{FB} = \Phi_{M} - \Phi_{S}$$

where Φ_{M} and Φ_{S} are the work functions of the metal and semiconductor respectively.

Since silicon is a semiconductor, the Fermi energy level lies in the energy gap. Thus the knowledge of whether the silicon is doped n- or p-type and what level of dopants are present is required to calculate the work function of the silicon. The formula for calculating Φ_{S} is [91]:

$$\Phi_{S} = X_{S} + \frac{1}{q}(E_{C} - E_{F})_{SILICON}$$

where X_{S} is the electron affinity of silicon and $E_{C} - E_{F}$ is the difference between the conduction band energy level and the Fermi energy level in the silicon. To calculate $E_{C} - E_{F}$ (which is usually measured in electron Volts or eV):

$$E_{C}-E_{F}= \begin{cases} kT[\ln(N_{C}/N_{D})] & \text{(n-type)} \\ 1.12 - kT[\ln(N_{V}/N_{A})] & \text{(p-type)} \end{cases}$$

where N_{V}, $= 1.04 \times 10^{19}$, is the effective density of states in the valence band, N_{C}, $= 2.8 \times 10^{19}$, is the effective density of states in the conduction band, and N_{A} and N_{D} are the number of acceptor and donor

impurities per cubic centimeter respectively.

The C-V curves presented so far are "ideal" characteristics. With any real process, some non-ideal effects can be introduced. Four different non-ideal effects that can be introduced are Q_{it}, Q_f, Q_m, and Q_{ot} . These are, respectively, the interface trap charge density, the oxide fixed charge density, the mobile ionic charge density, and the oxide trapped charge density [92]. These are all measured in coulombs per square centimeter. Each of these perturbs the C-V characteristics in its own particular way which will now be briefly described.

The oxide fixed charge is due to defects and strains in the SiO_2 located very near the silicon-silicon dioxide interface, usually within the first 30 Å and can be either positively or negatively charged. Q_f does not exchange charge with the silicon substrate, thus these defects can not be charged or discharged over a wide range of applied gate bias. The oxide fixed charge can therefore be thought of as a charge sheet located at the $Si-SiO_2$ interface.

Like the oxide fixed charge, the oxide trapped charge is due to defects and strains, such as incomplete bonds, but within the bulk of the oxide layer, usually several atomic layers from the silicon-silicon dioxide interface. These defects create energy levels within the oxide layer that act as traps for electrons and holes. Q_{ot}, then, can be either positively or negatively charged depending on the trapped carrier. Unlike the oxide fixed charge, Q_{ot} can be changed by, for example, stressing the oxide layer with an electric field to give carriers enough energy to surmount the barrier height at the metal-oxide or silicon-oxide interface and then become trapped by these defects in the oxide.

The effect of Q_{ot} and Q_f is to shift the entire high frequency C-V curve with respect to an ideal curve along the voltage axis. Hence knowing the real V_{FB} from the measured C-V curve and calculating the theoretical V_{FB}, one can measure the amount of Q_{ot} and Q_f that exists in the oxide. For positive charges, the curve is shifted negatively, and for negative charges the curve is shifted positively along the voltage axis. An example of positive oxide charges shifting the C-V negatively for a capacitor fabricated with a p-type silicon substrate is demonstrated in Figure 5-30.

As its name implies, Q_m is due to mobile ions in the oxide, mainly alkali ions such as sodium and potassium. These ions cause instabilities in devices operated at high temperatures and biases because with such temperatures and biases the ions can move between the metal-oxide interface and the silicon-oxide interface. As they move between the two interfaces, the flatband voltage of the device changes because of the charge they possess. Alkali ions are positively charged, so they shift a C-V curve positively along the voltage axis if located near the metal-oxide interface and negatively if located near the silicon-oxide interface. Historically, these contaminants are one of the reasons for the delay in the implementation of MOSFETs in integrated circuit manufacture.

The fourth and perhaps most critical charge in plasma grown MOS structures is the charge trapped by interface states, Q_{it}. At the interface between the silicon substrate and the oxide layer are thought to be incomplete crystalline bonds due to the disruption of the silicon crystal lattice. When an oxide layer is grown on top of a single crystalline silicon lattice, the first layer of oxide does not fit
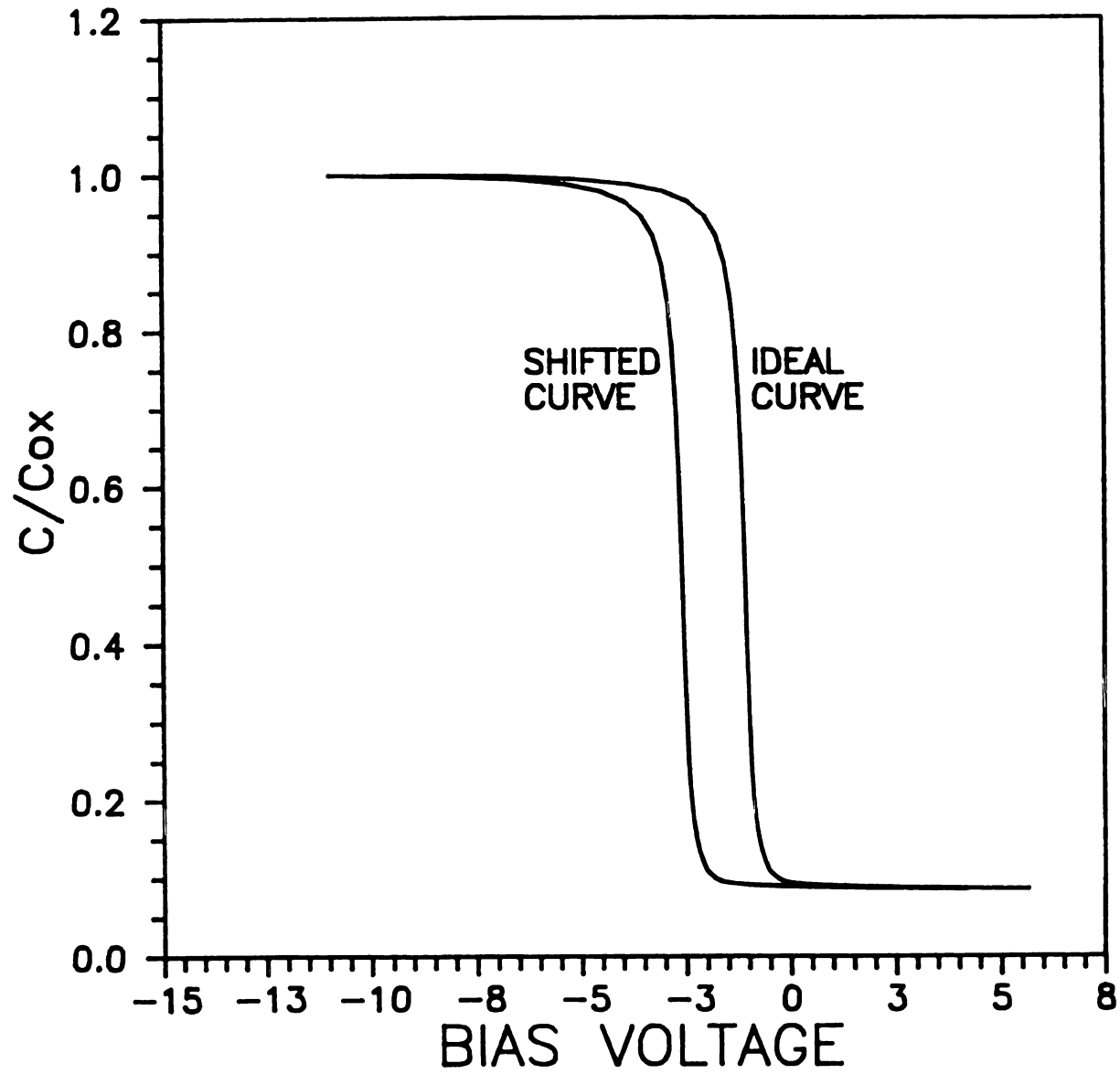
Figure 5.30 Example of the Shift of a High Frequency Capacitance
Voltage Curve by Positive Oxide Trapped Charge for an MOS
Capacitor with a P-Type Silicon Substrate

perfectly and hence it is really SiO_x with $1 < x < 2$. These weak or dangling bonds have a wide range of energies with many of them coinciding with levels in the silicon energy gap. These energy levels, or traps, are often called interface traps. The interface trap level density, D_{it}, can readily exchange and trap carriers with the silicon, i.e. be charged and discharged, which leads to the interface trap charge density, Q_{it}.

Since D_{it} is a function of energy in the band gap of silicon, the effect of these states is to "stretch-out" a high frequency C-V curve along the voltage axis. Figure 5.31 is qualitative example of such a case with interface traps in the transition region between the silicon and oxide layers. With such defects, a higher voltage operating range would be required in an integrated circuit.

The effects of each of these charges can be measured or calculated with knowledge gained from the measured high frequency, C-V curves. In this study, D_{it}, Q_f, and Q_m were quantified for the plasma grown oxides from C-V curves measured using the oxide as the dielectric in an MOS capacitor. A brief description of the methods used in the determination of each will be presented in the next section.

5.5.3 Measurement Systems and Data Extraction

Several different instruments, arrangements of equipment and computer software were used in measuring and extracting data from measurements in the analysis of the electrical properties of the plasma grown oxides. This section describes all measurement instruments and data analysis procedures.
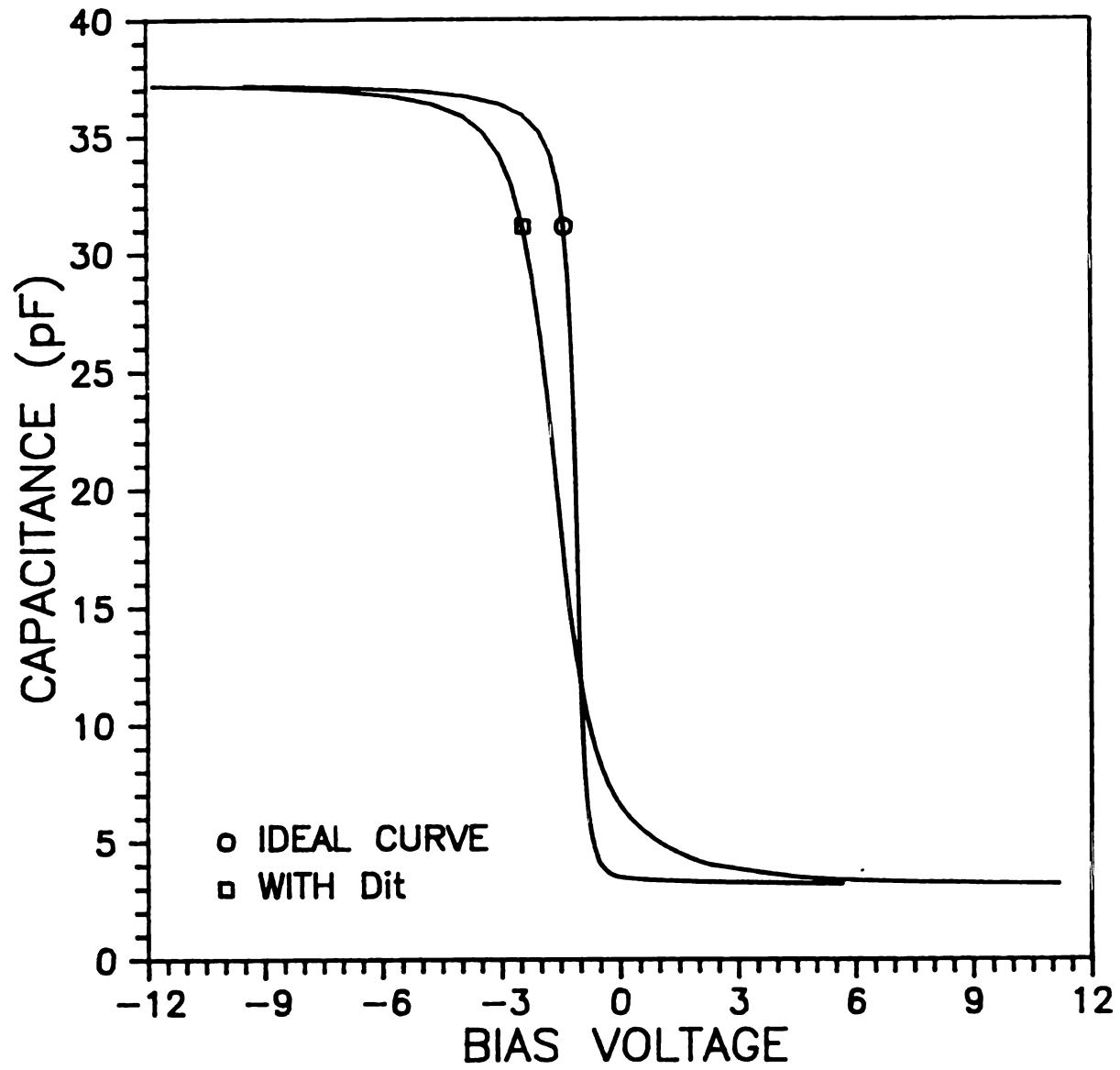
Figure 5.31 Comparison of an Ideal C-V Curve with a
Curve Stretched Out due to Interface Traps

To measure the high frequency, C-V characteristics of the capacitors fabricated as described in Section 5.5.1, two different instrumentation set-ups were used in this study. The first method utilized a Signatone Probe Station, an HP 4192A Low Frequency Impedance Analyzer and a personal computer (PC). The probe station has tungsten probes which were used to make contact with the gate of the capacitor. To make contact with the silicon substrate, the silicon wafer was mounted on a aluminum coated wafer with conducting silver paint, and another probe of the probe station was used to contact this aluminum coated wafer. The PC then controlled the impedance analyzer via a user specified program [93] to automatically trace out a high frequency (100 KHz or 1 MHz) C-V curve of the capacitor connected to the impedance analyzer via the probe station.

The second equipment arrangement to obtain C-V data is also an automated system controlled by a PC. The PC controlled several Keithley instruments: a 590 CV Analyzer, a 595 Quasistatic CV Meter, a 230 Programmable Voltage Source and a 5951 Remote Input Coupler. These instruments were connected to a light-tight probe box used to make contact to the capacitor. The probe box contained a sample platform which could be temperature controlled. This system could automatically measure both a high frequency and a low frequency C-V curve simultaneously. This set-up, (which when used was located at the Ford Motor Company's Scientific Research Laboratory, Dearborn, Michigan) with its temperature controlled sample platform, was also used in performing Bias/Temperature Stress Tests which are described below and the results of which are given in Section 5.5.5.

To measure the breakdown fields of the oxide, a Tektronix curve

tracer was used in conjunction with the Signatone Probe Station. Using the variable dc voltage control, the applied bias was slowly increased until the oxide broke down signified by a "spike" of current. Voltages where breakdown of the oxides occurred were hand copied into a lab note book and later divided by the oxide thickness to calculate the field at which breakdown occurred. These breakdown fields are reported in units of MegaVolts per cm (MV/cm). The current used to indicate the point of breakdown was 0.1 micro amp, which corresponds to a current density of approximately 3×10^{-4} amps per cm^2. This was a destructive test, i.e. the oxide was destroyed at this high field and current density.

The determination of the density of interface traps, D_{it}, was primarily done using the measured high frequency (100 KHz and 1 MHz), capacitance vs. dc voltage curves. These measured C-V curves were compared to calculated, ideal C-V curves to extract the density of interface traps. This method is commonly called the Terman method [94,95]. The implementation of this method is that of Roppel [30], who authored a computer program and thorough review of the method. Therefore, only a brief explanation will be given here.

As mentioned above, a theoretical, C-V curve is first calculated. In this calculation, the same values of d_{ox} and doping density as that of the test sample are used. To calculate the theoretical C-V curve, the silicon surface charge is first computed:

$$Q_s = \left[\frac{\varepsilon_s}{L_D}\right]\left[\frac{kT}{q}\right] \; \text{Sgn}(U_B - U_S) \; F(U_s, U_B)$$

where $U_B = -(q/kT)\psi_F = (1/kT)(E_F - E_i)_{BULK}$, and $U_S = (1/kT)(E_F - E_i)_{SURFACE}$ are dimensionless potentials due to the difference in the Fermi energy level and the intrinsic energy level in the bulk and at the surface of the semiconductor respectively. Sgn is the signum

function which returns the sign of the argument. The term $F(U_s, U_B)$ is a dimensionless electric field that is calculated as:

$$F(U_s, U_B) = (2)^{1/2} \left[(U_B - U_S)\sinh U_B - (\cosh U_B - \cosh U_S) \right]^{1/2}.$$

The next step is to calculate the silicon surface capacitance:

$$C_S = -Sgn(U_B - U_S) \left[\frac{\varepsilon_S}{L_D} \right] \frac{\sinh U_S - \sinh U_B}{F(U_S, U_B)} .$$

Now the total device capacitance is computed as C_S in series with C_{ox}:

$$C = \left[\frac{1}{C_S(\psi_S)} + \frac{1}{C_{ox}} \right]^{-1}$$

where ψ_S is the silicon surface band-bending, $\psi_S = (kT/q)(U_S - U_B) = 1/q(E_{iBULK} - E_{iSURFACE})$. Ideally, the gate voltage is the sum of the oxide voltage and the silicon band bending which is:

$$V_G = \frac{-Q_S}{C_{ox}} - \psi_S .$$

Since Q_S, $(U_S - U_B)$, and C_S are all dependent upon ψ_S, the amount of band bending in the silicon, this is chosen as the independent variable in the above equations. As should be noted, interface traps do not affect the variation of C_S with ψ_S. But, the presence of interface traps does decrease the fraction of the gate voltage, V_G, which is dropped across the silicon depletion layer. For a given bias, the band bending for the actual sample must be determined by comparing the measured C-V curve with the theoretical C-ψ_S curve. When this is done, the resulting ψ_S vs. V_G curve can be used to calculate the capacitance associated with the interface traps, C_{it}, according to the following expression:

$$C_{it}(\psi_s) = C_{ox} \left[(\frac{d\psi_s}{dV_G})^{-1} - 1 \right] - C_s(\psi_s)$$

From this expression, D_{it} can now be calculated from C_{it} by:

$$C_{it}(\psi_s) = qD_{it}(E_s) \ ,$$

here $E_s = E_i - E_v + \psi_s + (kT/q)U_B$ is a measure of the position of the Fermi energy relative to the valence band edge at the silicon surface. This $D_{it}(E_s)$ describes the distribution of the interface traps as a function of energy within the silicon bandgap. But since a C-V curve is measured from accumulation to strong inversion, the bandgap is investigated from a few kT/q energy units above (below) the valence-(conduction-) band to $\psi_s = 2\psi_F$.

To implement the entire procedure for calculating the density of interface traps, a computer program [96] was used which read each measured value of the C-V curve and then iteratively chose a ψ_s which corresponded to a theoretical value of C equal to the measured value. The values of C, ψ_s, C_s and the measured V were then stored in a new data file. From this data, D_{it} was calculated.

Another method that could be used to calculate D_{it} is called the Hi-Lo method. In this method two C-V curves, one measured at a high frequency and the other measured at a low frequency, are compared to determine C_{it}:

$$C_{it} = \left[\frac{1}{C_{LF}} - \frac{1}{C_{ox}} \right]^{-1} - \left[\frac{1}{C_{HF}} - \frac{1}{C_{ox}} \right]^{-1}$$

where C_{LF} is the capacitance from the low frequency C-V curve, C_{HF} is the capacitance from the high frequency C-V curve, and C_{ox} is the capacitance of the MOS structure in accumulation. With this procedure, the necessity of calculating C_s is eliminated. Then D_{it} is calculated

as above.

The capability of determining the D_{it} with the Hi-Lo method was available as part of the software that controlled the Keithley instruments. This option was tried several times, but the oxides grown in the plasma had too high a leakage current and therefore a good quasi-static (low frequency) C-V curve was not measurable.

A simple test, called a Bias/Temperature (B/T) Stress Test, was performed on some of the capacitors to determine if any mobile ionic charges were present in the plasma grown oxides. In this test, an initial high frequency C-V curve is first measured. Then, the temperature of the capacitor is elevated and an electric field is applied across the capacitor. In this study, a bias to maintain a positive or negative (with respect to the gate of the capacitor) one MV per cm electric field and a temperature of 160 $^{\circ}$C were applied for 10 minutes. After this B/T Stress is applied, the wafer is allowed to cool for about 2 minutes. Then, another C-V curve is measured to see if the characteristics have changed. Since Q_m are movable when given sufficient energy, this test, with its elevated temperature and electric field, causes the mobile ions to move between the silicon-oxide and oxide metal interfaces. Switching the electric field and again elevating the temperature of the capacitor moves the ions from one interface of the capacitor to the other. This test can be cycled several times to observe repeatability of the shifting of the C-V curve.

If the C-V curves do shift repeatably during the cycling of a B/T Stress Test, then this is evidence that mobile ions do exist in the oxide. To calculate the value of Q_m, the difference between two bias

voltage values corresponding to the same capacitance on two of the curves that are shifted from each other is calculated from the tests. Then using this measured voltage difference and then dividing by the the oxide capacitance will give the density of the mobile ions in the oxide:

$$Q_m = -1/2 \ \Delta V \ C_{ox}$$

For example, if an ideal capacitor has a flatband voltage of 4 V and the measured C-V curve has a flatband voltage of 5 V (Q_m at the oxide-metal interface) which shifts to 3 V (Q_m at the silicon-oxide interface) after a B/T Stress test, the actual ΔV, 2 V must be divided by two to determine Q_m.

To extract the density of fixed charges, Q_f, in the oxide, knowledge of the measured V_{FB} and theoretical V_{FB} is required. The theoretical V_{FB} is calculated as above. The measured V_{FB} is found by calculating C_{FB}, locating C_{FB} on the measured C-V curve and determining what voltage corresponds to this capacitance. Then using the difference between these two V_{FB}, the density of fixed charges, Q_f, in the oxide is calculated as:

$$\Delta V_{FB} = V_{FB}(real) - V_{FB}(theoretical) = Q_f/C_{ox}$$

or:

$$Q_f = - \ \Delta V_{FB} \ C_{ox}$$

However, if both Q_m and Q_f exist in the oxide, then the two equations must be combined in such a way as to account for where the charges are. If a B/T Stress Test is used, then this is simplified somewhat. When a B/T test is used to attract all the mobile ions to the Si-SiO$_2$ interface, then the two charges act in unison as:

$$\Delta V_{FB} = -(Q_f + Q_m)/C_{ox}.$$

This assumes that all the mobile ions have moved to the interface. Next if a B/T test is used to attract all the mobile ions to the metal-SiO_2 interface, then the two charges act against one another as:

$$\Delta V_{FB} = -(Q_f - Q_m)/C_{ox}.$$

So knowing the theoretical V_{FB} and being able to measure the real V_{FB} from C-V curves, in conjunction with a B/T Stress Test, the two charge densities can be calculated.

5.5.4 C-V Measurements and D_{it} Results

Capacitors were fabricated, as described in Section 5.5.1, on several oxides grown under various conditions so that they could be characterized with a high frequency C-V test. The oxides grown without the quartz tube in place during anodization exhibited a very large stretch-out. This stretch-out is evidence of a large interface trap density, D_{it}. Figure 5.32 is a representative example of the C-V characteristics of an annealed oxide from DS-15 which was anodized at 4 cm below the oxygen plasma discharge. When compared to the theoretical, ideal curve also shown, the stretch-out is very evident.

Figure 5.33 shows two curves from samples grown 6 cm below the plasma discharge again without the quartz tube. One curve is an as-grown sample from DS-21 and the other is an annealed sample from DS-27 measured at 100 KHz. Again, the stretch-out is quite severe. The measurement performed at 100 KHz gives the appearance of being better than it really is. This will be discussed, along with an example from DS-37, shortly.

In Figure 5.34 are shown measured C-V curves from oxides grown 8
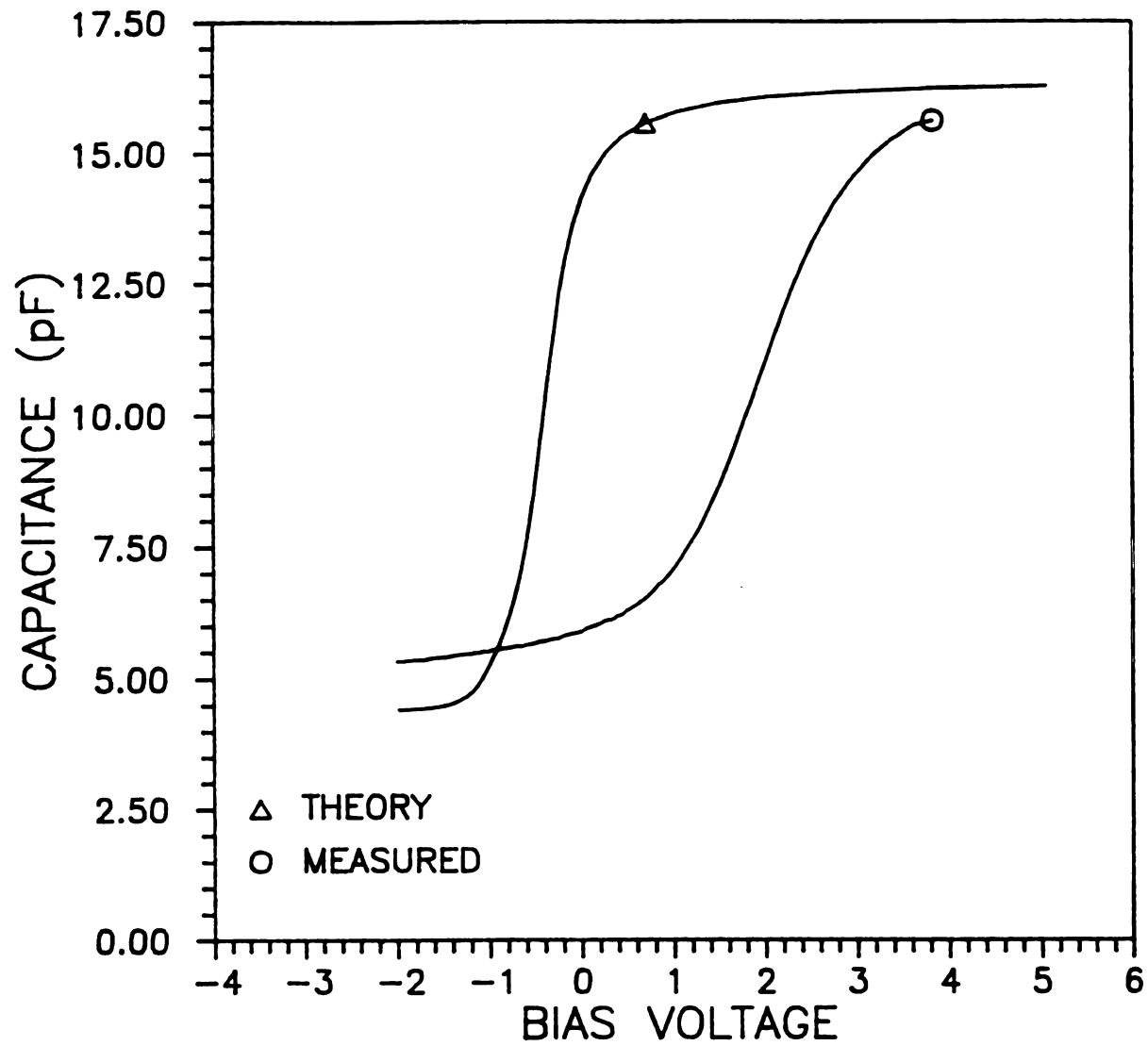
Figure 5.32 Measured High Frequency C-V Curve of DS-15
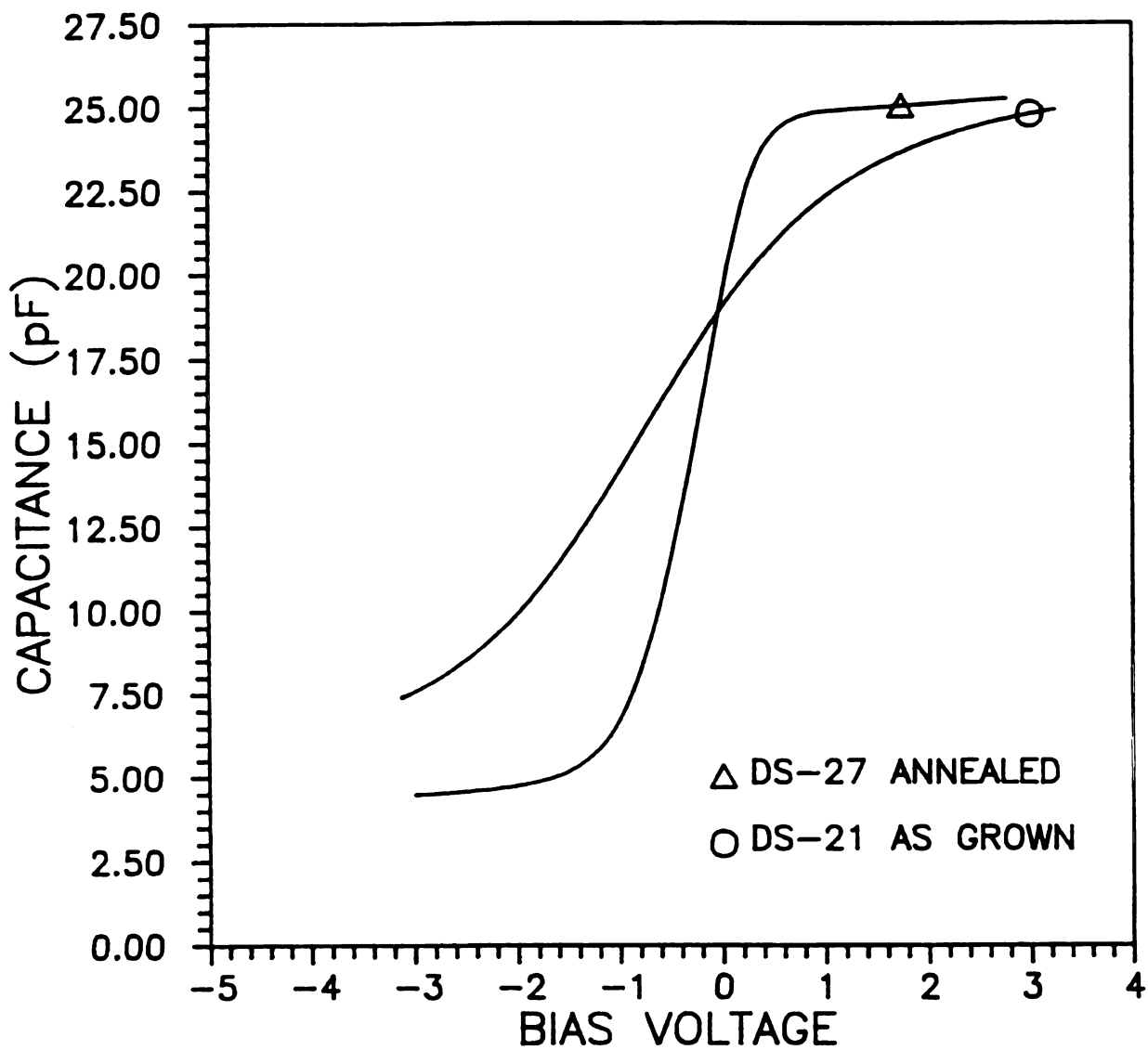
Figure 5.33 C-V Curves of DS-21 (as-grown) and DS-27 (annealed)
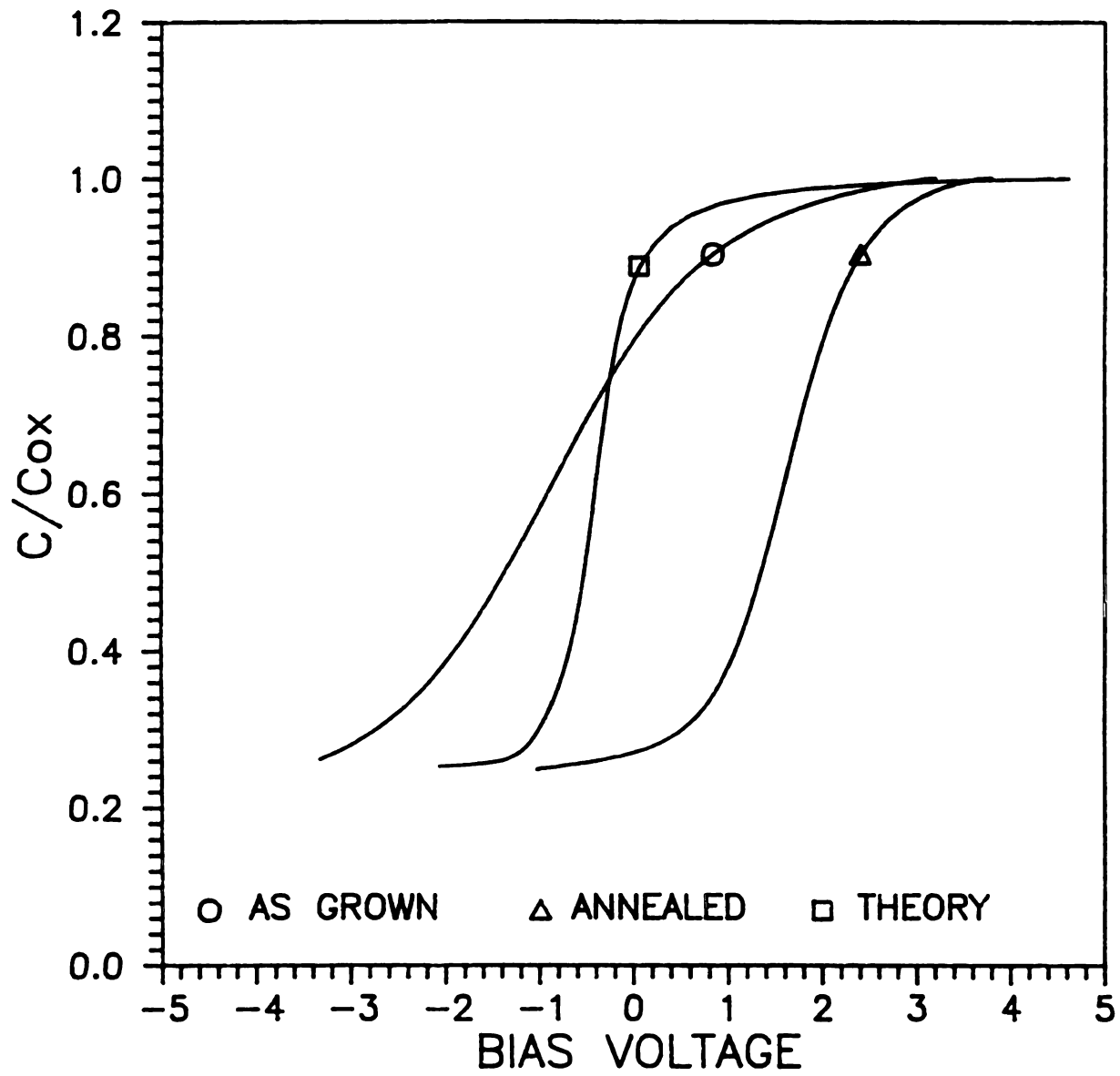
Figure 5.34   C-V Curves of DS-30 (as-grown and annealed)

cm downstream without the quartz tube. These two curves are from DS-30 and again are an as-grown and an annealed oxide sample.

As mentioned above, the oxides grown without baseplate shielding, i.e. without the quartz tube in place, all exhibited a large stretch-out. Consequently, D_{it} results were very high, in the upper 10^{12} and lower 10^{13} states per cm^2 per eV range even after annealing, for all downstream distances. However, the oxides grown with the quartz tube in place did not exhibit as large a stretch- out as will be shown below. Thus the large stretch-out of the C-V curves of the oxides grown without the quartz tube in place could be due, in part, to the metal content of these particular films.

The oxides grown with the quartz tube in place showed somewhat better C-V curves, i.e. did not exhibit as much stretch-out. Figure 5.35 is a representative example of measured C-V characteristics from DS-33 annealed and as-grown. Also presented for comparison is a calculated curve. The values of D_{it} extracted from these curves with the Terman method are shown in Figure 5.36. The annealed oxide exhibited a D_{it} minimum at mid-gap of approximately 8 X 10^{11} states per cm^2 per eV while the as-grown oxide showed a minimum of 1.1 X 10^{12}.

DS-34 was anodized under the same conditions as DS-33, i.e. 6.5 cm downstream from the plasma with the quartz tube in place. Figures 5.37 and 5.38 show the results of C-V measurements and D_{it} extraction from this curves for an annealed sample. The values are very close to those obtained for DS-33, showing that the process is indeed repeatable.

Figure 5.39 shows two curves measured on the same capacitor on DS-37, one measured at 100 KHz and the other at 1 MHz. As can be seen, the curve measured with an ac signal of 100 KHz is less stretched out,
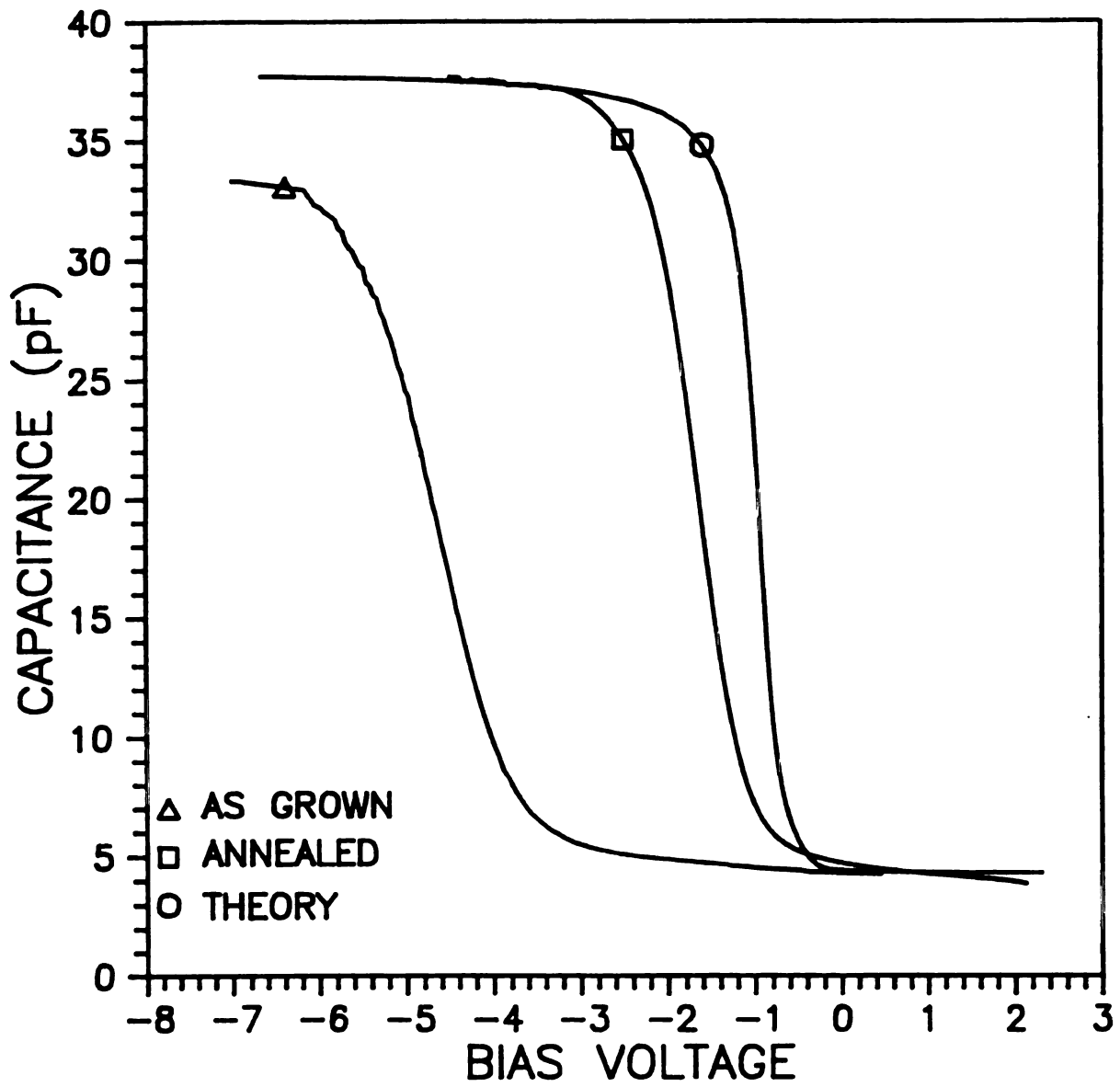
Figure 5.35 C-V Curves of DS-33 (as-grown and annealed)
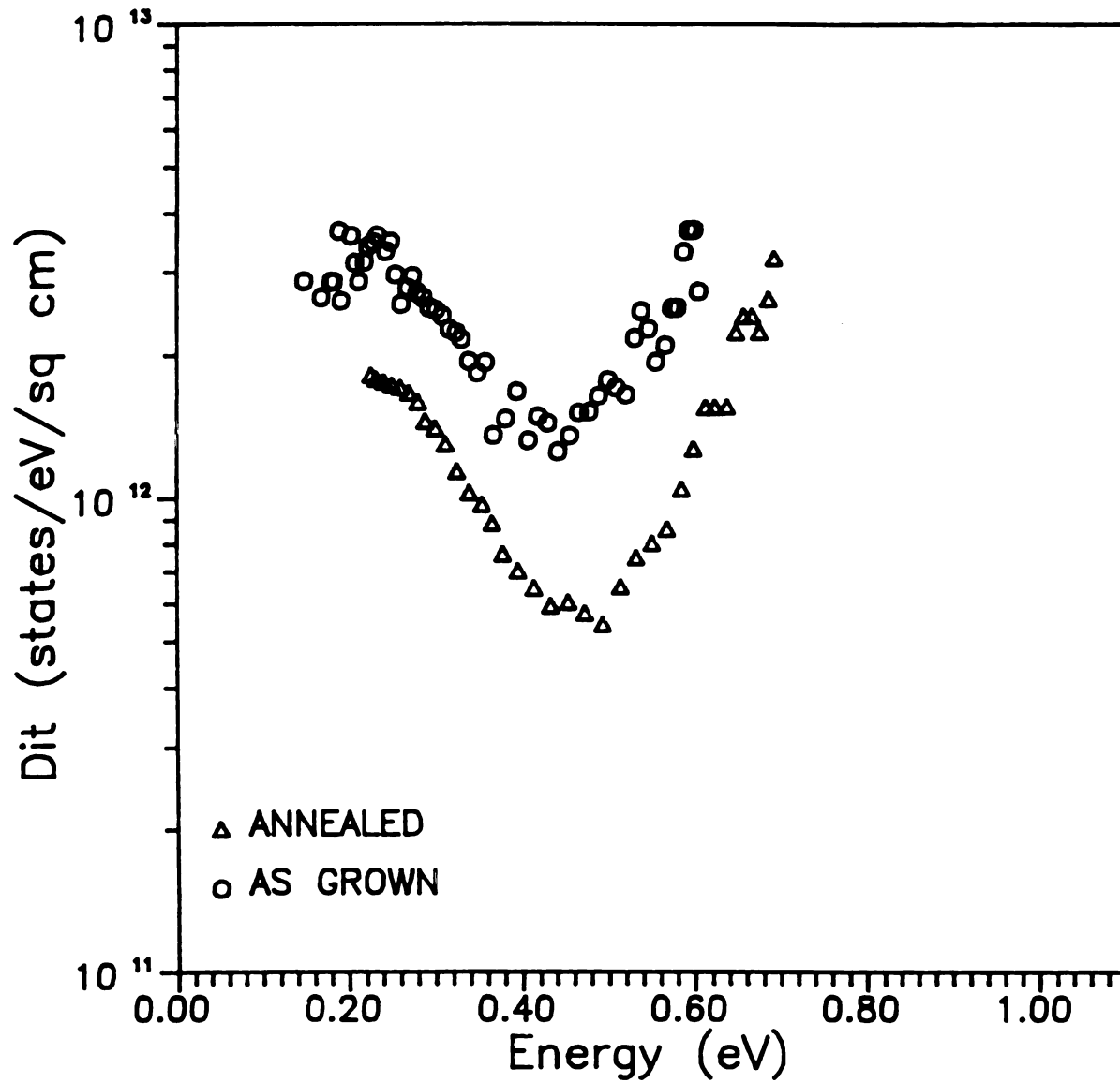
Figure 5.36 Density of Interface Traps of DS-33
from both the As-Grown and Annealed Oxides
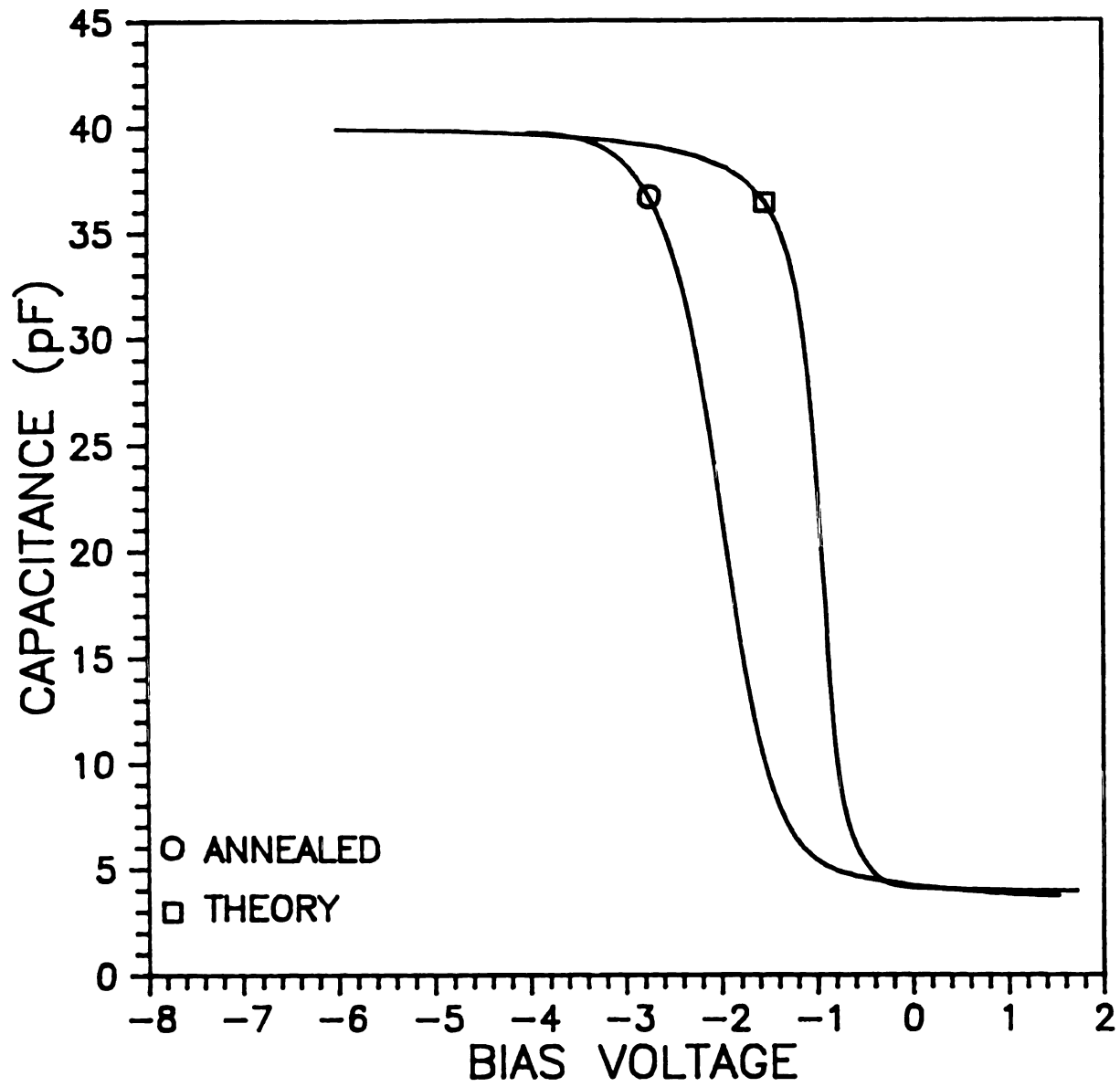
Figure 5.37   C-V Curve from DS-34 (annealed)
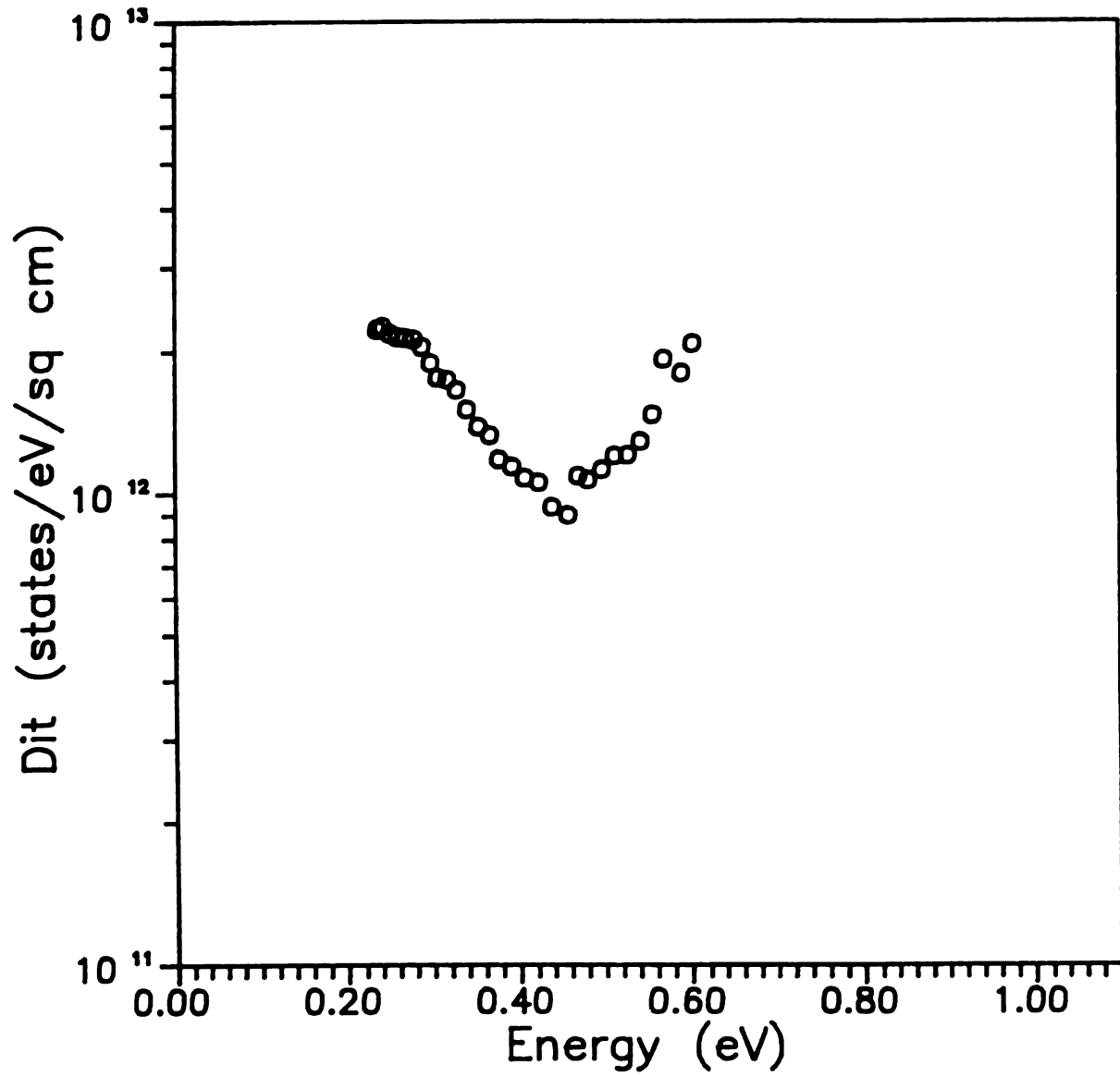
Figure 5.38 Density of Interface Traps from DS-34 (annealed)
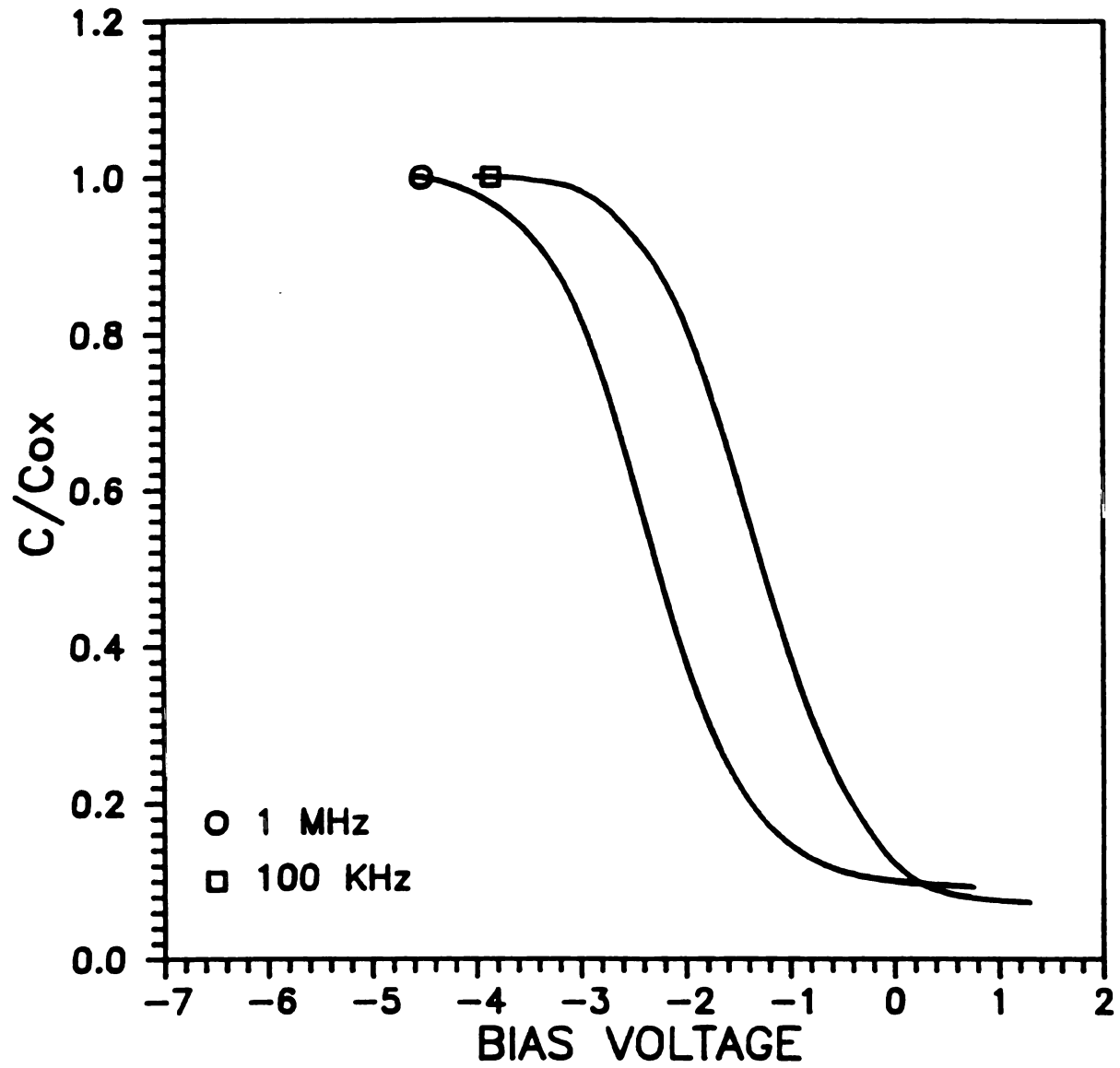
Figure 5.39 Measured C-V Curves of DS-37, 100 KHz and 1 MHz ac Signal

but shifted more than the curve measured with the 1 MHz signal. This is most likely due to some of the interface traps being able to react to the lower frequency signal and hence charge. The fact that there is less stretch out at the lower frequency is again born out in that the D_{it} is lower. The values for the interface trap density extracted from these two curves is shown in Figure 5.40 and indeed the midgap minimum is lower for the C-V curve measured with the 100 KHz signal.

State-of-the-art, thermally grown, annealed silicon oxides can have a density of interface traps in the low 10^{10} traps per eV per cm^2 range. The oxides grown in this study with plasma anodization are seen to have slightly more than an order of magnitude higher interface trap density. This could be due in part to the measurable heavy metal content in the films. Also, since this is a low temperature process, it is hypothesized that the temperature of this particular process is so low that even with a one hour, 450° C anneal, the energy to form the bonds between the silicon and oxygen, and hence reduce the number of dangling bonds thought to produce interface traps, is not present.

In comparison, Barlow et. al. [29] reported a density of interface traps minimum at midgap of 5 X 10^{10} states per eV per cm^2 for an oxide grown an O_2/Cl_2 combination plasma sustained with rf power. In addition to this gas mixture, the substrates were also heated to 500 $^{\circ}$C during anodization and then annealed with a two step process, 1 hour, 480 $^{\circ}$C H_2/N_2 post anodization anneal followed by a 1 hour 390 $^{\circ}$C H_2/N_2 post metal anneal. In another rf sustained oxygen plasma process, Nelson et. al. [33] report higher values for D_{it}, approximately 2 X 10^{11} states per eV per cm^2 for oxides grown with the substrate heated to 475° C. Ho and Sugano [19] reported a higher density of interface
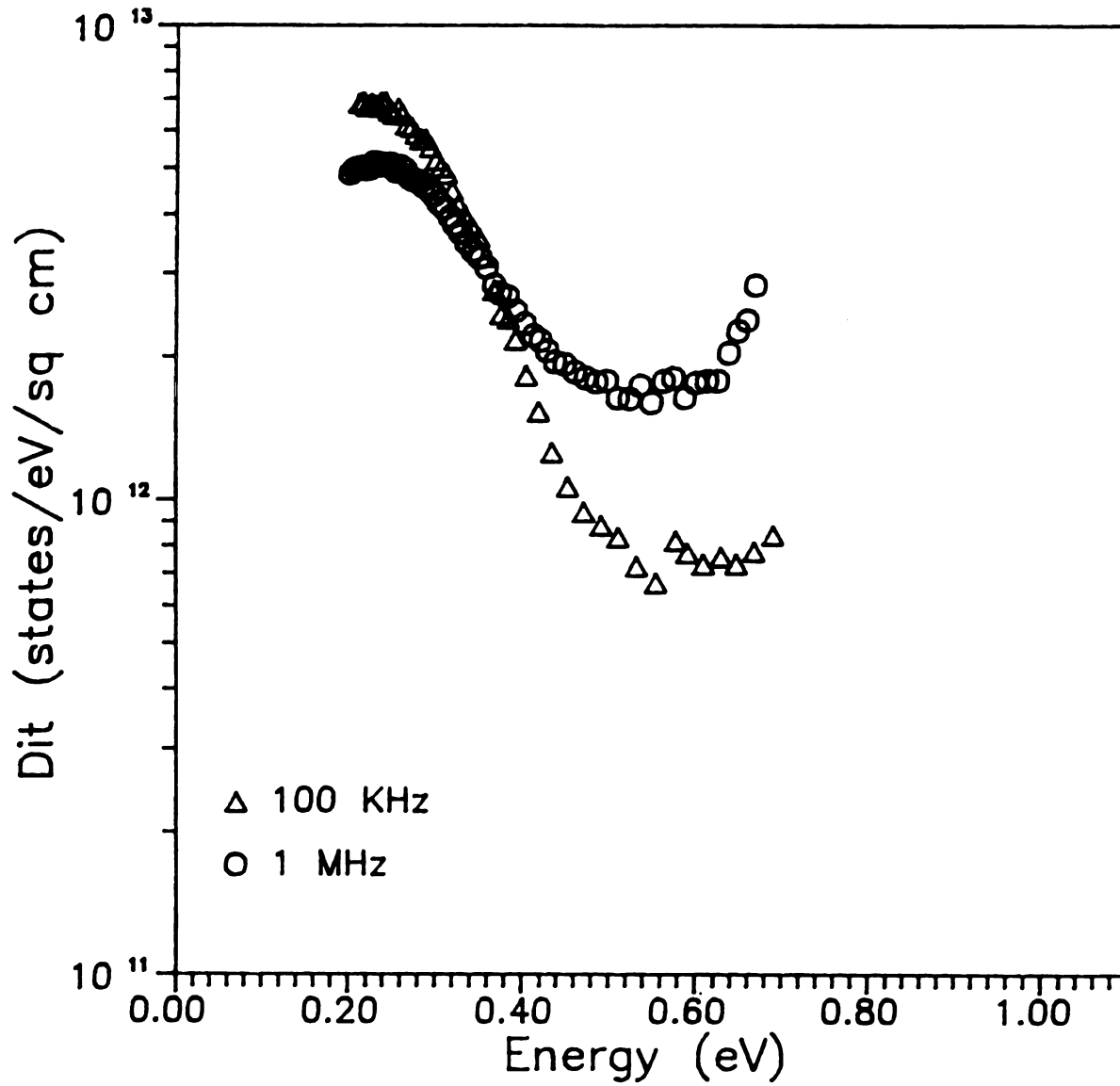
Figure 5.40 Density of Interface Traps from DS-37
Using the 100 KHz and 1 MHz ac signal C-V Curves

states, 10^{12} states per eV per cm^2 for as-grown oxides in which the substrate was heated to $600^\circ C$ during anodization in a 420 KHz rf power sustained plasma. But following a 1 hour $450^\circ C$ anneal in an H_2/N_2 ambient, this fell to the low 10^{10} range.

In the work of Roppel [30], the first work using an MPDR but without the ECR mode, the D_{it} minimum for as-grown oxides was found to be 1.7 X 10^{11} states/eV/cm^2 while those annealed in the same manner as in [19] were found to have a minimum of 1.8 X 10^{10} states/eV/cm. These values were determined from C-V curves measured at 100 KHz, this may lead to the possibility of a higher D_{it} than was actually reported as discussed above. For Roppel's work the substrates were small (1.2 cm diameter) and placed directly in the discharge region. While the substrates were not heated, it is very possible the temperature of the wafer during anodization was 300 to 350 $^\circ C$. The biasing of that work was such that no metallic contamination would be incorporated in the oxide films.

As mentioned above, heating the substrate in future work using the MPDR for plasma anodization of silicon will very likely reduce the interface trap density.

5.5.5 B/T Stress, Q_m, and Q_f Results

A B/T Stress Test, as described in Section 5.5.3, was used to test for the presence of mobile ions in some of the plasma grown oxide layers. Figure 5.41 shows C-V curves measured on a capacitor fabricated on sample DS-33 after several B/T Stress cycles. These results are a composite of five C-V curves. The first is an initial
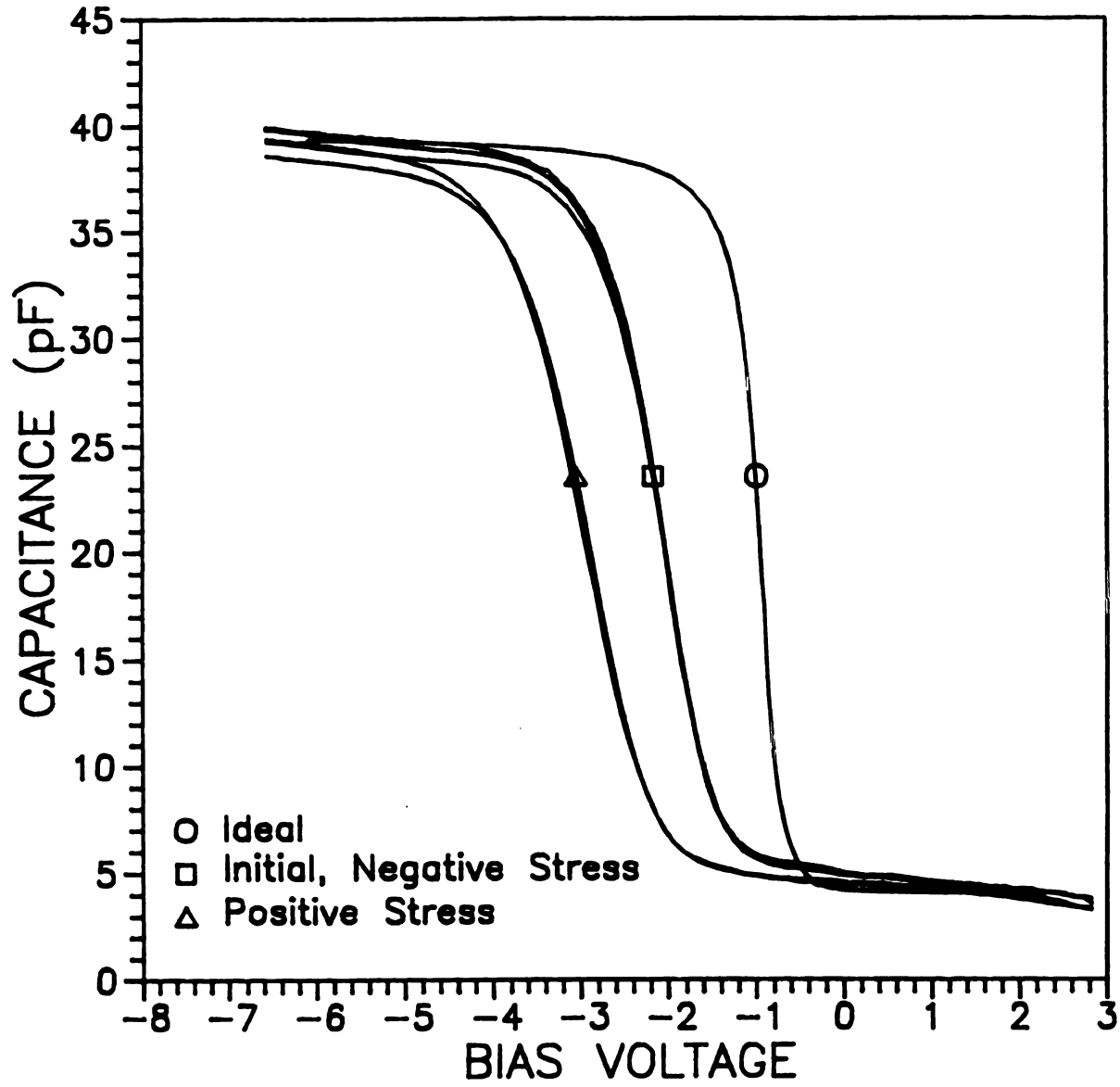
Figure 5.41 Results of a B/T Stress Test on Sample DS-33

measurement followed by a positive, a negative, a positive and lastly a negative B/T Stress. As can be seen, the test repeated almost exactly. Also presented in this figure, for comparison with C_{FB} and V_{FB}, is a theoretical curve. From this data and from the calculation of the C_{FB}, (≈ 16.7 pF), the measured and theoretical V_{FB} were found as:

$$V_{FB}(\text{theoretical}) = -0.894 \text{ V}$$

$$V_{FB}(\text{shift 1}) = -1.932$$

$$V_{FB}(\text{shift 2}) = -2.763$$

Using the equations at the end of Section 5.5.3:

$$\Delta V_{FB}(1) = -1.932 - (-0.894) = -q(Q_f - Q_m)/C_{ox}$$

$$\Delta V_{FB}(2) = -2.763 - (-0.894) = -q(Q_f + Q_m)/C_{ox}$$

($C_{ox} = 39.38$ pF) leads to a Q_f of 1.137×10^{12} and a Q_m of 3.25×10^{11} charges per cm^2. These values may be due in part to the measurable metal content in the oxide layers.

This value of Q_f found for the plasma anodized oxides is similar to that of as-grown thermal oxide which can have fixed charge density in the upper 10^{11} to low 10^{12} range. However, after annealing Q_f values for thermally grown oxides drops to the low 10^{11} range [97]. Reports for other plasma grown oxides, with the wafer heated during anodization, show, for example, 8×10^{11} charges per cm^2 for oxides grown in a pure oxygen plasma without an anneal and 6×10^{10} charges per cm^2 for an oxide grown in a combination O_2/Cl_2 plasma followed by an anneal [29]. In the work of Roppel [30] Q_f was determined to be 4×10^{11} to 1×10^{12} cm^{-2} for as-grown oxides while Q_f for annealed oxides was reduced to about 1×10^{11} cm^{-2}.

It is noted that the plasma apparatus was not in a clean room environment and the Q_m could be due in part to sodium contamination

which is omnipresent in non clean systems. Alternatively, this could be a result of metallic contamination. This is an issue for future study.

5.5.6 Oxide Break Down Field Results

The last electrical test performed on the oxide films grown with an oxygen plasma sustained in the MPDR was to investigate the oxide strength when subjected to an electric field. This test, described in Section 5.5.3, was carried out on 25 capacitors from each oxide for which breakdown data is reported.

Figures 5.42 and 5.43 show the breakdown fields for capacitors on DS-30 from a pre-anneal (as-grown) and an annealed sample respectively. This was one of the oxide layers grown without the quartz tube in place. Hence with the metal content of the film, the oxide strength was quite low. The as-grown oxide exhibited a very small break down field average of 2.67 MV/cm. The annealed sample of DS-30 showed a somewhat larger break down field average of 4.86 MV/cm but with two rather distinct populations. For a thermally grown, annealed oxide, one report for oxides with a similar thickness (400 Å) found a 50 % failure rate at a field strength of 7.6 MV/cm [98].

The oxides grown with the quartz tube in place to shield the films from sputtering contamination from the baseplate showed a somewhat higher oxide field strength. Figures 5.44 and 5.45 show the field strength for the annealed plasma grown oxide layers of DS-33 and DS-34 respectively. For DS-33, the annealed oxides had a break down field average of 5.66 MV/cm. DS-34 showed an even higher average of 7.80
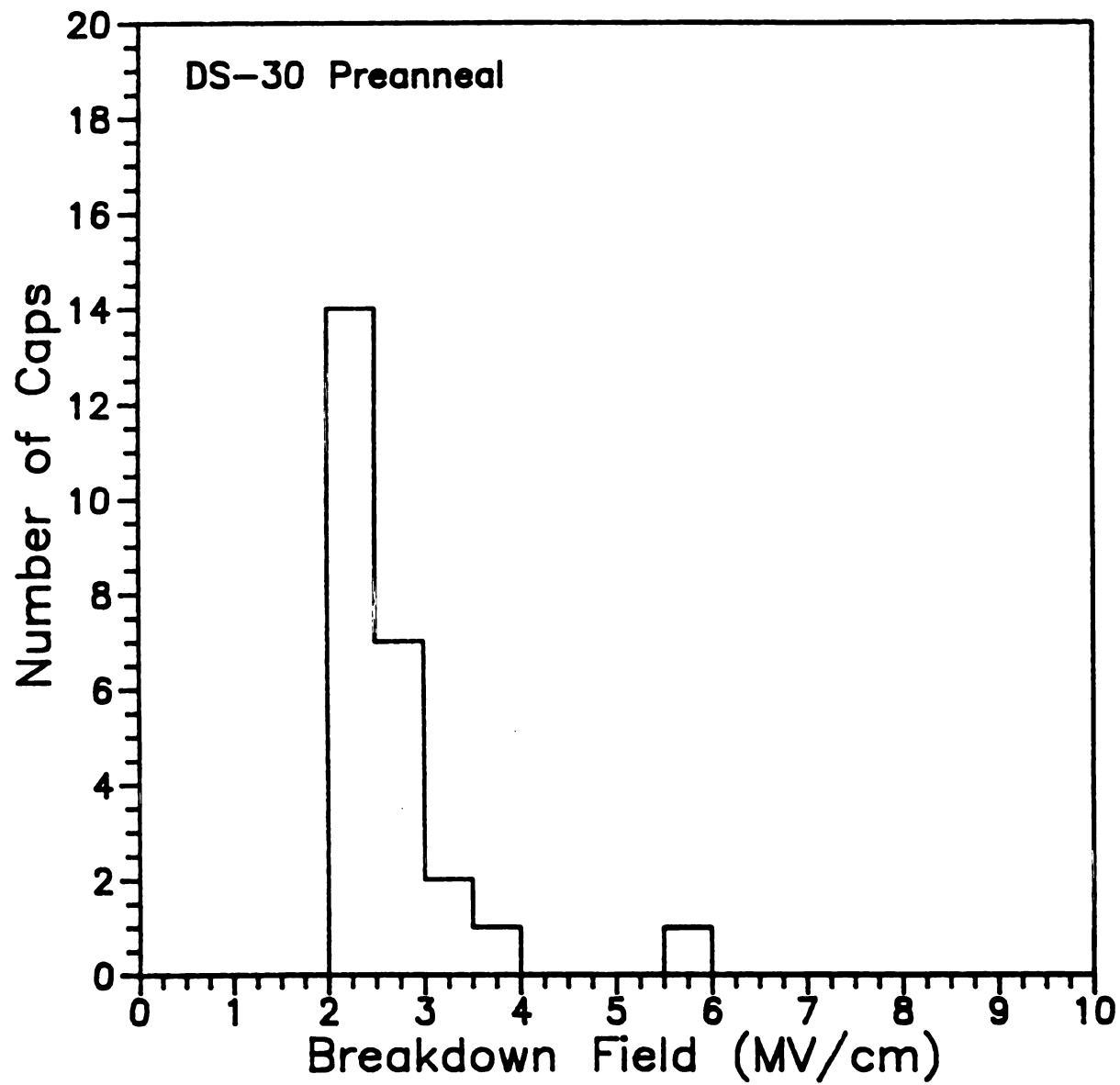
Figure 5.42 Breakdown Fields of 25 Capacitors of DS-30 (as-grown)
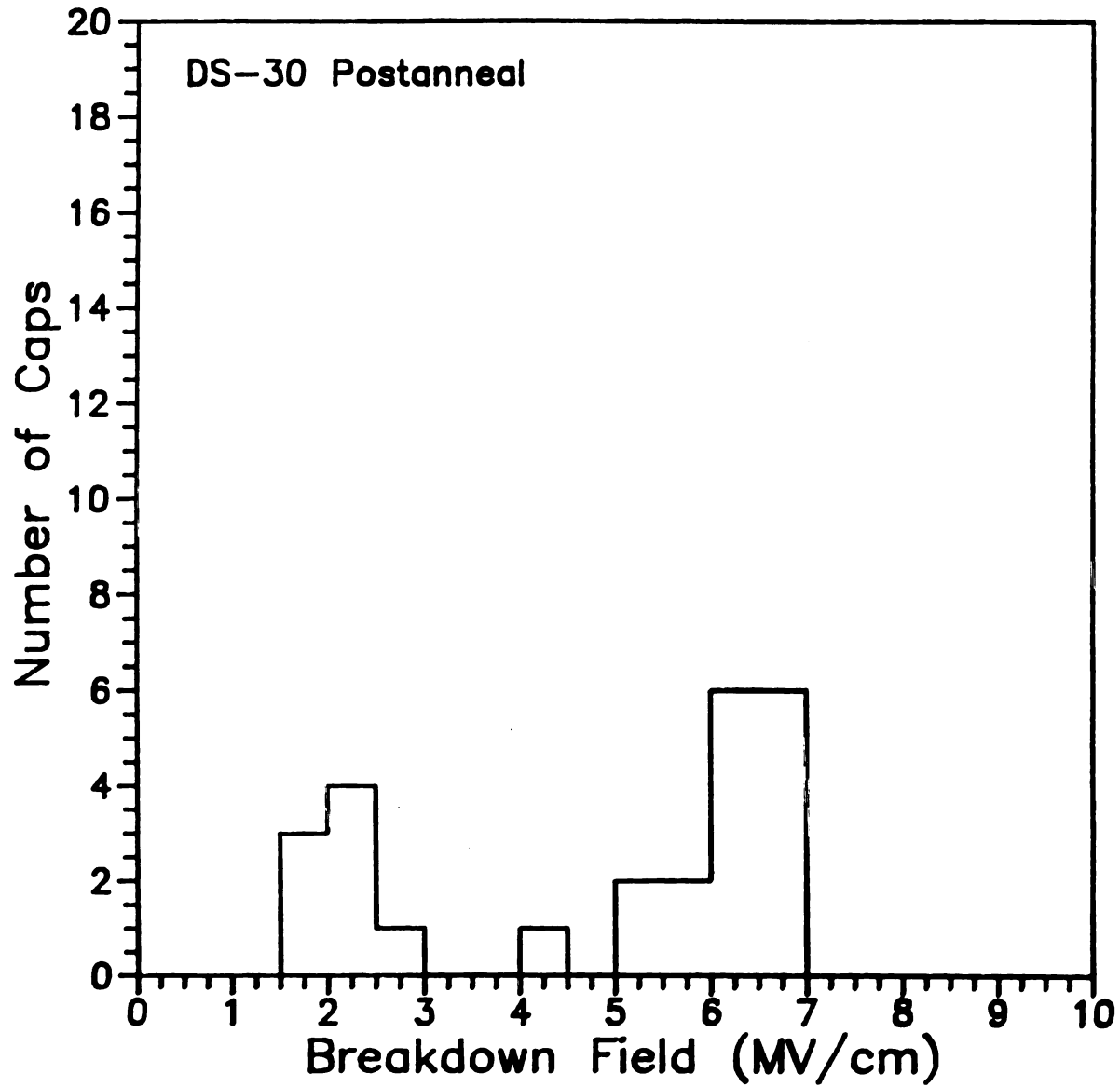
Figure 5.43 Breakdown Fields of 25 Capacitors of DS-30 (annealed)
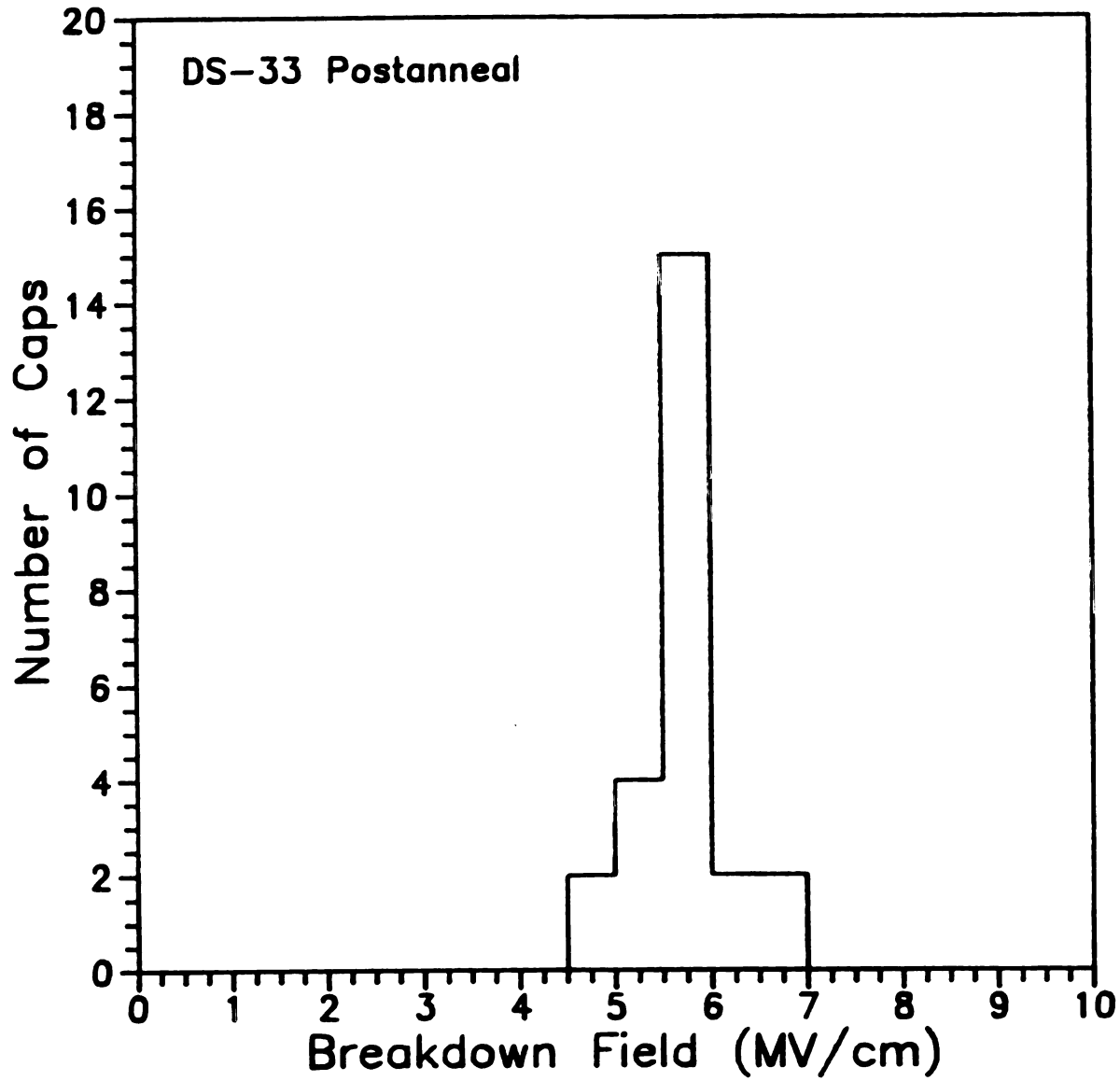
Figure 5.44 Breakdown Fields of 25 Capacitors of DS-33 (annealed)
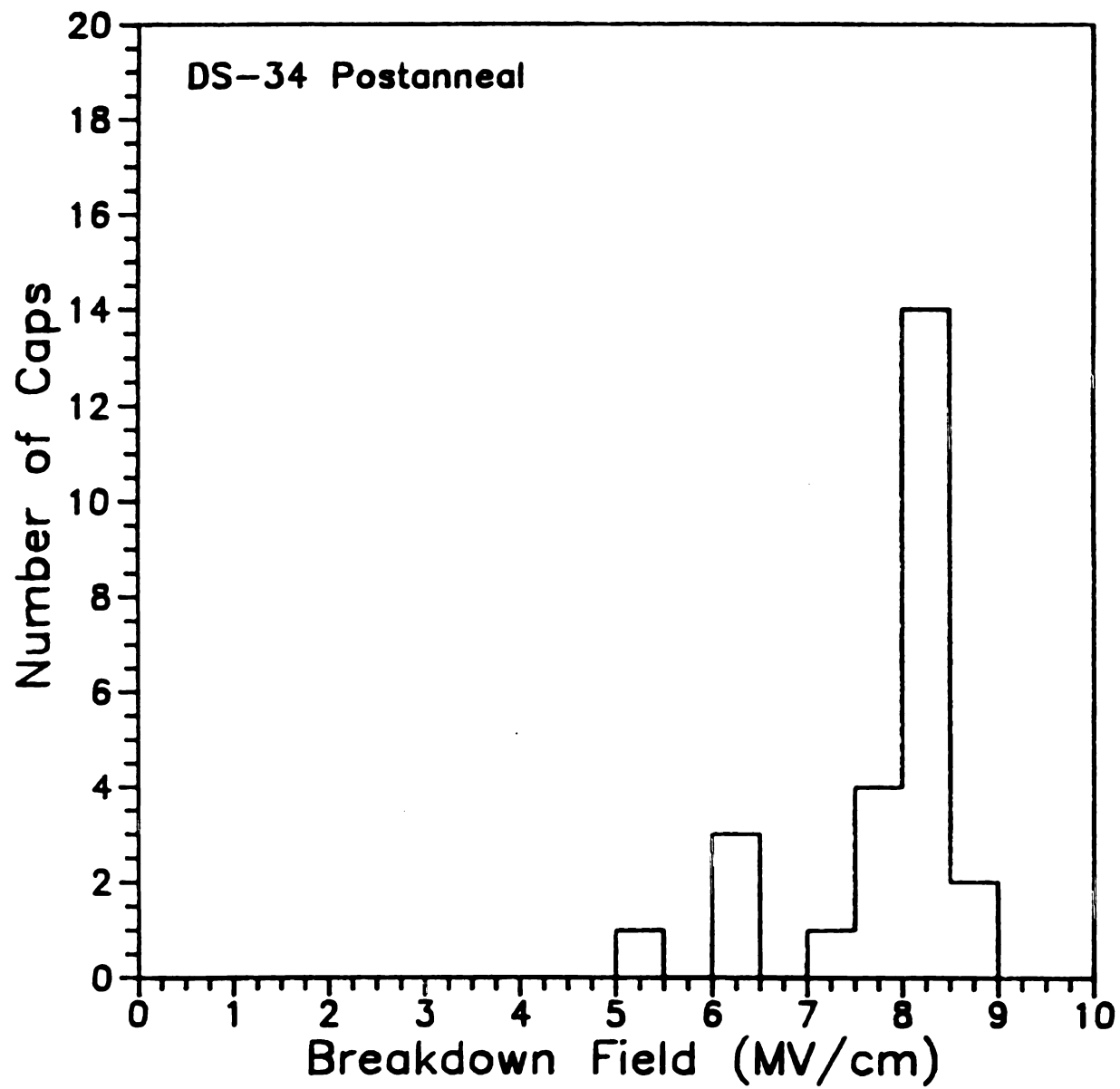
Figure 5.45 Breakdown Fields of 25 Capacitors of DS-34 (annealed)

MV/cm. These values are comparable with the study mentioned above for thermally grown oxides. In addition, the as-grown oxides of [29] using an oxygen plasma without an anneal exhibited break down fields between 5 and 8 MV/cm. (The oxides grown in [29] with a combination O_2/Cl_2 plasma followed by an anneal had somewhat higher break down fields which peaked sharply around 10 MV/cm .)

The work of Roppel [30] found very similar breakdown field results to the ones reported here. A breakdown field histogram for as-grown oxides peaked between 1 and 2 MV/cm while for annealed oxides the peak rose to very nearly 7 MV/cm for the work reported there [30].

l
u
A
a
5
■
i
b
p
o
p
s
ln
ap

CHAPTER SIX

ECR Argon Plasma Sputter Removal of Oxides

A sputtering!!   Show me a sputtering!!

6.1   EXPERIMENTAL METHOD AND CONFIGURATION

This chapter describes preliminary research into the use of the MPDR operating in the ECR mode to sustain an argon plasma which was used to sputter remove layers of silicon dioxide from silicon wafers. As mentioned in Section 2.5, an *in situ* method of removing small amounts of oxide layers and other contaminants from a wafer surface just prior to the deposition or growth of subsequent, overlying materials is becoming more and more desirable as device sizes and hence inter-layer contact sizes are shrinking.   Thus contact resistance between layers must be minimized, which leads to the need for a process for cleaning these inter layer contacts.   ECR sputter cleaning offers the combination of a useful sputtering rate (because of a high plasma density) with a low substrate/plasma potential (hence low sub- strate damage and contamination).

The same wafer holder as in the oxidation work was used in this investigation.   In this sputtering work, however, an rf bias was applied to the wafer holder to induce a negative self-bias on the wafer

as described in Section 3.2.3. Thus, the conduction path from the atmosphere to the wafer holder was different, i.e. co-axial conductors were used to carry the rf power from the matching network to the wafer holder.

The basic configuration used in this sputtering work was the same as that used in the anodization work. However, two different ECR base-plates, one designed by Dahimene [77], which was used exclusively in the anodization work, and one designed by Hopwood [78], were used in this study. Two differences between the baseplates are, the Hopwood design was thinner (1 inch thickness vs. 1.25 inch thickness) than the Dahimene design, and the Hopwood baseplate had newer, stronger magnets (3000 gauss vs. 2500 gauss pole face strength). The difference in the thickness of the baseplate may mean a higher density of plasma species, when using the Hopwood design, since there is a 0.25 inch reduction in the distance between the bottom of the quartz containment vessel and the wafer to be processed. Hence there is a smaller recombination area for plasma species. Additionally, with the stronger magnets, the 875 Gauss magnetic field which provides the ECR zones is further from the wall of the quartz containment.

Also in the sputtering work, two different belljars were used (18" diameter and 14" diameter). With a larger belljar diameter, the radial plasma density distribution will be, in principal, more uniform since the recombination surfaces will be at a larger radial distance, i.e. further from the center of the processing chamber. However, the densities would be lower because the plasma expands to fill a larger volume.

Another variation was the use of top plates {(19) in Figure 3.1}

with different size openings, (vacuum port sizes). Openings of 6.75, 7.00 and 7.75 inches were used in combinations with the above variables to investigate the effect each combination would have on the uniformity of the sputtering. As with a larger diameter belljar, a larger opening in this top plate would increase the radial density distribution uniformity, although the peak downstream density would be lower. A list of the various combinations of baseplate, belljar, and top plate opening for each trial is listed in Table 6.1.

Table 6.1 Equipment Combinations Used for Sputtering

TRIAL	BELLJAR DIAM (in)	PORT DIAM (in)	BASEPLATE	COMMENTS
RES3	14	6.75	MD	
RES4	14	6.75	MD	
RES5	14	6.75	MD	Magnets out of phase
RES6	18	7.00	JAH	
RES7	18	7.00	JAH	-70 V dc induced bias
RES8	14	7.75	MD	"old" magnets
RES9	14	7.75	JAH	"new" magnets
RES10	14	7.75	JAH	"new" magnets
RES11	14	7.75	JAH	"new" magnets
RES12	18	7.75	MD	"new" magnets
RES13	14	7.75	JAH	MPCS & "new" magnets
RES14	14	7.75	MD	MPCS & "old" magnets

The conditions used for sputtering are summarized in Table 6.2. Less power was needed in the sputtering work, 205 W of microwave input power for the argon plasma as opposed to 265 W for the oxygen plasma, because an argon plasma is easier to sustain. Taking advantage of this fact, a much lower pressure in the vacuum chamber was used which should increase the uniformity of the ion density distribution since plasma species can diffuse farther at a lower pressure. In all sputtering experiments conducted, except RES7, an rf bias sufficient to induce a -50 V dc wafer bias, as measured with the arrangement described in Section 3.2.3, was used (RES7 used an induced bias of -70 V dc). This was approximately 30 Watts incident 13.56 MHz rf power with 6 Watts reflected.

Table 6.2   Conditions for Sputtering Silicon Dioxide Layers

Vacuum chamber pressure	0.78 milli Torr
Microwave power input	200 - 210 Watts
Microwave power reflected	$\leq$ 3 Watts
Argon Flow	7.5 sccm
Input Probe Depth	1.9 - 2.1 cm
Cavity Height	7.1 - 7.3 cm
Sputtering Time	5 minutes

In all the trials performed, the wafer was located 8 cm downstream from the plasma discharge. This distance was chosen after consideration of the oxygen plasma anodization work in which it was found

that the processing uniformity reached its peak at this distance from the discharge.

The wafer served as the cathode in this work while the baseplate and the top plate of the vacuum chamber {(14) and (19) respectively in Figure 3.1} were grounded to serve as the anode. Also, an implosion cage around the belljar {(18) in Figure 3.1} was grounded to contain any rf radiation. The quartz tube which was used in some of the anodization experiments was not used in any of the sputtering trials since the bias was such that no heavy ions were accelerated into the baseplate or top plate of the vacuum chamber.

In an effort to improve uniformity of the sputtering results, use was made of a Multi-Polar Confinement Structure (MPCS) [99,100] in the last two experiments. This multi-cusp magnetic arrangement is used to confine the ions and hence improve the uniformity of the radial ion density distribution. The magnetic strength of the MPCS is high enough to provide confinement downstream of the plasma, but not high enough to provide ECR zones.

Figure 6.1 shows a cross sectional view of the sputtering arrangement including the MPCS. The eight alternating magnets of the MPCS were aligned with the eight alternating magnets in the baseplate but with the opposite pole face. In other words, a north pole in the baseplate was aligned with a south pole of the MPCS. The 6" X 0.50" X 0.50" MPCS magnets (27) were contained in 6" X 0.75" X 0.75" square aluminum tubes (26) to protect the magnets from the plasma species. The aluminum tubes were then attached to the top plate of the vacuum system (19) such that the MPCS magnets were inside the top plate vacuum port opening and in contact with the baseplate as shown in the figure.

Figure 6.1 The Sputtering Arrangement Including the MPCS

The inner diameter of the MPCS structure is 6.25" with the magnet faces at a diameter of 6.375". In contrast, the magnet faces of the baseplate are at a diameter of 4.25".

To characterize the sputtering, the thickness of silicon dioxide that was sputter removed and the uniformity of this thickness were measured with the ellipsometer described in Section 5.2.2. To do this, an 89 point X-Y grid measurement was made before and after a sputtering experiment and the latter measurement subtracted from the first. Every effort was made to measure the same 89 points by aligning the wafer with markings on the ellipsometer's stage to within $\pm$ 1 mm. The ellipsometer has a 50 micron (0.05 mm) diameter spot size.

As mentioned in Section 5.2.2, the ellipsometer is able to measure the oxide thickness to within $\pm$ 3 Å. Hence when subtracting the measured oxide thickness after a sputtering from the initial oxide thickness, there is an uncertainty associated with the result given by the expression presented in Section 5.2.1:

$$(x_1 \pm e_1) - (x_2 \pm e_2) = x_1 - x_2 \pm (e_1^2 + e_2^2)^{1/2}.$$

Thus the overall uncertainty in the amount of oxide sputtered off is $(3^2 + 3^2)^{1/2} = 4.2$ Å.

6.2 SAMPLE PREPARATION

The samples used in the sputtering work were three-inch, p-type, silicon wafers upon which a thermal oxide was grown. Before oxidation, the wafers were cleaned using the procedure described in Section 4.2.1. After this, the wafers were oxidized using conventional thermal techniques, i.e. placing the wafers in a quartz boat and pushing them

into a quartz tube that was concentric with a high temperature, resistively heated furnace. The temperature of the furnace was approximately 1050° C with 99.9997% pure oxygen flowing through the quartz tube. This is what is often termed a "dry oxidation". The wafers were left in the furnace for a sufficiently long enough time to grow 1500 to 1800 Å of oxide on the wafers, approximately 2 hours.

After the wafers were pulled out of the tube and allowed to cool, they were covered with positive photoresist and baked at 100° C for 20 minutes. Then the oxide was etched off the bottom side of the wafer using the buffered oxide etch described in Section 5.2.1. After the oxide was removed from the back side of the wafer, the photoresist was removed by rinsing with acetone, methanol, and DI.

Once the photoresist was removed from the silicon wafers, the ellipsometer was used to measure this initial oxide thickness as described above in Section 6.1. After the initial oxide thickness was measured, the wafer was mounted on the wafer holder with conducting carbon paint. The vacuum system was then assembled and evacuated as in Section 4.3. The sputtering procedure, as described above in Section 6.1, was then carried out. After the sputtering run, the carbon paint was washed off the wafer with isopropanol, acetone, methanol, and DI rinses. Then the second ellipsometer measurement was conducted.

6.3 PLASMA CHARACTERIZATION

As with the anodization work, the density of argon ions was measured using a double Langmuir probe arrangement described in Section 3.2.5. Knowledge about the ion density distribution was desirable so

that it could be compared with the sputtering results. Figure 6.2 shows the results of a double Langmuir probe measurement in a plasma of argon. Although all the sputtering work was done at 8 cm downstream from the plasma discharge, measurements were performed at 4, 6, and 8 cm below the discharge to compare them with the same theory developed by Hopwood [78] and described in Section 4.4. Figure 6.3 is this comparison assuming $\nu_i/D_a \ll (x_{on}/a)^2$. As can be seen, the measurements follow the theory quite well, much better than the oxygen results presented in Section 4.4. This may be because the assumptions made in deriving the Langmuir probe theory concerning the plasma species, i.e. equal number of positive and negative species, $\nu_i/D_a \ll (x_{on}/a)^2$, and ion mass, are more accurate for a plasma of a simple gas such as argon than for a plasma of a complex gas such as oxygen.

These measurements to determine the argon ion density were performed in the same manner as that for the measurements in oxygen described in Section 4.4, i.e. position the probe, assemble the vacuum system, evacuate the system, initiate gas flow, ignite the plasma, allow a "warm up" period of 15 minutes once operating conditions are reached, and take the probe I-V characteristics. Operating conditions for these probe measurements in argon were the same as those used for the sputtering work outlined in Table 6.2 above.
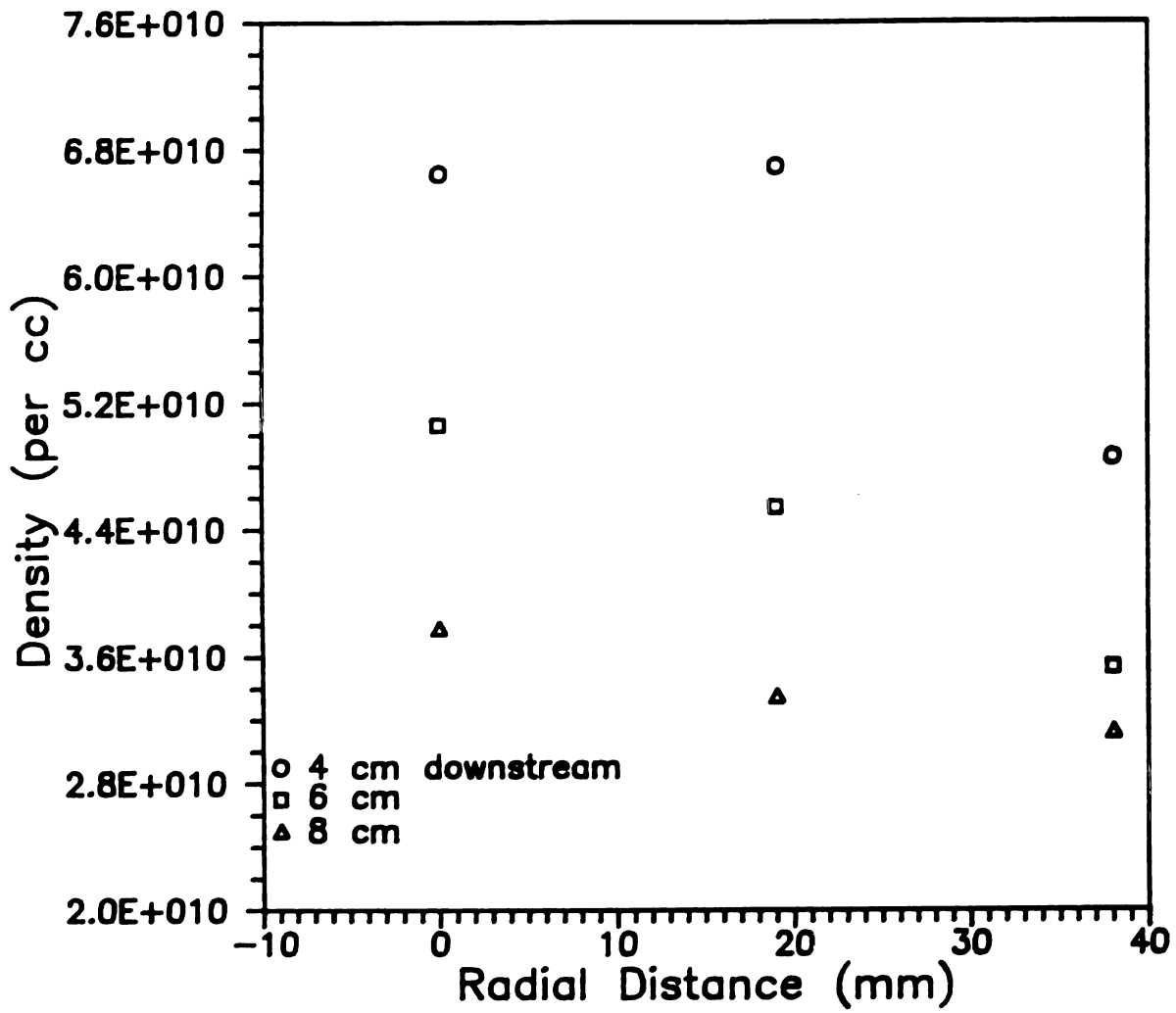
Figure 6.2 The Measured Density of Argon Ions
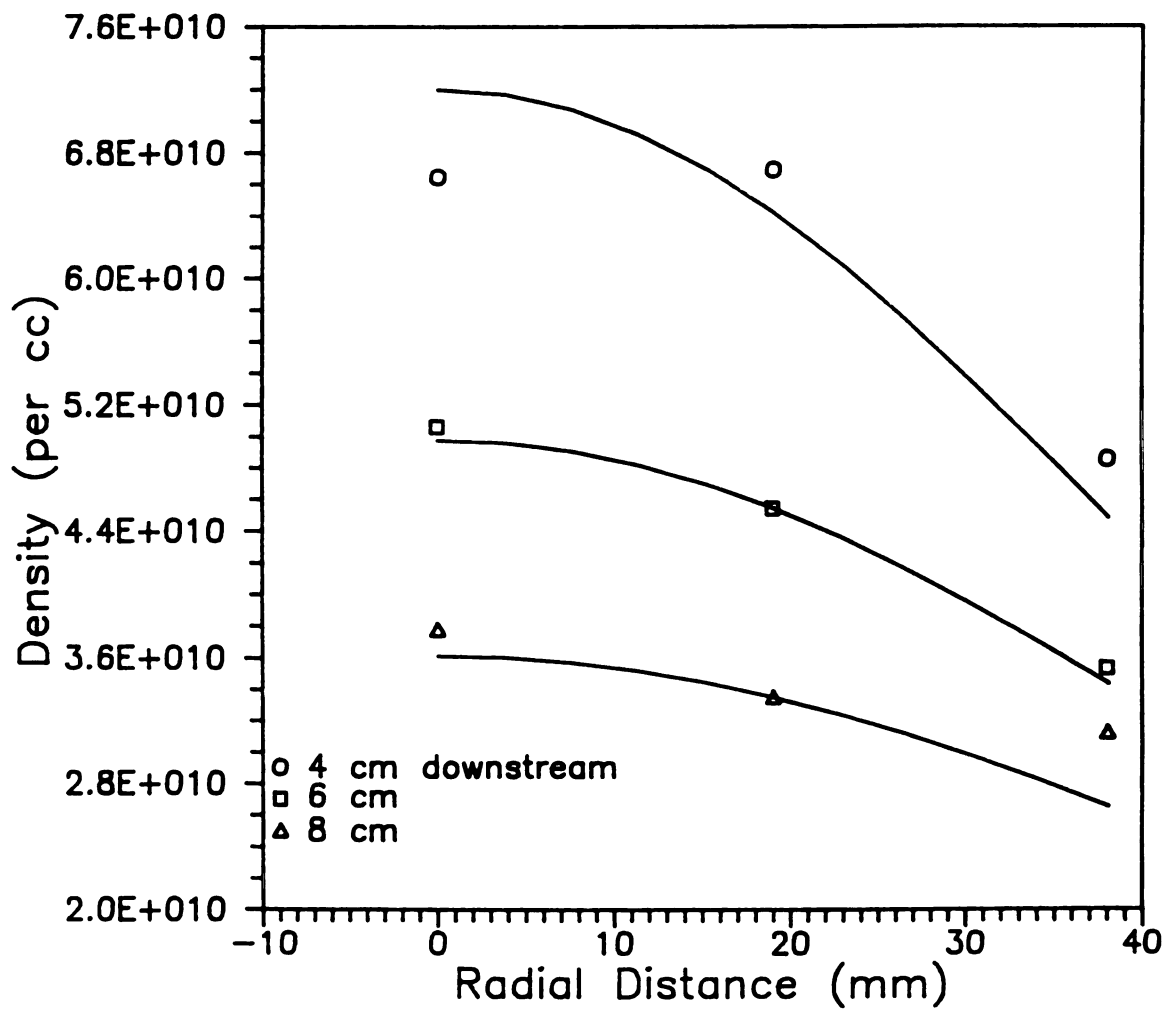
Figure 6.3 Comparison of the Measured Density
with the Calculated Density of Argon Ions

6.4 EXPERIMENTAL RESULTS

6.4.1 Uniformity

In this section, the uniformity of the thicknesses of SiO_2 that were sputtered off of the wafers is presented and discussed. The three dimensional figures representing these thicknesses were all normalized by dividing all the thicknesses by the average thickness and multiplying by 100 so that visual comparisons could be more easily made between different experiments. This was necessitated by the large differences in sputtering rates and uniformities. The reasons for these differences are not entirely clear, but Section 6.6 is a discussion of these results and possible reasons.

Table 6.3 is a summary of the amount and uniformity of the silicon dioxide thicknesses sputter removed from the wafers. As can be seen, there is a wide variation in both. For Table 6.3 all 89 sputtered off thickness points of the X-Y grid were considered to calculate the average, standard deviation, σ, and percent variation, %. This represents a radius of 35.7 mm across the wafer surface. For a 3 inch (76.2 mm) diameter wafer, this is only 3 mm from the edge of the wafer where it is unlikely any "chips" fabricated would actually be usable. Hence, it was desirable to see the effect of only taking into account the points which lie within a 31.5 mm radius. Table 6.4 is the result of omitting the outer 20 points of the grid. In each case, there is a slight increase in the uniformity of the amount of oxide sputtered off, about 1 to 4 percent.

Table 6.3   Summary of Sputtering Results (1)

TRIAL	HIGH	AVE	LOW	σ	% (σ/AVE)
RES3	250	171.4	106	39.7	23.2
RES4	290	244.1	184	29.7	12.2
RES5	96	67.1	33	18.1	27.0
RES6	165	141.6	103	14.7	10.4
RES7	411	351.8	285	37.2	10.6
RES8	133	103.1	71	17.4	16.9
RES9	173	119.1	52	37.1	31.1
RES10	106	58.4	15	27.7	47.4
RES11	47	35.6	16	6.0	16.9
RES12	155	119.7	72	20.3	17.0
RES13	129	115.6	96	7.1	6.1
RES14	182	95.6	20	52.3	54.7

Table 6.4 Summary of Sputtering Results (2)

TRIAL	HIGH	AVE	LOW	σ	% (σ/AVE)
RES3	250	180.6	112	38.4	21.3
RES4	290	254.0	196	25.2	9.9
RES5	96	72.1	35	16.8	23.3
RES6	165	147.2	122	10.8	7.3
RES7	411	365.3	294	30.3	8.3
RES8	133	108.6	80	15.6	14.4
RES9	173	122.1	55	36.2	29.6
RES10	106	59.1	21	25.8	43.7
RES11	46	36.8	22	4.8	13.0
RES12	155	126.5	97	16.8	13.3
RES13	129	117.5	104	6.3	5.4
RES14	182	95.8	28	51.2	53.4

The following 4 figures are three dimensional representations of the more uniform oxide thicknesses removed by sputtering. Each is a different combination of baseplate, vacuum port size, belljar size, and use or non use of the magnetic confinement structure. First is shown RES4 in Figure 6.4. This experiment was conducted with the smallest belljar and vacuum port opening. This particular result had the most oxide removed (aside from RES7 which used a much more negative induced bias). Figure 6.5 is a representation of RES6 which was conducted using the 18" belljar, the 7" diameter vacuum port and the baseplate
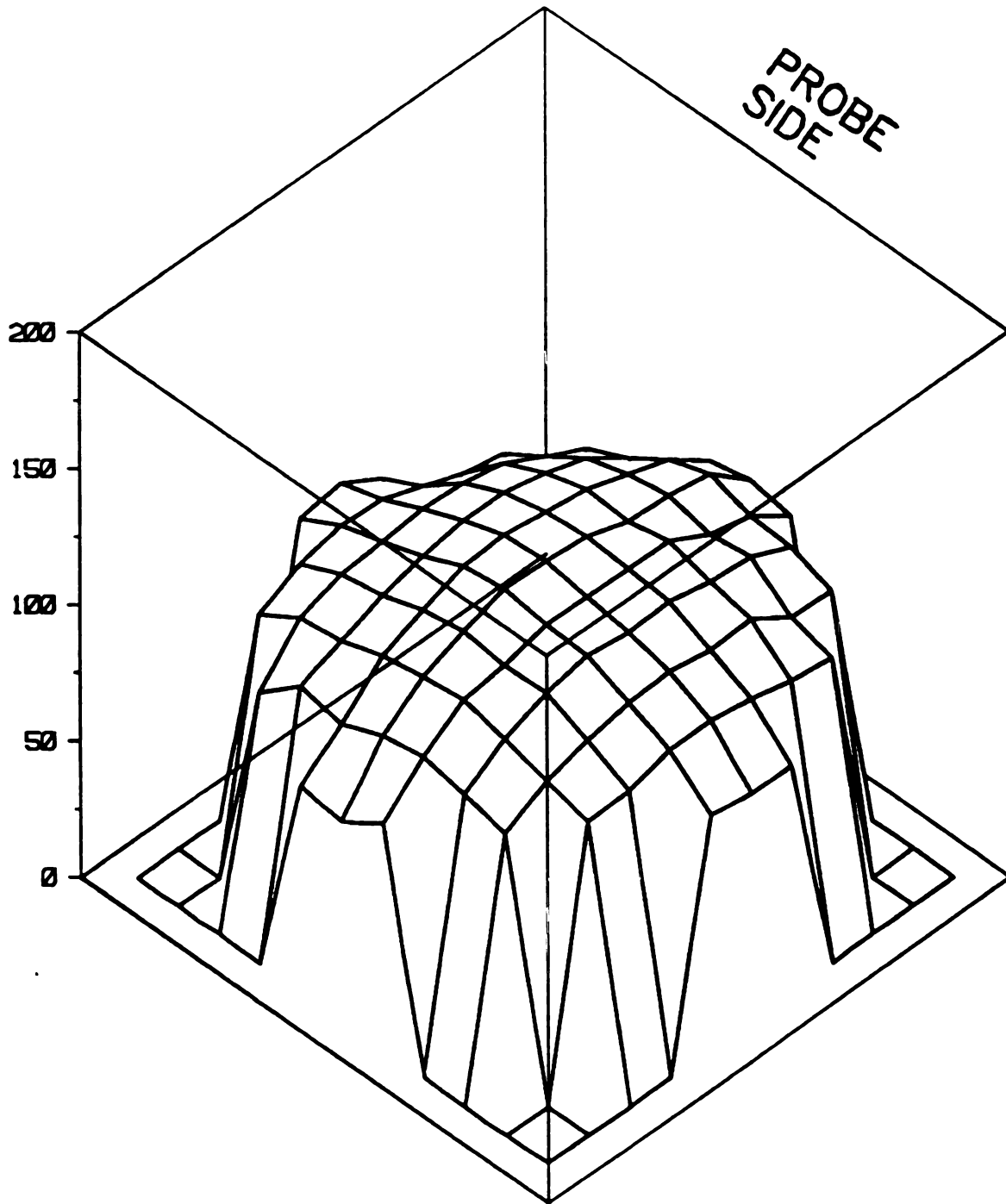
Figure 6.5   Three Dimensional Graph of the Amount
of Oxide Removed During Experiment RES6

with the stronger magnets. The amount of oxide remove in RES6 is smaller than that removed in RES4. This may be due at least in part to the larger diameter openings and still using the same power to sustain the plasma which leads to a smaller, though more uniform, density of ions. The average amount of oxide removed in this run is very close to the "average" of all the sputterings of 142 Å. This "average" will be presented and further discussed in Section 6.4.2.

Figure 6.6, RES12, shows the result of using the largest belljar, the largest vacuum port and the stronger magnets. The amount of oxide sputtered off is again slightly smaller. Lastly, Figure 6.7 is RES13 which was conducted using the MPCS. This particular experiment was the most uniform of all the experiments performed which is most likely due to the use of the magnetic confinement.

Because of the relative simplicity of argon sputtering as compared to plasma processes that involve chemical reactions, such as etching and oxidation, these experiments represent a good platform to compare: (1) plasma modeling and simulation, (2) measured plasma properties, and (3) processing results. Figure 6.8 shows that there is in fact very good agreement between the ambipolar diffusion model prediction, the ion density measurements obtained with a double Langmuir probe, and the ellipsometer determined thicknesses of oxide sputtered from the wafers. The model results in this figure were calculated for an 8 cm downstream distance and were normalized to 165 Å at the center to agree with the experimental sputtering results. Likewise the Langmuir probe results are normalized to the wafer center. The percent variation (high-low/high) along the diagonal of the simulated ion density is 22.4% over a 70 mm radius. As Figure 6.8 shows, this agrees well,
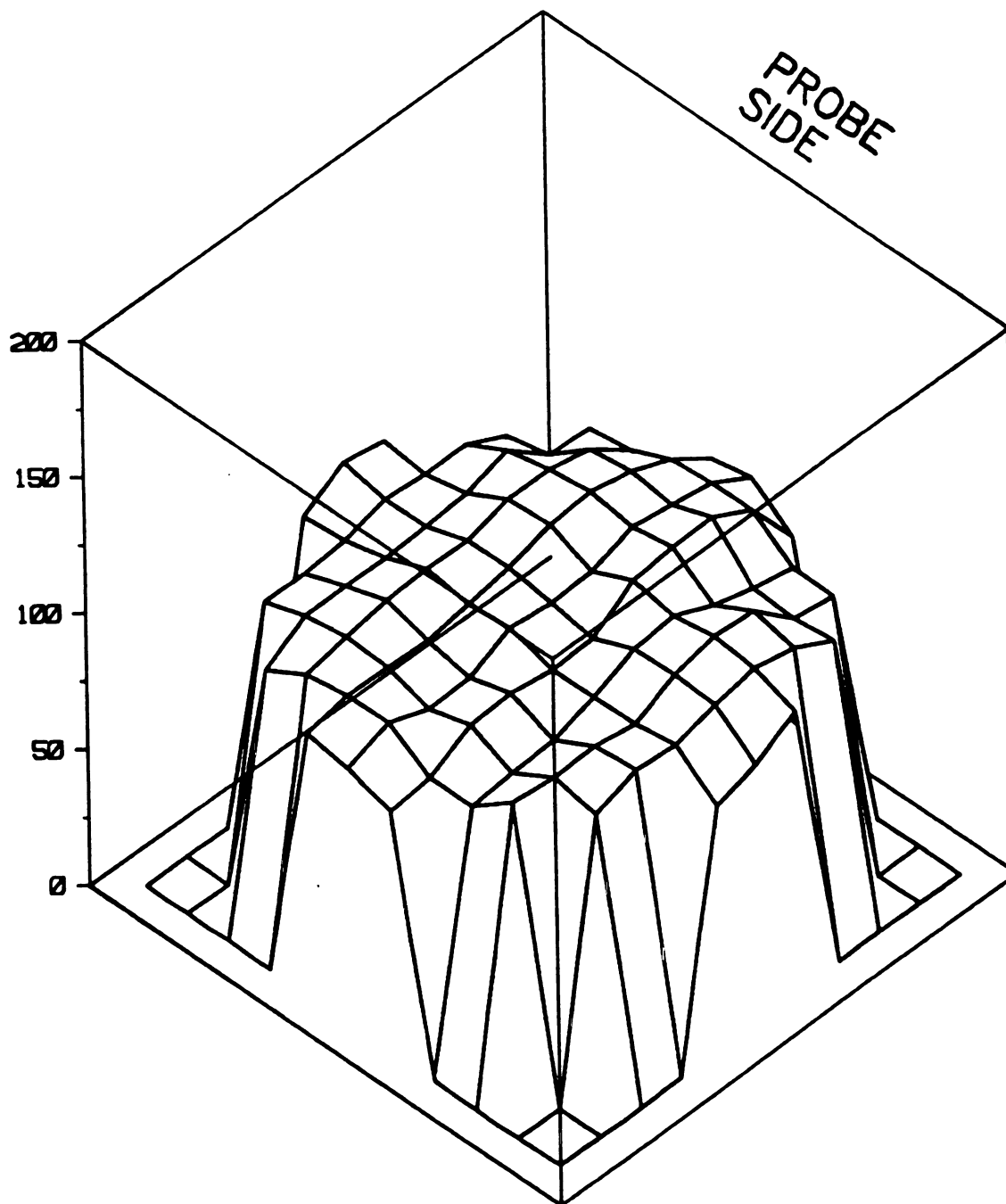
Figure 6.7 Three Dimensional Graph of the Amount
of Oxide Removed During Experiment RES13
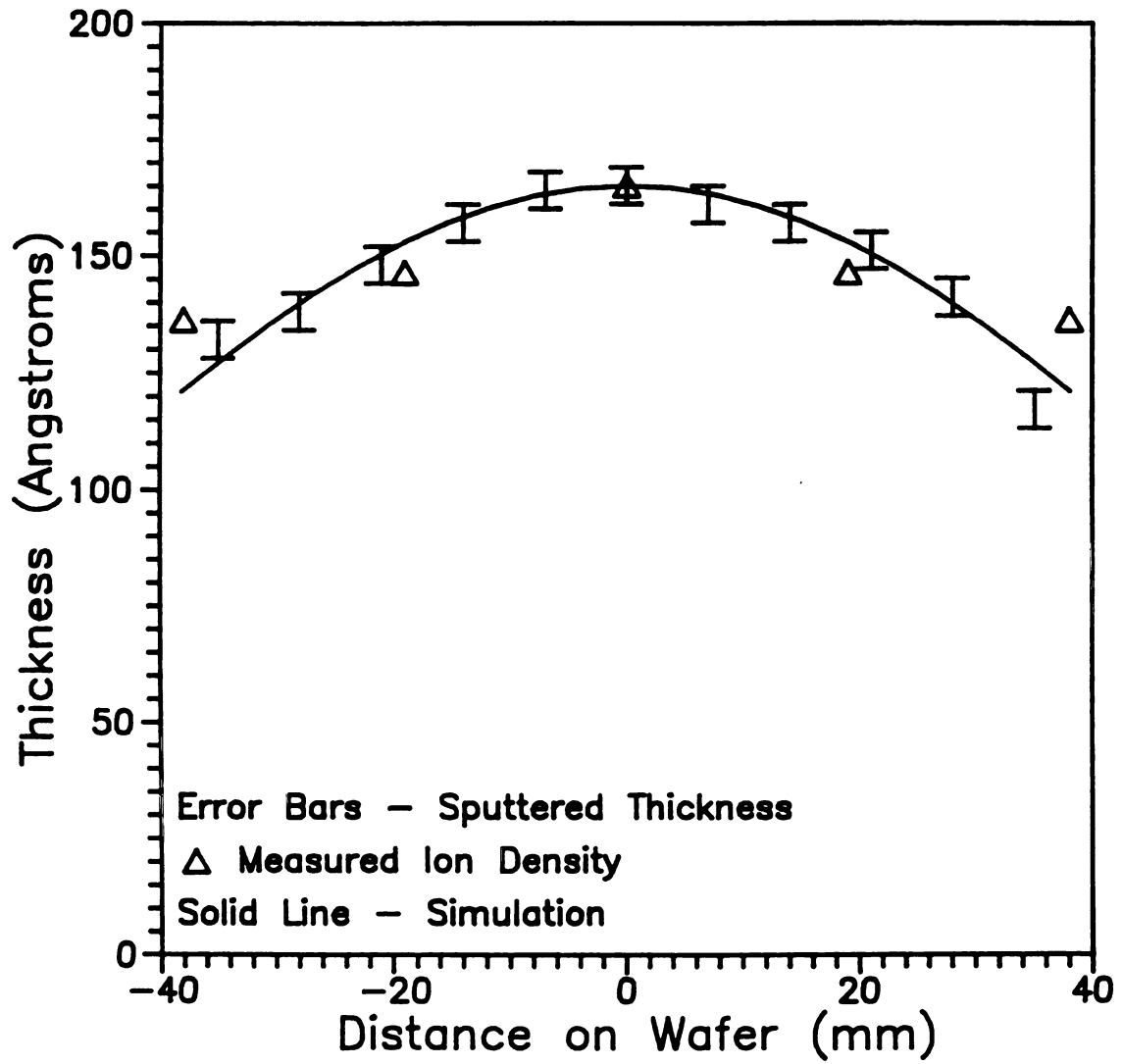
Figure 6.8 Comparison of the Oxide Thickness Removed with
the Measured and Simulated Ion Density Distributions

within experimental error, with the shape of the curve of the amount of oxide removed from the wafer. Calculating the percent variation for the amount of oxide sputtered from the surface of the wafer using only these 11 points results in a 24.5% variation over a 70 mm radius (here the average of the two end points, was used for the low value). The variation in the measured ion density (double Langmuir probe results) is 17.5%.

As noted in Table 6.1, RES5 was performed with the magnets "out of phase". In this experiment the magnets in the baseplate that provide the static magnetic field for the ECR zones were rotated so that the input power probe was over one of the magnets instead of between two magnets. The reasoning behind this was that the ECR zones would be closer to the inside wall of the quartz containment thereby putting the higher density of ions at a larger radius to possibly improve the radial ion density distribution uniformity. This however was not the case. Uniformity did not increase which indicates that the uniformity of the radial ion density distribution depends more heavily on the diffusion of the plasma species than the distribution of the plasma species in the discharge.

6.4.2 Sputter Rate

In this section the sputter rate is calculated and compared for all the sputtering experiments performed in this research on the three inch wafers. Table 6.5 is a list of all the sputter rates determined by dividing the average oxide thickness removed during the experiment by 5 minutes, the length of time that each sputtering was performed.

Table 6.5 Summary of Sputtering Rates

TRIAL	AVE(1) (Å)	AVE(2) (Å)	Rate(1) (Å/min)	Rate(2) (Å/min)
RES3	171.4	180.6	34.3	36.1
RES4	244.1	254.0	48.8	50.8
RES5	67.1	72.1	13.4	14.4
RES6	141.6	147.2	28.3	29.4
RES7	351.8	365.3	70.4	73.0
RES8	103.1	108.6	20.6	21.7
RES9	119.1	122.1	23.8	24.4
RES10	58.4	59.1	11.7	11.8
RES11	35.6	36.8	7.1	7.4
RES12	119.7	126.5	23.9	25.3
RES13	115.6	117.5	23.1	23.5
RES14	95.6	95.8	19.1	19.2

AVE(1) is the average thickness removed calculated by considering all 89 points, as in Table 6.3 and AVE(2) is the average thickness removed by considering only the innermost 69 points. Rate(1) and Rate(2) then correspond to AVE(1) and AVE(2) respectively.

An "average" of Rate(1), omitting RES7 which was sputtered using a -70 V dc bias, is a sputter rate of 23.1 Å per minute with a standard deviation of 10.9 Å per minute. Doing the same for Rate(2) the rate is 24.0 Å per minute, with an 11.5 Å/min standard deviation, only about 1 Å per minute more. "Average" is used here since this is really the

average rate of 11 average rates for the 11 samples processed with a -50 V dc induced bias.

As will be shown in Section 6.5, the experimental sputter rate is in good quantitative agreement with measured plasma properties. The large experimental standard deviations are discussed in Section 6.6.

6.4.3 Impurity Assessment

An ESCA analysis (ESCA analysis is described in Section 5.3.1) was performed on one of the sputtered samples to determine if any contamination resulted from the sputtering process. One ESCA survey was done on the surface of the sample and another was done after sputter removing approximately 10-15 Å of the surface with this machine's argon ion sputter gun. No metallic contamination, other than surface carbon, was found in the sample. The fact that no metallic contamination, in contrast to the situation for oxides grown anodically with the same system, was found is expected since the biasing for the sputtering work (wafer biased to -50V dc) was such that no heavy ions were accelerated into a metallic surface. Thus no sputtering of the baseplate occurred. Often in argon sputter cleaning, some argon is implanted into the sample. But ESCA results show that this was not the case here. The fact that a low bias was used such that the argon ion energy was quite low accounts for this and demonstrates an advantage of ECR sputter cleaning.

6.5 CALCULATED RATE PER mA/cm^2 vs. ENERGY

Of interest to the sputtering work is what could be expected from theoretical calculation of the sputtering rate. Knowledge of the plasma ion density and energy imparted to the ions from the applied bias plasma plus theoretical models for ion flux are the information that can be used to calculate a theoretical rate of sputtering.

Part of the knowledge needed to calculate a sputtering rate is the number of molecules of a particular sample that can be sputtered off by an ion of a given energy. Experimental information for the sputtering yield of silicon dioxide by argon ions versus energy has been compiled by Maissel and Glang [101]. As mentioned above, the induced bias on the wafer provided by the rf bias was -50 V dc. For an argon ion of 50 eV energy, the yield is 1.65×10^{-2} silicon dioxide molecules per argon ion.

Another factor that must be determined is the flux of argon ions to the wafer surface. This can be inferred from plasma physics and the measured density of argon ions and electron temperature. Following the work of Chapman [102] and Mahoney [103], an analytic expression for the ion flux to a surface under the conditions of free fall diffusion is:

$$\Gamma_i = 0.61 \, n_i (kT_e/M_i)^{1/2}$$

where n_i is the ion density of the plasma, k is Boltzman's constant, T_e is the electron temperature, and M_i is the mass of the ions (for argon, 6.63×10^{-26} kg).

Using the measured values of n_i and T_e at z = 8 cm below the plasma and r = 1.91 cm from the center of the vacuum chamber (the average values at z = 8 cm) of 3.349×10^{10} ions/cm^3 and 27,200°K, as

presented in Section 6.3, the flux of ions is found to be:

$$\Gamma_i = 4.86 \times 10^{15} \text{ ions per cm}^2 \text{ per sec}$$

or expressing this in mA per cm^2:

$$J_i = 0.78 \text{ mA per cm}^2.$$

Combining this information, a theoretical sputtering rate can now be calculated:

$$S.R. = (\text{yield}) \times (\text{flux}) / (\text{density of SiO}_2)$$

$$= 1.65 \times 10^{-2} \times 4.86 \times 10^{15} / (2.3 \times 10^{22})$$

$$= 3.49 \times 10^{-9} \text{ cm/sec}$$

$$= 20.9 \text{ Å/min.}$$

This is only slightly smaller than the average experimental sputtering rate of 23.1 Å/min presented in Section 6.4.2. It is noted that though the average induced bias that was measured was -50 V dc, this bias had an ac component of approximately 7 V peak to peak impressed upon it. This ac signal was due to the rectification of the line voltage for the rf power supply to provide a needed high voltage dc supply. With this added potential, the predicted sputter yield would have been slightly higher, since the sputter yield increases superlinearly with ion energy. This would then increase the predicted sputtering rate.

For RES7 which was sputtered using -70 V dc induced bias, the yield is 4×10^{-2} silicon dioxide molecules per argon ion. This increased the predicted sputtering rate to 50.7 Å/min. The observed rate for RES7 was slightly above 70 Å/min. If again the peak to peak variation is taken into account, and -80 V dc was the induced bias, then the yield increases to 7×10^{-2} molecules/ion and the predicted rate rises to 89 Å/min, which is somewhat higher, but closer to the

actual, observed rate.

6.6 DISCUSSION

Data presented in this chapter shows that uniform ($\pm$ 5%) sputter cleaning without baseplate or argon contamination is achievable. It also shows that the sputtered uniformity agrees well with Langmuir probe measurements and diffusion theory and that the average experimental sputtering rate agrees well with the free-fall diffusion model. However, some of the experimental runs showed widely varying thicknesses, and in some cases, highly non-uniform thicknesses of oxide removed. As an extreme example of the non-uniformity of the amount of oxide sputtered removed in some of the experiments, Figures 6.9 and 6.10 depict the results of RES10 and RES14. These two experiments are very off-centered, with most of the sputtering taking place on the extreme edge of the wafer. A discussion of possible reasons why is clearly in order.

The most probable reason for the widely varying results and the random, highly non-uniform amounts of oxide removed on certain samples is the electrical contact between the wafer and wafer holder. After compiling the results, some of the back sides of the wafers were inspected for stains left by the carbon paint. In the cases with the most uniform thicknesses of oxides removed by sputtering, nearly the entire back side of the wafer was stained. For RES13 in particular, the entire wafer holder had to be soaked in isopropanol for approximately 3 minutes in an ultrasonic bath unit before the wafer could be dislodged from the wafer holder. In the cases with very
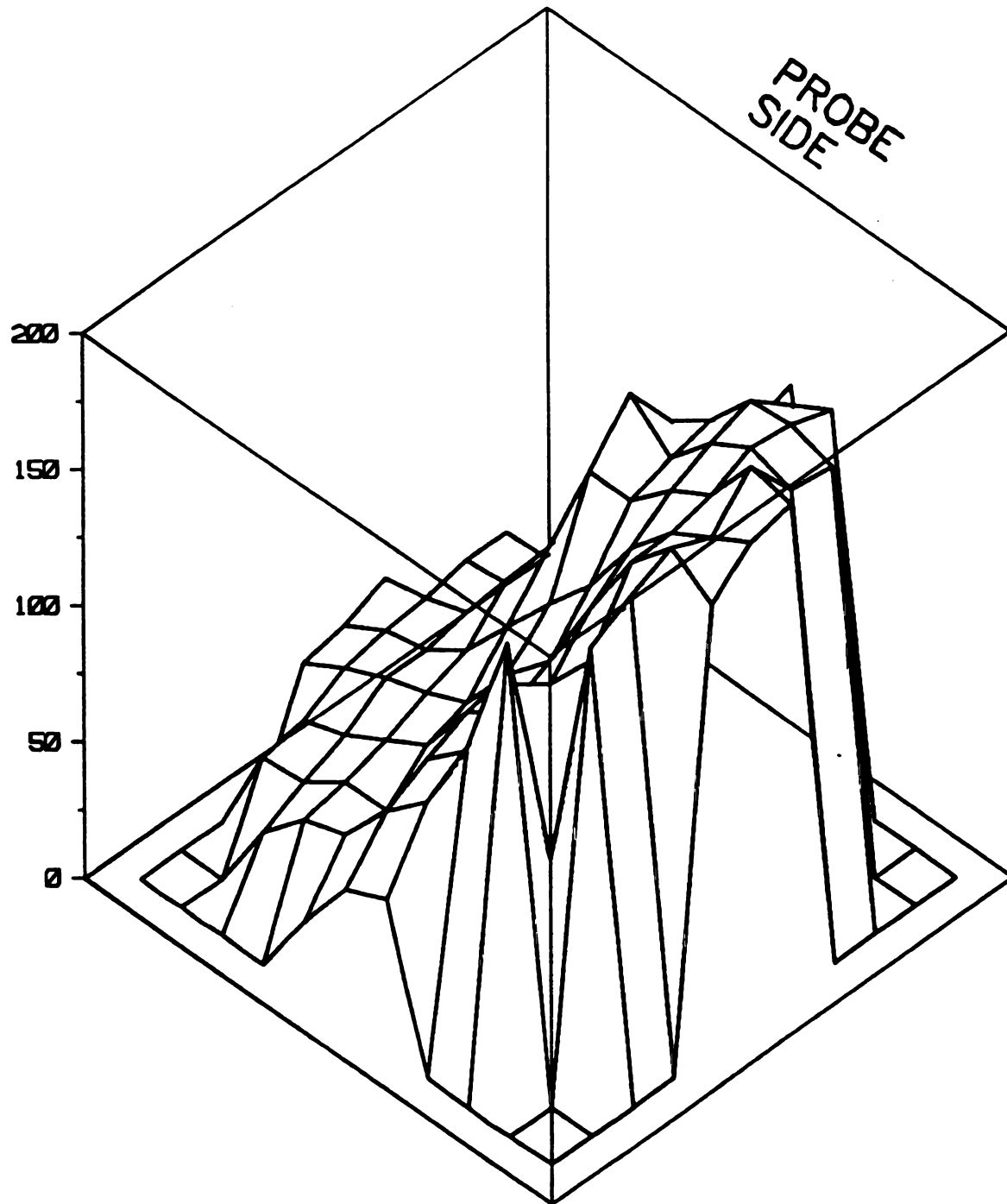
Figure 6.9   Three Dimensional Graph of the Amount
of Oxide Removed During Experiment RES10

non-uniform thickness removal, some of the wafers had only a small portion of the back side stained, in particular RES14 and RES10 had only one side with only a small amount of staining by the conductive paint evident. The highest sputtering rates were observed over these stained areas. For the unstained areas, there was a physical gap between the wafer holder and the wafer so that there was not good rf contact in those areas. One solution to this apparent contact problem could be to evaporate aluminum over the entire back side of the wafer and to not use any conductive paint but to use small clamps or clips to hold the wafer on the wafer holder. More simply, with an rf bias, the wafer may be placed directly on a flat chuck without any intervening layer.

Another possible reason for random variations in uniformity could be that some nonuniformities could have existed in the plasma. While all the experiments were conducted with the MPDR tuned (probe depth and cavity height adjusted) for minimum reflected power, some of the "lobes" of the plasma were sometimes observed to be slightly more intense than other lobes. However, since changing the magnet configuration had negligible effect on uniformity, it is not believed that this slight variation in plasma brightness is responsible for the large asymmetries observed on some samples.

There are also two possible sources of a systematic asymmetry in uniformity, namely the lack of a ground shield and a perturbation in the vacuum system (3.5 cm of the support shaft for the wafer holder was above the surface of the wafer approximately 4.5 cm from the side of the wafer holder). However since systematic variations were not observed, their effect appears negligible.

Also observed in the sputtering work was a large variation in the average amount of oxide sputtered off of the wafers (or the sputtering rate). Before the first sputtering run, the top plate and the base plate were thoroughly cleaned ("Metal Brite" pad buffing and rinsing with acetone and methanol). Between RES7 and RES8, the anodization using the silicon cathode arrangement was performed with an oxygen plasma. Then more sputterings were performed without any further cleaning of the vacuum system surfaces. Switching processes in this manner may change the surface of the walls of the vacuum system in such a way that the sputtering process was changed, i.e. the walls become oxidized by the oxygen plasma which reduces the amount of current able to be drawn from the plasma during sputtering with an argon plasma.

CHAPTER SEVEN

Summary and Conclusions

All in all, a nice little bit of work

7.1 SUMMARY OF RESULTS

7.1.1 Uniformity and Thickness of the Plasma Grown Oxides

The process of growing silicon dioxide layers by anodization in an oxygen plasma sustained at low pressures with a microwave plasma disk reactor (MPDR) operating in an electron cyclotron resonance mode (ECR) was studied. This process is a low temperature one, the highest temperature measured for any growth conditions was $265°C$. Oxide layers were grown on single crystalline silicon wafers, 7.6 cm (3 inches) in diameter (area = 45.6 cm^2) placed between 2 and 10 cm below the discharge region. The wafers were biased positively, between 30 and 50 V dc, to attract negative oxygen ions and electrons to the surface of the wafers. Anodization was performed for 2 hours for each wafer. Pressure in the vacuum chamber was 3 mTorr with 260 - 265 Watts of microwave power used to sustain the plasma.

Oxide layers were grown on the silicon wafers under all conditions investigated. The amount of oxide grown varied considerably with

choice of downstream distance. Using an anodization voltage of 40 V, the largest amount of oxide grown occurred at 2 cm below the discharge, with 1106 Å of oxide grown in the center of the wafer. In terms of uniformity, the standard deviation of oxide thickness across the wafer surface was 61 Å corresponding to a percent deviation (σ/average X 100) of 6.2%. The uniformity of the oxide layers peaked for films grown at 8 cm below the discharge, with a wafer center thickness of 484 Å, a σ of 8 Å and a percent deviation of 1.7%.

The amount of silicon dioxide grown decreased with increasing distance from the plasma discharge in a decaying exponential fashion. A data fit for a plot of the oxide thicknesses measured in the center of the wafer versus downstream distance was d_{ox} = 1245 exp [-0.111 z]. This qualitatively follows the theory of the diffusion of plasma species under ambipolar diffusion conditions.

Plasma characterization of the oxygen discharge with double Langmuir probe measurements was performed to compare the plasma density distribution with the uniformity of the oxide layers grown. The radial distribution of the plasma species was found to decay faster than the oxide thickness grown across the surface of the wafers, i.e. the radial oxide thickness was more uniform than the plasma distribution. This is due in part to the boundary the wafer creates in the plasma during anodization which "flattens out" the ion distribution and in part to the fact that the oxidation rate decreases as the thickness of the oxide increases which provides a built-in tendency toward uniformity.

7.1.2 Characterization of the Plasma Grown Oxides

Chemical analysis of the plasma grown oxide films, using AES, XPS and FTIR, was performed to determine the elemental content and stoichiometry of the oxides. One of the first findings was that of metallic contamination of the oxide films. Most of the experiments were carried out using the wafer as the anode and the baseplate of the MPDR as the cathode. Hence positive oxygen ions were collected at the baseplate with enough energy to sputter off metallic species. This material was incorporated in the growing silicon dioxide films. Therefore several variations were investigated to remove this contamination: quartz tube shielding of the baseplate, floating baseplate with an alternative cathode, and a silicon cathode. The quartz tube shielding greatly reduced the metal content of the films and the silicon cathode completely eliminated ESCA measurable contamination. A reduction in growth did occur in both cases.

Stoichiometry of the films, X in SiO_x, was found to be higher than that of thermally grown silicon dioxide films. The range of X for the plasma grown films was found to range from 2.05 to 2.28. AES analysis versus sputtering time (depth into the oxide film) revealed that the stoichiometry was uniform throughout the entire film however.

Wet etching of the oxide films found that the etch rate for the plasma grown oxide layers was higher than that for thermally grown oxides, between 2.6 and 10.5 Å/sec as compared to 2.0 Å/sec. Also, the ellipsometer results show a refractive index lower than that for thermal oxides. Combining this information with the stoichiometry results, it is hypothesized that the non-stoichiometry of the plasma

grown oxides at this low of a temperature may lead to a less dense material.

MOS C-V measurements were performed on the oxides to characterize their electrical properties. For the as-grown oxide layers, the density of interface traps for oxides with a large metallic content and no annealing was very high, in the upper 10^{12} to lower 10^{13} states/ eV/cm^2. The as-grown oxides shielded with the quartz tube during anodization had a lower D_{it}, approximately 1.7 X 10^{12} states/eV/cm^2 at midgap.

Annealing of these latter samples in a forming gas (5% H_2, 95% N_2) for one hour at 450°C reduced D_{it} to 8 X 10^{11} states/eV/cm^2. These values for D_{it} for both the as-grown and annealed oxides are higher than thermally grown oxide layers, which typically have a D_{it}, after annealing, in the low 10^{10} states/eV/cm^2 range. Possible explanations are the metal content of the films and the very low temperature during anodization.

Combining the C-V measurements with a Bias/Temperature Stress Test for one of the annealed plasma grown oxide layers revealed a fixed oxide charge density, Q_f, of 1.37 X 10^{12} cm^{-2} and a mobile ion density, Q_m, of 3.25 X 10^{11} cm^{-2}. These values are again higher than those for thermally grown oxides. The low temperature during the growth of the films is again believed to be a factor in the high values of Q_f. The Q_m, however, should be eliminated if the process is performed under cleaner circumstances.

Another electrical property of the oxides that was investigated was the dielectric strength of the oxides. The oxides were stressed with a dc bias until the oxides underwent breakdown. For the as-grown

oxides with the higher metallic content, the breakdown field average was 2.66 MV/cm. After annealing, the average oxide strength rose to 4.86 MV/cm. The oxides grown with the quartz tube shielding had significantly higher strengths, a 7.80 MV/cm average after annealing for sample DS-34.

7.1.3 Sputter Removal of Silicon Dioxide Layers

An ECR argon plasma was sustained in the MPDR with 200 - 205 Watts of microwave power and used for the sputter removal of silicon dioxide layers from 3 inch diameter silicon wafers. The wafers were placed 8 cm below the plasma discharge region in the vacuum chamber which was held at a pressure of 0.78 mTorr. A small, 13.56 MHz rf bias was applied to the wafers such that a -50 V dc bias was induced on the wafer to accelerate the argon ions to the surface. An average sputtering rate of between 23 and 26 Å/minute was found when considering the most uniform results. This sputtering rate compared well with predictions made from considering diffusion theory. A predicted value of 20.9 Å/min was calculated using the measured density of argon ions, the measured electron temperature and using the free fall diffusion equation for flux of ions to a boundary surface.

The peak uniformity was found for RES13 in which the average amount of silicon dioxide removed was 115.6 Å in the 5 minute sputtering experiment (23.1 Å/min) with a 7.1 Å standard deviation. The percent variation associated with this is 6.1% (σ/average).

Diffusion theory predictions were also in good agreement with the uniformity of the oxide thicknesses removed during sputtering. When

comparing the percent variation (high value - low value / high value) the variation found in the simulation of the ion density across a 70 mm diagonal was 22.4% while the variation in the sputtered-off oxide thickness was 24.5% across a 70 mm diagonal on the wafer surface. The measured density of ions was also in close agreement with a 17.5% variation.

7.2 RECOMMENDATIONS FOR FUTURE RESEARCH

7.2.1 Oxygen Plasma Anodization Recommendations

While the goal of growing uniform oxide layers over 3 inch silicon wafers at a low temperature was achieved, this was done for a very limited set of parameters, i.e. 265 W of microwave power, 3 mTorr vacuum chamber pressure, 40 V dc anodization voltage, and the wafer placed 8 cm below the plasma discharge. Much was learned, but there are many more variations of the parameter space that should be studied to improve the process. Therefore, the following suggestions and recommendations are made for further work involving the MPDR operating in the ECR mode to sustain an oxygen plasma for the anodization of silicon.

7.2.1.1 Contamination Reduction

A very preliminary refinement to the system of using silicon as a cathode to eliminate the metallic contamination was successful. However, the amount of oxide grown for this one experiment was slightly

less than half of the amount grown under similar conditions using the baseplate as the cathode. Another refinement is in order, possibly using a much larger area silicon cathode near the plasma discharge such as a cylindrical silicon sleeve which could be inserted in the discharge zone and which fits tightly against the walls of the baseplate.

A second possibility for reducing the contamination would be to electrically float the baseplate and place a large conducting plate near the wafer itself, but downstream of the wafer so that the cathode area is large, but without the line-of-sight path from this plate to the wafer. This would greatly reduce the possibility of sputtering contamination from this plate.

7.2.1.2 Substrate Heater

As mentioned earlier, in Section 5.5, it is entirely possible that the temperature of the substrate was in fact too low to effectively grow, in terms of MOSFET fabrication, high quality oxides. Heating the wafer during anodization would in all likelihood improve the oxide in terms of its electrical properties, i.e. reducing D_{it} and Q_f. Heating the silicon substrate during anodization would also increase the amount of oxide grown for the same conditions used without substrate heating. Knowledge gained from investigating this option would aid in the under-standing of the temperature dependence of the formation of silicon dioxide using plasma anodization.

7.2.1.3 Scale-Up

While 3 inch diameter wafers are a substantial increase in size as compared to earlier work [30] using the MPDR to grow oxide layers on silicon (though not in the ECR mode), industrial fabrication has moved, in most cases, to 6 inch and 8 inch diameter silicon wafers. Thus anodization experiments should be performed using a larger system such as the ones described in [99], i.e. a 45.7-cm-diam cylindrical cavity with a 20-cm-diam discharge (18" diam cavity, 8" diam discharge) or a 37-cm-diam cavity with a 25-cm-diam discharge (14" diam cavity, 10" diam discharge). Similar anodization results should be readily attainable on these larger diameter wafers without major changes in the procedures used in this research.

7.2.1.4 MPCS

Recent studies [99] using a magnetic Multi-Polar Confinement Structure (MPCS) indicate that a much more uniform ion density distribution, in terms of radial uniformity, is possible for smaller separations between the silicon wafer and the plasma discharge. Not only would this improve the uniformity of the processing, but placing the wafer nearer the discharge would increase processing rates. This would make the use of the MPDR for plasma processing even more attractive. Thus, in addition to the use of a scaled-up version of the MPDR, oxidation research should be conducted with an MPCS to investigate improvements in the uniformity of anodization.

7.2.1.5 Combination with RTP

More and more, the use of Rapid Thermal Processing (RTP) is gaining attention as an alternative method of processing semiconductor substrates. This method involves the use of high-intensity lamps to rapidly, within seconds, raise the temperature of a substrate to a given temperature, process the substrate for a desired amount of time, and then to rapidly reduce the temperature of the substrate by extinguishing the lamps. Annealing the plasma grown oxides (RTA) in this manner may preserve the advantages of the low temperature anodization process while providing enough energy to form high quality silicon dioxide. Research combining the two processes is recommended.

7.2.1.6 Mixture of Gases

Investigations using a combination of gases to form the plasma, such as O_2/Cl_2 or O_2 with a small partial pressure of TCE vapor, have already been documented using other plasma applicators [21,29] to improve the oxide quality. In addition to a vapor or gas containing chlorine, a small percent of argon added to an oxygen plasma may increase the rate of anodization of silicon by providing more electrons to the plasma and positive ions to complete the current flow between the anode and cathode. A silicon cathode would have to be used in conjunction with such an experiment since the argon ions are quite massive and would sputter material from the cathode. This would also keep the silicon cathode from growing a thick insulating layer of SiO_2 which was found to reduce the current flow in the one experiment

described in Sections 4.1.3 and 5.2.3. The suggestion for future work is a combination of all three gases along with a silicon cathode.

7.2.2 Argon Plasma Sputtering Recommendations

7.2.2.1 Analysis and Modeling Considerations

The sputtering work performed in this research again utilized only a limited number of possible processing parameters. It was demonstrated that soft sputtering did occur using an argon plasma sustained with the MPDR and there are strong indications that uniform sputtering without contamination is possible, but much work is needed to improve the process.

As was also demonstrated, there was good agreement between experimental sputtering results and modeling of the process with the use of diffusion theory. It would be useful to extend this modeling and processing to the scaled-up plasma processing designs mentioned in Section 7.2.1.3. Since the most uniform results in the sputtering research conducted occurred with the use of magnetic fields to confine the ions, further extending this modeling and processing to include the use of magnetic confinement such as that provided by an MPCS would also be informative. The extension of the modeling in these two ways would aid in refining the designs such that they are applicable for current industrial needs, i.e. the processing of larger diameter wafers.

7.2.2.2 System and Procedural Considerations

As described in Section 6.6, the use of a ground shield to contain the rf power such that it appears only at the surface to be processed, may increase the uniformity of the amount of material sputtered from the substrates. Use of such a device should be incorporated in further research in this area.

Of minor consideration in the modification of the sputtering system, is the procurement of a low-power, rf-impedance-matched, vacuum feedthrough. The present system of introducing the rf power into the vacuum system is adequate for the preliminary research performed here, however, such a device would improve the match between the rf power generator and the wafer thereby extending the life of some of the components by reducing the reflected power.

7.2.3 Wafer Preparation Recommendations

Recent investigations by Ohmi, *et. al.* [104, 105] of the cleaning procedures used on silicon wafers before processing has shown that high ratios of NH_4OH in the degrease etch described in Section 4.2.1 have detrimental effects on the operation of MOSFETs because this solution increases dramatically the surface microroughness of the silicon. The report by Ohmi show that the solution of $1:1:5$ $NH_4OH:H_2O_2:H_2O$ increased the average surface microroughness (*Ra*) of an as received silicon surface from 2 Å to 12 Å, while a 0.25:1:5 mixture only increased the *Ra* to 3 Å. This was correlated with the electron channel mobility which decreased from 360 $cm^2/V \cdot$ s to 100 $cm^2/V \cdot$ s with the increase in

Ra. This high *Ra* may contribute to the higher D_{it} and Q_f observed in the plasma grown oxides. Thus it is recommended that other, more current methods of wafer cleaning be implemented in future work.

7.2.4 General System Considerations

Both the anodization and sputtering work would benefit, in terms of increased process cleanliness and hence reduction of contamination, if the plasma system were housed in a clean room setting. As found in the plasma grown oxides, some mobile ion contamination was found.

Another improvement would be a load lock for introducing samples into the vacuum system. This would eliminate the need to partially disassemble the apparatus after every run and would allow the main chamber to remain evacuated between experiments. This would improve both repeatability and cleanliness since the chamber would not be vented to atmosphere which allows condensation on the vacuum chamber walls.

LIST OF REFERENCES

LIST OF REFERENCES

[1] Shimoda, et al. "An 18-ns 1-Mbit CMOS SRAM", *IEEE J. Solid State Circuits,* **23**, 1073 (1989).

[2] M. Inoue, et al. "A 16 Mbit DRAM with a Relaxed Sense-Amplifier-Pitch Open-Bit-Line Architecture", *IEEE J. Solid State State Circuits,* **23**, 1104 (1989).

[3] B.E. Deal, "The Oxidation of Silicon in Dry Oxygen, Wet Oxygen, and Steam", *J. Electrochem. Soc.,* **110**, (6), 1963.

[4] B.E. Deal and A.S. Grove, "General relationship for the Thermal Oxidation of Silicon", *J. Appl. Phys.,* **36**, (12), 1965.

[5] W.A. Tiller, "On the Kinetics of the Thermal Oxidation of Silicon I. A Theoretical Perspective", *J. Electrochem. Soc.,* **127**, 619, (1980).

[6] W.A. Tiller, "On the Kinetics of the Thermal Oxidation of Silicon II. Some Theoretical Evaluations", *J. Electrochem. Soc.,* **127**, 625, (1980).

[7] P. Pan, L.A. Nesbit, R.W. Douse, and R.T. Gleason, "The Composition and Properties of PECVD Silicon Oxide Films", *J. Electrochem. Soc.*:SOLID-SCIENCE AND TECHNOLOGY, **132**, 2012, (1985).

[8] P.D. Richard, R.J. Markunas, G. Lucovsky, G.G. Fountain, A. Mansour, and D.V. Tsu, "Remote Plasma Enhanced CVD Deposition of Silicon Nitride and Oxide for Gate Insulators in (In,Ga)As Devices", *J. Vac. Sci. Technol. A,* **3**, 867, (1985).

[9] B.R. Bennett, J.P. Lorenzo, K. Vaccaro, and A. Davis, "Low Temperature Pyrolytic Deposition of High Quality SiO_2", *J. Electrochem. Soc.,* **134**, 2517, (1987).

[10] Y. Shacham-Diamand, T. Chuh and W.G. Oldham, "The Electrical Properties of Hg-Sensitized 'Photox'-Oxide Layers Deposited at 80 ^{o}C", *Solid-State Electronics,* **30**, (2), (1987).

[11] L.G. Meiners, "Electrical Properties of SiO_2 and Si_3N_4 Dielectric Layers on InP", *J. Vac. Sci. Technol.,* **19**, 373, (1981).

[12]   B.R. Bennett, K. Vaccaro, J.P. Lorenzo, K.M. Sleboda and A. Davis, "Properties of Low-Temperature (80-300 °C) Pyrolytic SiO_2 on Si and InP", *J. Electronic. Mater.*, **17**, 365, (1988).

[13]   J.R. Ligenza, "Silicon Oxidation in an Oxygen Plasma Excited by Microwaves", *J. Appl. Phys.*, **36**, 2703, (1965).

[14]   J. Kraitchman, "Silicon Oxide Films Grown in a Microwave Discharge", *J. Appl. Phys.*, **38**, 4323, (1967).

[15]   J.R. Ligenza and M. Kuhn, "DC Arc Anodic Plasma Oxidation- a New Vacuum Process for Solid State Device Fabrication", *Solid State Technol.* pp 33-38, December 1970.

[16]   J. O'Hanlon, "Plasma Anodization of Metals and Semiconductors", *J. Vac. Sci. Tech.*, **7**, 330, (1970).

[17]   D.L. Pulfrey, F.G.M. Hathorn, and L. Young, "The Anodization of Si in an RF Plasma", *J. Electrochem. Soc.*, **120**, 1529, (1973).

[18]   D.L. Pulfrey and J. J. Reche, "Preparation and Properties of Plasma-Anodized Silicon Dioxide Films", *Solid State Electron.*, **17**, 627, (1974).

[19]   V.Q. Ho and T. Sugano, "Selective Anodic Oxidation of Silicon in Oxygen Plasma", *IEEE Trans. Elec. Dev.*, **ED-27**, 1436, (1980).

[20]   V.Q. Ho and T. Sugano, "An Improvement of the Interface Properties of Plasma Anodized SiO_2/Si System for the Fabrication of MOSFET's", *IEEE Trans. Elec Dev*, **ED-28**, 1060, (1981).

[21]   N. Haneji, F. Arai, K. Asada, and T. Sugano, "Anodic Oxidation of Si in Oxygen/Chlorine Plasma", *IEEE Trans. Electron Devices*, **ED-32**, 100, (1985)

[22]   J.L. Moruzzi, A. Kiermasz and W. Eccleston, "Plasma Oxidation of Silicon", *Plasma Physics*, **24**, 605, (1982).

[23]   A. Kiermasz, W. Eccleston and J.L. Moruzzi, "Theory of the Growth of SiO_2 in an Oxygen Plasma", *Solid-State Electronics*, **26**, 1167, (1983).

[24]   K.J. Barlow, A. Kiermasz and W. Eccleston, "The Efficiency and Temperature Dependence of the Growth of Silicon Dioxide in a Gaseous Plasma", in *Proceedings of the International Conference on Insulating Films on Semiconductors (INFOS '85)*, edited by J.J. Simonne and J. Buxo.

[25]   W. Eccleston, K.J. Barlow and A. Kiermasz, "The Gaseous Anodization of Silicon and Its Applications", *Vacuum*, **35**, 455, (1985).

[26]   S. Taylor, K.J. Barlow, W. Eccleston and A. Kiermasz, "Comparison of RF and Microwave Oxidation Systems for the Growth of Thin Oxides at Low Temperatures", *Electron. Lett.*, **23**, 309, (1987).

[27]   S. Taylor, W. Eccleston and P. Watkinson, "Advances in Electrical Properties of Plasma-Grown Oxides of Silicon", *Electron. Lett.*, **23**, 732, (1987).

[28]   S. Taylor, W. Eccleston, and K.J. Barlow, "Theory for the Plasma Anodization of Silicon Under Constant Voltage and Constant Current Conditions", *J. Appl. Phys.*, **64**, 6515, (1988).

[29]   K. J. Barlow, S. Taylor, W. Eccleston and A. Kiermasz, "The Low-Temperature Anodization of Silicon in a Gaseous Plasma," *IEEE Trans. Electron Devices*, **ED-36**, 1279, (1989).

[30]   T. A. Roppel, "Anodic Oxidation of Silicon in a Microwave Plasma Disk Reactor", Ph.D. Dissertation, Michigan State University (1986).

[31]   T. Roppel, D.K. Reinhard, and J. Asmussen, "Low Temperature Oxidation of Silicon Using a Microwave Plasma Disk Source", *J. Vac. Sci. Technol.*, **B4**, 295, (1986).

[32]   T. Roppel, D. K. Reinhard, G. T. Salbert, and J. Asmussen, "Properties of Silicon Oxide Films Grown in a Microwave Oxygen Plasma", Presented at 1986 IEEE International Electron Devices Meeting, Los Angeles, California, December (1986).

[33]   S.A. Nelson and R.A. Buhrman, "Thin Silicon Oxides grown by Low-Temperature RF Plasma Anodization and Deposition", *Appl. Phys. Lett.*, **50**, 1095, (1987).

[34]   S.A. Nelson, H.D. Hallen, and R.A. Buhrman, "A Structural and Electrical Comparison of Thin SiO_2 Films Grown on Silicon by Plasma Anodization and Rapid Thermal Processing to Furnace Oxidation", *J. Appl. Phys.*, **63**, 5027, (1988).

[35]   S.S. Wong and W.G. Oldham, "A Multiwafer Plasma System for Anodic Nitridation and Oxidation", *IEEE Electron Device Letters*, **EDL-5**, 175, (1984).

[36]   J. Perriere, J. Siejka, and R.P.H. Chang, "Study of Oxygen Transport Processes During Plasma Anodization of Si Between Room Temperature and 600 °C", *J. Appl. Phys.* **56**, 2716, (1984).

[37]   J. Perriere, J. Siejka, N. Remili, A. Laurent, A. Straboni, and B. Vuillermoz, "Transport Number Measurments During Plasma Anodization of Si, GaAs and $ZrSi_2$", *J. Appl. Phys.*, **59**, 2752, (1986).

[38] C. Vinckeir and S. De Jaegere, "Yields of the Plasma Oxidation of Silicon by Neutral Oxygen Atoms and Negative Oxygen Atom Ions", Ions", *J. Electrochem Soc.*, **137**, 628, (1990).

[39] A. K. Ray and A. Reisman, "The Formation of SiO_2 in an RF Generated Oxygen Plasma, I. the Pressure Range Below 10 mTorr", *J. Electrochem. Soc.* **128**, 2460, (1981).

[40] A. K. Ray and A. Reisman, "The Formation of SiO_2 in an RF Generated Oxygen Plasma, II. The Pressure Range Above 10 mTorr," *J. Electrochem. Soc.*, **128**, 2466, (1981).

[41] A.K. Ray and A. Reisman, "Plasma Oxide FET Devices", *J. Electrochem. Soc.*:SOLID-STATE SCIENCE AND TECHNOLOGY, **128**, 2424, (1981).

[42] S. Kimura, E. Murakami, T. Warabisako, and H. Sunami, "Microwave-Discharge Plasma Oxidation of Silicon in a Cusp Magnetic Field", *J. Electrochem. Soc.*:SOLID-STATE SCIENCE AND TECHNOLOGY, **135**, 2009, (1988).

[43] S. Kimura, E. Murakami, K. Miyake, T. Warabisako, H. Sunami, and T. Tokuyama, "Low Temperature Oxidation of Silicon in a Microwave-Discharged Oxygen Plasma", *J. Electrochem. Soc.*, **132**, 1460, (1985).

[44] T. Warabisako, S. Kimura and T. Tokuyama, "A 600 °C Process for MOSFET Fabrication Using Microwave Plasma-Stream Gate Oxidation", *1985 IEDM Technical Digest,* pp.216-219, (1985).

[45] K. Miyake, S. Kimura, T. Warabisako, H. Sunami, and T. Tokuyama, "Microwave Plasma Stream Transport System for Low Temperature Plasma Oxidation", *J. Vac. Sci. Technol. A,* **2**, 496, (1984).

[46] S. Kimura, E. Murakami, T. Warabisako, H. Sunami, and T. Tokuyama, "Low-Temperature Fabrication of MOSFET's Utilizing a Microwave-Excited Plasma Oxidation Technique", *IEEE Electron Device Letters,* **EDL-7**, 38, (1986).

[47] L. Bardos, G. Loncar, I. Stoll, J. Musil, and F. Zacek, "A Method of Formation of Thin Oxide Films on Silicon in a Microwave Magnetoactive Plasma", *J. Phys. D,* **8**, 1195, (1975).

[48] L. Bardos, J. Musil, F. Zacek, and L. Hulyeni, "The Negative Role of the Fast Electrons in the Microwave Oxidation of Silicon", *Czech J. Phys.* **B28**, 639, (1978).

[49] G. Loncar, J. Musil, and L. Bardos, "Present Status of Thin Oxide Films Creation in a Microwave Plasma", *Czech J. Phys.*, **B30**, 688, (1980).

[50] S. Gourrier and M. Bacal, "Review of Oxide Formation in a Plasma", *Plasma Chemistry and Plasma Processing,* **1**, 217, (1981).

[51] T. Sugano, **Applications of Plasma Processing to VLSI Technology**, J. Wiley and Sons, New York, 1985.

[52] D.V. McCaughan and J.A. Heilig, Jr., "Dielectric Strength and Interface-State Behaviour of Oxygen Plasma-Grown SiO_2 Films Annealed at High Temperature", *Int. J. Electronics*, **34**, 737, (1973).

[53] E.K. Broadbent, "Ion Beam Etching in an Evaporator", *Solid State Technol.*, **26**, 201, (1983).

[54] T.J. Donahue, W.R. Burger, and R. Reif, "Low-Temperature Silicon Epitaxy Using Low Pressure Chemical Vapor Deposition with and without Plasma Enhancement", *Appl. Phys. Lett.*, **44**, 346, (1984).

[55] W.R. Burger, and R. Reif, "Bulk-Quality Bipolar Transistors Fabricated in Low-Temperature (T_{dep}=800 °C) Epitaxial Silicon", *Appl. Phys. Lett.* **50**, 1447, (1987).

[56] W.R. Burger and R. Reif, "An Optimized *in situ* Argon Sputter Cleaning Process for Device Quality Low-Temperature (T<800 °C) Epitaxial Silicon: Bipolar Transistor and *pn* Junction Characterization," *J. Appl. Phys.*, **62**, 4255, (1987).

[57] J.H. Comfort, L.M. Garverick and R. Reif, "Silicon Surface Cleaning by Low Dose Argon-Ion Bombardment for Low-Temperature (750 °C) Epitaxial Silicon Deposition. I. Process Considerations" *J. Appl. Phys.* **62**, 3388, (1987).

[58] L.M. Garverick, J.H. Comfort, T.R. Yew, R. Reif, F.A Baiocchi, and H.S. Luftman, "Silicon Surface Cleaning by Low Dose Argon-Ion Bombardment for Low-Temperature (750 °C) Epitaxial Silicon Deposition. II. Epitaxial Quality," *J. Appl. Phys.* **62**, 3898, (1987).

[59] S. Ohi, W.R. Burger, and R. Reif, "Fabrication and Characterization of Bipolar Transistors with *In-Situ* Doped Low-Temperature (800°C) Epitaxial Silicon", *IEEE Electron Device Letters*, **EDL-10**, 383, (1989).

[60] M. Sadamoto, J.H. Comfort, and R. Reif, "Low Temperature Si_2H_6 Si Epitaxy *In-Situ* Doped with AsH_3/SiH_4," *J. Electron. Mater.*, **19**, 1395, (1990).

[61] S. Ohi, W.R. Burger, and R. Reif, "Electrical Characterization of Junctions and Bipolar Transistors Formed with *in-situ* Doped Low-Temperature (800°C) Epitaxial Silicon," *IEEE Trans. Electron Devices*, **ED-38**, 128, (1991).

[62] T.R. Yew and R. Reif, "*In Situ* Dopin in Silicon Selective Epitaxial Growth at 800 °C by Ultralow-Pressure Chemical Vapor Deposition", *Appl. Phys. Lett.*, **57**, 2010, (1990).

[63]   T.J. Faith, J.J. O'Neill, Jr., R.S. Irven, J.L. Vossen, J.M. Shaw, and J.H. Thomas, III, "Comparative Investigation of CF_4-Plasma, Ar-Plasma, and Dilute-HF-Dip Cleaning Methods for (Al-Si)/n$^+$Si Contacts", *J. Electochem. Soc.*: SOLID-STATE SCIENCE AND TECHNOLOGY, **134**, 665, (1987).

[64]   T. Ohmi, T. Ichikawa, T. Shibata, K. Matsudo, and H. Iwabuchi, "*In situ* Substrate-Surface Cleaning for Very Low Temperature Silicon Epitaxy by Low-Kinetic Energy Particle Bombardment", *Appl. Phys. Lett.*, **53**, 45, (1988).

[65]   T. Ohmi, K. Hashimoto, M. Morita, and T. Shibata, "Study on Further Reducing the Epitaxial Silicon Temperature Down to 250 $^\circ$C in Low-Energy Bias Sputtering", *J. Appl. Phys.* **69**, 2062, (1991).

[66]   S. Salimian, C.B. Cooper, III, and A. Ellingboe, "Etching of SiO_2 in an Electron Cyclotron Resonance Argon Plasma", *Appl. Phys. Lett.*, **56**, 1311, (1990).

[67]   R.J. Holwill, "The Current Status of Metallization in Integrated Circuit Applications," *Mater. Sci. Eng.*, **A116**, 143, (1989).

[68]   F. Hawley, A. Levi, G. Vasche and J.M. Caywood, *IEEE VLSI Multilevel Interconnection Conf.*, IEEE, New York, 1988, p.142.

[69]   R. Wolters, *IEEE VLSI Multilevel Interconnection Conf.*, IEEE, New York, 1988 p149.

[70]   J.A. Bittencourt, Fundamentals of Plasma Physics, p. 9, (Pergamon Press, New York, 1986).

[71]   J. Asmussen, "Electron Cyclotron Resonance Microwave Discharges for Etching and Thin-Film Deposition", *J. Vac Sci. Technol.* A 7, 883, (1989).

[72]   J. Hopwood, M. Dahimene, D.K. Reinhard, and J. Asmussen, "Plasma Etching with a Microwave Cavity Plasma Disk Source", *J. Vac. Sci. Technol.* B 6, 268 (1988).

[73]   C. Pomot, B. Mahi, B. Petit, Y. Arnal, and J. Pelletier, "Anisotropic Etching of Silicon using an SF_6/Ar Microwave Multipolar Plasma", *J. Vac. Sci. Technol. B,* **4**, 1 (1986).

[74]   J. Asmussen, and J. Root, "The Characteristics of a Microwave Plasma Disk Ion Source", *Appl. Phys. Lett.*, **44**, 396, (1984).

[75]   J. Root and J. Asmussen, "Experimental Performance of a Microwave Cavity Plasma Disk Ion Source," *Rev. Sci. Instrum.* **56**, 1511, (1985).

[76]   J. Asmussen and M. Dahimene, "The Experimental Test of a Microwave Ion Source in Oxygen," *J. Vac. Sci. Technol.* **B5**, 328 (1987).

[77] M. Dahimene, "Development of a Microwave Ion and Plasma Source Immersed in a Multicusp Electron Cyclotron Resonant Magnetic Field," Ph.D. Dissertation, Michigan State University, 1987.

[78] J.A. Hopwood, "Macroscopic Properties of a Multipolar Electron Cyclotron Resonance Microwave-Cavity Plasma Source for Aniso- tropic Silicon Etching," Ph.D. Dissertation, Michigan State University, 1990.

[79] G.T. Salbert, D. K. Reinhard, and J. Asmussen, "Down-Stream Oxidation of Silicon Using an ECR Microwave Plasma Disk Reactor," Presented at the 1989 IEEE International Conference on Plasma Science, Buffalo, New York, May (1989).

[80] G.T. Salbert, D.K. Reinhard, and J. Asmussen, "Oxide Growth on Silicon Using a Mirowave Electron Cyclotron Resonance Oxygen Plasma", *J. Vac Sci. Technol.*, **A8**, 2919, (1990).

[81] J. Asmussen, J. Hopwood, and F.C. Sze, Presented at the International Conference on Ion Sources, University of California at Berkely, California, July (1989), Proceedings to be published in Review of Scientific Instruments, January (1990).

[82] J.A. Bittencourt, <u>Fundamentals of Plasma Physics,</u> p. 291, (Pergamon Press, New York, 1986).

[83] The current-voltage measuring program and the analysis program that are part of the automated system used in this work were first developed by Leonard J. Mahoney. The programs were further refined by Jeffery A. Hopwood, Pung-Un Mak, Fan-Cheung Sze and Aseem K. Srivistava. Special thanks goes out to Fan-Cheung Sze for advice and instruction in the use of these two programs.

[84] L.J. Mahoney, "The Design and Testing of a Compact Electron Cyclotron Resonant Microwave-Cavity Ion Source", MS Thesis, Michigan State University, 1989.

[85] W. Kern and D.A. Puotinen, "Cleaning Solutions Based on Hydrogen Peroxide for use in Silicon Semiconductor Technology", *RCA Review* **31**, 187 (1970).

[86] B.E. Cherrington, <u>Gaseous Electronics and Gas Lasers,</u> p. 145, (Pergamon Press, Oxford, 1979).

[87] F.C. Sze, B.D. Musson, D.K. Reinhard, and J. Asmussen, "Correlation of Plasma Properties and Etching Performance in a 23 cm diameter Microwave Multicusp ECR Plasma Reactor", presented at the 18th IEEE International Conference on Plasma Science, June 3-5, 1991, Williamsburg, Virginia.

[88] P.G. Pai, S.S. Chao, and Y. Takagi, "Infrared Spectroscopic Study of SiO_x Films Produced by Plasma Enhanced Chemical Vapor Deposition", *J. Vac. Sci. Technol.* A **4**, (3), 689, May/June (1986).

[89]   J.S. Johannessen, W.E. Spicer, and Y.E. Strausser, "An Auger Analysis of the SiO_2-Si Interface", *J. Appl. Phys.* **47**, (7), 3028 (1976).

[90]   M.A. Taubenblatt and C.R. Helms, "Ion Knock-On Broadening Effects in Auger Sputter Profiling Studies of Ultra-Thin SiO_2 Layers on Si", *J. Appl. Phys.* **54**, (5), 2667, May (1983).

[91]   D.K. Reinhard, Introduction to Integrated Circuit Engineering, p. 91 (Houghton Mifflin Company, Boston, 1987).

[92]   E.H. Nicollian and J.R. Brews, MOS (Metal Oxide Semiconductor) Physics and Technology, p. ix (Wiley and Sons, New York, 1982).

[93]   Special thanks to Michal J. Ulczynski for help in writing and refining the program to automatically take the C-V data with the HP Low Frequency Impedance Analyzer.

[94]   L.M. Terman, "An Investigation of Surface States at a Silicon/ Silicon Oxide Interface Employing Metal-Oxide-Silicon Diodes", *Solid-State Electron.*, **5**, 285 (1962).

[95]   E.H. Nicollian and J.R. Brews, MOS (Metal Oxide Semiconductor) Physics and Technology, p. 325 (Wiley and Sons, New York, 1982).

[96]   The computer program used in the extraction for the D_{it} was first written by Roppel [30] for n-type silicon and subsequently modified by D.K. Reinhard and G.T. Salbert for p-type silicon along with corrections to both programs.

[97]   E.H. Nicollian and J.R. Brews, MOS (Metal Oxide Semiconductor) Physics and Technology, p. 787 (Wiley and Sons, New York, 1982).

[98]   G.A. Swartz, "Gate Oxide Integrity of MOS/SOS Devices", *IEEE Trans. Electron Devices*, ED-33, 119, (1986).

[99]   F.C. Sze, D.K. Reinhard, B.D. Musson, J. Asmussen, and M. Dahimene, "Experimental Performance of a Large-Diameter Multi-polar Microwave Plasma Disk Reactor", *J. Vac. Sci. Technol.*, B **8**, 1759, (1990).

[100]   Peng-Un Mak designed the MPCS used in this work.

[101]   Leon I. Maissel and Reinhard Glang, Handbook of Thin Film Technology, page 3-20 (McGraw-Hill 1970).

[102]   B. Chapman, Glow Discharge Processes: Sputtering and Plasma Etching, p. 69, (John Wiley and Sons, New York, 1980).

[103]   L.J. Mahoney, "The Design and Testing of a Compact Electron Cyclotron Resonant Microwave-Cavity Ion Source", MS Thesis, p. 79, Michigan State University, 1989.

[104]   T. Ohmi, K. Kotani, A. Teramoto, and M. Miyashita, "Dependence of Electron Channel Mobility on Si-SiO$_2$ Interface Microroughness", *IEE Elect. Dev. Lett.*, **12**, 652, (1991).

[105]   T. Ohmi, M. Miyashita, M. Itano, T. Imaoka, and I. Kawanabe, "Dependence of Thin-Oxide Films Quality on Surface Microroughness", *IEEE Tans. Electron Devices*, **39**, 537, (1992).